Optimisation of a Wearable Neuromodulator for Migraine Using Computational Methods

Enver Salkim

A thesis submitted in partial fulfilment of the requirements for the degree of **Doctor of Philosophy**

Analogue and Biomedical Electronics Group

Department of Electronic and Electrical Engineering

University College London

Official declaration

I, Enver Salkim, confirm that the work presented in this thesis is my own. Where information has been derived from other sources, I confirm that this has been appropriately indicated in the thesis.

"To people worldwide who suffer from migraine."

Abstract

Migraine is the third most common neurological disorder and the sixth cause of disability. It may be characterized by a headache, nausea, vomiting, photophobia and phonophobia. Available pharmaceutical treatments of migraine are not completely effective and have troublesome side-effects. Thus, there is a need for alternative treatments such as neuromodulation. Neuromodulation may be delivered invasively; however, this exposes the patients to the associated risks. Transcutaneous electrical nerve stimulation is a non-invasive technique that is widely used to relieve pain. A significant number of migraine sufferers complaint the symptoms of pain originating in the frontal region of the head. Thus, migraine may be associated with the supraorbital nerve and supratrochlear nerve which passes below the frontal bone exits from the orbital rim and penetrates the corrugator and frontalis muscles. Transcutaneous frontal nerve stimulation has been applied on a large group of patients who have episodic migraine using a device called Cefaly. This study produced mixed results (50% response rate). A post–marketing survey led to 53% satisfaction while the most limiting factor is reported to be paraesthesia and painful sensation. The possible causes of these inconclusive results may be associated with neuroanatomical variations, patient compliance and neurophysiological effects. The most plausible cause may be related to the neuroanatomical variations across different subjects. The neuroanatomical variations may lead to excessively high current levels being required. Since this solution is patient–operated, these relatively high required levels are not applied. In addition, as the electrodes are positioned near pain–sensitive

structures, pain may be induced even at low current levels, further limiting the efficacy of the solution.

There has been no robust investigation identifying the underlying causes of inefficacy. This is partly due to the physical limitations of studying the neuroanatomy of each subject and different settings of electrode arrangements. Computational models may enable researchers to estimate current stimulation thresholds in neuromodulation therapy and investigate the effects of various parameters. Such computational models are composed of a volume conductor model and an advanced Hodgkin–Huxley–type model of neural tissue referred to as a hybrid model.

Once the human head anatomy, the human nervous system and available solutions for migraine are detailed, the computational model of the human head is generated. A highly detailed human head model based on magnetic resonance imaging (MRI) studies, microscopic structure of the skin(including sweat ducts, keratinocytes and lipid) and those of a simplified head model (which built from geometric shapes) are compared based on neural excitation to assess the usability of geometrically realistic(simplified) human head models in the subsequent studies to save computations cost. The induced electric field due to an electrode setting is simulated in the volume conductor model and the resulting electric potential values along the nerve are passed on to the neural model to simulate nerve's response. It is shown that a simplified model may be used with a marginal error ($\approx$2%) in the subsequent work when assessing the effect of neuroanatomical variations on the efficacy of the target solution and possible ensuing optimizations.

The first step is to identify if neuroanatomical variations had any effect on the required stimulus current levels using state of the art computational bio–models. Ten realistic human head models are developed by varying thirteen neuroanatomical features including human head size, thicknesses of the tissue layers and variations in the courses of the nerve by considering their respective statistical distri-

butions as reported in the literature. A novel algorithm is developed to account for the variations of the nerve in different individuals and mimic statistically relevant large population. In each case, the required stimulus current levels are simulated. The findings show that the combined neuroanatomical variations have a significant effect on the neural response for the electrode setting used in Cefaly device.

Therefore, a potential improvement is to align the axis of electrodes with the target nerve, so that the electrical potential along the trajectory of the nerve changes polarity. This may lead to lower required stimulus current levels. Aligning electrodes with the nerve, the required current may be reduced by at least 60%. This new orientation reduces current density near pain– sensitive structures by diverting the current away from them, which may lead to a higher level of patient compliance, further improving the efficacy of the solution. Using an electrodes array arrangement, the required current levels is further reduced due to incorporating multiple electrodes array elements to maximise the variations of the electrical field in the simulation of the fibres in one phase.

The findings of this thesis indicate that the highly detailed human head model can be simplified while minimally affecting the outcome. Additionally, it is shown that neuroanatomical variations have a significant impact on the stimulus current thresholds but it is not possible to conclude if these thresholds solely depend on a specific neuroanatomical variation. The relatively high required levels of the stimulus currents are beyond the current capabilities of existing device and possible pain thresholds. Furthermore, the proposed new electrode arrangement has multiple benefits including the reduction of the stimulus current levels and diversion of current spread from possible pain–sensitive structures. This improvement, based on modelling, can potentially improve the clinical outcome of the neuromodulator substantially if confirmed in the subsequent clinical studies.

Impact statement

Migraine is a highly disabling neurological disorder which may affect patients both socially and economically. Transcutaneous electrical nerve stimulation (TENS) has fewer complications compared with the pharmaceutical and invasive neuromodulation methods on the treatment of migraine. A solution based on transcutaneous frontal nerve stimulation for the prevention of an episodic migraine is commercially available and is called Cefaly.

This non–invasive method has been tested in a clinical study and the tolerability and the safety of the device has been evaluated based on a survey. The results showed limited efficacies and led to side effects including pain. It has been claimed that the principal reasons for the interruption of the stimulation are the sensation of the paraesthesia and pain with high current stimulation. These may also be associated with neuroanatomical variations which leads to high levels of required stimulus current and may result in painful sensations due to activation of pain fibres (nociceptive). Furthermore, as the electrodes are positioned near pain–sensitive structures (e.g., eyes, frontal sinuses, veins and nerves), pain may be induced even at low current levels, further limiting the efficacy of the solution. Using a new electrode configuration that shifted away from these sensitive anatomical layers, it may be possible to stimulate all nerve fibres of frontal nerve at a reduced threshold with a lower risk of inducing pain. This study investigates the effect of neuroanatomical variations, electrode orientation and electrodes array configuration on the stimulus current thresholds and current density using a computational hybrid model involving a volume conductor and nerve models.

Ten human head models are developed considering statistical variations of key neuroanatomical features, mimicking a large population. Simulating the required stimulus current level in each case, it is shown that the current levels may not solely depend on one specific neuroanatomical feature.

The results show that excessive current levels may be required in 50% of variations. Aligning electrodes with the nerve, the required current may be reduced by at least 60%. The current levels are further reduced using electrodes array configuration. This new configurations reduce current density near pain–sensitive structures by diverting the current away from them, which may lead to a higher level of patient compliance, further improving the efficacy of the solution. If this improvement is confirmed in the clinical study for migraine patients, as future work, the target neuromodulator can be optimised substantially.

Acknowledgement

I would like to thank my principal supervisor, Prof Andreas Demosthenous for guiding me throughout my PhD journey. I am grateful for his invaluable guidance, support and contributions in my work. Working with him has allowed me to both gain academical and professional skills.

I would also like to acknowledge the efforts of my second supervisor, Dr Arsam N. Shiraz, for his immense support so far. I am also grateful for his valuable feedback, suggestions and discussions that helped me strengthen the different aspects of my work and overcome arduous challenges.

It has been a pleasure to share the same atmosphere with the friendly and pleasant group of colleagues in Analogue and Biomedical Electronics Group. I have gained a lot from their feedback and discussions throughout this journey.

Additionally and most importantly, I would like to acknowledge my sponsors, Turkish Educational Ministry and Mus Alparslan University, who have provided this platform for my educational development. Special thank goes to staffs in Turkish Embassy who have always helped me by generating a bound between me and my sponsors.

Finally, a special and very big thank you goes to my dear family: my parents, my beloved and supportive wife and my baby boy for their constant unending love, encouragement and moral support throughout this period. I would like to express my special gratitude to everyone who always support me and wishes the best for me.

Contents

List of Figures

List of Tables

Acronyms

AE Adverse event

AHP After Hyper polarisation Adenosine

AP Action potential

CAD Computer-aided designing

CGRP Calcitonin generelated peptide

CH Cluster headache

CI Chloride

CM Chronic migraine

CNS Central nervous system

CSF Cerebrospinal fluid

CSM Corrugator supercilii muscle

CT Computed tomography

DAP Depolarising after-potential

ECG Electrocardiogram

EEG Electroencephalogram

EM Episodic migraine

EMG Electromyogram

EN Endoneurium

EP Epineurium

ETI Electrode tissue interface

FDA Food drug administration

FDM Finite difference method

FEM Finite element model

FVM Finite volume model

GHK Goldman-Hodgkin-Katz

GON Greater occipital nerve

HH Hodgkin-Huxley

HT Hydroxytryptamine

K Potassium

MRG McIntyre Richardson Grill

MRI Magnetic resonance imaging

Na Sodium

NSAIDs Nonsteroidal anti-inflammatory drugs

ONS Occipital nerve stimulation

PE Perineurium

PNS Peripheral nervous system

Pt Platinum

SC Stratum corneum

SD Sweat duct

SON Supraorbital nerve

SPGS Sphenopalatine ganglion stimulation

STN Supratrochlear

tDCS Transcutaneous direct current stimulation

TENS Transcutaneous electrical nerve stimulation

TES Transcutaneous electrical stimulation

tFNS Transcutaneous frontal nerve stimulation

TTH Tension type headache

TMS transcranial magnetic stimulation

TNC Trigeminal nucleus caudalis

VGS Vagus nerve stimulation

Chapter 1

Introduction

1.1 Overview

Migraine is a neurological disorder that may be characterized by a recurrent, unilateral or bilateral throbbing headache, which is usually accompanied by nausea, photophobia, and phonophobia [2]. It is the third most common neurological disorder and the sixth cause of disability, affecting about 15% of the general population [3]. This socioeconomic burden has led to substantial constraints globally [4], [5]. Available pharmaceutical treatments of migraine are associated with moderate to severe side effects including headache chronification due to overuse [6]. These may lead to inefficacy, dissatisfaction and/or abandonment of medication. A recent study has shown the profound need for alternative treatment methods [6].

Neuromodulation has been implemented in managing pain by affecting peripheral or central pathways via applying stimulus current using implantable electrodes or non-invasively through surface electrodes [7]. Based on gate control theory [8], the peripheral nerve stimulation leads to the activation of Aβ afferent fibers and subsequently this inhibits Aδ and C pain fibers. Pain suppression may be due to neural plasticity, defined as the ability of the nervous system to modify itself. This can be achieved over a period of time, often weeks to months [7] triggered by external stimuli.

Stimulation of occipital and vagus nerves, and sphenopalatine ganglion stim-

ulation, delivered invasively, and stimulation of vagus and frontal nerves, and transcranial magnetic stimulation (TMS), delivered non-invasively, are examples of using neuromodulation to manage migraine. Invasive methods are used in the most medically intractable patients due to their associated risks [9]. The induced electrical stimulation by TMS activates a mixture of neurons in the brain and may lead to unorganized pattern of activity. Additionally, studies have shown that the stimulation protocols (e.g., stimulation frequency, current waveform and coil position of TMS have not been optimized [10]. Moreover, the vagus nerve contains sensory and motor fibers and its stimulation may cause neck muscle contractions [11].

Migraine sufferers commonly report that migraine pain is centred in the regions innervated by supraorbital (SON) and supratrochlear (STN) nerves [12]. These sensory peripheral nerves are branches of the frontal nerve stemming from the ophthalmic division of the trigeminal nerve. STN and SON transmit frontal head pain through the trigeminal nucleus caudalis to thalamus which is then transmitted to higher brain centres [13]. Transcutaneous frontal nerve stimulation (t–FNS) using the Cefaly neurostimulator (Cefaly, CEFALY Technology, Lige, Belgium) has been shown to prevent episodic migraine [7]. Bipolar stimulus current is applied via transcutaneous electrical stimulation (TES) electrodes on the forehead to stimulate the target nerves.

The t–FNS using Cefaly has been tested in a double blind randomized controlled trial (n=67) [14] in which the efficacy, tolerability and safety of the device have been studied. This study produced mixed results (50% response rate). A post-marketing survey (n=2313) led to 53% satisfaction [15] while the most limiting factor was reported to be paraesthesia and painful sensation [16]. These inconclusive results may be associated with neuroanatomical variations that may lead to excessively high current levels being required [16] . Since this solution is patient-operated, these relatively high required levels are not applied. Such high stimulus current levels may lead to the co-excitation of Aδ and C (nociceptive) fibers re-

sulting in painful sensation. In addition, as the electrodes are positioned near pain sensitive structures (e.g., eyes, frontal sinuses, veins and nerves), pain may be induced even at low current levels, further limiting the efficacy of the solution.

1.2 Project aims

The main aim of this thesis is to investigate the effect of neuroanatomical variations and electrode arrangements on the efficacy of the transcutaneous frontal nerve stimulation using the state of the art of the bio–computational modelling methods. There has been no robust investigation identifying the underlying causes of the inefficacy of t–FNS using Cefaly device. This may be associated with the physical limitations of studying the neuroanatomy of the individuals and challenging nature of designing the optimal electrode settings for each subject by experimental methods. Using the state of the art of bio–computational methods, the effect of neuroanatomical variations and different electrode settings on the efficacy of the target solution can be readily investigated. The neuroanatomical features can be readily changed using their statistical distributions in anatomical data, creating a powerful tool for assessing how these variations lead to different neural responses for a given electrode setting using these computational models which are composed of a volume conductor model and an advanced Hodgkin-Huxley-type model of neural tissue referred to as a hybrid model.

The diversity of neuroanatomical elements and the complexity of the volume conductor impede the investigation of the aims of the project. To reduce the computation cost, a simplified model can be used with a marginal error in the subsequent work when assessing the effect of neuroanatomical variations on the efficacy of the target solution and possible ensuing optimizations.

To identify if the effect of neuroanatomical variations have any influence on the stimulus, statistically relevant group of human head models are developed by varying the key anatomical layers including human head size, thicknesses of the

tissue layers and variations in the courses of the nerve by considering their respective statistical distributions as reported in the literature. In each case, the induced electric field due to an electrode setting is simulated in the volume conductor model and the resulting electric potential values along the nerve are passed on to the neural model to simulate nerve's response.

As the electrode patch is placed in the vicinity of the pain–sensitive structures and also the required high levels of the stimulus current is led to patient discomfort, a new electrode configuration is proposed to reduce the nerve fibre stimulus current thresholds as well as patient discomfort. Thus, a potential improvement is to align the axis of electrodes with the target nerve, the consequence of this the electrical potential along the trajectory of the nerve changes polarity in one phase. This may result in lower stimulus current thresholds being required. In the target solution, this can be achieved by rotating the existing electrode setting in Cefaly by 90 degrees to participate both electrodes in the stimulation of the fibres in one phase. In this way, less stimulus current levels are required and the current spread is shifted away from sensitive structures.

Based on the findings of electrode orientation, an optimal electrodes array is designed and applied to all of the generated statistically relevant group of human head models to examine its effect on the stimulus current levels and patient discomfort using bio–computational modelling. The existing electrode arrangement (horizontal), the rotated version of the existing electrode (vertical) and the optimal electrode configurations are compared based on the nerve fibre stimulus current thresholds and current density in the vicinity of pain–sensitive structure. The results show that the required current thresholds are even further reduced using the optimal electrode configuration and it is noted that these thresholds are relatively less fluctuated for different individuals. Thus, if the results are validated in clinical study for migraine patients, the neuromodulator can be improved substantially.

1.3 Contributions

- The socioeconomic burden of the neurological disorder is targeted and discussed; the available solutions with their underlying neural circuitry are categorised and their key features are highlighted for readers' convenience.

- The transcutaneous neuromodulation of the frontal nerve may be the solution based on the provided literature. Thus, the overall concept of the project is put into perspective.

- The models and the underlying formulations regarding the biophysics of the phenomena under investigation are thoroughly analysed.

- Highly complex human head model with subsequent anatomical layers is developed from a magnetic resonance imaging (MRI) data set. The trajectory of the frontal nerve is generated based on anatomical data in literature. The effect of highly complex human head model, the simplified human head model (generated from simple geometries such as sphere) and the microscopic structure of the skin layer on the nerve fibre stimulus current thresholds and the computation cost are analysed using a state of the art hybrid computational methods. The main finding of the Chapter 3 is that the simplified human head can be used with a marginal error (2 to 3% based fibre activation) to assess the effect of the neuroanatomical variations across different individuals and electrode settings with different arrangements in future investigations.

- A novel algorithm was developed to provide a statistically relevant group of variations, incorporating the possible variations of the nerve trajectories and other anatomical structures. The samples of the entire statistical distribution of each variable was included for each case by ensuring that the variables are sufficiently separated in their respective distributions. The

finding in Chapter 4 suggested that the neuroanatomical variations have substantial impact on the target neuromodulator efficacy, but it was shown that the current levels may not solely depend on one specific neuroanatomical feature.

- By a thorough theoretical analysis, a new electrode orientation was proposed to investigate the possibility of reducing relatively high current levels that are obtained based on neuroanatomical variations using target electrode setting. The results show that by aligning the electrode with the axis of the nerve trajectory, the stimulus current thresholds may be reduced considerably by changing the polarity of the electrical potentials.

- Based on the idea of the changing the polarity of the electrode which may lead to low stimulus current being required, an optimal electrode was proposed to more increase the variation of the electrical potentials polarity along the nerve trajectory. It was observed that the required current thresholds for the nerve fibers of the target nerve can be further reduced.

- The proposed new electrode arrangements have multiple benefits including the reduction of the stimulus current levels and diversion of current spread from possible pain sensitive structures. This improvement can potentially improve the clinical outcome substantially if confirmed in the subsequent clinical studies.

1.4 Author's publications

The work reported in this thesis has resulted in the following publications:

E.Salkim, A.Shiraz and A.Demosthenous, "Effect of Neuroanatomical Variations and Electrode Orientation on Stimulus Current in a Device for Migraine Suppression: A Modelling Study", *IEEE Transactions on Neural Systems and Rehabilitation Engineering*, Submitted.

E.Salkim , A.Shiraz and A.Demosthenous, "Influence of Cellular Structures of Skin on Fiber Activation Thresholds and Computation Cost", *Biomedical Physics & Engineering Express*, , vol. 5, no. 1, p. 015015, 2018.

E.Salkim , A.Shiraz and A.Demosthenous, "Optimisation of a Wearable Frontal Neuromodulator Using Computational Methods", *Manuscript in preparation for submission to IEEE Transactions on Neural Systems and Rehabilitation Engineering.*

E.Salkim, A.Shiraz and A.Demosthenous, "Effect of Nerve Variations on the Stimulus Current Level in a Wearable Neuromodulator for Migraine : A Modeling Study", *8th International IEEE EMBS Conference on Neural Engineering, pp. 239-242, 25-28 May 2017, Shanghai, China DOI: 10.1109/NER.2017.8008335.*

E.Salkim, A.Shiraz and A.Demosthenous, "Effect of model complexity on fiber activation estimates in a wearable neuromodulator for migraine", *2017 IEEE Biomedical Circuits and Systems Conference (BioCAS), 19-21 October 2017, Turin, Italy, DOI: 10.1109/BIOCAS.2017.8325080.*

E.Salkim, A.Shiraz and A.Demosthenous, "Computational Study on Transcutaneous Frontal Nerve Stimulation: Simplification of Human Head Model", *2017 COMSOL Conference in Rotterdam, 18-20 October 2017, 2017 held in Rotterdam, Netherlands.*

1.5 Thesis organisation

In this section a summary of every chapter and the overall progression of the presented narrative are presented.

Chapter 2: **Fundamental of Migraine Management.** The fundamental of migraine management are reviewed in this chapter with a particular attention to the neurophysiology of migraine.

The general concepts of the human nervous system with subsequent divisions together with their roles are provided. Furthermore, from a cell level understanding of the neuroscience to complex neural circuits mediating different functions are

discussed. The main principles of the generation and propagation of the neural signal are particularly emphasised as these are the central concepts in the subsequently presented modelling studies in Chapter 3. At the next stage, the mechanism of the general pain and migraine pain and their functions are explored. Migraine pathophysiology and its underlying pathway theories are discussed in further. Then, available migraine management solutions including pharmaceutical, surgical and electrical neuromodulation techniques and their underlying neural circuitry are introduced. Finally, the limitations of the transcutaneous frontal nerve stimulation using Cefaly device are introduced to put the presented work in this thesis into perspective.

Chapter 3: **Computationally Efficient-Accurate TES Head Model Development**. The importance of the computational neuromodulation in the design and development of the neurostimulation therapy system is introduced to the reader. Then, the nerve and volume conductor modelling are reviewed. In particular, the attention is drawn to the fundamental of the HH type cable models and the general principles of the cable theory to be able to model the associated nerves accurately in the subsequent works. After introducing the fundamentals of the volume conductor models including associate equations, their approximations, the choice of the boundary conditions and the way they are solved numerically, then, the chronological and conceptional development of the human head model based on different numerical solutions were tabulated and their key points were discussed to choose the best platform for volume conductor modelling.
The development processes of the MRI based highly complex multi–layer human head model, nerve model and electrode model are provided. Then, the limitation of the highly complex human head volume conductor is provided and also it is discussed that these limitations can be reduced when using simplified geometries, that is generated by mimicking the realistic human head model, with a marginal error when compared to the highly detailed models. Additionally, the effect of the

microscopic structures and their statistical distributions in the skin layer on the nerve fibre activation is evaluated and the results are compared to the simplified human head model. After applying the boundary conditions, electrical properties of each layer and optimal mesh characteristics for each model; the electrical potential is simulated in volume conductor, interpolated and imported to the available workstation to calculate the response of nerve fibres to given current levels.

The results show that the simplified human head model can be used in future work when assessing the effect of neuroanatomical variations and different electrode configurations on the efficacy of the target solution.

Chapter 4: **Effect of Neuroanatomical Variations on Stimulus Current Levels**. In the previous chapter, It was shown that the simplified human head model can be used with a marginal error to investigate the effect of neuroanatomical structures on the stimulus current thresholds. Therefore, the statistical distribution of the of the human head size, key subsequent anatomical layers (including skin, fat, muscle, skull, CSF(Cerebrospinal fluid) and brain) and trajectories of the nerve and their branches are provided. To account for the variations of the nerve in different individuals and mimic statistically relevant large population, a novel algorithm is developed based on the statistical distribution of the neuroanatomical features. This results in ten different human head model which are generated by varying thirteen neuroanatomical features including human head size thicknesses of the tissue layers and variations in the courses of the nerve by considering their respective statistical distributions as reported in the literature. After providing the development processes of the three dimensional (3D) modelling of these statistically relevant models; the electrical properties of each tissue layer and adjustment of the optimal mesh features are applied to simulate electrical potentials in each model. The neural excitation is measured using hybrid computational methods based on current levels versus

percentage activation of the nerve fibre

The findings indicate that the variations of the neuroanatomical layers highly affect the required stimulus current thresholds using electrode settings of the target solution, it can not be concluded which neuroanatomical variations mainly affect these thresholds levels. The results show that the required current levels are higher than the existing neuromodulator stimulus current range. Thus, it is emphasised that there is a need for a new electrode arrangement that helps to reduce the current levels as well as patient discomfort.

Chapter 5: **Optimal Electrode Design**. The fundamentals of the electrode design including the effect of electrode orientation, electrode materials, electrode sizes and spacing, and electrodes array configuration on the excitation of the neural tissue are introduced.

It is discussed, in Chapter, 4 that the higher stimulus current ranges needed to activate all nerve population in the statistically relevant models. Therefore, a new electrode configuration is proposed to stimulate the nerve fibers with relatively lower current levels and reduce the patient discomfort. It has been shown that by aligning the axis of the electrode with the trajectory of the nerve, the stimulus current thresholds may be reduced due to changing the polarity of the electrical potential along the nerve trajectory. Therefore, the first step is to align the existing electrode setting with the trajectory of the nerve by rotating it 90 decrees to evaluate the effect of electrode orientation on the stimulus current thresholds and current density. The electrical potentials along the nerve are simulated for all generated human head models and the response of each nerve fibre is measured based on stimulus current thresholds. The results suggest that the required current thresholds and current density in the vicinity of pain–sensitive structures highly reduced when using new orientation.

This finding of electrode orientation leads to design an optimal electrodes array. In this way, the polarity of the induced electrical potentials on the nerve trajectory

are changed at the multiple places, thus, the stimulus current levels may further be reduced. After introducing the steps of the development of the optimal electrodes array configuration, the required current levels for each model is recorded to assess the effect of the optimal electrodes array on the target solution. It shows that the stimulus current thresholds even further reduced using the optimal electrode configuration. Thus, it is suggested that using new electrode arrangements provide multiple benefits including the reduction of the stimulus current levels and diversion of current spread from possible pain sensitive structures.

Chapter 6: **Conclusions and Future Directions**. The overall summary of the work presented in this thesis are provided and draws some conclusions about the contributions of the work presented and outlines possible future works including the experimental study on the effect of electrode orientation, and development of a hardware for novel electrodes array configuration.

Chapter 2

Fundamentals of Migraine Management

2.1 Introduction

In this chapter, the fundamentals of the migraine management procedures are discussed. The anatomy of human head structures related to this work is summarised. The human nervous system and underlying neural circuits are detailed. Then, the mechanism of the neural circuitry of the sensory pain, primary headache are explored to be able to optimise the available solution. The available neural or neurovascular pathway theories for migraine are studied and well accepted proposed theory is emphasized. After comprehensively reviewing the existing solutions for a migraine based on pharmaceutical, surgical and neurostimulation techniques and their possible adverse events, the transcutaneous supraorbital neuromodulation technique is explored as a possible solution. Finally, the possible reasons which are limiting the target solution's efficacy are discussed to put the presented work in this thesis into perspective.

2.2 Review of human head anatomy

It is necessary to explore human head structures related to this study, to generate a model of the human head. The skin, muscle, eyeball, skull, and cerebrospinal fluid (CSF) may be of interest due to the vicinity of the target nerve. The brain will be discussed in the human nervous system section in detail.

Skin

The first layer which contacts the electrode is skin. For this reason, knowledge of the electrical properties and structure of the skin is valuable. The trajectory of target nerve lines underneath the skin. Therefore, the conductivity of the skin may affect the activation of the target nerve. Thus, it is vital to summarise the morphological and electrical features of the skin and its sublayer which are summarised in Table 2.1 [17], [18].

The skin responsible for protecting the body from physical, chemical and biological assailants and mainly consists of **epidermis** and **dermis** layers. The outermost epidermis layer is called the stratum corneum (keratin layer). This layer is mainly composed of corneocytes (dead cells) which contribute significantly to the impedance of the skin (i.e., it is poorly conductive when dry). These subsequent layers of the skin are depicted in Figure 2.1a. [19], [20].

The skin thicknesses on the forehead varies between about 1 millimetre to 2 millimetre [19], [20]. The epidermis layer is one millimetre thick [21] in general and it is penetrated by sensory nerve ending. This layer consists of keratinocytes cells, which has a function of producing keratin to maintain skin's toughness and hardness. The dermis underlying the epidermis has a variable thickness and has both collagen and elastic fibres which maintain toughness and elasticity of the dermis layer. It contains blood vessels, sensory receptors (free nerve endings) and related nerves. These specialized receptors send physical stimuli (e.g., pain, pressure, temperature) from the peripheral nervous system (PNS) to the central

Table 2.1: The range of the investigated skin layers and fatty tissue conductivity and thickness values.

Tissue layer	Conductivity(S/m)	Thickness(mm)
Stratum corneum	0.0002–0.002	0.01-0.05
Epidermis	0.0002–0.3	0.08–1.0
Dermis	0.1–0.7	0.5–2.5
Fat	0.01–0.1	5–20

nervous system (CNS) for interpretation [22], [23]. This is discussed in the human nervous system section in detail.

The deep tissue in the dermis is subcutaneous (fatty layer) tissue which is not considered as a part of the skin. It connects the skin layer with the underlying organs and contains fat which protects the body from shocks and insulates the underlying organs from high–temperature variations [22], [23].

Muscle

The target nerve comes out from above eyes, pierces the frontalis nerve and underlines the skin. Thereby, it may useful to overview the facial muscles. The frontalis muscle covers the forehead area and it has roughly rectangular shape with bilateral symmetry. This muscle consists of approximately vertically oriented fibres and lies uniformly at a depth beneath the skin of the forehead. Its depth can vary considerably (2–7 mm) from one individual to another and on average is around 1 mm greater in men than in women [24]. The function of this muscle is to raise the eyebrows and to wrinkle the forehead [24]. The supraorbital and supratrochlear nerves, which are the target nerves, are mostly located in the frontalis muscle. The facial muscles are illustrated in Figure 2.1b.

The orbicularis muscle consists of fibres that are localised around eyes. It is innervated by the facial nerves, supplying the eyes' closing movement. The corrugator muscle is located under orbicularis muscle and medial aspect of eyebrows which allows eyebrow movement functions.

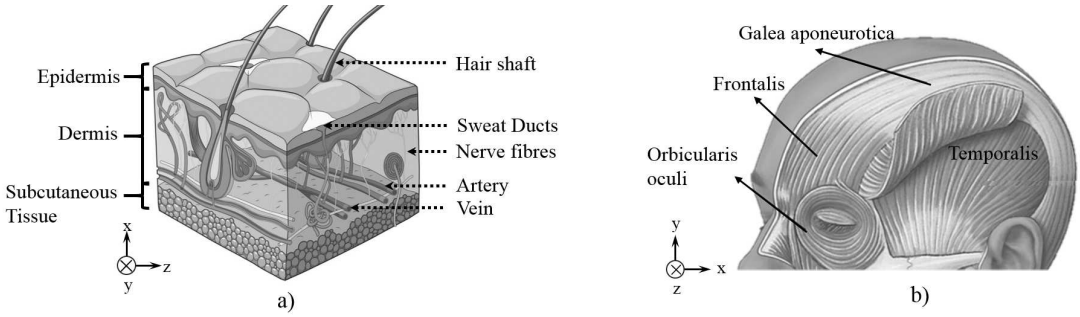

Figure 2.1: The anatomy of the skin and muscle in the human head, a)indicates the general structure of the skin which are mainly composed of epidermis, dermis and fat; b) shows different muscle types which are covered human head and facial areas. Different parts of the figure was obtained from [25] to construct the present here.

Skull

The human skull is responsible for protecting the brain and mainly composed of two sets of bones which are cranium and facial bones which are displayed in Figure 2.2a. These bones contain calcium salts and large numbers of collagen fibres which helps to protect and support body organs. Specifically, the cranium bones protect brain tissues while facial bones hold the eyes and maintain the muscle activity. The cranium layer mainly consists of frontal, parietal, temporal, occipital, sphenoid, and ethmoid bones. The facial bones are composed of fourteen small bones [23], [25].The cranium layer is subdivided as skull's outer and inner layer. Between these two layers, the skull dipole layer is present.

Eyeball

The target nerve trajectory comes out just above the eyes. During stimulation of the target nerve, the electrical potential may be induced in the vicinity of eyes. To prevent any soft tissue damage, the anatomy of the eyes should be reviewed in this work, as demonstrated in Figure 2.2b. The eye comprises a hollow sphere which is generally called the eyeball. Its interior is filled with humors to maintain the shape and lens which focus on objects at various distances. The retina can be

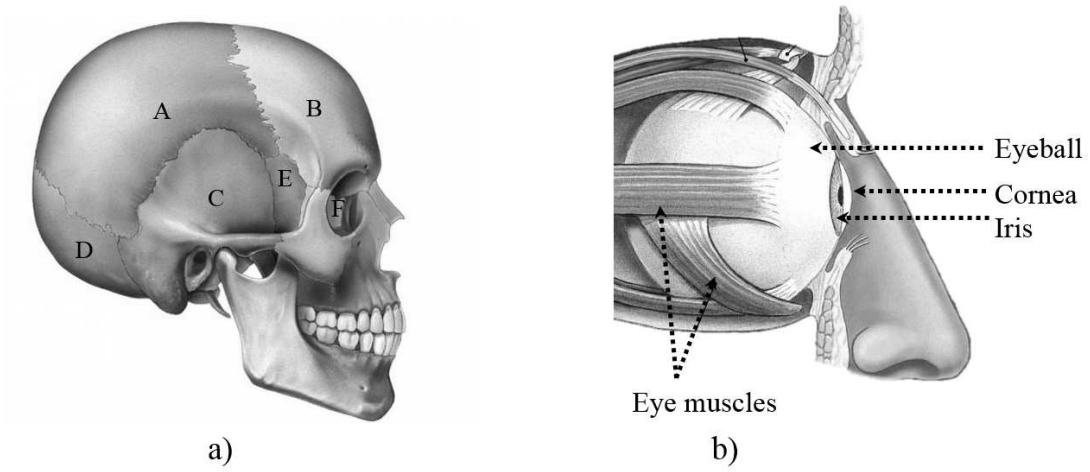

Figure 2.2: The anatomy of the human's skull and eye, adapted from [25], a) shows different parts of skull, namely; A, B, C, D, E, and F represent cranium bone layers and remaining layers are called facial bones, b) shows the parts of the human's eye and muscles in the vicinity.

divided into two subdivisions; the pigmented layer includes pigmented cells that help to absorb or reflect the light from inside of eyes. The neural layer consists of photoreceptors which respond to light. In order for the visual perception to happen, the bipolar cells (which are detailed in the nervous system section) transmit the electrical signal to photoreceptors through ganglion cells then the optic nerve conveys impulses to the optic cortex [23], [26].

2.3 Human nervous system

It is necessary to understand the nervous system before designing a system to suppress a neurological disorder. This section focuses on the human nervous system divisions and cell tissues in general regarding their functions and structures. The human nervous system divisions are CNS and PNS; the CNS mainly comprises of the brain and spinal cord, which occupy the dorsal body cavity and act as the integrating and command centres of the nervous system. The brain mainly comprises medulla oblongata, pons, cerebellum, midbrain, diencephalon, and cerebral hemispheres. The components of the CNS and PNS were shown in

Figure 2.4. The PNS comprises mainly of the nerves that extend from the brain and spinal cord; spinal nerves carry neural signals to and from the spinal cord and cranial nerves carry neural signals to and from the brain. The CNS and PNS structures will be covered later in this chapter. The nervous tissues are mainly nerve cells (neuron) and supporting cells (glia cells) which will be discussed in the following section.

2.3.1 Fundamentals of nerve tissues

The cellular structures of the nervous system can be grouped into neurons and glia cells based on histological studies. These will be detailed in this section.

Neurons

Neurons, also called nerve cells, are the main functional unit of the nervous system. Their role is to carry neural impulses from one part of the body to another. Although neurons may have different structures from one another, The typical neuron contains four main structures with differing functions and these are; a cell body (soma), an axon, group of dendrites, and axon terminals (as illustrated in Figure 2.3) [27].

The cell body or soma contains the nucleus and surrounding cytoplasm. It branches out various short dendrites and one long axon. The dendrites extend out–ward from the cell body and are specialised to transmit electrical signals toward the cell body. These signals may have an excitatory or inhibitory effect on the neuron (detailed in the pain mechanism section). Whereas, axons, long nerve fibres, are responsible for generating action potentials (AP will be discussed in detail on the latter section) and typically conduct them away from the cell body. Mammalian axons diameters usually vary between $1 - 20\mu m$ [27]. Although neurons have only one axon, they may have hundreds of the branching dendrites (depending on the neuron type). Axons originate from the cell body and the first segment of axon is called axon hillock. The axons spread out branches at

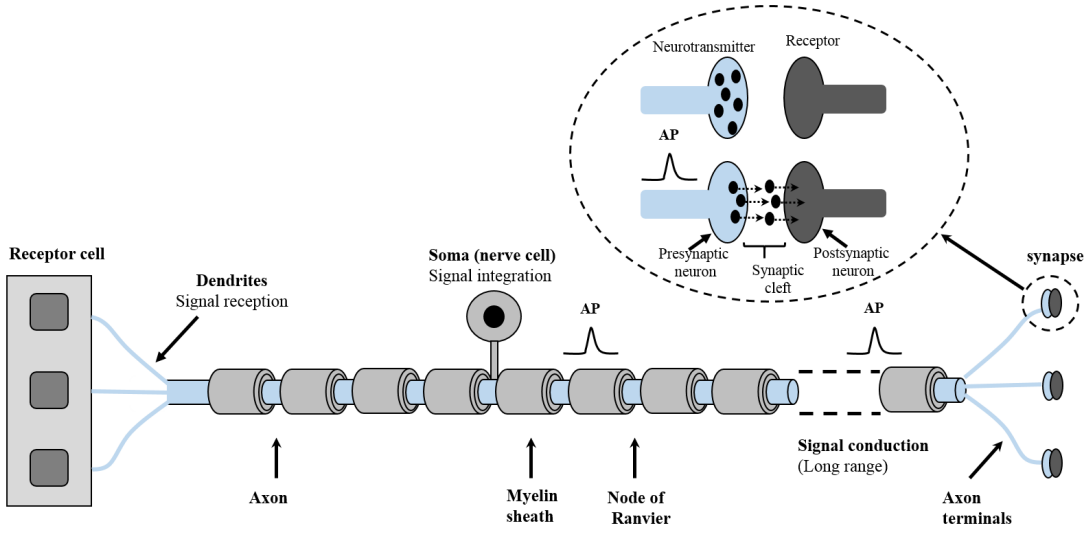

Figure 2.3: A typical sensory neuron structure.

the end of their terminal is called axon terminals which contain neurotransmitters. These are chemical messengers whose purpose is to provide communication between neurons (for the most cases). The functional junction that provides communication between two neurons is called a synapse. The axon terminals release neurotransmitters to the synaptic cleft which is a tiny gap and separates axon terminals from the next neuron. These are diffused across synapses and bind with the receptors on the opposing neural membrane. Electrical stimulation of sensory nerve fibres acts on the nerve through these junctions. The cell that transmits the signal is known as a presynaptic neuron and the cell that receives the signal is called postsynaptic neuron. The signal transmitted by the synapsis on the neuronal dendrites and read out at the origin of the axon [27], [28]. The electrical signal transmission steps from one neuron to another is displayed in Figure 2.3.

Neurons may be classified according to their functionality or based on their structure. In terms of the direction of neural signal (i.e., AP) that is travelling relative to the CNS, neurons may be grouped as sensory, motor, and interneuron (association neuron). The sensory or afferent (meaning to go toward or to go inward) neurons carry neural signals from sensory receptors (skin or in the internal organ) to the CNS. The motor or efferent (meaning to go outwards or to go away)

neurons carry neural signals from the CNS to the muscles and glans. Interneurons form the largest group of the neuron, the function of which is to connect the sensory and motor neurons in the neural pathway and transmit neural signals from one neuron to the other. The cell bodies of sensory neurons are located in a ganglion outside the CNS, while the cell bodies of motor and interneuron neurons are located in the CNS [27].

The structural classifications are grouped based on the number of processes extending from their cell body. The most common structural type is the multipolar neuron which has many dendrites spreading out from the cell body. Bipolar neurons have two processes which are an axon and a dendrite. Many sensory neurons have a bipolar structure in which the neural signal is received by dendrites and transmitted to the through the axon to the CNS. Bipolar neurons are rare in adults; they are located only in some special sensing organs such as eye and nose. Frontal nerve fibres are a typically bipolar and are the target nerves of this study. Neurons which have a single process originating from the cell body are called unipolar neuron. They are short and divided into central and peripheral processes. The axons in these types of neurons conduct neural signals both toward and away from the cell body [25], [27].

Sensory neurons have receptors which are responsible for converting different types of stimuli (pain, touch, light, and pressure) into electrical signals to transmit to the CNS. These signals are determined by the electrical properties of the cell membrane. While the cell is at rest, the membrane has resting potential which is typically -65mV in mammals [27]. However, the resting voltage can be varied for different cells between -40mV to -90mV [27]. The resting membrane potential occurs as a consequence of two factors; unequal distributions of Na^+(Sodium) and K^+(Potassium) ions and selective permeability of the membrane [27], [28], [29]. The underlying principles are discussed in AP section.

Supporting cells

Supporting cells in the CNS are is called neuroglia or glia cells or simply called glia. Neuroglia cells surround the nerve cells and have different functionalities. It is thought that the glia cells do not participate directly in information processing. Rather, they support, insulate, and protect the delicate neurons. Although neuroglia and neurons resemble each other in having a cell and cell extensions, neuroglia are not able to transmit neural signals. However, neuroglia never lose their ability during the dividing process, whereas most of the neurons do not have that ability. Each of the different neuroglia has different functions; oligodendrocytes cells insulate axons in the CNS. Schwan cells and Satellite cells are supporting cells in the PNS. Schwan cells form the myelin sheath around the axons and satellite cells are cushioning cells that give protection. Most of the long fibres are wrapped with a whitish, fatty structure called myelin. It protects and insulates the axons and increases the speed of conduction of the AP (which is explained in more detail in the following section).

Fibres may be grouped as myelinated and unmyelinated which is discussed detail in a further section. Myelinated fibres are wrapped by a myelin sheath which is interrupted at regular intervals by gaps called nodes of Ranvier. These help to the regenerate the AP provide fast propagation of AP [25], [27].

2.3.2 Central nervous system

Brain neuroanatomy

The main structures of the human brain are shown in Figure 2.4a. An adult brain is composed of cerebral hemispheres, the cerebellum, and the brainstem. The cerebral region is the largest part of the brain and is divided into two hemispheres. Each of these cerebral hemispheres has a wrinkled outer layer which is called the cerebral cortex. The cortex has a grey appearance hence it is called grey matter which mainly consists of the cell bodies. Underneath of the grey matter, there

are axons which are long myelinated fibers to increase the conduction speed. The myelin sheath delivers a white appearance to fibres hence thet are termed as white matter. The cerebellum layer consists of a thin grey matter and white matter which contains nuclei. The function of this layer is to precise coordination of muscle action and help proper posture in response to gravity [23], [27].

The brainstem is a part of the CNS and is covered by the cerebral and cerebellum layers. All the cranial nerves, apart from the trochlear nerve (will be mentioned in the section 2.3.3), pass out from the ventral aspect of the brainstem. The brain stem is responsible for receiving sensory information from the skin and the muscles that are present in the head and supplies motor control for these muscles. In addition to this, the brain stem transmits sensory signals from the spinal cord to the brain and from the brain to the spinal cord. Cranial nerve nuclei and cell bodies are present within the brain stem. Importantly, some of these nuclei are responsible for receiving sensory information from the skin and muscles of the head and remaining nuclei control motor output to the muscles of the face, neck, and eyes (trigeminal system). The medulla oblongatas main role is to control some vital autonomic functions such as digestion, breathing, and control of the heart pulse. The pons is located between the midbrain and the medulla and its function is to transmit movement information from the cerebral hemisphere to the cerebellum.

The cerebellum is responsible for regulating general force and movements and also has a role of learning motor skills. The midbrain lies above the pons which modulates many sensory and motor functions such as hearing and vision. The diencephalon consists of two structures which are thalamus and hypothalamus. The chief function of the thalamus is relaying most of the sensory and motor information to the cerebral cortex (from the rest of the central nervous system). One of the main tasks of hypothalamus is to regulate autonomic, endocrine, and visceral functions [27], [28].

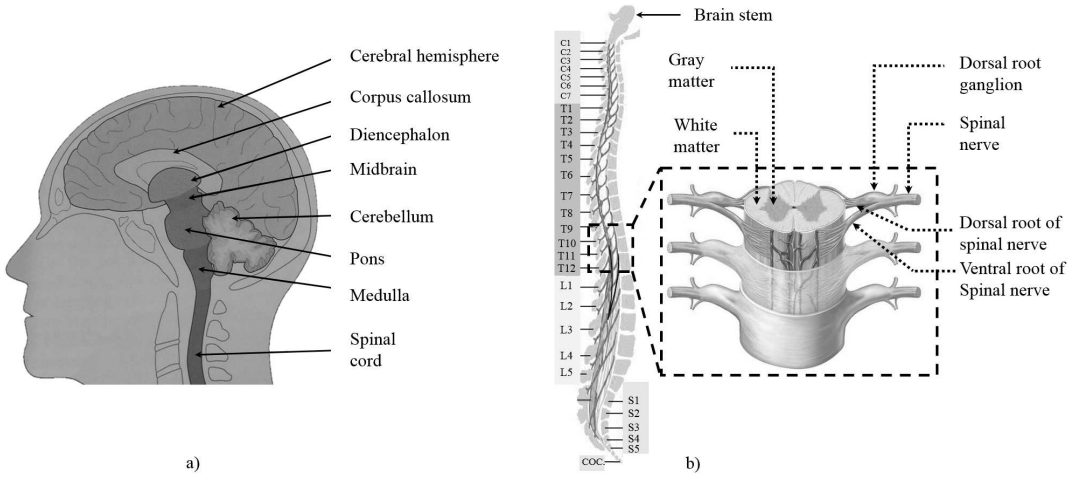

Figure 2.4: The main structures of the CNS which are mainly brain and spinal cord shown in this figure, adapted from [25], [28] with changes, a) shows parts of human brain in general, b) shows the structure of spinal cord.

Spinal cord

The spinal cord is adjoining and structurally continuous with the brain stem which is a cylindrical structure of nervous tissue composed of white and gray matter. It consists of bundles of nerve fibres that receives and processes sensory information from the skin, joints, and muscles and controls their movement. There are 31 segments which can be defined 31 pairs of nerves exiting the cord. These are divided into 8 cervical (C), 12 thoracic (T), 5 lumbar (L) and 5 sacral (S), and 1 coccygeal nerve, as shown in Figure 2.4b.

A cross section of the adult spinal cord shows white matter in the periphery and gray matter inside. The white matter containing myelinated and unmyelinated nerve fibers. These fibers conduct information up (ascending) or down (descending) the cord. The gray matter is subdivided into dorsal and ventral horns. The dorsal horn conveys the sensory information while the ventral horn conveys the motor signalling. The interneuron in the gray matter modulate information flowing from the sensory neurons towards the CNS and information from the CNS to the motor neurons. The cell bodies of sensory neurons are clustered together in

the dorsal root ganglion.

The dorsal horn of the spinal cord may be allocated into six distinct layers (laminae). The nociceptive neurons (will be detailed in the pain mechanism section) are located in the marginal layer (laminae I) and substantia gelatinase (laminae II) layers of dorsal horn. The substantia gelatinase layer mostly consists of interneurons which are both excitatory and inhibitory. Thus, some of neurons in this layer respond to pain stimulation while others respond to non-pain stimulation. Laminae III and IV layers contain neurons which respond to non-pain stimuli. Lastly, laminae V primarily consists of wide dynamic range neurons that project to the high level of brain parts. The distributions of these layers are presented in Figure 2.9b [27], [28].

2.3.3 Peripheral nervous system

The PNS is connected to the CNS with nerves that are present within the various tissues of the body. These nerves are spinal nerve and cranial nerves; the spinal nerves transmit impulses to and from the spinal cord and cranial nerves are responsible for conveying neural impulses to and from the brain. These nerves connect all parts of the body by transmitting impulses from the sensory receptors to the CNS and from the CNS to glands or muscles. The PNS may be classified into the somatic nervous system and autonomic nervous system. The somatic system is responsible for gathering sensory information from the receptors present in periphery and for sending out motor signals, such as controlling our skeleton muscle. In contrast, the autonomic nervous system principally includes motor nerves which carry out non-voluntary processes. The autonomic nervous system may be further divided into the sympathetic and parasympathetic nervous systems. The sympathetic are primarily responsible for the responses that may be associated with fighting or fleeing, such as increasing heart rate and blood pressure. However, the parasympathetic nervous system responses are related to resting and digesting [28], [30].

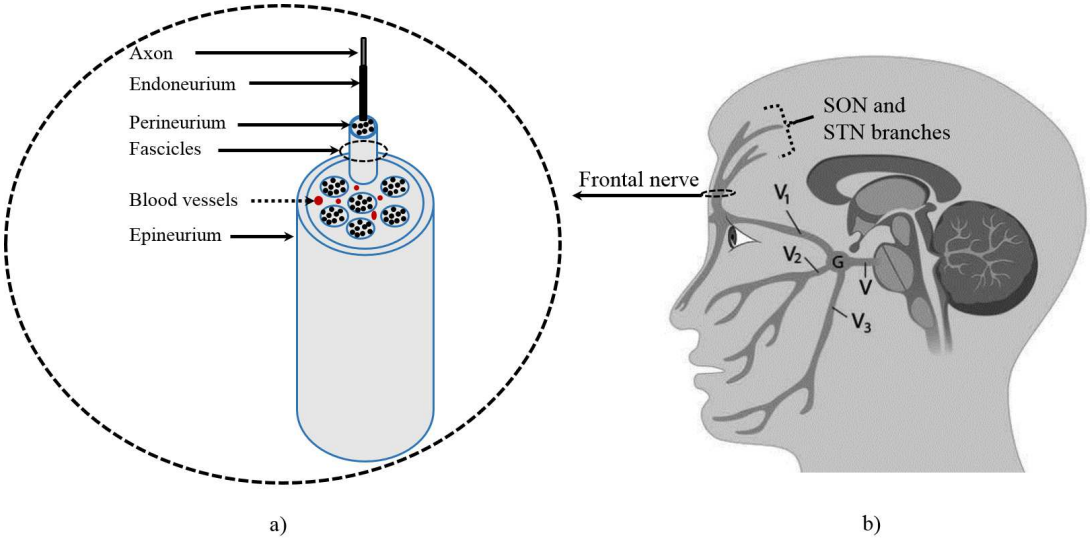

Figure 2.5: Nerve anatomy and trigeminal nerve distribution, a) shows general structure of a nerve, b) shows the distributions of the trigeminal nerve and its branches. Frontal nerve is sub-branched as SON and STN. The trigeminal ganglion is represented with 'G'.

Nerve

A nerve is composed of a bundle of neuron fibres outside of the CNS. Each fibre is wrapped in a delicate endoneurium connective tissue sheath. A group of fibres that are surrounded by perineurium connective tissue is referred to as a fascicle. These fascicles are covered by the epineurium tough fibrous sheath [25]. A nerve and constituent tissues are depicted in Figure 2.5a. Since a solution for migraine is to stimulate branches of the trigeminal nerve, it is necessary to outline the trigeminal nerve and its branches in this study. The trigeminal nerve is the largest cranial nerve and also known as the fifth cranial (V) nerve. It is extensively distributed in the head and neck and has both sensory and motor components. It is composed of three branches which are ophthalmic (V1), maxillary (V2), and mandibular (V3), as their distribution is shown in Figure 2.5b. The ophthalmic and maxillary branches are supplying sensory innervation, while mandibular is supplying both motor and sensory sensations [31]. The frontal nerve passes below the frontal bone, exits from the orbital rim and penetrates the corrugator and

frontalis muscles. It is divided into the supraorbital (SON) and supratrochlear (STN) nerves. These branches have multiple sub branches, supplying sensory sensation to upper the eyelid, forehead and the scalp [23], [25].

The common complaint of migraine sufferers is generally the symptoms of pain originating in the frontal region of the head [32]. This may be because of the fact that migraine is primarily related to SON and STN. Thus, in this situation a solution targeting this nerve is of interest.

2.3.4 Action potential(AP)

As discussed in the overview of the human nervous system and its bioelectrical phenomena, the AP is the most fundamental event in the nervous system. The underlying principles of the AP is detailed here. It is an electrical signal that is generated in the neuron via ionic exchanges. These ionic exchanges occur when there is a concentration difference between inside and outside of the neuron that results in a potential across the membrane, called transmembrane potential (V_m). Naturally, the activation in the form of AP is first seen in the axon hillock and travel along the neuron. The nerve cell is able to carry this signal over long distances with different velocities ranging from 1 to 100 m/s depending on the fibre type and size [27]. Importantly, the AP generation is an all-or-none process, meaning that if the excitatory stimulus that pushes the V_m to reach the threshold is strong enough, the AP will be generated. However, if the triggered V_m is not exceeding the threshold, then the AP will not be generated. The underlying dynamics of the AP propagation are discussed further in this chapter. Importantly, to generate AP, a series of electrical impulses occur near the cell portion of the neuron. This electrical signal moves across the neural membrane in much the same way as the electrical signal does in an electronic device.

There are three main phases in an AP. When the nerve cell is stimulated by the excitatory or inhibitory stimulus, the V_m changes. If the excitatory stimulation is applied, there is an increase of V_m and becomes more positive than the resting

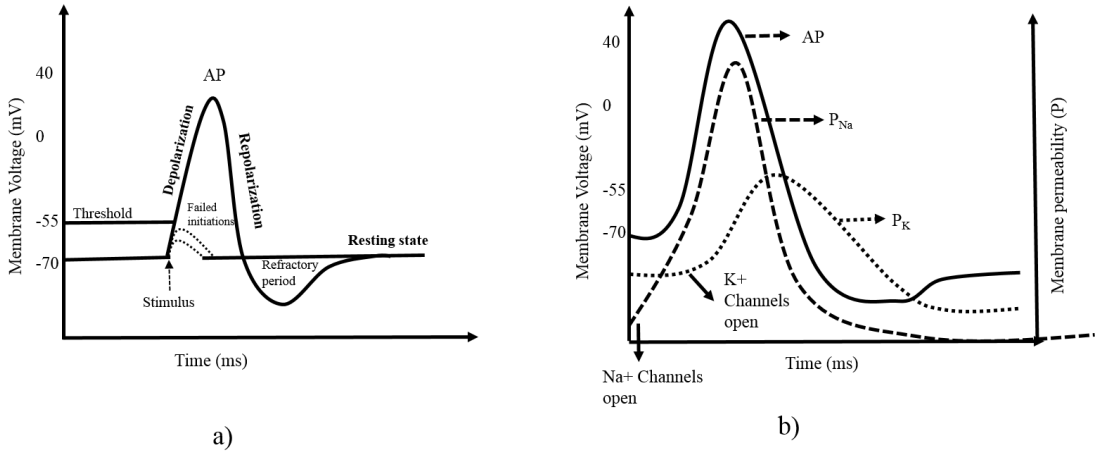

Figure 2.6: AP phases and ion channels permeability, a) shows an AP phases during stimulation, b) shows ion channels permeability changes for Na^+ and K^+ during an AP. Figures adapted from [30] with changes.

potential and exceeds the threshold potential. This phase is called depolarisation period. The following reduction in the V_m after depolarisation phase is called repolarisation phase. If the inhibitory stimulation is applied, the V_m reduced below resting potential. This phase of AP is called hyperpolarization. After this phase, the membrane reaches the resting state. The variations of these phases are depicted in Figure 2.6a [27], [33].

AP generation

The AP is generally generated and propagated by voltage–gated ion channels. These channels allow ions to pass through the membrane which is ion specific, meaning that when they are open they allow only one ion type to pass through the membrane and prevents all other ions from crossing the membrane through that channel. They are either passive or active. Passive channels, which are always open, exist for Na^+, K^+ and Cl^-. The active channels (Na^+, K^+), or gates, are either opened or closed depending on an external electrical or chemical stimulation. To understand the regulation of the movement of these ions between the extracellular and intracellular spaces, the Nernst formulation is explored in

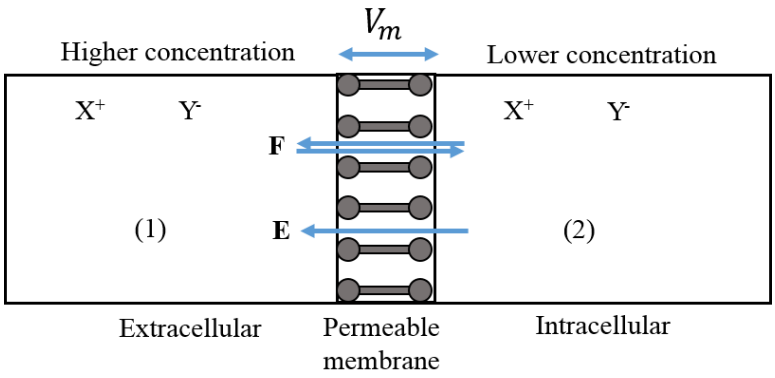

Figure 2.7: Concentration of membrane. X and Y show the different ions, F are electrostatic forces which cause charges to reside on the membrane, the electric field is represented with E, V_m is electrical potential difference across the permeable membrane.

more details here. Due to the fact that the ion composition inside the cell differs from the outside of the cell, a concentration gradient exists for all permeable ions that contribute to the net ion movement or flux. These ions flow based on the principle of the diffusion; meaning ion flows from the high concentration region of the membrane to the low concentration region. Based on the movement of the ions, an electrical field (E) is established in the direction of the gradient within the membrane. This field applies forces on the ions to cause them to cross the membrane (to the electric field be equal and opposite to the force due to diffusion). This results in a difference of V_m across the membrane, as shown in Figure 2.7. The diffusional force balances and the electric field force reach the equilibrium when there is no net ion flow. These opposing forces, transmembrane electrical potential, equilibrium voltage and ions concentration ratio is calculated by the Nernst equation as shown in Equation 2.1.

$$V_m = (\frac{RT}{zF}) \ln(\frac{[X]_{out}}{[X]_{in}}) \tag{2.1}$$

Where V_m the equilibrium potential, R is is the gas constant, T is the temperature (in degrees Kelvin), z is the valence of the ion, F is the Faraday constant, $[X]_{out}$ and $[X]_{in}$ are the concentrations of the ion outside and inside the cell, re-

spectively. The Goldman-Hodgkin-Katz equation (GHK), as shown in Equation 2.2, is used to calculate the transmembrane voltage when there are several types of ions in the intracellular and extracellular media, and when the membrane is permeable to all of them. The GHK equation is a straightforward extension of the Nernst equation.

$$V_m = (\frac{RT}{zF}) \ln(\frac{P_K[K^+]_o + P_{Na}[Na^+]_o + P_{CI}[CI^-]_i}{P_K[K^+]_i + P_{Na}[Na^+]_i + P_{CI}[CI^-]_o}) \tag{2.2}$$

Where, P is the permeability of the membrane to a given ionic species which is referred to the ease of which ion crosses the membrane. The permeabilities are governed by the voltage-gated channels. It is assumed that when several permeable ions are present, the flux of each is independent of the others. This is called independence principle, formulated by Hodgkin and Huxley (HH) [33]. The current existing systematic understanding of the channel mechanisms is based on this principle. These channels have gates that depending on the voltage across them the rate at which they open or close is various. For a channel to conduct, all its gates should be open.

According to HH, depolarisation of the membrane leads to Na^+ channels to open rapidly which means membrane becomes temporarily permeable to Na^+, thereby inward current is increased. Accordingly, the membrane depolarisation potential approaches V_{Na} that provides a rising phase of the action potential, as compared in Figure 2.6a.

On the other side, inactivation of the Na^+ permeability and activation of the K^+ permeability causes an increase of the permeability of the K^+, resulting in increasing g_K (potassium conductance). Consequently, these ions diffuse from inside of the neuron to outside and membrane potential is transiently hyperpolarised (repolarisation). The HH model of the channel dynamics is presented in detail in Chapter 3.

In general, the AP is followed by hyperpolarisation in most of the nerve cell.

However, as can be seen from the Figure 2.6b, there is a transient shift in the membrane potential which is more negative than resting potential. This is because of the K^+ channels remain open for some time after the membrane potential has reached its resting potential. The refractory period can be determined as some K^+ channels begin to close and some Na^+channels reactivated. It may generate an action potential at the refractory period but only applying by stimuli which generate higher level potentials than normal threshold level [27], [28], [33].

AP propagation

AP propagates in a different way for both unmyelinated and myelinated fibre as demonstrated in Figure 2.8b and Figure 2.8c, respectively. Apart from a little transmembrane current, most of the transmembrane currents are confined to the nodes. Thus, a myelinated fibre can only produce AP at the nodes of Ranvier due to the high insulation of the myelin sheath. Thereby, the AP propagates from one axon to the other. This gap allows the current to flow passively within the myelinated segment until the next node reached. This current flow then generates AP at the vicinity of the segment, and this cycle is reoccured along the length of the axon [28]. In the unmyelinated fibre, there is a continuous conduction of AP along the axon however, the current flows along the fibre to induce an increase in the transmembrane potential in the vicinity of the depolarised segment. [27], [33]. It is essential to understand the underlying neural mechanisms and stimulus features to predict the dynamics of the generation of APs. These properties are detailed in Chapter 3. After detailed the fundamentals of the AP generation and propagation, the impact of the fibres size on these features is examined in the following section.

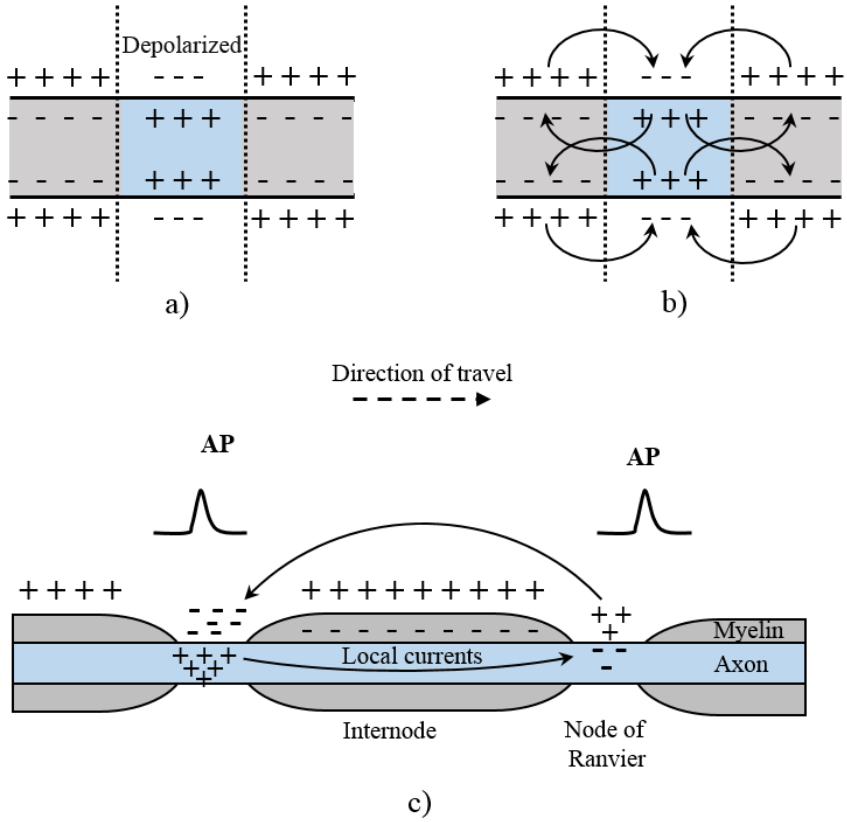

Figure 2.8: Generation and propagation of APs in both myelinated and unmyelinated fibres. The figure adapted from [34] with modifications, a) shows the pattern of ion movement during extracellular stimulation in unmyelinated fibre, b) shows how AP is propagating in unmyelinated fibre, c) shows propagation of an AP pattern in a myelinated fibre.

Effect of fibre features on AP

Myelination and the diameter of nerve fibres are vital for determining the conduction velocity of APs. There is a linear relationship between the conduction velocity and both the thickness of myelin and the fibre diameter. Meaning that the conduction velocity is higher for the fibres which have a larger diameter and thicker myelin sheath. The required amount of charge to achieve a certain potential is determined by the capacitance of the membrane per unit length. The small capacitance values, with other parameters remaining the same, mean a faster conduction velocity. The resistivity of the medium inside and outside also has a role in the velocity of conduction which affects depolarisation time constant. The meaning that, the smaller the resistance and the smaller time constant resulting

Table 2.2: Erlanger's fibre classification (in mammalian).

Type	**Diameter**(μm)	**Conduction velocity**(m/s)	**myelination**
$A\alpha$	12–22	70–120	thick myelinated
$A\beta$	5–12	30–70	thick myelinated
$A\gamma$	2–8	15–30	myelinated
$A\delta$	1–5	5–30	thin myelinated
B	<3	3–15	myelinated
C	0.1–1.3	0.6–2	unmyelinated

in faster conduction velocity. The velocity propagation of APs in unmyelinated fibre can be expressed by Equation 2.3. The velocity propagation of APs in myelinated fibres may be correlated with the fibre diameter (d) and can be expressed by Equation 2.4.

Additionally, it was experimentally proved that the threshold of the excitation fibres is lowest in the largest fibres. In general, the conduction velocity and electrical excitation can be correlated in myelinated fibres however, there is no such correlation within the unmyelinated fibre population. The electrical stimuli excite not only the most rapidly conducting unmyelinated fibres but also those belonging to the more slowly conducting subgroups at the threshold.

Also, absolute refractory period is longer in a smaller size, which may result in the lower conduction of APs signals during propagation [33], [35].

$$\theta = \sqrt{\frac{i_{Na}}{r_i c_m^2 V_{th}}} \tag{2.3}$$

where θ is velocity of the nerve impulse (m/s), i_{Na} is maximum sodium current per unit length (A/m), V_{th} is threshold voltage (V), r_i is axial resistance per unit length (Ω/m) and c_m is the membrane capacitance per unit length (F/m).

$$\theta = 6d \tag{2.4}$$

Table 2.3: Llyods's fibre classification (in mammalian).

Type	**Diameter**(μm)	**Conduction velocity**(m/s)	**myelination**
I	12–20	70–120	thick myelinated
II	6–12	30–70	thick myelinated
III	3–4	<30	myelinated
IV	1–5	2.5	unmyelinated

There are two main studies which have been proposed for a classification of fibres based on the diameter and conduction velocity. The first classification scheme was devised by Erlanger and Gasser who divided peripheral nerve fibres in three (A, B, C) main groups based on the nature of the conducted potential in various nerves. They further subdivided group A into $\alpha, \beta, \gamma, \delta$ fibres. It is proposed that motor nerves are composed of the $A\alpha, A\beta, A\gamma, A\delta$ and pure sensory nerves are composed of the $A\beta, A\delta$ and C fibres in mammalians. It is worthy to have a precise border between the different fibres, Beside this classification, Lloyd introduced a terminology of afferent in both muscle and cutaneous nerves. $A\alpha, A\beta$ have thicker myelination sheath thereby they have highest conduction velocity. However, $A\delta$ is composed of thick mylenation and C fibres are unmyelinated fibres. He classified nerve fibres based on fibre size. In his system, the myelinated afferent fibres were allocated into three broad groups with different ranges of the diameters which he named I, II and III, respectively. The unmyelinated fibres were referred as IV. The fibers are classified based on aforementioned features and two approaches, shown in Table 2.2 and 2.3 [35], [36].

So far the fundamentals of the human nervous system and human head anatomy were generally reviewed. The neurophysiology and underlying neural circuits of the primary headache disorders, mainly migraine and pain, related to the target application of this thesis, is elaborated in the following section.

2.4 Pain mechanism and primary headache

The causes of the headache range from short–lived and trivial (e.g., hangover headache) to the intermittent and quality of life–threatening (e.g., migraine). The diversity of causes and high prevalence in the general population mandate a diagnostic categorisation system to provide the framework for a clinical approach. Based on those diagnostic rules, the headache can be grouped as a secondary and primary headache. Former disorders have an identifiable underlying cause, such as an infection, brain tumour, or stroke. The latter disorders have no apparent underlying causes. The primary headache disorders may be grouped as migraine, cluster headache and tension-type headache which are most common diseases and leading causes of disability worldwide. To better understand the mechanism of the headache disorder, the pain and underlying mechanism is discussed first. Then, different types of a primary headache with their explanation are detailed. After explaining a cluster headache (CH) and tension-type headache (TTH), migraine is explored in detail. The relationship between general pain mechanism and migraine is elaborated. Furthermore, the available neural circuitry theories about migraine are discussed and the solution which based on well–accepted theory is targeted in this thesis.

2.4.1 Pain mechanism

Pain can be described as an unpleasant sensation or conscious experience that arises from the consequence of an inflammatory response with substantial tissue injury, or damage to the nervous system [37], [38]. This disorder can consequently have an impact on an individuals physical and mental well being. An individual that suffers from pain would be affected in numerous ways where their daily responsibilities (such as work) would become unmanageable and social life would be disturbed due to significant ensuing psychological problems like anger, depression, hence causing the inability of adaptation [39]. The pain is mediated from

PNS to CNS by certain tissues those have specialised sensory receptors which are called nociceptors. These neural mechanisms are called nociception. The perfection of pain is subjective and depends on many factors which mean an identical sensory stimulus can elicit different results in the same subject under different conditions.

Pain has been categorised in a variety of different ways and one of the most important divisions are the nociceptive and neuropathic pain. The nociceptive pains result from the direct activation of nociceptors in the skin or soft tissue to actual tissue damage or potentially tissue-damaging stimuli. When activated, they transmit pain signals (via the peripheral nerves as well as the spinal cord) to the brain. Neuropathic pain is the result of an injury or malfunction in the PNS or CNS. The pain is often triggered by an injury, but this injury may or may not involve actual damage to the nervous system. Many different conditions and diseases cause neuropathic pain, such as diabetes, stroke, cancer. It is different from nociceptive pain because it does not develop in response to any specific circumstance or outside stimulus.

The noxious stimuli to the cutaneous or subcutaneous may activate several groups of nociceptors. These primary sensory nerves have afferent nerve endings with cell bodies and are located in the dorsal root ganglia and trigeminal ganglia. They have a small diameter, thinly myelinated $A\delta$ and unmyelinated C fibres. The role of these fibres is to transmit pain stimuli from PNS to CNS. Conversely, there are non-noxious nociceptors, meaning they are not activated by noxious stimuli. These may consist of $A\beta$ fibres which are highly myelinated and have large diameters. These fibres may suppress or block the transmission of nociceptive input from $A\delta$ and C fibres based on the gate theory. These primary fibres specifications and their AP versus time are illustrated in Table 2.4 and Figure 9a, respectively. The underlying principle of pain pathway mechanisms and gate theory will be elaborated in here.

Nociceptive afferent fibres are mostly located in the dorsal horn of the spinal

Table 2.4: Features of primary afferent fibres.

Type	Carried information	Activation threshold
$A\beta$	Light touch, non-noxious	High
$A\delta$	Rapid, sharp(first pain), localised pain	High and low
C	Slow, diffuse, dull Pain(second pain)	Low

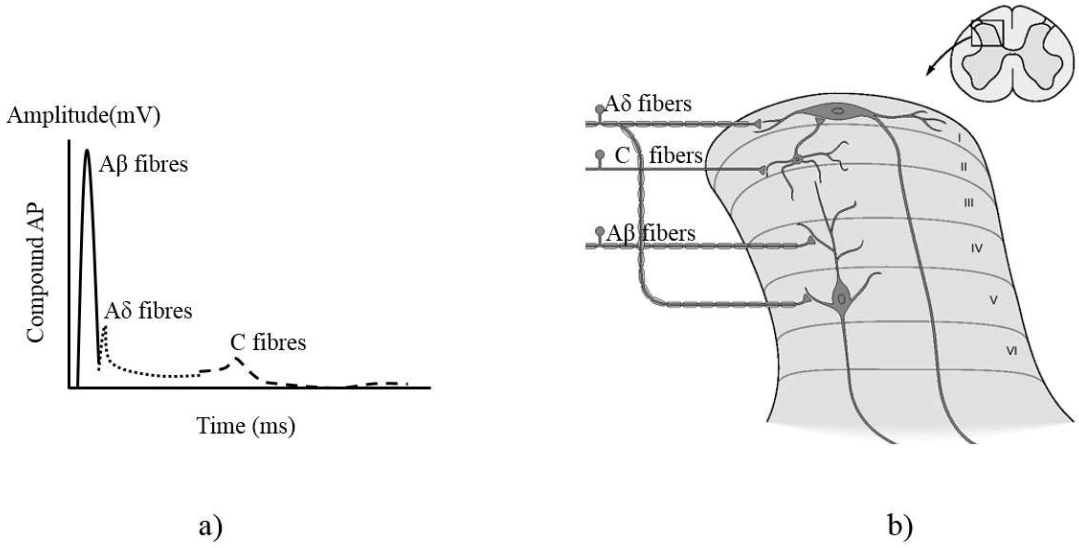

Figure 2.9: The compound action potential of a mammalian cutaneous nerve fibers and their location in spinal cord, a) shows nociceptive and non- nociceptive fibres with their velocity, redrawn figure was adapted from [35], b) shows distributions of these fibers in dorsal horn of spinal cord which adapted from [27].

cord, as shown in Figure 2.9b. The nociceptive neurons are located in the laminae I and laminae II layers of dorsal horn. Most of these neurons in the lamina I are nociceptive specific. However, some neurons, called wide dynamic range neuron, in this layer respond to both non-noxious and noxious stimulation. The lamina II layer mostly consists of interneurons which are both excitatory and inhibitory. Thus, some of the neurons in this layer respond to noxious stimulation while others respond to non-noxious stimulation. Laminae III and IV layers contain neurons which respond to non-noxious stimuli and receive information from $A\beta$ fibres. Lastly, laminae V primarily consists of wide dynamic range neurons that project to the high level of brain. The stimuli signal is conveyed from $A\beta$ and

$A\delta$ fibers to this layer [27]. The synaptic transmission between nociceptors and dorsal horn neuron is mediated by chemical neurotransmitters. During peripheral sensitisation of the pain, nociceptors release peptides and neurotransmitters, such as glutamate, substance P, calcitonin gene–related peptide (CGRP), and ATP, in the vicinity of the synaptic terminal to help pain transmission from presynaptic cell to postsynaptic cell. In addition to that, some non-neuronal cells are released in the vicinity of injury to interact directly with receptors or ion channels of nociceptive fibres to augment their response. For example, the prostaglandins decrease the threshold for activation of nociceptors.

The pain may be controlled by brain modulation circuits function of which is to regulate the perception of pain. Owing to the fact that there is an interconnection between nociceptive and non-nociceptive afferent fibre in the spinal cord, the afferent pain transmission pathways from the spinal cord to high centres in the brain may be controlled. The pain pathway from the peripheral side to the high centre of the brain is shown in Figure 2.10a. Although the nociceptive afferent fibres are involved the transmission of nociceptive information, pain results from the balance of activity in nociceptive and non-nociceptive afferents. The association between these two afferent neuron groups was formulated in the 1960s by Ronald Melzack and Patrick Wall that is called gate control theory [8]. The concept of this theory has emphasized the importance of synaptic interactions in the spinal cord for modulating the perceived pain of intensity. The underlying principle of the theory is discussed here and the mechanism of gate theory is shown in Figure 2.10b. Neurons in the laminae V, and possibly laminae I receive a neural signal from both non-nociceptive $A\beta$ fibres and nociceptive $A\delta$ and C fibres. The large diameter $A\beta$ fibres inhibit the firing of neurons which are located in laminae V by activating inhibitory interneuron in laminae II. The $A\delta$ and C fibres can activate neurons in laminae V and they can inhibit the firing inhibitory interneuron in laminae II which are activated by non-nociceptive fibres. The function of non-nociceptive afferents system is to close and nociceptive afferents function is

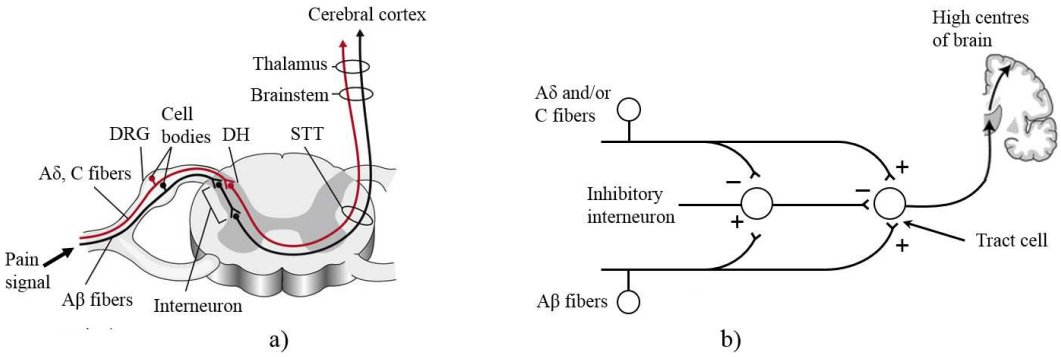

Figure 2.10: Pain mechanism, a) shows ascending neural pathway of pain, DRG, DH, and STT represent dorsal root ganglion, dorsal horn, and spinothalamic tract, respectively, b) shows gate control of pain mechanism [40], [41].

open a gate to the central transmission of pain signal input. The gate control theory may be an appropriate control mechanism for the use of transcutaneous electrical nerve stimulation to relieve the pain. In this technique, the current is applied through the skin via surface electrodes to activate large diameter fibres that overlap the area of injury and pain [8], [27].

Although the gate control theory is used for migraine pain, the migraine pain pathway is not fully understood yet [40]. After elaborating on pain and its pathway, the primary headache disorders and other postulated neural theories about migraine and their pathways with underlying circuits are discussed in detail in the following section.

2.4.2 Tension-type headache(TTH)

Although research on TTH is limited compared to migraine, it is the most common among all age groups over the world (ranging between 30% and 78% in different studies) and has the greatest socioeconomic impact of any primary headache type. It has recurrent episodes of a headache lasting from 30 minutes to 7 days. The pain occurs bilateral in location, and generally does not have any effect on an individual's routine physical activity. The pain of TTH may be identified as dull, pressure like constricting or giving a sense of fullness in the head. Up to now, the

exact cause and neural mechanisms of the TTH remain elusive. It may also be characterised by nausea and vomiting and photophobia or phonophobia may also be present. The best criteria to distinguish the TTH from migraine is associated with features that are commonly seen in migraine typically absent or minimal, including nausea, vomiting, photophobia, and phonophobia. It is generally divided into either episodic or chronic. Although the episodic can be managed with medical treatment, the chronic form has serious effect on the quality of life of the individual [2].

2.4.3 Cluster headache (CH)

The CH is a worldwide disorder with a prevalence of about 1% in the general population [42]. It is more painful than other types of headache. The pain is severe and mostly one sided. Due to the intensity of the pain, patients are usually unable to lie down and characteristically pace the floor. During the cluster period, the pain usually recurs on the same side of the head. The location of the pain is orbital, supraorbital, temporal or in any combination of these sites. The pain lasts for a short time; generally,15-180 minutes and occurring from once every other day to eight times a day. The CH may be associated with one or more of the following symptoms: conjunctival injection, lacrimation, nasal congestion, forehead and facial sweating, miosis, ptosis and/or eyelid oedema, and/or with restlessness or agitation. One of the discriminate points of the CH is its periodicity. It was reported that attacks occur repeatedly at a different time of the day or evening, particularly at night. Although the cluster headaches are not associated with symptoms of migraine, it is possible for someone with cluster headaches to also have migraines. The treatment of the CH is usually based on drug therapy. Decompression of the trigeminal nerve, alone or in a combination with microvascular decompression, decreased the pain (50% relief or greater) [43]. However, this method may lead to surgical risks including death, permanent neurological deficits, corneal anaesthesia and visual loss [2], [43]. Although the

prevalence CH is less than TTH, it is a serious disorder and affects an individual's life both economically and socially. It is the fact that there is room to improve the methods of low risks techniques(e.g., non-invasive neuromodulation) to help individuals tormented by CH. The existing invasive options are not effective due to having irreversible complications and side effects [44].

2.4.4 Migraine

Migraine is a common neurological disorder with substantial personal, societal, and economic consequences. Its associated symptoms are throbbing headache, nausea and/or vomiting, photophobia and phonophobia [2]. It is the third most common neurological disorder and the seventh cause of disability which affects an estimated one in six of the population. The most common type of a headache is firstly TTH, and then migraine in the general population. It is the leading causes of suffering and disability at the national and global level. Migraine prevalence varies between 2.6% to 21.7% with variation between countries and between studies [4]. It is common amongst the European population which is estimated at about 15% in adults [45]. Its impact in American society remained stable over many years that affects almost 20% of population [46]. The prevalence of migraine across different continents are displayed with bars for both males and females in Figure 2.11. It may be seen in the productive life of an individual and can affect the ability to work or carry out activities during daily living. During migraine attacks, only 25% of patients can function without help from others, rest of the patients need help to do their daily activity which results in a loss of 20 million working days a year [2], [4], [47].

There are two main types of migraine; migraine with aura and migraine without aura. However, these two types are not mutually exclusive because people who have migraine with aura also may have migraine without aura. Migraine with aura is also referred to as a classic migraine, they have recurrent attacks; lasting minutes which may be characterised by visual symptoms (spots of light, zigzag

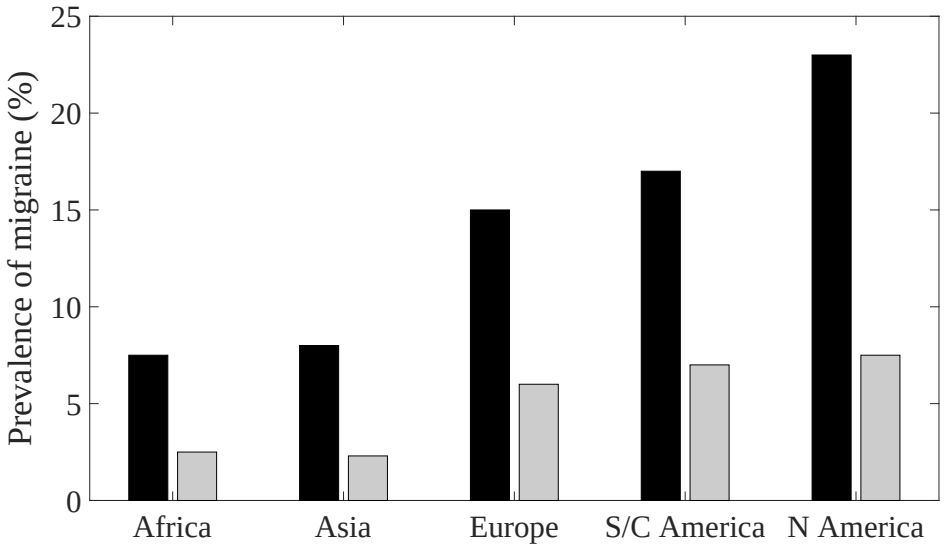

Figure 2.11: The prevalence of migraine across different geographic area and sex, N = North; S/C = South/Central. The prevalence of migraine among female and male were represented with black and gray bars, respectively. The data in the figure was obtained from [48].

lines, or greying out of vision), sensory symptoms (tingling and numbness), or language disturbances. Whereas, migraine without aura is recurrent headache disorder manifesting in attacks lasting 4-72 hours. This may be characterised by pulsating quality, moderate or severe intensity, aggravation by routine physical activity and association with nausea and/or photophobia and phonophobia [2]. In terms of headache duration; migraine may be divided into an episodic migraine (EM) and chronic migraine (CM). The EM headaches occur on less than 15 days per month, while, CM headache is described by occurring on 15 or more days per month for more than three months, with the condition that the headache should have the features of migraine for at least eight days per month [2].

2.4.5 Migraine pathophysiology theories and neural circuit pathways

Understanding the pathophysiology of migraine is an important first step to discover the optimal treatment option for this condition. There is an increase in interest around migraine pathophysiology which may allow researchers to discover neurophysiological mechanisms and neurotransmitter involvement culminating in the recent development of novel therapies. This might substantially change the clinical approach to migraine patients. Although the pathophysiology of migraine is not fully understood yet, it can be deduced much from what is known of the pathophysiology and its treatment [32]. One of the theories about the pathophysiology of migraine is a vascular theory. It is claimed that migraine aura is due to an abnormally low concentration of oxygen in the blood which results in an increase in blood pressure (vasoconstriction) and that a headache is the result of rebound vasodilation. In other words, vascular changes do not directly have an impact on the neural theory of migraine, yet the consequences of the vascular changes cause a headache. However, as stated in the review study [49], several experimental and clinical studies have been indicated that the reduced blood flow was still present when the headache of migraine with aura had started. Therefore, the original vascular theory of migraine is untenable for most patients [49], [50]. The alternative and widely accepted theory suggestion is that the headache of migraine attack originates from the inactivation and sensitization of trigeminal sensory afferents. This activation innervates innervating pial, arachnoid and dural blood vessels, as well as large cerebral arteries and sinuses. This theory may be validated by electrical, mechanical, and chemical stimulation. When these anatomical structures are stimulated, the headaches were risen up and were remarkably similar to the pain of migraine; moreover its most common associated symptoms were observed as discussed in the review paper [49]. The nociceptive innervation of the mentioned tissues consist of C fibres and $A\delta$ fibres axons sur-

rounding blood vessels of the pia and dura mater can release vasoactive peptides producing a sterile inflammatory reaction. Neurons in the trigeminal ganglion contain calcitonin gene-related peptide (CGRP) or substance P. The stimulation of the trigeminal ganglion induces the release of these neurotransmitters (The cells in the trigeminal ganglion possess peripheral and central processes) to reach the dura mater mainly through the ophthalmic branch of the trigeminal nerve [51]. Its activation is thought to lead to the cascade of events resulting in the migraine pain due to its direct connection with key brain centres such as diencephalic and brainstem nuclei.

Furthermore, there is evidence showing antimigraine drugs such as triptans ergot derivatives and the novel CGRP receptor antagonists can specifically modulate activity in the trigeminal nucleus caudalis (TNC), which might explain their effect in aborting migraine. Thus, it can be deduced that migraine headache is chiefly related with the ophthalmic nerve and its sub–branches such as supraorbital and supratrochlear nerves which result in head pain in migraine is often localized in the fronto-orbital or cervico–occipital region [32], [50].

The assumed migraine pathway mechanism for a targeted solution is illustrated in Figure 2.12. The head pain is carried from PNS to CNS by the trigeminal system (rather than a single nerve pathway, the term trigeminal system refers to a complex arrangement of nerve transmission fibres, interneurons, and synaptic connections). The sensory information from the peripheral process is conveyed to the trigeminal ganglion through the ophthalmic division by afferent neurons. Once the signal is received by the first–order neurons in the trigeminal ganglion, the myelinated and unmyelinated trigeminal fibres descend from pons through caudal medulla as a form of the spinal trigeminal tract (or can also be called spinal tract of trigeminal nerve) and terminate in TNC which distribution of headache pain to regions of the upper neck and head can be attributed to the convergence of projections from the trigeminal nerve at the TNC. The pain signal is transmitted from TNC by second–order neurons (which they have both

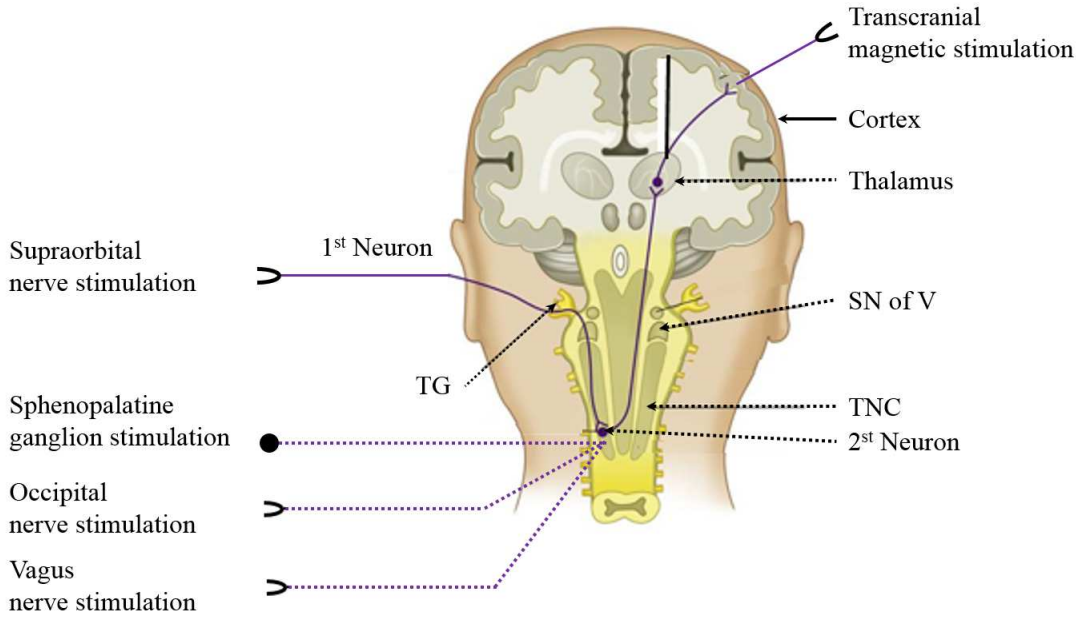

Figure 2.12: Migraine pain pathways targeted by different neurostimulation techniques. A simplified diagram of the various peripheral and central pain pathways which are targeted by current neurostimulation devices. The head figure was adapted from [52] with modifications. TNC: trigeminal nucleus caudalis; TG: Trigeminal ganglion; SN: sensory nerve, 1st and 2nd represent first and second nerve fibers, respectively.

nociceptive and non-nociceptive fibres and) to trigeminal thalamic tract. Then, the axon fibres convey data over the trigeminothalamic tract through ventral posteromedial of the thalamus. Following the previous process, the pain signal is relayed from the thalamus to the higher centre of the brain such as primary somatosensory cortex.

With respect to anatomical convergence and influence of the pain–matrix on the activity of second-order sensory transmission neurons within the TNC, gate control theory suggests that there is an inverse relationship between activity in small-diameter nociceptive afferents and large-diameter nerve fibres. Meaning that stimulation of large-diameter fibres leads to suppression of small diameter fibre nociceptive input and elevation of pain thresholds. The activation of $A\beta$ fibres in the TNC may inhibit the nociceptive fibres signals, thus the migraine pain signal may be blocked or suppressed to reach the second order of neuron

through the trigeminal spinal nucleus. Therefore, the pain signal may not reach the high centres of brain.

The available neuromodulation techniques use the different mechanism of migraine, as summarised in Figure 2.12. Although these techniques convergence in the TNC, one of the main reasons for choosing the frontal nerve as a target of this study is that all fibres are sensory. On the other hand, the vagus nerve consists of both motor and sensory types which lead to complexity during the stimulation process. After discussing on migraine headache mechanism, existing treatment methods will be detailed in the next section.

2.5 Existing treatment methods

This section describes the existing solutions for migraine headache suppression. Migraine may be managed by acute and preventative treatments. The acute treatments may be interrupted an attack and restore normal function, while preventive treatments may be reduced frequency of attacks and its severity [7]. Although there are many new therapeutic solutions and novel approaches for acute and preventative migraine treatment, the efficacy of these existing approaches has not achieved the expected level. In general, these solutions may be categorised as pharmaceutical, surgical and neuromodulation techniques. Using drugs to treat migraine attacks have been especially disappointing, as they have a limited efficacy (on average 50%) and the most effective drugs often induce intolerable side effects [53]. Whereas due to the associated risks of the surgical treatments, this method is not desired. Although some neuromodulation techniques have given some positive results, most of them had small numbers of participants. Therefore they are underpowered and do not provide long-term outcome data [53]. After an overview of all types of the possible solutions, the target solution and the assumed reasons which lead to the inconclusive response of this neuromodulation procedures, that are objective of this thesis, will be detailed.

2.5.1 Pharmaceutical therapy

The most commonly used drugs to prevent migraine attacks are analgesics, non-steroidal anti-inflammatory drugs (NSAIDs), and specific anti-migraine drugs such as ergots and triptans. For the mild to moderate attacks, analgesics are generally the first choice. Although ergots have been used with some success for many years, they may induce severe side effects. Thus, triptans are preferred instead due to having fewer side effects. It is believed that they exert their effects via serotonin (5-hydroxytryptamine, or 5-HT) receptors. This receptor can be found throughout the peripheral and central trigeminovascular system and they are an agonist for an acute migraine. The calcitonin gene-related peptide (CGRP) is a pain signalling neuropeptide that is released from trigeminal sensory afferents and the spinal trigeminal nucleus. It is one of the validated therapeutic targets for migraine which increase the levels of the peptide in blood and saliva during migraine attacks. It was shown that CGRP receptor antagonists can specifically modulate activity in the TNC, which might explain their effect in aborting migraine. It was shown that triptans and ergot derivatives and CGRP receptor antagonists can modulate activity in TNC that might prove their effect in aborting migraine [50], [53]. Effective preventive drugs include beta-blockers (e.g., metoprolol, propranolol, bisoprolol, candesartan), calcium channel blockers (such as flunarizine or verapamil), and the anticonvulsants topiramate and valproate. Majority of these migraine preventive drugs have contraindications and are associated with moderate to severe intolerable effects such as sleepiness, exercise intolerance, impotence, nightmares, dry mouth, weight gain, tremor, hair loss, or fetal deformities [54].

The available treatment drugs for attacks may be further classified into nonspecific (e.g., aspirin, non-steroidal anti-inflammatory drugs (NSAIDs), etc.) and migraine–specific (e.g., ergotamine, dihydroergotamine, and the triptans). The former is used to treat a wide range of pain disorders. The latter is effective

for treating neurovascular headaches including migraine. The high doses of prescribed nonspecific drugs may cause more bothersome attacks and may even lead to addiction. Also, due to their pharmacological complexity, some of them may cause unseen diseases. The overall efficacy of the preventive pharmaceutical migraine treatments is about 50%. Some other available drugs have fewer side effects but works with lower efficacy rates [55].

In conclusion, the aforementioned side effects and insufficient efficacy may lead to dissatisfaction and discontinuations. In addition to this, the overuse of drugs may cause a chronic migraine. Furthermore, 80% of patients are willing to change their current medication for a treatment with similar efficacy but fewer side effects. Medication-related adverse effects and lack of efficiency thus underscore the need for better anti-migraine treatments and have created a niche for non-pharmacologic therapies such as neurostimulation [7], [55].

2.5.2 Surgical treatment

The theory behind the surgical treatment was postulated that muscles, vessels, fascia, and bone may compress peripheral nerves in retrospective trials and anatomic studies. Further to this, extra-cranial trigger sites of migraine have been identified. It is believed the decompression of these peripheral sites may result in some positive results with respect to pain suppression. However, it should be noted that this method is only applied to the patients who failed to respond the available conservative medical management methods. Although there are other more infrequent potential sites of compression, the operation of the decompression is mainly based on four major sites. These peripheral trigger sites are frontal, temporal, nasal and occipital. Depending on these trigger sites, the patient is approached based on several diagnostic tools including a constellation of symptoms, migraine headache starting point, nerve block, ultrasound Doppler, CT scan and rarely injection of botulinum toxin–A. The surgical decompression is mainly applied to the peripheral nerves to manage migraine as discussed in the

following paragraphs. The procedure of these methods are beyond the scope of the thesis.

The surgical treatment of migraine has been investigated mainly by decompression of frontal trigger site. The pain in the frontal territory usually starts the supraorbital area of the forehead. Deactivation of this site may be achieved with a surgical endoscopic approach (an instrument which can be introduced into the body to view inner parts) or through an upper eyelid incision on patients. The pain can be suppressed by decompression of the corrugator myofascial unit through subtotal resection of the corrugator supercilli muscles (CSM) or It may be possible to decompress the STN and SON by removing the glabellar muscle group (corrugator supercilii, depressor supercilii, and procerus muscle). Using either a transpalpebral approach or an endoscopic approach through small hairline incisions, it has been shown that endoscopic approach has a higher success rate, compared to other surgical decompression methods for frontal trigger site. This is due to more complete resection of the CSM and easier visualization and identification of supraorbital foramen and accessory SON branches.

At the temporal trigger site, pain is generally seen in the vicinity of the temporal side of the head. The patient can be diagnosed by pointing to a hollow area in the non-hair bearing territory. The course of the zygomaticotemporal (ZT) arises from the inner side through the temporalis muscle. Thus, the temporal trigger site can be related to compression of the ZT nerve branch of the maxillary division of the trigeminal nerve which believed the main reason for the ZT compression is temporal muscle. The surgical operation is performed to decompress or remove the ZT using an endoscope. Mostly, the endoscope is used for the patients who experience both frontal and temporal symptoms to easily view the inner structure for surgical operation.

At the occipital trigger site, patients generally experience upper neck and occipital pain, muscle tightness, and trigger point tenderness. This trigger point can be associated with the greater occipital nerve (GON) which is a sensory branch

of the spinal nerve. A recent study suggested that the compression of the GON may cause the initiation of migraine.

The nasal trigger site is identified based on the symptoms such as patient waking up with migraine pain, usually cyclic and sensitive to weather, allergy, and hormone changes.

Although surgical treatment methods for migraine are yielded some positive results, there is a limited portion of the patients who respond to the surgery. The most common reason for this inconclusive response may be a failure to detect all trigger sites. Additionally, as it is believed the extra-cranial trigger sites exist the consequence of the compression of the STN, SON, zygomaticotemporal and/or the greater occipital nerves however and decompression of these nerves relieve some pain, but effects are temporary. Generally, clinical studies have lack of appropriate control of following-up and most of them have lack of evidence regarding safety and adverse effects. The most common side effects include transient numbness or paresthesias at the surgical site, incisional alopecia, controlled intra-operative bleeding, and transient uneven brow movement. The advantage of the surgical operation to the aforementioned nerves is to help identify the target nerve. The associated studies and their positive effects and adverse effects are listed in Table 2.5 [12], [56], [57].

Table 2.5: Clinical studies of the surgical treatment of migraine, reference is shorted as Ref, and Adverse effects are represented with AEs in table. F: Frontal; T: Temporal; O: Occipital; N: Nasal.

Ref.	Patient No	Duration(month)	Migraine free	Trigger site	Notes
[58]	39	46.5	38.5%	F	[1]
[59]	22	11.4	45%	F,T	[2]
[60]	60	12.8	28.3%	F	[3]

Continued on next page

[1]The study was investigate the correlation between corrugator supercilii muscle (CM) and migraine. Meaning that there was a some improvement in migraine after removing CM by surgical operation. Any adverse events (AEs) were not reported in this study.

[2]In this study, the patients were underwent the foreheadplasty by removing corrugator supercilii muscles. The common complaints were transient surgery site numbness

[3]The common AEs were reported by patients was transient surgery site paresthesia

Ref.	Patient No	Duration(month)	Migraine free	Trigger site	Notes
[57]	89	13	34.8%	F,T,O,N	[4]
[61]	18	16	16.7%	F,T,O	[5]
[62]	49	12	57.1%	F,T,O	[6]
[63]	69	60	29%	F,T,O,N	[7]
[64]	24	21.7	8.3%	F,T,O,N	[8]
[65]	169	>11	39.1%	F,T,O,N	[9]
[66]	25	–	–	O	[10]
[67]	86	12	–	F	[11]
[68]	335	12	35.2%	F,T,O,N	[12]
[69]	253	>12	63.2%	F	[13]
[70]	170	>12	55.9%	O	[14]

Continued on next page

[4]The complications of the surgical treatments were temporary nasal dryness, rhinorrhea, slight recurrence of septal deviation, intense itching, minor hair loss, temporary neck stiffness Itching. The 19.4% of the patients underwent the re–surgery operations due to associated complications.

[5]This study aimed to evaluate the effectiveness of surgical decompression of multiple migraine trigger sites in a clinical practice setting. The various combinations of the surgical decompression of STN, SON, ZT and GON were performed on 18 consecutive patients. Three patients had complete relief of their migraine. The reported AEs were itching, numbness, scar alopecia

[6]The efficacy of the independent surgical deactivation of frontal, temporal and occipital sites on migraine headaches was investigated. The most common surgical complications were numbness, temporal hollowing, temporary itching, uneven brow movement, temporary hair loss or thinning, residual corrugator function, neck stiffness

[7]The study was designed to evaluate the long term efficacy of the surgical decompression of the common four trigger sites for migraine. The twelve percent of the patient experienced no significant change in their migraine. The reported AEs were neck stiffness or weakness, numbness, hypersensitivity.

[8]Deactivation of the four trigger sites of migraine underwent the surgical decompression to assess efficacy on migraine attacks. Among the entitled population, just two patients reported migraine elimination. The complication mostly experienced were immediate post-op headache, transient surgery site paresthesia, incisional alopecia, periorbital ecchymosis.

[9]The surgery was performed on 169 patients who met the inclusion criteria. However, the study was shown only 39.1% of patients did not experience migraine pain after study period. Any AEs were not reported.

[10]The study was evaluated the possibility of any improvement on migraine pain by performing surgical decompression of occipital artery and greater nerve junction. The study was not reported any AEs.

[11]The decompression of the SON was performed by removing muscle. Any AEs were not declared.

[12]A large population of the patients underwent the surgical treatment to improve migraine headaches. They only obtained about 35% of patients who relief migraine headaches. The study did not include the AEs

[13]Scalp paresthesia, forehead asymmetry, frontalis paralysis, eyebrow elevation, dimpling on animation

[14]The effect of occipital artery surgery was evaluated on the migraine headache. However any AEs were not reported

Ref.	Patient No	Duration(month)	Migraine free	Trigger site	Notes
[71]	188	>12	34.6%	F,T,O,N	[15]
[72]	229	>6	27.5%	O	[16]
[73]	71	33	-	O	[17]
[74]	43	6–24	69.24%	F,O	[18]
[75]	13	21.6	–%	F	[19]
[76]	30	11.1	46.7%	T	[20]

2.5.3 Neuromodulation techniques

Available pharmaceutical and surgical treatments of migraine are not completely effective and have troublesome side-effects [50], [53]. Thus, there is need for alternative treatments such as neuromodulation. Recently, the neuromodulation techniques have raised great interest thanks to technological and scientific advances. Neuromodulation can be defined as the process of inhibition, stimulation, modification, regulation or therapeutic alteration of activity, electrically or chemically, in the central, peripheral or autonomic nervous systems [77]. There are a variety of central and peripheral nerve stimulation methods that have been studied and these techniques have shown at least some improvement. Neuromodulatory treat-

[15]The surgical operation was performed to remove trigger sites associated muscles to decompress STN, SON, GON and ZT. However, the migraine headache was not removed from nearly 65% of patients. The complications of the study was not discussed

[16]The large population of patients was followed up for short–term. The effect of occipital nerve on the migraine was evaluated by removing the associated nerve. However, the operation was not completely successful for nearly 75% patients. Another drawback of the study was not to mention any AEs during the study.

[17]The patients underwent the surgical decompression of the occipital nerve. However, they did not discuss the population of patients who relief from the migraine. The AEs are numbness, headache and hypersensitivity.

[18]They performed the endoscopic surgical treatment to frontal site and surgical isolation procedure to occipital trigger site to compare their efficacy on migraine. Although most of the patients relief from migraine, but the efficacy of the study on large population is not clear and the long–term AEs unknown

[19]The study was designed based on low population patients group to assess the effect of the frontal trigger site on migraine. The efficacy of the study for large population remains unclear and any possible AEs were not reported.

[20]it was aimed to decompress the STN, SON, and ZT by performing the surgical operation on the CM. The rate of patients who relief the migraine was less than 50% although the study was based on low population and short–term follow–up. The general complications of the surgical treatment were experienced in this study

ment approaches may be grouped as invasive and non-invasive neurostimulation methods (regarding their implementation to the body). They can be grouped as peripheral and central regarding their effect on the neural circuitry. The peripheral neurostimulation is applied to peripheral (pericranial) nerves and the central neurostimulation aims to activate the central structures (the cerebral cortex). The function of these neurostimulation techniques is to manipulate central or peripheral pain pathways using electrical or magnetic impulses to supply preventative or acute treatment. The preventative treatment function is to suppress the central sensitisation of migraine headache, while the acute treatment function is to block the processes which are responsible for generation of attacks.

The invasive methods are occipital nerve stimulation (iONS), vagus nerve stimulation (iVNS), and sphenopalatine ganglion stimulation (SPGS). The non-invasive methods are transcutaneous single–pulse transcranial magnetic stimulation (tsTMS), transcutaneous vagal nerve stimulation (tVNS), transcutaneous occipital nerve stimulation (tONS), and transcutaneous frontal nerve stimulation (tFNS). The underlining principles of non-invasive techniques may apply the electric pulses through the skin via surface electrodes to depolarize the neural tissue underneath, without requiring any surgery or percutaneous invasive act. Thus, this technique is safer and can be used in all migraine patient [50], [53], [78].

Invasive neurostimulation techniques

Subcutaneous stimulation consists of several components, including electrodes and their leads (bundle wires), anchors to fasten the leads to the associated tissue and power source. Generally, there are two types of electrode leads in peripheral stimulation. These are percutaneous leads which are thin and cylindrical and paddle leads which are flat and broad. The electrodes are metallic points on the lead which may be made of platinum–iridium. These contact points can be designed either from anodes or cathodes to convey the current to the target structure. One of the main differences between lead and paddle electrodes is

that the leads can be inserted through a needle, however, a surgical dissection is required for paddle electrode. Additionally, the paddle electrode is shielded on one side and the percutaneous lead electrode is not; the current is directly transmitted through the target structure opposed to percutaneous lead. This may require less current levels to activate the neural structure which would result in a prolonged battery life. However, both electrodes types have been used for occipital stimulation. The power source for PNS is typically implanted in a subcutaneous pocket which is similar to pacemaker battery. The available options are an external Radio frequency (RF) transmitter/receiver system, a primary cell implantable pulse generator and a rechargeable implantable pulse generator. The RF receiver can be powered by an external RF transmitter coil placed on the skin over the device. Since rechargeable and non–rechargeable batteries are quite new, the implanted batteries are commonly used to power the stimulator system. The typical implant location in the body are upper buttock, abdomen and upper chest [79], [80]. The available invasive neurostimulation therapeutic procedures for migraine are shown in Figure 2.13.

Besides the STN and SON, the subcutaneous stimulation of the occipital nerve has been used to treat refractory headache disorders. The iONS is the most widely used for CM. However, it was shown that iONS has only been given some improvements for preventative treatment but no acute effect (apart from a few cases). The stimulating lead is implemented subcutaneously in the occipital region by the surgical operation to activate the GON and lesser occipital nerves. It is worthy to note that electrode leads can be either placed on the target structure or may be implanted just above the level as minimally invasive to propagate electrical impulses in neural tissue. The stimulator device is often implanted under the collarbone (clavicle), but the abdominal and buttock (gluteal) areas are also options. Although the exact mechanism of the ONS is not fully understood, the study on the animal showed that it has an antinociceptive effect on the second–order neurons in the TNC. The most common adverse events of the

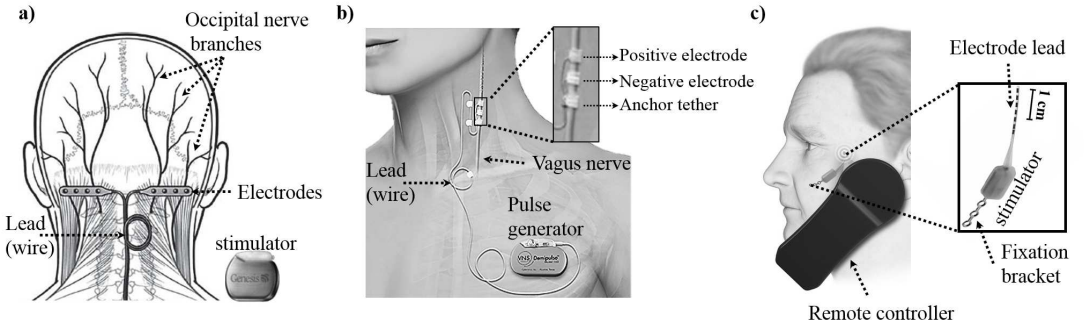

Figure 2.13: Available invasive neurostimulation procedures. (a) shows ONS where electrodes are placed on the branches of the occipital nerve at the back side of the head. Two leads are used to cover both side of the neck (single lead can also be used to provide bilateral stimulation coverage). A small pocket is implemented in the subcutaneous tissues around the incision where the lead(s) will be looped and anchored [80] (b) shows placement of the vagus nerve stimulation device, a pulse generator is implanted in the tissues of upper chest and electrical pulses are transmitted to the associated nerve via electrode lead. The end of the electrode helical lead is wrapped around the nerve and helps to anchor the lead to the vagus nerve [81]. (c) The SPG microstimulator implanted with an integral lead and a battery. The lead is placed within the pterygopalatine fossa structure. The microstimulator can be controlled by a hand–held remote control device [9].

iONS were lead migration, battery depletion and infection which may require another surgery. The other experienced complications are painful stimulation, pain over the battery site, paresthesia intolerance and hardware related adverse events. Overall, among the patients who had iONS treatment methods for migraine, 40%of them underwent new surgery and 70% of them experienced at least one adverse event according to based on a large population–study.

The iVNS technique has been used in the treatment of refractory epilepsy and depression. The experiments on the animals showed that stimulation of the vagus nerve aborted or reduced their frequency. Although there are many studies about the efficacy of the iVNS for epilepsy, it was shown in small studies that provided efficacy benefits in CM. In this method, the stimulating electrode is implanted and wrapped around the vagus nerve in the neck. The current pulse transmitted by a pacemaker–like device (generator) through a flexible wire (lead). The vagus nerve consists of both motor (80%) and sensory fibres (20%). The potential

mechanism of action of VNS in the treatment of migraine disorder has not been fully elucidated, however, it is postulated that nociceptive transmission may be modulated through the activation of vagus nerve afferents that goes to the higher centre of the brain through the TNC. This may explain the effect of the VNS on headache, ultimately through a reduction of glutamate levels and neuronal firing in the spinal trigeminal nucleus. These potential mechanisms will need to be more fully explored and, the efficacy of VNS for migraine still awaits properly designed, randomized, sham-controlled studies. The common AEs of this method are a surgical infection, temporary excessive salivation, permanent voice alteration mild coughs, paralysis of the vocal cord, lower facial weakness and the coercive feeling of coughing. Depending on the surgical improvements, the battery of the stimulator may need replacement thereby necessitating additional surgery. Although stimulation of the vagus nerve has a role in the reduction of migraine pain, the potential risks associated and the high cost limits the use of the procedure [78], [82].

The sphenopalatine ganglion is the largest extracranial structure which is situated in the pterygopalatine fossa and it has a connection with the trigeminal nerve and multiple neural roots. Although SPGS technique is mostly used for CH, it has shown a degree of pain frequency reduction in migraine as well. This neuromodulation technique aims to either stimulate or inhibit neural function by electrical impulses. The stimulator can be designed from multiple electrodes and all the features of the neuromodulator are adjustable including location, duration, and intensity of stimulation, frequency, band-width of stimulation, and so forth. However, in general, the electrode and pulse generator is implanted through the mouth above the teeth and screwed to the skull. Although the neurostimulator with electrode arrangements are implanted, the power is supplied by a small wireless handheld remote controller. The efficacy of the SPGN is low and has limited safety due to subcutaneous implementation. The most common complication of this method are hardware failure, mild-to-moderate hypoesthesia within

the maxillary nerve territory, sensory disturbances, limited jaw movements and dry eye [83], [84].

Since all invasive neurostimulation treatment methods require surgery, there are certainly risks involved. In consequence, invasive methods may be used for the most serious and chronic patients who have failed to respond to the available multiple therapies [80]. Table 2.6 summaries the trail studies have been carried out based on these techniques.

Table 2.6: Invasive neurostimulation trail studies, t:time.

Ref.	Year	Technique	Patient No	t(month)	Study	Treatment	Notes
[85]	2017	ONS	35	84	open-label	Preventive, acute	[21]
[86]	2017	ONS	20	12	RCT	Preventive	[22]
[87]	2012	ONS	177	4	RCT	Preventive	[23]
[88]	2009	SPGS	11	-	Open label	Preventive	[24]
[89]	2008	VNS	29	6	Open label	Preventive	[25]

Continued on next page

[21]The open labeled study investigated the long-term efficacy and tolerability of ONS for CM. The subcutaneous double sets electrode leads placed at the extracranial exit of the greater and lesser occipital nerves. The stimulator was programmed to generate pleasant paresthetic sensation spreading throughout the occipital region. The stimulation was performed at 40 Hz pulse frequency and 250μs pulse width. The migraine frequency decreased by 50% for 31 patients and less than 50% for 3 patients. Only one patient did not experience any reduction.

[22]In this study, neurostimulator was implemented in the body of 20 patients to observe any therapeutic improvements on CM. The migraine reduction range was between 30% to 50%. 75% of the patients reported at least one AE.

[23]This is a randomized control study which was applied to large groups of patients. The permanent implementation of PNS device was performed only for 157 patients. The electrode leads were placed either along or perpendicular to the course of the nerve and this process can be unilaterally or bilaterally depending on the pain distribution. Patients experienced reduction in migraine-related disability. The common AE was persistent implant site pain

[24]The study investigated possible role of SPGS on treatment of CH. The stimulation was performed under 1.2V, 67 Hz pulse frequency and 0.462 s pulse width. It was shown that nearly 50% of patients did not have any reduction in their migraine attacks.

[25]In this study, the aim to investigate the effect of VNS on the seizures and migraine for 6 months follow up duration. The efficacy of VNS on the seizures has been well established. However the results showed that stimulation of the vagus nerve may provide small encouraging results for migraine. To have more accurate results, large and long–term studies are needed to observe the effect of VNS on migraine.

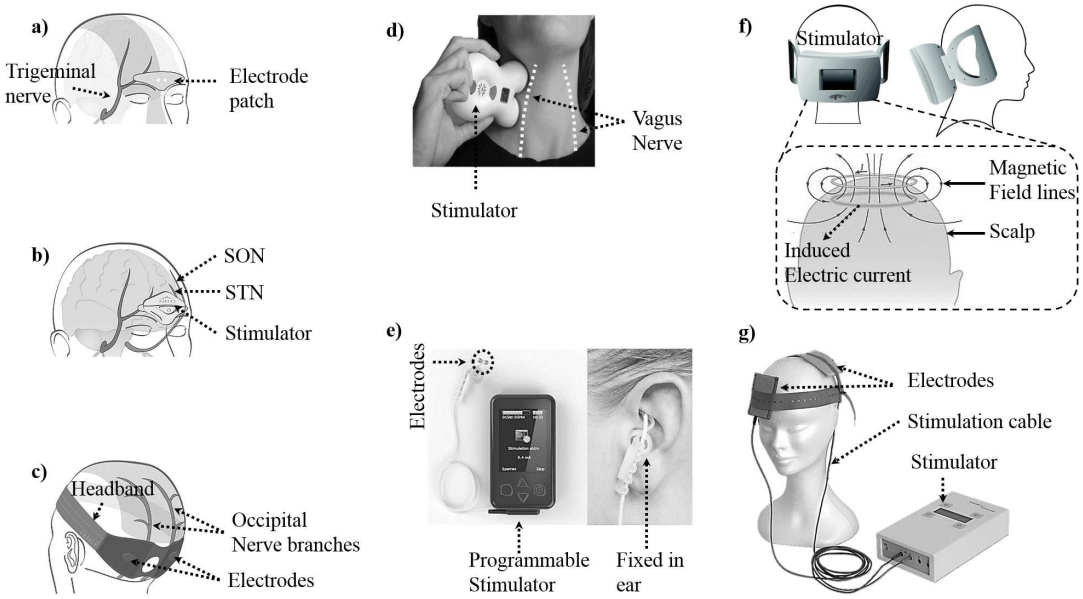

Figure 2.14: Available non-invasive neurostimulation devices. (a) shows Cefaly stimulator which is placed over the forehead and covering frontal nerve. (b) shows Cefaly bipolar electrode patch [7]. (c) shows Kit Arnold headband stimulator with electrodes covered occipital nerve [78]. (d) shows GammaCore device, the electrode is applied on the neck via gel [91]. (e) shows Nemos device which has mobile phone-like stimulator. User can control the stimulator manually [92]. (f) shows SpringTMS device, the electromagnetic current is applied through the coils to back side of head [93], (g) represents NeuroConn stimulator device which aims to change the cortex excitability using relatively large electrodes [94].

Ref.	Year	Technique	Patient No	t(month)	Study	Treatment	Notes
[90]	2005	VNS	6	13	Open label	Preventive	[26]

Non–invasive neurostimulation techniques

Table 2.7 summaries the technical aspects of non-invasive neurostimulation devices. The trial studies of these devices and their effect on migraine headache are discussed in Table 2.8.

[26]The stimulation of vagus nerve on migraine and cluster headache was investigated based on small open labeled study. The stimulation current range was 1.5 to 2.27 mA and pulse width was 0.25 s. Patients experienced some therapeutic benefit in both CM and CH.

Table 2.7: Non-invasive neurostimulation devices and their technical aspects, P.Width: Pulse width and S.Wave: Stimulation wave.

Ref.	Device	Electrode	Intensity	Frequency	P. Width	S.Wave	Use
[85]	Cefaly	Bipolar	16 mA	60 Hz	$250\mu s$	Biphasic	EM
[85]	Nemos	Biploar	25 V	10 Hz	$0.3ms$	Biphasic	CH, Epilepsy
[85]	GammaCore	Disc	up to 24 V	25 Hz	$1ms$	Biphasic	Epilepsy, CM
[85]	SpringTMS	Disc	$4mA/cm^2$	-	$180\mu s$	Biphasic	Acute Migraine
[85]	NeuroConn	Rubber	$\pm 4.5mA$	Adjustable	Multiple	Multiple	Prevention

TMS procedure is to activate the human motor cortex based on the principle of electromagnetic induction which in turn has the effect of changing the firing pattern of neurons. TMS has been shown to disrupt the wave of cortical spreading depression (CSD), which is thought to be the experimental correlate of migraine aura. The current pulse passes through a coil located within the neuromodulator to depolarise neurons (depends on correct size, duration, and location of current) within a target area to alternate neurotransmitter levels. The animal studies have shown the nociceptive trigeminothalamic neurons can be inhibited by this approach. Thus a portable neuromodulator (SpringTMS) was developed to acute or reduce migraine pain levels. However, according to a post–marketing survey, majority of the patient population (55%) were not satisfied possibly due to inadequate benefit, cost, or inconvenience. 62% of the patient groups who have completed the survey reported some reduction in migraine and reported 59% some reduction in attack duration. However, there is no controlled evidence to support the use of the TMS device in the prevention of migraine. The common complications are transient and mild; these include dizziness, light–headedness, tingling and worsening of migraine pain. Also, this method can not be applied to the patients who have epilepsy, skull defect or with a pacemaker, cardiac lines, metal in the head (electrodes, stimulation devices) or other apparatus that could be

influenced (dislocation, induction of electric currents) by magnetic field [93], [95]. Usage of the implantable VNS for migraine leads to the development of the non–invasive neuromodulator treatment methods to activate vagus nerve. The underlying mechanism for tVNS in headache treatment is likely to be similar to the iVNS, as mentioned above. There are two types of the tVNS that have been released on the market and their long–term and large–scale efficacy on the primary headache acute or prevention therapy is currently being assessed. One of the VNS treatment methods(Nemos neurostimulator) is aimed to treat or reduce pain attacks of migraine by giving electrical current to the left auricular branch of the vagus nerve fibres (thick myelinated sensory $A\beta$ fibre afferents) based on TENS technique. The battery–driven neuromodulator connected to an ear electrode placed in contact with the skin of the concha. The electrical pulses released from the stimulator during stimulation had following characteristics (pulse width: 250 s, frequency: 1Hz or 25Hz, duty cycle: 30s on, 30 s off, to avoid habituation) released from the stimulator during stimulation. The stimulation can be and should be fixed by the individual when tingling sensation occurred [78], [96]. Other method (GammaCore) stimulate vagus nerve sensory afferents transcutaneously via disc electrodes in the neck region. This therapy is administered with a handheld device which is placed on the neck to activate the vagus nerve through the skin as shown in Figure 2.14d. Although methods are mainly designed with epilepsy, the small studies have shown there was some improvement for migraine pain as well. However, the devices are not available on the government clinics (they are not FDA approved) but individual funding requests may be considered. Additionally, most of the studies, based on this procedure, lack of having control group. Thus, to have an objective, safe and well–tolerated results, the long–term randomised control studies of tVNS are required and the exact underlying mechanism of the pain remains unclear. The AEs are local discomfort, a mild skin irritation, worsening pain [47], [78].

The tDCS may modulate cortical excitability by an anodal (excitatory) or catho-

dal (inhibitory) electric current applied to the scalp using NeuroConn device. Although there are limited studies which investigate the effectiveness of tDCS on migraine, it was suggested that tDCS may have a positive impact on migraine (reduced pain intensity about 36–40%). In this technique, the weak electrical current (e.g., 1–2 mA) is supplied by one or two relatively large electrodes that are placed on the scalp to modify membrane potential which alters cortical excitability and activity depending on the current flow direction through the target neurons [97]. In other words, this procedure can induce neural plasticity. The experienced complications of this method are unpleasant sensations after tDCS, a mild tingling sensation may occur directly under the electrode, moderate fatigue, occasional headache. Although most of its adverse effects of this technique are mild and disappear soon after stimulation, several papers have reported that some adverse effects, most commonly skin problems, can persist even after stimulation. The limitations of tDCS are mainly the use of large electrodes due to the low spatial resolution and difficulty in defining the treatment protocol (e.g., localisation, current density and electrode position). Thus, further large random controlled studies are necessary to optimise the correct stimulation settings. [98]. The transcutaneous supraorbital nerve stimulation has also been proposed for suppression of migraine pain. This approach will be discussed in detail in the following section.

Table 2.8: Non-invasive (TENS) neurostimulation trail studies for migraine, t: time.

Ref.	Year	Technique	Patient No	t(month)	Study	Treatment	Notes
[99]	2018	sTMS	263	3	Open label	Preventive	[27]

Continued on next page

[27] The objective of this study was to measure the efficacy and tolerability of sTMS for migraine headache. Although a large group of patients were recruited, nearly 50% of those completed the study due to many reasons including safety consideration. It was shown that there was nearly 50% reduction in the number of migraine days for 46% patients. Concerning to safety and tolerability, it was reported 62 AEs in total including scalp discomfort, light headedness, ringing in ears(tinnitus), tingling. The limitation of the study were lack of long-term randomised control study and open label based.

Ref.	Year	Technique	Patient No	t(month)	Study	Treatment	Notes
[100]	2017	tSNS	57	1	CT	Preventive	[28]
[101]	2017	tSNS	37	3	open label	Preventive	[29]
[102]	2017	tSNS	33	4	Open label	Preventive	[30]
[103]	2017	tSNS	31	7	Open label	Acute migraine	[31]
[104]	2017	tVNS	9	1	Open label	Acute,Preventive	[32]
[97]	2017	tDCS	50	1	open label	Preventive	[33]

Continued on next page

[28]The tSNS with Cefaly neuromodulator was used to prevent primary headache attacks (migraine, CH,TTH) by stimulating both STN and SON. The postulated mechanism is to activate $A\beta$ fibers to inhibit nociceptor fibers. Thus, the pain attacks may be reduced either by gate control theory or neural plasticity. The pain attacks were reduced in both migraine group and patients with other types of headache(range was 22.5% to 28.8% in control group). No AEs were reported

[29]The efficacy and safety of Cefaly neurostimulator was investiagted on 37 patients who have either EM or CH. Although about 65.5% of patients expressed their satisfaction and willing to continue treatment, there was a small decline in migraine days and frequency. Furthermore, 34.5% patients complained about AEs. The major limitation of this study is the lack of a control group and the small sample size

[30]The tSNS with Cefaly is used to prevent EM, however there is no available data for CH till this study. It was aimed to investigate efficacy of the Cefaly device on CH with or without medication overuse. The study showed that 35%of patients achieved benefit over four months following time. Although the results were encouraging and suggested that this form of neurostimulation may have an efficacy similar to that of established pharmacological prophylactics for CM, the study was an open label and had limited participants

[31]The aim of this study was to evaluate the safety and efficacy of the tSNS via Cefaly neuromodulator as an acute treatment for migraine attacks. The stimulation was applied for an hour at 100 Hz (60 Hz used in the migraine prevention studies), $250\mu s$ and the current intensity was increased over the first 14 minutes. The pain intensity was labeled from 0 to 10 and patients were asked to rate their pain intensity. The results regarding to the efficacy showed that pain intensity was reduced by 57% in an hour stimulation. With regards to safety, no AEs or complaints were reported during the trial

[32]A small group of patients who have migraine without aura were trained to use gammaCore neuromodulator device to treat these disorder's attacks. Although the study showed some improvements in migraine attacks, the RCT based on large scale of patients is required to assess the efficacy of available application.

[33]The study investiagted the impact of tDCS on consumption of drugs and on pain conditions. The tDCS was performed on 30 patients by given a weak direct electrical current (2 mA) passed through the cortex to change the degree of cortex excitability and pharmacological methods were applied for the rest of the patients. Although it was shown that the tDCS has more effect on reduction of migraine than pharmacological methods, the measurement was based on subjective assessment.

Ref.	Year	Technique	Patient No	t(month)	Study	Treatment	Notes
[105]	2016	tVNS	56	3	Open label	Preventive	34
[106]	2016	tVNS	59	2	RCT	Preventive	35
[107]	2015	tSNS	24	10	CT	Preventive	36
[93]	2015	sTMS	190	3	Open label	Acute, Preventive	37
[108]	2014	tVNS	30	-	Open label	Acute	38
[14]	2013	tSNS	67	3	RCT	Preventive	39
[15]	2013	tSNS	2313	36	Open-marketing	Preventive	40

Continued on next page

[34]The study investigated the efficacy of tVNS using gammaCore neuromodulator with stimulation vagus nerve fibers in the neck. Although the results showed that there was a reduction in migraine attacks, randomised control studies are required to validate these results. The most commonly self-reported AEs were mild or moderate application site reactions (e.g., tingling) and facial/neck twitching

[35]The study aimed to assess feasibility, safety, and tolerability of tVNS for the prevention of CM attacks using GammaCore device. This is the only randomised controlled study to evaluate the efficacy of tVNS in CM to date. The study failed to show a significant difference in active versus sham group.

[36]The safety and efficacy of the tSNS using Cefaly neuromodulator for migraine without aura was investiagted. The results showed that there was nearly 50% reduction in migraine attacks frequency. Furthermore, there was reduction in monthly migraine attacks and migraine days. However, the results were not different from previous study. Concerning safety, no AEs were reported. Although there was some encouraging results to decrease migraine days and attacks, long-term studies based on large populations and random control procedures are required.

[37]Single pulse TMS device was used through the post market pilot program in the UK to treat migraine with aura for a period of three months. A single magnetic field pulse is delivered of nominally 0.9 Tesla on the scalp and underlying cortex, measured 1 cm from the device surface, with a rise time of 180 s and a total pulse length of less than 1 ms. According to this post marketing survey, the 55% of patient population was not satisfied possible due to an inadequate benefit, cost, or inconvenience. From the patient group who completed the survey, 62% reported some reduction in migraine and 59% reported some reduction in attack duration. However, there is no controlled evidence to support the use of SpringTMS in the prevention of migraine. The common complications are transient and mild; these include dizziness, lightheadedness, tingling and worsening of migraine pain.

[38]This is the first open label study which evaluate the efficacy of gammaCore to acute treatment of migraine. Although 21% of patients reported to be pain free after the two hours of treatment, the study was open label and uncontrolled. The stimulation caused to tense neck, frequent urination, shoulder pain and lip or facial drooping.

[39]The efficacy and safety of Cefaly neuromodulator based on TENS was assessed. Sixty seven patients with episodic migraineurs have been used daily tSNS of Cefaly or sham sessions. The length of this treatment of the study was 20 minutes sessions per day and this was repeated for three months. After three months, the responder rate (50%) was much higher than active group (38.2%). The episodic migraine attacks were reduced (the therapeutic gain was 26%) however, the headache severity did not change and the drug intake was also reduced. With respect to safety, no AEs or side effects occurred during the trial, either in the verum or in the sham group

[40]This is one of the large post marketing survey of 2313 headache sufferers in the general population. The Cefaly device was provided via internet for a free 40 days trial. It was

Ref.	Year	Technique	Patient No	t(month)	Study	Treatment	Notes
[109]	2013	VNS	46	3	RCT	Preventive	[41]
[110]	2013	tDCS	10	2	open label	Preventive	[42]
[111]	2006	sTMS	42	-	Open label	Preventive	[43]

2.5.4 Transcutaneous frontal nerve stimulation (t-FNS)

Transcutaneous stimulation of the frontal nerve is peripheral neuromodulation method that has shown some positive results in migraine treatment. This promising non-invasive neurostumulatory therapy is called transcutaneous supraorbital nerve stimulation (t-SNS) or trigeminal nerve stimulation,(eTNS). The tSNS with Cefaly (Cefaly, CEFALY Technology, Lige, Belgium) stimulator has been developed to prevent an episodic migraine by stimulating the STN and SON nerves. The Cefaly generates electrical pulses and transmits them via a self-adhesive

recommended the each patients used the device for 20 minutes for per day for 40 days. However, nearly half of the patients (46.6%) were not satisfied and returned the device in short time.

[41]The trial study was evaluated nVNS for CM using Nemos device. In this controlled study, the nVNS was received by chronic migraineurs patients at either 1 or 25 Hz frequency in the left ear. Patients in the 1 Hz group had a more migraine headache reduction days than those of the 25 Hz group. However, further data is required to support its regular use in clinical practise They did not define why 1 Hz is more effective than 25 Hz. The VNS for CM may be different from those who have epilepsy. As the vagus nerve have both myelinated and non–myelinated effrents as well as afferent fibers, the stimulation of target nerve may require different patters. Although animal data showed that afferent vagal stimulation can reduce the activation of nociceptive neurons in the caudal trigeminal nucleus, it is not clear how vagus nerve interferes with migraine generation. Most common treatment related AEs were mostly characterized by local pain, paresthesia and ulcers at the stimulation site.

[42]The impact of anodal tDCS on visual activity in healthy volunteers and on possible prevention for patients who suffer from episodic migraine without aura were investiagted. The stimulation was performed using programmable DC stimulator with 2 rubber electrodes ($5 \times 7cm$). The anode electrode was placed in the occipital region to activate cortex region and the cathode was fixed on the chin to avoid any inhibition of cerebral cortices. Low current intensity (1 mA) was stimulated on patients and current level was gradually increased to minimise possible discomfort. There was a degree of reduction in both drug intake and migraine frequency, however the results need to be confirmed in a long term random control study and long follow up duration.

[43]This is the first open label study of sTMS that aimed to assess the impact of TMS on migraine pain. The stimulation was performed on 42 patients with a two brief pulses of TMS at the pain area. The frequency of headache recurrence decreased by 48% for one trail. The limitations of the study was low stimulation group and lac of randomised control group. It is important to note that the heart rate was decreased during stimulation.

supraorbital electrode to excite on the SON and STN located under the skin of the forehead as shown in Figure 2.14.a. Symmetrical rectangular biphasic stimulation through the bipolar electrodes and 60 Hz low–frequency pulses set were delivered. The current level can be varied between 1–16mA, depending on a patient sensation of tingling on the forehead. Meaning that stimulus current threshold is decided based on tingling sensation. There is no well-controlled evidence for the use of the Cefaly device in the acute treatment of an episodic migraine. However, it may be useful during the migraine pain attack and in a chronic migraine. The physiological communication between the spinal nerve roots and the spinal trigeminal tract, involving the ophthalmic branch of the trigeminal nerve, could trigger migraine attacks. Although the exact pain mechanism of this method is unknown, it is believed TENS with Cefaly neurostimulator may use this nerve pathway to convey electrical stimulation by acting therapeutically on the inhibitory circuit in the TNC. That pain may be inhibited by gate control theory which activates $A\beta$ to inhibit the nociceptor fibres ($A\delta$ and C), as discussed in the pain mechanism subsection. Another possible mechanism in pain attacks may be reduced by neural plasticity. The effectiveness of tSNS in an episodic migraine was proven in a randomised double–blinded and sham–controlled study with a positive response rate of 50%. Additionally, a post–marketing survey of 2313 subjects using the device, as a preventative treatment of an episodic migraine, reported 53% satisfaction with the treatment. This as determined by the number of subjects continuing the treatment after the 40 day trial period. 46.6% of the patients were not satisfied with the Cefaly device(among them 40% of patients using the device at least 20 days). The efficacy of Cefaly is nearly the same as topiramate(one of the best preventive medication for an episodic migraine, as mentioned in pharmaceutical therapy subsection) and Cefaly has better safety. Thus, Cefaly may be superior for episodic migraine prevention when safety and efficacy are considered together. The Cefaly was approved by FDA as the first medical device for prevention of migraine. The most common AEs reported were

pain and paresthesia induced by the stimulation [14], [15], [85].

The Cefaly device thus appears to be a novel and suitable alternative to drugs for the preventive management of an episodic migraine. The effectiveness in the management of a chronic migraine, however, is yet to be confirmed. As with other neurostimulation devices, issues of adherence are reported with Cefaly and may be managed with adequate patient education and reinforcement.

After reviewing existing solutions for migraine headache, it can be deduced that the tFNS neuromodulation with Cefaly device is safe, has more objective results and includes large–scale studies, among other neuromodulation techniques based on preventing episodic migraine. Although invasive electrical nerve stimulation (IENS) methods, such as occipital nerve stimulation, have shown encouraging results to prevent migraine, this method is only used in the most medically intractable patients due to the inevitable exposure of the patients to the associated risks. TENS has fewer complications compared with the IENS. Although transcutaneous vagus nerve and transcranial magnetic stimulation provide a sensible degree of positive results, most of these techniques are based on small numbers of participants and lack long–term data about their tolerability, convenience, effectiveness and side effects in the treatment of migraine. In addition, the induced electrical stimulation by TMS activates a mixture of neurons in the brain and may lead to unorganized pattern of activity. Additionally, studies have shown that the stimulation protocols (e.g., stimulation frequency, current waveform and coil position) of TMS have not been optimized [10]. Moreover, the vagus nerve contains sensory and motor fibers and its stimulation may cause neck muscle contractions [11]. Although the t-FNS has been tested in double–blinded randomized controlled studies and the tolerability and the safety of the device are studied, it has not been effective in many cases. These complications can be associated to the required high current levels, due to the variations of the neuroanatomical structures. Usage of high levels of stimulus current may result in activation of both $A\delta$ and C fibres (i.e., pain fibres). In addition, as the electrode patch is

close to the pain-sensitive intracranial structures (e.g.; eyes, sinuses and nerves) in the existing device, this may cause discomfort to patients. In addition to this, the electrode patch may allow the stimulation of any structure in the vicinity of target nerve, resulting in unforeseen responses. Thus, by using a new electrode arrangements that shifted away from these sensitive anatomical layers, the required stimulus current levels and inducing pain may be reduced. No study has investigated these possible underlying causes of low efficacy in all subjects. This is partly due to the physical limitations of studying the neuroanatomy of individuals. One of the most useful tools to investigate these various parameters is computational study. Thus, using hybrid computational models of the human head, neural tissue and a neuromodulator, the effect of different electrode arrangements and neuroanatomical variations on the stimulus thresholds may be readily investigated as presented in the subsequent works.

2.6 Summary

The aim of this chapter was to detail the fundamentals of migraine management and its available solutions with underlying neural circuits presented in this thesis and bring into attention the work presented in the subsequent chapters into perspective. The divisions of the human nervous system and underlying neural circuits were discussed. The neural signals pathways from periphery site to the centre of the brain through the sensory fibres and, conversely, the way the motor fibres relay the neural signals from the central neurons to the periphery (to invoke an effect with neurotransmitters) were introduced. The generation and propagation of the AP in the neural circuits for both myelinated and unmyelinated nerve fibres were explained. Then, the effect of the features of the nerve fibres on the AP was evaluated.

Once general sensory pain mechanism was discussed, the primary headache disorders and their impact on the global populations, the neurophysiology of migraine

and its functions were introduced with a particular attention paid to neural circuits and their attributes. Namely, the central and peripheral control, the nerves involved and their presumed roles, the type of fibres and pathways and, finally, the kind of receptors and transmitters involved were discussed. It was emphasized that understanding migraine pathophysiology is probably the most challenging point in migraine management since an efficient acute and preventive treatment should rely on clear pathophysiological bases. Advances in the understanding of migraine pathway neural circuits are leading to the identification of new therapeutic targets at a rapid rate. The available pharmaceutical and invasive and non–invasive neuromodulation treatment methods and their underlying neural mechanisms, for migraine, were introduced. After a comprehensive reviewing of the available solutions for migraine pain management, noninvasive neuromodulation is an exciting and useful method that is being increasingly recognised as a valid strategy for migraine management. It offers a safe and effective alternative to pharmacological treatments. Among them, the supraorbital nerve stimulation with Cefaly neuromodulator was introduced as a promosing treatment method. The main cause of the inconclusive response of the tSNS may be neuroanatomical variations across different individuals and electrode settings which results in high stimulus current levels. Thus, the motivation for the subsequent work presented in the thesis was the optimisation of this wearable neurostimulator.

Chapter 3

Computationally Efficient-Accurate TES Head Model Development

3.1 Introduction

Transcutaneous electrical stimulation is derived based on the knowledge of the anatomy of the human head and nervous system as introduced in the previous chapter. In this chapter, the underlying principles of the neural tissue excitability based on the existing models are detailed. After discussing the general concepts of the computational neuromodulation, the nerve fibre excitation modelling based on the HH type cable models of an axon and associated cable equations are elaborated. Following this, the volume conductor with relevant boundary conditions and associated Maxwell's equations with quasi-static approximation are detailed. In addition, the existing studies on human head modelling are tabulated chronologically and discussed in terms of numerical solution and mathematical approximations. Lastly, different types of mammalian myelinated nerve fibre models with their channel mechanisms are compared.

When the computational complexity increases, the time and computational re-

sources may limit the investigations. Alternatively, to reduce the complexity and save computation time, the human head model may be built from simplified geometries with a level of error. Thus, the anatomically realistic multilayer human head model was extracted from MRI data set and the simplified model was constructed by imitating the realistic human head model. After applying the electrical features of the tissue in both models, the appropriate boundary conditions and discretisation setting are used to obtain electrical potential in their volume conductors. Then, the current thresholds, the amount of charge injection and computation cost are compared and discussed with the one that constructs from geometric shapes.

Finally, since the electrode patch is in contact with the skin, thus the effect of the microscopic structure of these layers on the neural tissue excitation may be necessary to investigate. The statistical variations of the highly conductive microscopic layer are generated and the constructed with the other layers to asses the effect of these layers on the stimulus current thresholds and computation cost. The obtained results are compared and discussed with the results of the simplified model to evaluate the use of the simplified model for future work when assessing the effect of neuroanatomical variations and electrode orientation on the efficacy of the target solution and possible ensuing optimizations.

3.2 Computational modelling of neuromodulation

Application of neuromodulation is growing rapidly for different therapy systems [112]. The computational models can provide important insight into the design, operation, and clinical application of the neurostimulation these therapy systems. It is infeasible to test all neuromodulator parameters using trial–based approach in human or animal. This may require massive trail studies which result in costly expensive. Alternatively, these models can be used to readily find

out solutions for the many concerns in the literature about pain related brain disorders, deep brain stimulation, spinal cord stimulation which would be difficult to obtain using other methods. For instance, the location of stimulation and the effect of the stimulation to the tissues in the vicinity and the effectiveness of stimulation can be readily examined using computational models.

These models are being used with substantial increases in computational neuroscience and bioelectrical field modelling. The former uses the computational tools to solve the nervous system problems. The latter evaluates the effect of the electric and magnetic field on the volume conductor of the biological tissue. The volume conductor models have been used to make detailed predictions of the bioelectric fields produced during stimulation based on a detailed geometric and biophysical characterisation. Nerve fibre models are created to predict neural firing patterns in response to stimulation using detailed neuron geometries with Hodgkin-Huxley ion channel kinetics. These predictions have been used as a starting point for further analysis such as stimulation safety, neural response, neurostimulation system design, or clinical outcomes.

The study of Hodgkin-Huxley was one of the earliest examples that deriving a set of governing equations for the nonlinear behaviour ion channels in the squid's nerve membranes. Finite element modelling (FEM) has matured as a numerical approach to solve bioelectrical field distributions within a complex volume conductors based on their isotropic and anisotropic tissue properties. NEURON software aimed to quantify the response of these multicompartmental neuron models with Hodgkin-Huxley ion channel kinetics. Also, the computational models were updated by recent studies such as Lorente, Rattay, Ranck and McNeal. They have provided some of the foundations of modern computational models [113], [114], [115].These are will be detailed in the following subsections.

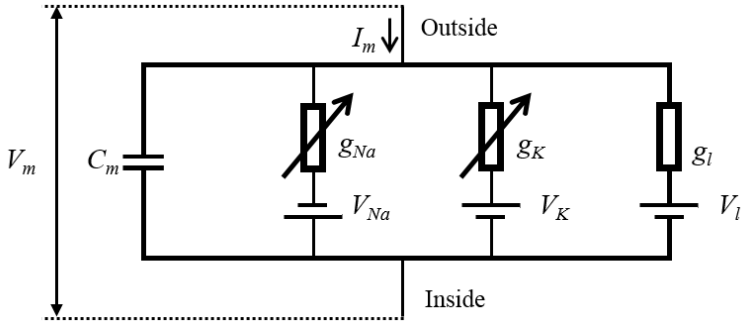

Figure 3.1: The HH axon model. The membrane capacitance C_m is parallel with ions electrical representation which each consists of a series of conductance and transmembrane potentials(V_{Na}, V_K, V_l). The arrows indicate that the voltage-gated conductance varies with time, while the leak conductance does not change over time. The potentials of sodium and others ions have opposite sign due to their concentrations.

3.2.1 Nerve fibre modelling

The following paragraphs will take the engineers point of view and look at the nerve fibers regarding membrane conductances and equivalent circuits. HH studied on ion channels based on first order kinetics in the squid giant axon which provides a very accessible way for electrophysiological measurements [116]. The HH fibre model composed of two voltage-dependent channels selective for sodium and potassium, respectively, and one (virtual) leak channel. The equivalent electrical circuit of fibre is represented with channels conductance g_{Na}, g_K, g_l and with associated currents I_{Na}, I_K, I_l, respectively as shown in Figure 3.1. The first two channels are called active channels, whose conductance changes in time based on the effect of the electric field on the distribution or orientation of molecules with a charge or dipole moment and the last one is called passive channels, which have a constant conductance. Based on Kirchhoff's current law for a parallel circuit, the total membrane current can be obtained from capacity current and an ionic current as shown in Equation (3.1).

$$I_m = C_m \frac{dV_m}{dt} + I_{ion}, \tag{3.1}$$

Where I_m and V_m are the total membrane current and membrane voltage, respectively and I_{ion} is the total ionic current which also can be expanded as in Equation (3.2).

$$I_{ion} = g_{Na}(V_m - V_{Na}) + g_K(V_m - V_K) + g_l(V_m - V_l). \tag{3.2}$$

The above ion conductance can be expressed in terms of conductivities (which commonly in units mS/cm^2). These are derived based on the HH empirical study as indicated in Equation (3.3).

$$I_{ion} = \overline{g}_{Na} m^3 h(V_m - V_{Na}) + \overline{g}_K n^4 (V_m - V_K) + \overline{g}_l (V_m - V_l). \tag{3.3}$$

where $\overline{g}_{Na}$, $\overline{g}_K$ and $\overline{g}_l$ are the maximum conductance of sodium, potassium and leakage channels, respectively. n, m and h are dimensionless variables which can take values from the interval [0,1] and are associated with the potassium channel activation, sodium channel activation and sodium channel inactivation variables, respectively. The conductance of the each active channel variation is defined by different order in equating. The kinetics of gating particles are given by the following equations.

$$\frac{dn}{dt} = \alpha_n(1 - n) - \beta_n n, \tag{3.4}$$

$$\frac{dm}{dt} = \alpha_m(1 - m) - \beta_m m, \tag{3.5}$$

$$\frac{dh}{dt} = \alpha_h(1 - h) - \beta_h h. \tag{3.6}$$

It is noteworthy to that models are that derived from the original HH are called *HH-type models* and are probably the most successful ones in modelling membrane excitation.

Although HH developed a merely empirical formulation for the observations but the overall macroscopic system of equations they defined is compatible with the microscopic understanding which exists today [27]. The description of the for-

mulation presented here is based on the current understanding where α_x and β_x are voltage–dependent rate constants (depending on the difference between transmembrane and resting membrane potentials). The neural membrane consists of large numbers of microscopic ion channels, each of has some gates which may be open or closed. Unless all associated channels gates open, the channel does not conduct. In equation (3.4), n can then be defined as the probability of having a gate open α as the rate at which the closed gate opens and β the rate at which the open gate closes.

Cable theory

So far, the description of the HH model for nerve fibre is completed. However, it is important to note that the HH axon model is not spatial dependent. The fact is that the neuron is reduced to a point in space. However, neurons may have complex morphologies in the real word. In addition to this, their voltages channels types and densities may vary, depending on different parts of the neuron. This complexity is defined by cable theory (originally developed to study signal decay in underwater telegraphic cables by Lord Kelvin) to describe electrical potential and current spread neuron fibres. Figure 3.2 shows the cable model of an axon. This model is a series of membrane compartments, connected by resistors. Each compartment is itself an electrical circuit that includes a capacitor representing the membrane capacitance of the lipid bilayer, resistors representing the ionic conductances of the transmembrane proteins (ion channels), and batteries representing the differences in potential (Nernst potential) arising from ionic concentration differences across the membrane. It should be emphasised cable theory works based on two assumptions. First, it is considered that the potential on any cross–section of the fibre is equal due to short fibre diameter respect to its length. Second, the extracellular space is isopotential and set to be zero due to low extracellular resistance along the cable exterior. Although the fibres in neuron structure can be oriented in any direction, the cable equation is assumed

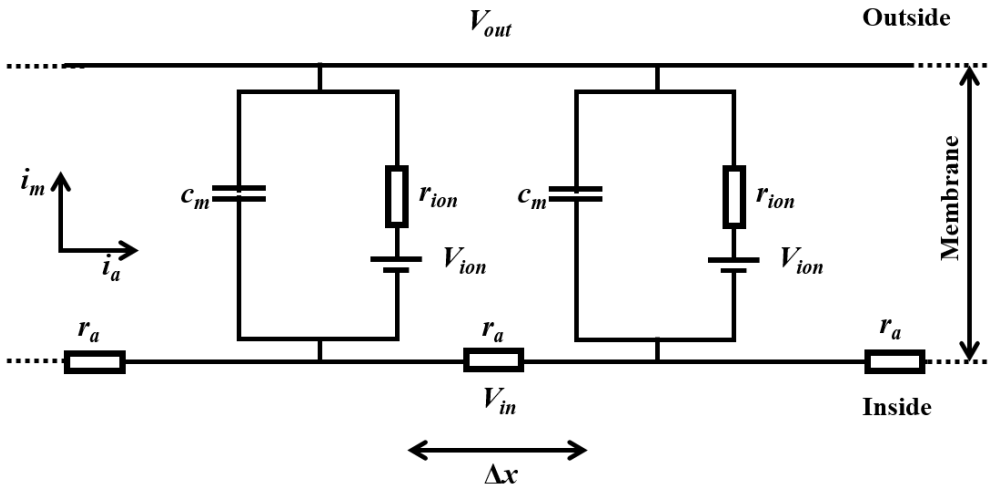

Figure 3.2: Cable model of an axon. Outside of the membrane is at the top, inside at the bottom. Multiple membrane patches are connected through axial resistance ($r_a[\Omega m^{-1}]$). The other channel mechanism features are active sodium and potassium resistance ($r_{Na}[\Omega m]$), ($r_K[\Omega m]$), respectively. The passive membrane channel resistance ($r_l[\Omega m]$), and the lipid bilayer capacitance ($c_m[Fm^{-1}]$).

one dimensional. Thereby, the current can either flow along the fibre or through the membrane at any point along the fibre [115], [117]. It is possible to model a phenomenon such as the initiation and propagation of APs with a complete set of differential equations. The cable theory aims to find a set of partial differential equations which can be varied with time and space. Considering that $\Delta_x \rightarrow 0$, the axial current (i_a) and membrane current (i_m) can be related as $\frac{\partial i_a}{\partial x} = -i_m$ which means the variations in i_a, as named leaking out current, is equal to i_m. The i_a encounters the cytoplasm resistance, producing a voltage drop, from the Ohms law, the Equation (3.7) can be derived. Then, the variation in the i_m can be formulated by Equation (3.8).

$$\frac{\partial V_{in}}{\partial x} = -i_a r_a \tag{3.7}$$

$$i_m = \frac{1}{r_a}\frac{\partial^2 V_{in}}{\partial x^2} \tag{3.8}$$

Rearranging the Equation (3.8) and follow the Ohms law, the second-order partial differential equation for membrane potential can be formed in $V(x,t)$ as shown

in Equation (3.9).

$$\frac{1}{r_a}\frac{\partial^2 V_{in}}{\partial x^2} = c_m\frac{\partial V_{in}}{\partial t} + \frac{1}{r_a}(V_{in} - V_l) \tag{3.9}$$

The cable equation has been widely used for modelling excitation of spatially extended neurons with the NEURON [118] stimulation by solving the set of partial differential equations using backward Euler integration.[1]

Myelinated nerve fibre modelling

Although myelin sheath was considered during nerve modelling in early studies [119], [120], however most models have treated the myelin as a perfect insulator based on McNeal [121] nerve model. The available myelinated nerve model mainly can be divided into three group based on assuming regarding the internodal segments. The Figure 3.3a shows the basic method which is considered that the myelin sheath is a perfect insulator [121], [122]. The behaviour of the model is decided based on the node of Ranvier. Although this model can be represented with a single cable electrical circuit, however, it has been shown that the myelin sheath is not a perfect insulator, has a capacitance that leads current to flow in the internode and this approximation is not consistent with experimental study [123], [124]. The Figure 3.3b shows the electric representation of the second model which assumes that the myelin is an imperfect insulator, passive mechanism in parallel with the membrane capacitance to indicate the capacitive and passive current flows through the myelin sheath. The studies which are underlined based on this model is here [119], [120], [125], [126], [127].

The most recent model is illustrated in Figure 3.3c with a double layer which is developed to explore possible mechanisms for depolarising afterpotentials (DAPs) in myelinated axons [129], [130]. It is important to note that Richardson et al. [128] and McIntyre et al. [131] are made the main contribution for this model with the investigation of the suitability of implementing these three models and for-

[1] As of November 5 2018, Google Scholar showed over 2208 citations of the original NEURON paper by Hines and Carnevale.

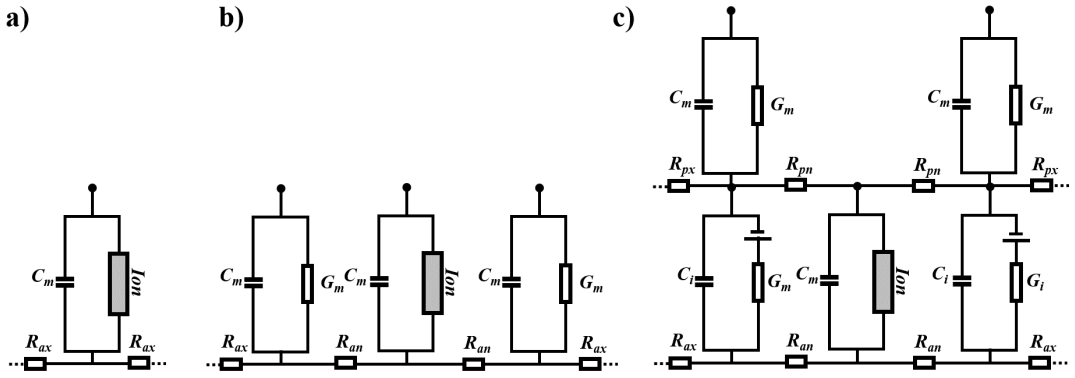

Figure 3.3: The myelinated fibre schematic diagram and different cable models. (a) assumes a perfect insulation for the myelin sheath, while (b) and (c) assume an imperfect insulation. (c) is superior as it considers more realistic features of the fibre. Redrawn with changes from [128].

malisation a set of equations and specifications for mammalian fibres of various diameters by replicating experimental data, respectively. The postulated model by McIntyre et al. [131] is named as MRG model hereafter. This model has been used by a wide range of neural activities based studies. Kuhn [132] has been compared the various models based on TES, the results showed that MRG based model matched the experiments data best.

The underlying channel mechanisms of this model is discussed here. The MRG model aim is to explore a distinct pattern of threshold fluctuation, known as the recovery cycle. It is important to explore the excitability of a fibre after an episode of the AP generation. The AP lasts about 1 ms at physiological temperatures in mammalian fibres as discussed before. However, it can affect the axons excitability due to its long–continued effect. Following the AP, a distinct pattern of threshold fluctuation, known as the recovery cycle has been generated from postspike afterpotentials and sodium channel activation and inactivation [131]. This cycle is constructed from absolute and relative refractory periods followed by supernormal (decreased threshold) and subnormal (increased threshold) periods mainly due to inactivation of fast Na^+ channels [133]. These followed oscillations in axonal transmembrane potential periods are referred to

as the depolarizing afterpotential (DAP) and the afterhyperpolarization (AHP), respectively [129], [130], [134]. The former has been related to both discharging of the internodal axolemma and activation of nodal persistent Na^+ channels mechanisms, while the latter has been associated with the activation of slow K channels [131]. It has been proposed that myelin attachment section has an important impact in the DAP [129], [130], [134]. Thus, McIntyre et al. [131] thought to represent explicitly of the fibre morphology. They used a double cable model which is constructed from two myelin attachment segments (MYSA), two paranode main segments (FLUT), and six internode segments (STIN) between every subsequent node of Ranvier. It is important to note that the geometry and membrane dynamics of the model are derived from the experimental studies on the human, cat, and rat for fibre diameters scaling from 5.7m to 16. It is noteworthy to that this model is developed for motor neurons, however, it has been proved that it can be used for sensory neuron as well [135].

3.2.2 Volume conductor modelling

The presence of current sources and their effect in conductive tissue layers can be investigated by the volume conductor theory. The sources of current in conductive media may be APs or stimulating electrodes. The volume conductor can be defined as a conducting medium that surrounds the region, occupied by the source [114]. This field deals with the propagation of electric and magnetic fields within volume conductors. To describe the static and transient potential distributions in volume conductor, Maxwells equations as shown in Equations (3.10-3.14) are solved.

$$\nabla D = \rho \tag{3.10}$$

$$\nabla B = 0 \tag{3.11}$$

$$\boldsymbol{\nabla} \times \boldsymbol{E} = -(\frac{\boldsymbol{\partial B}}{\boldsymbol{\partial t}}) \tag{3.12}$$

$$\nabla \times \boldsymbol{H} = \boldsymbol{J} + (\frac{\partial \boldsymbol{D}}{\partial \boldsymbol{t}}) \tag{3.13}$$

where $\boldsymbol{E}$ is the electric field and is related to $\boldsymbol{D}$ based on $\boldsymbol{D} = \boldsymbol{\epsilon E}$, where $\boldsymbol{D}$ is the electric displacement, $\boldsymbol{E}$ is the electric field and $\boldsymbol{\epsilon_r}$, $\boldsymbol{\epsilon_0}$ are relative and vacuum permittivity, respectively. $\mathbf{H}$ is the magnetic field and is related to $\boldsymbol{B}$ based on $\boldsymbol{B} = \boldsymbol{\mu_r \mu_0 H}$, where $\boldsymbol{\mu_r}$, $\boldsymbol{\mu_0}$ are the relative and vacuum permeability, respectively. The charge density is $\boldsymbol{\rho}$ and the conductivity of the domain is $\boldsymbol{\sigma}$. The volume conductor is usually assumed to be a monodomain (whose meaning will be amplified later), isotropic, resistive, and (frequently) homogeneous. The permeability of biologic tissues is important when examining magnetic fields and is usually assumed to be that of free space. The permittivity is a more complicated property, but outside cell membranes (which have a high lipid content) it is also usually considered to be that of free space.

Quasi-static approximation of Maxwell's equations

The set of *Maxwell's Equations* (3.10–3.13) describe complex phenomena evolving on time scales of nanoseconds. Neural activity may extend from a scale of milliseconds to seconds. The transient dimensions where neuronal electric events develop, together with the conductivity and permittivity of the extracellular medium imply that charges decay instantly in the extracellular space. Additionally, a study of sources of physiologic origin shows that their transient behaviour lies in mainly up to 1 kHz frequency. These are proved that influence of magnetic fields on the electric field and the existence of any free charges in the medium can be neglected in a certain frequency. Meaning that in the static case the quantities in *Maxwells Equation* are independent of time. This is valid as well for charges which move at a steady rate in time. This approximation is called *quasi-static Maxwells Equations*. In this approximation, the tissues are considered to be purely resistive with no capacitive and inductive effects. This is valid for the low stimulation frequency (close to DC) used in TENs. Based on these assumptions, *Maxwell's*

Equations reduce to (3.14–3.17) [30], [114], [136], [137].

$$\nabla \cdot D = \rho \tag{3.14}$$

$$\nabla \cdot B = 0 \tag{3.15}$$

$$\boldsymbol{\nabla} \times \boldsymbol{E} = \mathbf{0} \tag{3.16}$$

$$\boldsymbol{\nabla} \times \boldsymbol{H} = \boldsymbol{J} \tag{3.17}$$

Electrical field and current in excitable tissue

$\boldsymbol{E}$ behaves like a static field at each instant of time for both time varying and quasi–static conditions. Thus, it can be expressed from the gradient of a scalar potential, $\boldsymbol{V}$, in Equation (3.18).

$$E = \nabla \cdot V \tag{3.18}$$

The presence of the $\boldsymbol{E}$ in a conducting medium results in the flow of the charge(i.e., current). Therefore, the relationship between $\boldsymbol{J}$ and $\boldsymbol{E}$ can be identified by Ohm's Law Equation (3.19)

$$J = \sigma E = \sigma \cdot \nabla V. \tag{3.19}$$

Generally, the conduction region considered containing current sources which may occur either naturally (e.g., in the membrane) or artificially (e.g., from a stimulus electrode) can be described by a source density (current per volume parameter) $I_v(x, y, z)$ in Equation (3.20). There is two case for I_v in the volume conducting region. First, if I_v is zero, the meaning is that the volume is either source free or total current across the boundary surface is zero (net charge is zero, meaning that sources equal to sinks). If the volume integral is non zero, then the conducting region is net positive or net negative which requires compensating sources to make all sources equal to zero. These relationships between current sources and

potentials can be expressed by *Poisson's Equation* (3.21).

$$\nabla \cdot J = I_v. \tag{3.20}$$

$$\nabla^2 V = \frac{I_V}{\sigma}. \tag{3.21}$$

From a known source configuration, a solution for electrical potential V can be calculated by *Poisson's Equation* (3.22).

$$V(x', y', z') = \frac{1}{4\pi\sigma} \int\int\int \frac{I_v d_v}{r} \equiv \int\int\int \frac{I_v(x, y, z)}{r(x, y, z, x', y', z')} \tag{3.22}$$

If the I_v is equal to zero everywhere in the region of interest, then *Poisson's Equation* is simplified to *Laplace's Equation* as shown in Equation (3.23).

$$\nabla \cdot J = \nabla \cdot ([\sigma]\nabla V). \tag{3.23}$$

Choice of boundary conditions

After chosen of the volume conductor equation and its parameter (e.g., biological tissue conductivity) are set, one of the most important steps for modelling is boundary condition set of volume conductors. They are used to determine a unique solution for the whole domain. The homogeneous Neumann boundary condition insulates the boundaries which result in where no current flows out of volume conductors. These mentioned conditions can be formulated by Equation (3.24) [138].

$$\sigma \nabla V \cdot n = 0, \tag{3.24}$$

where $\boldsymbol{n}$ is the unit vector normal to the boundary. Generally, Equation (3.24) is used for insulating elements such as an air–tissue interface or surrounding insulating materials. The inhomogeneous model has a different conductivity at the boundary of different media. Equation (3.25) shows the continuity of the

normal component of the electric potential field at the boundaries in which the subscripts indicate the variables in the corresponding media.

$$\sigma_1(\nabla V \cdot n)_1 = \sigma_2(\nabla V \cdot n)_2. \tag{3.25}$$

The Dirichlet boundary condition is the most widely used condition. It consists of settings the value of the electrical potential at the corresponding boundaries. This condition sets potential at the boundaries to zero at infinity (the most external boundary ($\delta\Omega$)) as shown in Equation (3.26) [138], [139].

$$V(\delta\Omega) = 0. \tag{3.26}$$

The Dirichlet boundary condition has been used by many studies, however, this condition does not consider the potential drop that occurs at the interface between the electrode and the conductive volume [138].

The electrode–tissue impedance effect in the volume conductor can be incorporated into the boundary conditions at the interface. This may be expressed by using the following Robin boundary condition in Equation(3.27) which can be obtained by the combination of Neumann and Dirichlet boundary conditions with some modifications.

$$\sigma\nabla V \cdot n = g(V_{metal} - V_0), \tag{3.27}$$

where g refers to surface conductance of the electrode and V_0 represents voltage of the electrode on the metal side. This does not consider any capacitive effects. Only the magnitude of the impedance in a similar quasi-static condition is considered.

Numerical solution and computational considerations

The electrical potentials within domains were derived based on the relevant equations and boundary conditions in previous sections. These space and time–

dependent problems are usually expressed in terms of partial differential equations based the laws of physics. These partial differential equations cannot be solved with an available analytic method for many of geometries and problems. However, they can be approximated based on different types of discretisation which meaning approximate the partial differential equation with numerical model equations. In this section, different approaches are overviewed that can be used to solve these equations numerically and it is justified why the finite element method (FEM) was used in this thesis. These discretisation methods may be divided as finite difference method (FDM), finite volume method (FVM), and finite element method (FEM). The FDM does not allow to use different mesh size for different geometries. Thereby, to have accurate results, all geometries may be discretised with the much finer meshes. The consequence of this is that a very large number of elements will be obtained and the computation time of these simulations (especially for the low frequency that is required for TES (1kHz)) would be impractically long in reality. This approach is too slow. Although the FVM allows more detailed geometries, it is required to a deeper understanding of the underlying mathematical methods. The FEM has become a popular numerical tool in the optimisation of bio–medical applications [140]. The FEM is chosen as the numerical method for solving the partial equations. This method provides a robust numerical algorithm for approximating the solution in the discrete domain. The FEM discrete the geometries into small sub-domains which are called 'elements' whose individual solutions match accordingly to provide a global, consistent solution [137], [141]. As discussed in Table 3.1 the FEM is used by many studies due to the availability of well-established methods and platforms in solving the problem. Therefore, Simpleware ScanIP(Synopsys, Mountain View, USA) and COMSOL Multiphysics (COMSOL, Ltd., Cambridge, UK) operating based on FEM is chosen for this study.

Table 3.1: A review of studies on the human head volume conductor modelling (VCM).

Reference	Year	VCM	Approximation	Notes
[142]	2018	FEM	Quasi-static	2
[143]	2017	FEM	Quasi-static	3
[144]	2016	FEM	Quasi-static/Linear	4
[145]	2015	FEM	Quasi-static	5
[146]	2015	FDM	Quasi-static	6
[147]	2015	FEM	Quasi-static	7
[148]	2015	FEM	Quasi-static	8
[149]	2014	FEM	Quasi-static	9

Continued on next page

[2]They constructed 3D human head models based on MRI scans top quantify the corresponding current distribution and current density strength in the brain using TES electrode configurations. The DC stimulation of the current density was calculated by formulation of Maxwell's equation which was solved by the FEM and applying proper boundary conditions.

[3]This is a comprehensive review paper which is consists major of the published FEM based human head modelling about brain injury.This paper summarized all these published efforts, models, data, fining, and understandings of concussion mechanisms reported in the open literature.

[4]It was investigated the effect of changing human head structures on the electrical current density with using electrode montage types. To determine this, the quasi static based FE simulations was performed on the nine human head models which were constructed from a single MRI data set. The stimulation current level was 2mA.

[5]It was investigated traumatic brain injury based on mathematical modelling of human head. The 3D human head model was obtained from high resolution male subject MRI scan. The applied pressure on the frontal head was quantified from FEM with using quasi-static and linear elastic equations approximation and the results were compared with the experimental data.

[6]The study was aimed to investigate the effect of the microscopic modeling of the skin on internal electrical potential distributions and temperature elevation around the electrodes. The FDM was used to discrete the domains to solve potential distributions by using Maxwell's approximation equations.

[7]The human head model was constructed based on T1 weighted MRI data set to investigate the current density based on finite element models and smoothed tetrahedral finite element models. Three electrode montages were used and anode was set to 1mA and cathode was set to as ground. The electrostatic approximation was used.

[8]The multiple electrodes (73 pairs of surface electrode) were applied non-invasively auditory cortex stimulation to treat tinnitus based on current stimulation. They aimed to explore the influence of inter-individually varying conductivity profiles on optimal electrode configuration. The related tissue layers of human head was built from MRI scan of male subject and modelling current density field was calculated based on the quasi-static approximation of the Maxwells equations.

[9]Transcranial direct current stimulation was applied on the detailed anisotropic head model (constructed from MRI) to investigate long lasting changes in cortical excitability that can benefit cognitive functioning and clinical treatment. The FEM used to calculate electrical

Reference	Year	VCM	Approximation	Notes
[150]	2014	FEM	Quasi-static	[10]

Hybrid model

So far, the general concepts of the two major modelling components in the bio-modelling context have been introduced: cable models of an axon and models of the volume conductor. To calculate the response of the nerve fibre, the target nerve fibre is segmented in compartments and the stimulation potential field along the trajectory of the nerve separately calculated in the volume conductor.
The Hybrid model aims to combine these two models together, in an attempt to model the response of the neural tissue to an extracellular generated field. For this purpose, the NEURON software provides a suitable environment to calculate the response of the neural tissue to the extracellular potential along the trajectory of the nerve. Shiraz *et al.* [151] summarised the key contributions in the literature on developing hybrid models.

3.2.3 Electrode–tissue interface (ETI)

One of the important issue during electrical stimulation is electrode and tissue interface (ETI). The detailed analysis of this is beyond the scope of this thesis. The actual process is much more complex (detailed in Appendix B) but the general principles mentioned here should suffice to arrive at a functional understanding of the interface and a model. When an electrode is placed in contact with the skin, an interface is formed. The transfer of the charge from the electrode level is carried by electron while, this transfer process in the tissue medium (general

potential distribution on the head model with using quasi-static approximation.

[10] They have been developed 3D FE head model to investigate the treatment of brain disorder based on the subdural cortical stimulation. The electrical current was injected beneath the dura matter through single or array electrodes configuration and the effect of isotropy and anisotropy white matter conductivity was investigated. In addition to this, the realistic brain model and simplified model was compared. The voltage variation which induced by current was governed by quasi-static approximation.

term is called electrolyte) is done by ions. The charge can be transferred between ETI either by a non-faradic or faradic processes.

In the non–faradic process, electrons are not transferred from the electrode to tissue. Instead, it is a mechanism of the redistribution of charge in the tissue which leads to electrode polarisation. This process can be represented by a capacitor which formed by a plane of charge at the surface of the electrode and a plane of opposite charge in the electrolyte. Conversely, the electrodes are transferred from the electrode to tissue in the faradic process which resulting in reduction (electrons transfer from the tissue to the electrode) or oxidation (electrons transfer from the electrode to the tissue) of ions in the tissue. Such interactions at the ETI may provide quasi-capacitive effects. These capacitive and pseudo-capacitive effects of the ETI may be referred to as the double layer capacitor (C_{dl}).

Also, there is an actual charge transfer at the ETI depending on the level of the applied signal and the electrode material due to occurring of the oxidation and reduction processes. Thus, there are C_{dl} and the Faradic current flow involved at the ETI. Therefore, the impedance at the ETI may be modelled by a parallel combination of a C_{dl} and charge transfer resistor (R_{ct}) as detailed in Appendix B [152], [153], [154].

Besides the electrode size, the impedance of ETI also depends on the tissue properties such as anisotropy, inhomogeneous, time-variant. However, It is important to note that current based stimulation is independent of the impedance of ETI due to having serial circuits at the ETI as shown in Figure 3.4 [155]. Thus, since this study is based on current stimulation and as only the potential at the tissue side is of interest, the ETI can be ignored under the quasi–static approximation.

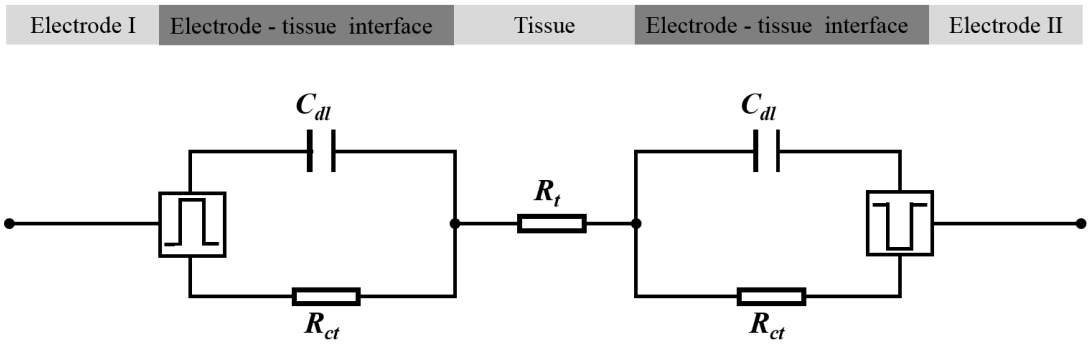

Figure 3.4: Equivalent electrical model of the bipolar electrode system. The circuit was designed based on current stimulation.

3.3 Objectives

Computational models may enable researchers to estimate current stimulation thresholds in neuromodulation therapy and investigate the effects of various parameters. Such models are usually implemented in FEM involving a volume conductor model representing various anatomical structures and the electrodes by their respective conductivities and appropriate boundary conditions. However, when the computational complexity increases, the time and computational resources may limit the investigations. Therefore, to reduce the complexity and save computation time, the human head model may be built from simplified geometries that only describe the region of interest with a level of error. First, the highly realistic human head and mammalian nerve fibre models should be generated based on an MRI. Then, simplified human head and mammalian nerve fibre models should be generated by mimicking the features of the realistic human head model. Two models can be compared based on stimulus current thresholds, safety criteria and computation cost. After obtaining marginal error between two models, the effect of microscopic structures should be investigated and the results should be compared with the simplified human head models to obtain computationally efficient TES human head model for further investigation.

3.4 Materials and methods

3.4.1 Realistic human head model development

MRI study and tissue segmentation

There is a substantial advance in image processing techniques to develop high resolution 3D medical imaging modalities. The MRI and computed tomography (CT) are most widely used techniques for reconstruction of the human anatomy. MRI provides detailed information about the soft tissues of the body and does not involve the use of ionising radiation hence is preferable over CT. Also, development in 3D scanning systems and computer-aided desig (CAD), the highly accurate 3D head and associated tissues can be easily constructed [156]. Thus, the 3D realistic model of the human head was obtained from a high–resolution MRI set. The dataset was composed of 350 slices, each of which comprised of 480×480 pixels. Voxel dimensions were $0.5 \times 0.5 \times 0.5$ mm for each of the x, y and z planes [157]. The MRI data was imported to Simpleware ScanIP v2016.09 (Synopsys, Mountain View, USA) for image processing and data segmentation. The head tissue layers, mainly, skin, fat, muscle, eyeball, skull, cerebrospinal fluid (CSF), and the brain (grey and white matter) were segmented using both automatic and manual segmentation processes. Most of the layers were given a specific grey scale threshold range to facilitate automatic segmentation process. However, it is noteworthy that manual segmentation is required for some tissue layers due to the discontinuity (such as CSF) and having similar greyscale values at the neighbouring regions. If the manual segmentation process is not applied to overcome these problems, a tissue with high conductivity (such as CSF) would considerably affect the current flow in the modelling [158]. Additionally, manual segmentation was used to correct the automatic segmentation errors using smoothing filters (recursive Gaussian, median and mean filters), edit the morphology or fill cavities (dilate, erode, open and close functions) in ScanIP

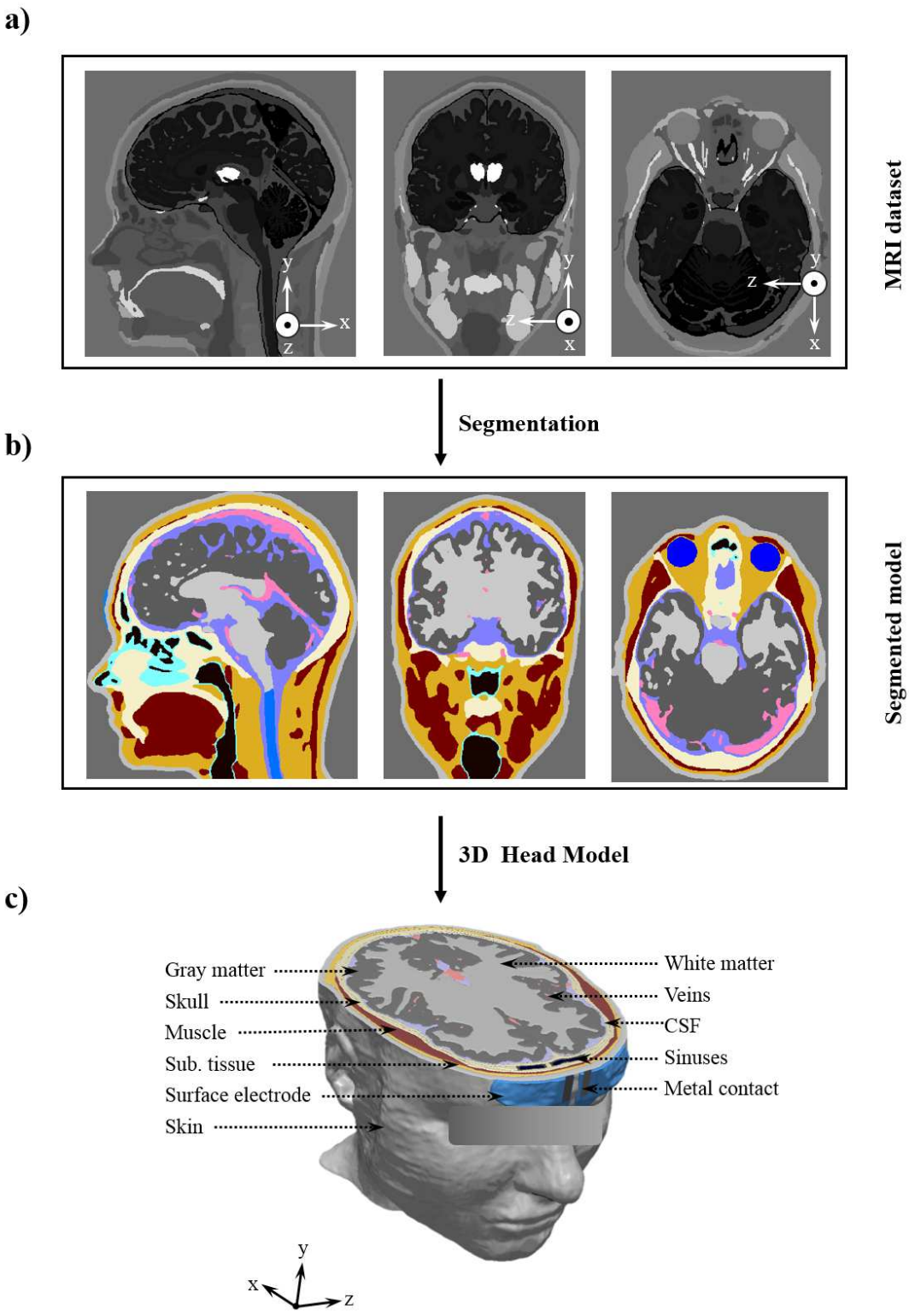

Figure 3.5: A realistic human head development process. (a) MRI data set shown in different plane for the same slice. (b) Different anatomical layers of human head are segmented based on gray value using both automatic and manual segmentation in ScanIP software; the electrode patch model is separately constructed and merged with the head model. (c) Generated anatomical layers and electrode patch are labeled.

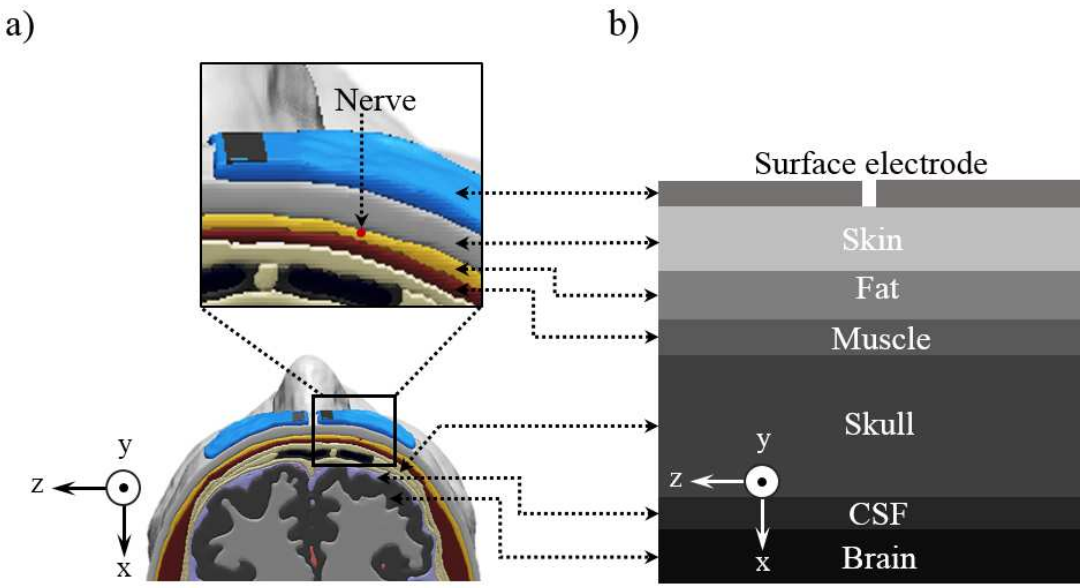

Figure 3.6: Simplified human head development. A realistic (a) and a simplified human head model (b) and relative tissue layers are shown. The small structures such as mucus, veins were not studied in the simplified model. The stratum corneum typical thickness is 40 μm and was incorporated in both models as boundary condition [1].

software. Finally, the Boolean operations were applied to remove any overlapping sections between the tissue layers.

The trajectories of the SON and STN cannot be observed in the MRI due to their relatively small diameters (i.e., $\approx$ 1mm) [159]. The 3D model of these nerves were constructed from geometric shapes (e.g.; cylinder) in ScanIP based on available literature [160], [161] . It was assumed that the human head is symmetrical. Therefore, the nerve models were generated only for the left side. The electrode model was generated separately and merged with the skin. The full list of segmented anatomical tissue layers and electrode patch can be found in Figure 3.5.

3.4.2 Simplified human head model development

The anatomically realistic model is computationally expensive and it has been shown that the human head can be represented with simple geometric shapes

(e.g.; sphere) at the cost of a level of error. Thus, to model the distribution of current flow and electric field in the tissue layers from the surface electrodes such models may be used [162]. The volume conductor model of human head tissue layers and Cefaly patch electrode were constructed from geometric shapes in COMSOL Multiphysics v5.2a (COMSOL, Ltd., Cambridge, U.K.). The head model consisted of six concentric spheres to represent the skin, subcutaneous tissue, muscle, skull, CSF and brain as the block diagram shown in Figure.3.6b. To increase geometric similarity between anatomically realistic and simplified head models, the curvature of the forehead of the simplified model was constructed to follow that of the realistic human head model. In addition, the average thicknesses of each tissue layer in the realistic model were used to construct the layers of the simplified model. However, the white and grey matters were merged and modelled as brain as the electrical potential field decays considerably inside them (The variation of the electrical potential inside these layers is shown in Figure 3.11). The same nerve trajectories were used for both of the two models to obtain sufficient accuracy. Meaning that the trajectories of the associated nerves were generated in ScanIP module and saved as standard tessellation language (STL) CAD format. Then, these were imported to COMSOL to complete volume conductor of the simplified human head. Since stratum corneum (SC) layer is thin compared to other tissue layers, it was modelled as a boundary condition at the outermost boundary of skin, defined in COMSOL as contact impedance with its typical thickness for both models.

3.4.3 Cellular structure of skin model development

Since the electrode patch, as the interface for delivering the stimulus current, is in contact with the skin, incorporating microscopic details of this layer may be important in simulating the resulting electrical potential fields accurately. Mammalian skin is comprised of epidermis and dermis layers. The outer layer of the epidermis is SC [163]. The thickness of SC is between 10 um and 50 um and

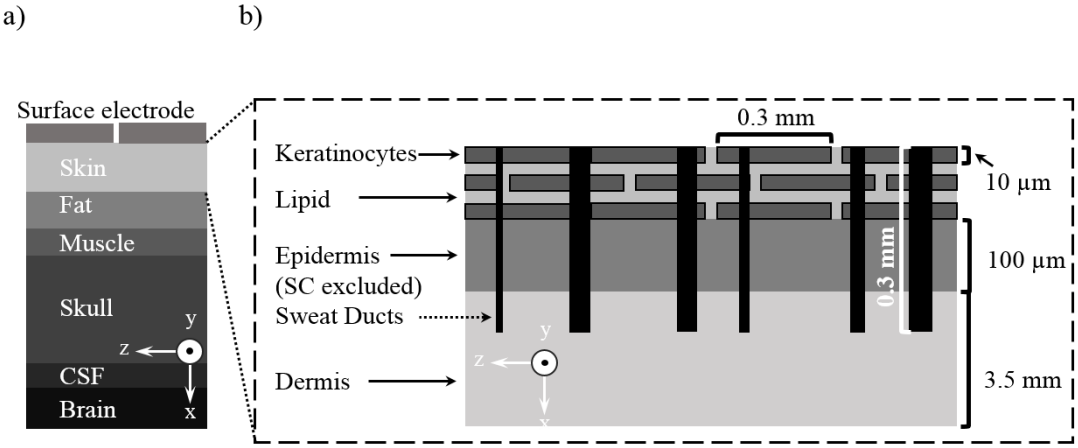

Figure 3.7: Cellular structure of skin.(a) Block diagram of the simplified human head model components, small structures such as mucus, veins were not included. (b) Block diagram of the cellular levels of the skin. The skin was divided into cellular levels and associated dimensions are displayed, the other tissue layers (e.g., fatty tissue) are not shown in (b) [1].

contains 10-20 layers of dead keratinized cells (keratinocytes) with lipid lamellae filling the intercellular regions and sweat ducts (SDs) [164]. Since the sizes of these layers are considerably smaller than other tissue layers involved, a large dimensional ratio between these structures will lead to a significant computation cost in FE models. Microscopic structures may be ignored at the cost of a degree of error to provide manageable computational requirements.

The stimulating current flows through the skin via lipid lamellae, keratinocytes and SDs [164]. These layers may have an impact on the potential distributions in the VCs which may affect percentage activation (PA) of the nerve fibres. Therefore, the cell level model was designed to examine the impact of these layers on TES modelling. The block diagram of these layers is shown in Figure 3.7a and b. Stimulation currents generally have the highest intensity underneath electrodes. Thus, only the cellular structures of the skin layer immediately below them were considered. The rest of the tissue layers (e.g., fatty tissue) were of the same dimensions as those in the simplified model. The cellular structures in the skin layer were derived from their typical morphological parameters. However, the

Table 3.2: Morphological parameters of the cellular structures in FEM. The σ_{pt}(m) shows tissue thickness which used in this study and σ_{tt}(m) shows typical thickness of each tissue [1].

Tissue layer	$\sigma_{pt}(m)$	$\sigma_{tt}(m)$	**Source**
Stratum corneum	50	10-50	[165]
Epidermis	150	75-2000	[163]
Dermis	1500	500-2500	[163]
Lipid lamellae	10	≈ 1	[165]
Keratinocytes	10	1	[165]
Sweat ducts	98±11	98±11	[164]

values of σ_{tt} of the lipid and keratinocytes were limited by the memory size of the existing PC. The typical and proposed morphological parameters of the cellular structures are detailed in Table 3.2.

The cellular structures of the skin cannot be evaluated in a simplified model of the entire head due to the computational cost. Therefore, a region of interest (forehead) with all subsequent tissue layers were considered for this study. Two models were developed for further analysis. In one, the cellular structures of skin were incorporated, referred to as the cellular model, and in the other, the microscopic structures of skin were excluded, here referred to as the simplified model. In the cellular model, the skin was delaminated into multiple layers (as shown in Figure 3.7b). The effect of the lipid lamellae, keratinocytes and uniform random variations of the SDs on the estimated current thresholds and the current density of the nerve fibres were studied using hybrid (coupling the FEM results with the NEURON model) computational modelling. The simplified and cell level models were further compared based on electrode size with respect to their current thresholds and computational features to obtain an efficient and reliable TES VC for further studies. The lipid- keratinocytes layers are crossed by SDs as shown in Figure 3.7b. These SDs start from the dermis layer and extend upwards to the surface. The average density of SDs on the forehead of human

is $3/mm^2$, their length is approximately 0.3 mm and their diameter is 98±11 μm [166], [167]. Based on the given data, the distributions of the SDs across the human forehead were generated using a uniform random function in MATLAB v.R2015b (MathWorks, Inc., Natic M, USA). SDs with various diameters were generated from smooth geometric shapes (to decrease complexity) and designed accordingly in the VC based on their average density per mm^2 in the region of interest. During the modelling of SDs in the cellular model, random spacing was chosen for x and y–direction to obtain more realistic results. It is vital to have the same trajectory of the nerve for both models for a fair comparison [1].

Electrode settings

The electrode size was assumed to be smaller than the Cefaly electrode due to the limitations of the computation. Although the same electrode size was used for both models, it is important to investigate the range of electrode sizes that minimally affect the outcome. It is assumed that the activation of the nerve fibres mostly depends on the extracellular potential variations across the trajectory of the nerve fibres [168]. Thus, if an electrode setting leads to similar extracellular potentials and PAs versus stimulus current levels variations for both simplified and cellular models, this electrode setting can be used to compare the computation features for both models. The smallest electrode size was derived from Cefaly electrodes. The parameters of this electrode were proportionally increased until they resulted in similar extracellular potential variations and PAs across the nerve fibres for both models. Four different electrode patch sizes (L×W) were used: E1:9.4×3 mm, E2:7.5×2.5 mm, E3:6×2mm, E4:4.5×1.5mm, which were parameterised and designed in COMSOL. During the electrode design, the nerve trajectory was positioned under the centre of the electrode to obtain the maximum possible difference for both models. This procedure was then repeated for each different electrode size.

In this study, the largest electrode **E1** had the smallest error between cellular and simplified models with respect to the electrical potential field and required current thresholds. This size was used to evaluate the current density and computation cost [1].

3.4.4 Finite element method simulation

Since in a complicated geometry (such as head volume conductor) the underlying differential equations cannot be solved analytically, FEM was used to compute the electrical potential distribution for all volume conductors. The model domains were discretized using tetrahedral finite elements (first order) to solve the numerical solution of partial differential equations in COMSOL to obtain electrical potential distribution on the trajectories of the nerves. For all the subsequent simulations and operations, a computer with an Intel Core i7-6700 CPU @ 3.4 GHz with 64 GB RAM was used. As the frequency of the applied pulses is relatively low, the simulation results can be obtained by means of a quasi–static approximation of Maxwells Equations in COMSOL that can be expressed through Laplace formulation. The exact methods of applying such formulations in COMSOL Multiphysics are mentioned here. In the *AC/DC* Module of COMSOL, the *Stationary* equation form selected in *Electric Currents* physics. Under this condition, the software the associated assuming equations are $\nabla.J = Q_j$, $J = \sigma E + J_e$ and $E = -\nabla V$ where J is current density, Q_j is the current source, E is the electric field and J_e is the external current density. When Q_j and J_e are set to zero everywhere in the model in *Electrical Currents* settings, a quasi–static approximation is implemented. Also, Dirichlet boundary conditions is used to obtain a unique solution for the associated volume conductor.

Boundary condition and discretisation

To ensure sufficient accuracy, the maximum element size was adjusted in the regions of interest. Whilst skin, muscle, electrode patch and nerves were meshed

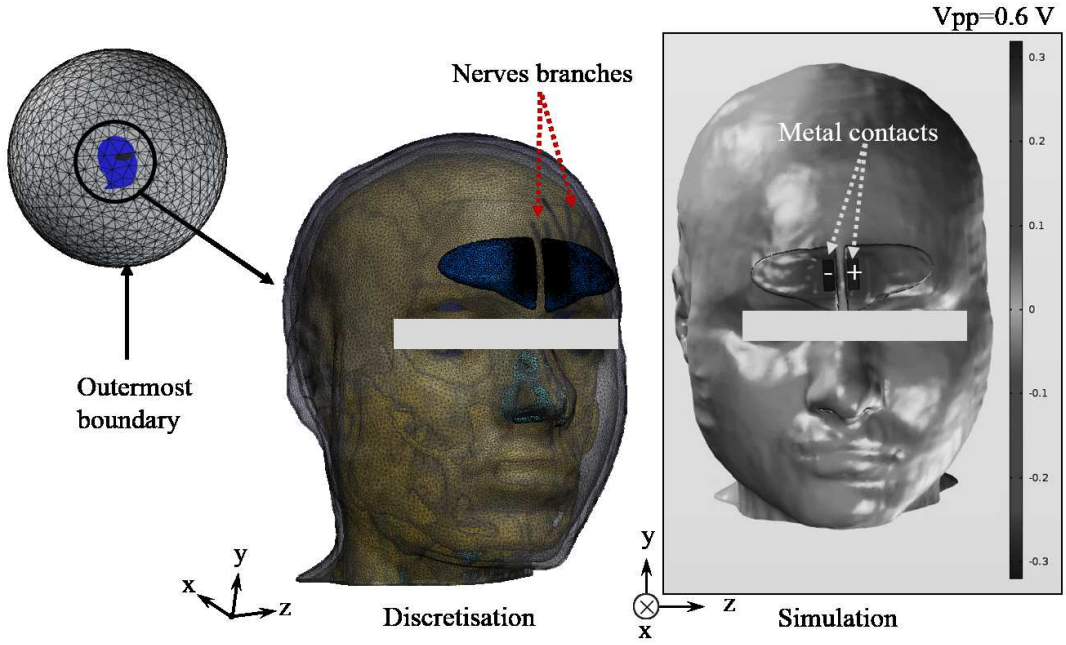

Figure 3.8: Discretisation and simulation of the realistic human head model.

with finer discretisation settings using adjusted maximum and minimum element sizes, brain and skull layers were meshed with relatively higher maximum and minimum element sizes to decrease computation cost for the realistic human head model in ScanIP. The boundary, discretisation and simulation in the realistic human head, simplified and cellular models are shown in Figure 3.8, 3.9, 3.10, respectively. As the simplified human head models composed of the smooth geometric shapes, relatively finer discretisation settings can be used to obtain optimum meshing quality. Thus, most of the domains in this model were discretised based on finer settings with adjusting maximum and minimum elements sizes in COMSOL. The same boundary conditions in the realistic one is used for the simplified human head model. The realistic and simplified models are compared with their computation features in the results section.

Since the cellular model is composed of microscopic structures and also has higher wide spatial difference ratio, the region of interest should be meshed relatively with finer discretisation settings. Thus, the maximum and minimum element sizes of the SDs, lipid- keratinocytes layers, electrode and nerve trajectory were

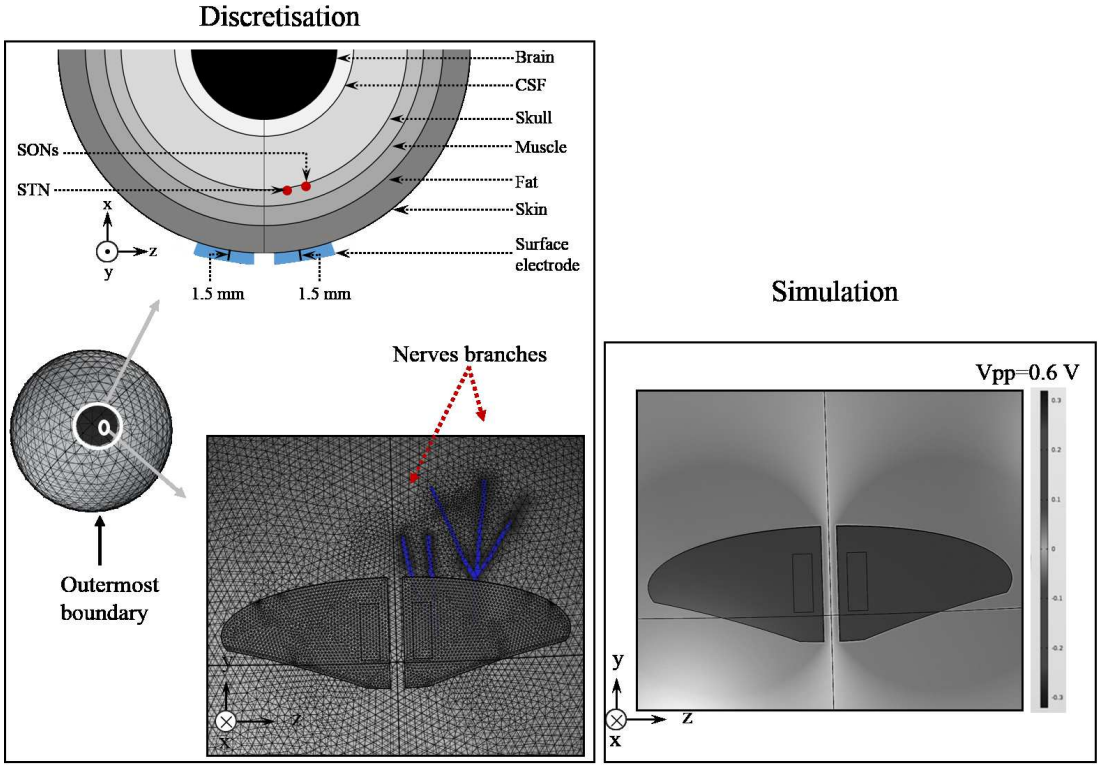

Figure 3.9: Discretisation and simulation of the simplified human head model.

selected as 1 mm and 1μm, respectively. This resulted in about 18 million elements. The discretisation and simulation features of the simplified and cellular models were compared in Results section.

Since zero electrical potential is defined at infinity in physics, a sphere with large diameter was determined around the volume conductor model to imitate the appropriate boundary. Thus, the Dirichlet boundary condition was applied to the external boundaries of the sphere. This approximates ground at infinity boundary condition. For instance, the radius of the external sphere was changed from 0.25 meter(m) to 10 m gradually. Only a shift in the voltage along the nerve trajectory was observed. This variation was less than 2% when the radius was changed from 0.5 m to 1 m. Thus the radius of the external medium was set to 0.5 m during the development of the realistic human head model. These values were the same for the simplified model as well. However, it was relatively small during the design of the cellular structure as a result of modelling just the region

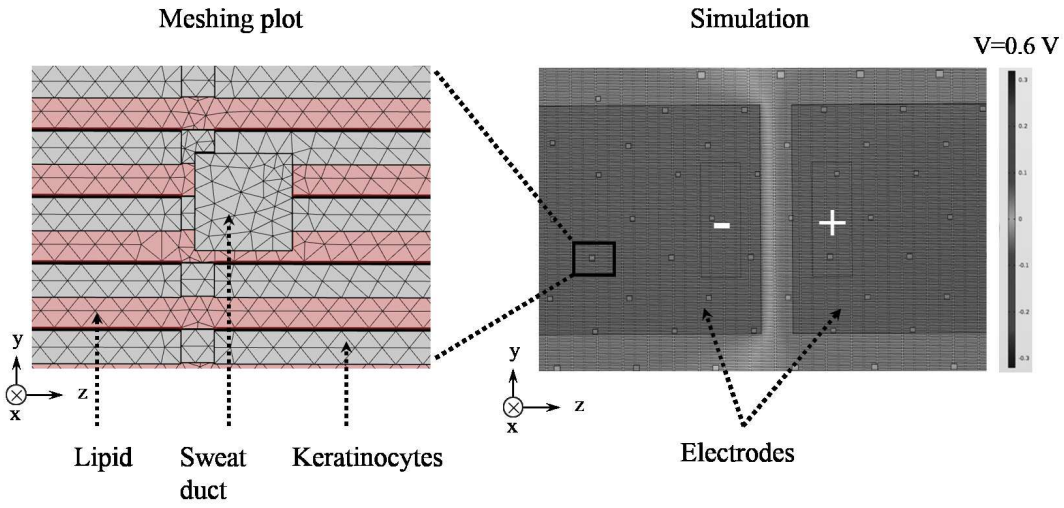

Figure 3.10: Discretisation and simulation of the cellular human head model.

of interest.

The electrode was assumed to be as equipotential surfaces on which the current density distribution was non-uniform. The metal contacts on the electrode were designed as boundary and the current level was set to positive 1 mA in the boundary of *Terminal1* for the anodes and the same value with opposite polarity for the cathodes in the boundary of *Terminal2* in COMSOL. As the stimulation is based on current–controlled bipolar stimulation setting, it is expected to that ETI has a marginal effect on the neural activations thresholds due to the impedance of the electrodes and incorporated tissue all being in series. Meaning that the same current passes through them as it has been shown in previous studies [169], [151]. Thus, ETI impedance was ignored under the quasi–static approximation as only the potential at the tissue side is of interest.

Conductivity

As we discussed earlier in this section, one of the crucial anatomical layers in the stimulation is skin. Thus, the conductivity of this layer may have an impact on the electrical current flow through the inner layer of the associated model. There is a controversial measurement data on the conductivity of the skin in the

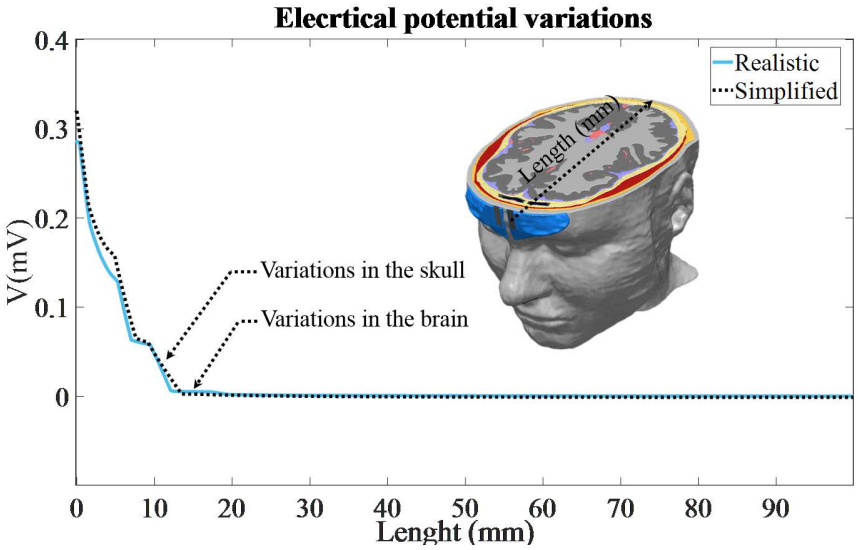

Figure 3.11: Voltage decaying in the skull and brain layers.

literature based on low frequency [18], [170], [171], [172]. For instance, the skin conductivity value of 0.1 (S/m) was used as a weighted average between the skin and the subcutaneous fat tissues. Schmid *et al* [172] used very low skin conductivity values (0.0002 S/m, at 50 Hz). However, they did not mention whether they considered several skin layers as a single layer. The study which has carried out by Gabriel and co–workers [18] were recommended the usage of low values (0.0002, at 50 Hz). However, the measurements were based on the surface of the skin and therefore mainly representative of the uppermost skin layer (i.e., SC). Yamamoto and Yamamoto [170] used the value of 0.22 (S/m) at 10 Hz for the conductivity of the skin and their study was incorporated in the literature survey published by Gabriel and co–workers [18]. The average conductivity of all the layer in the skin is about 0.2 (S/m) based on low frequency (at 50 Hz) [173] which is matched with the study of Yamamoto and Yamamoto. Thus, this value of the conductivity is used for skin in this study.

The conductivities of tissue layers were selected based on low frequencies. After generating VCs, the associated conductivity of each tissue layer was obtained to solve underlying equations. The anisotropy of the muscles and SDs were considered in their conductivities. Since frontalis muscle fibres are nearly ver-

Table 3.3: Tissue conductivities I [1].

Tissue layer	Conductivity(S/m)	Source
Skin	0.22	[170]
Sub.tissue	0.025	[174]
Muscle(long.)	0.33	[175]
Muscle(trans.)	0.11	[175]
Nerve	0.083	[176]
Eyeball	0.5	[174]
Sinuses	1.8	[177]
Skull	0.015	[178]
CSF	1.8	[177]
Brain	0.1	[174]
Gel	0.1	–

tically oriented at the longitudinal plane, the diagonal matrix of the conductivity was applied. As the SDs were surrounded by lipid and keratinocytes layers, It was assumed that the most of the current flows through the SDs in the cellular modelling study. Remaining tissue layers were defined as isotropic. The conductivities of different components are summarized in Table 3.3. Since the skin layer was divided into multiple layers in the cellular model, the conductivities in Table 3.4 were used for cellular structures. The conductivity of the outermost layer (epineurium) of the nerve was used for nerve conductivity. To highlight, the sphere (air) domain conductivity is set to a low value ($1e^{-10}S/m$) to obtain efficient voltage distribution on the volume conductor.

3.4.5 Myelinated nerve fibre model

Two main aspects are required to model myelinated nerve fibres. These are membrane dynamic which refers to distributions of the ion channels, and compartment representations are used to identify the number and type of compartments on the nerve fibre. To detect nerve fibre excitation, a double layer cable model of myelinated fibres in the frontal nerve were developed with imperfect myelin insulation

Table 3.4: Tissue conductivities II [1].

Tissue layer	**Conductivity**(S/m)	**Source**
Lipid lamellae	0.1	[165]
Keratinocytes	0.001	[165]
Sweat ducts (long.)	$1e^{-}6$	-
Sweat ducts (trans.)	0.7	[132]
Epidermis	0.1	[18]
Dermis	0.22	[18]

and implementing MRG channel mechanisms for the nodes of Ranvier [131] similar to [151]. The compartments between two nodes comprised two MYSA, two FLUT and ten STIN passive compartments. The number of STIN compartments was increased compared to the original MRG model to ensure a smooth electrical potential variation.

Aβ fibers, whose diameters followed a Gaussian distribution with a mean of $\mu_D = 12.5\ \mu m$ and standard deviation of $\sigma_D = 2\ \mu m$, were modeled based on the experimental data [26] while the associated parameters were derived by interpolating experimental measurements as shown in Figure 3.12 . The first node of Ranvier was randomly placed between 0 and Δx of the course of the related nerve, where Δx is node to node distance for a given fibre. The compartments were inserted between every two active nodes along the nerve trajectory and the fibre model was terminated by a node based on the trajectory defined in the FEM model. This process was repeated for all 100 fibers in the nerve. To generate 100 double layer cable model of associated fibers with imperfect insulation of the myelin sheath, the geometric properties of all the fibers and the numbers of compartments and their positions along the nerve trajectory were exported to NEURON v7.4 [118]. The electric properties of the channels and the underlying HH–type differential equations (which can be found in Appendix A) for the channel mechanism were obtained from the work in [131]. The electrical parameters of the fibres shown in Table 3.5. The node dynamics were extracted from the files on Model DB with

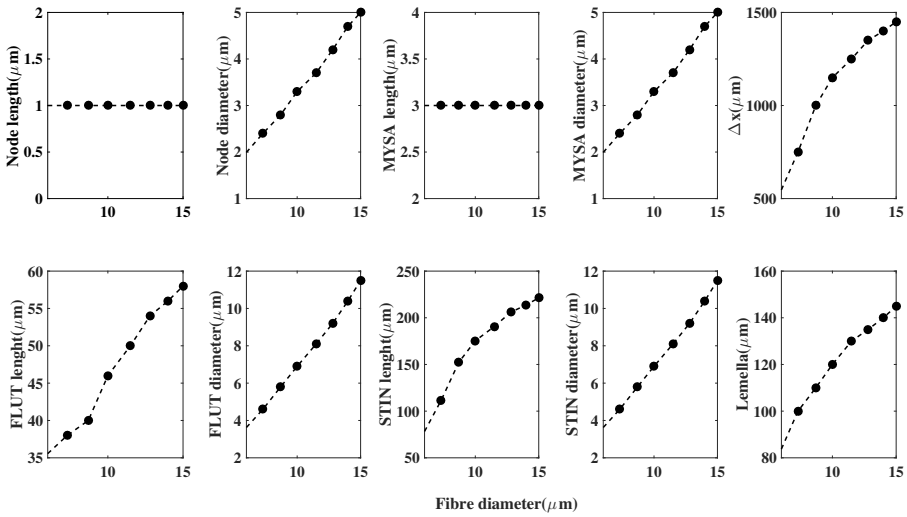

Figure 3.12: The geometric parameters of fibre models as a function of the fibre diameter based on [131].

accession number 3810 [179].

3.4.6 Hybrid model

To quantify the PAs of fibers, the electrical potential solutions of FEM were coupled with NEURON models. The electrical potential along the nerve was solved in COMSOL, interpolated in Matlab, and imported as extracellular potentials in NEURON to excite myelinated fibers. In NEURON, the extracellular potentials were pulsed as symmetrical biphasic pulses of 250 μs repeated at 60 Hz as used in [7]. For different amplitudes, the values were simply multiplied until the generation of action potential which is appropriate under quasi-static approximation. The PAs of the fibers were measured for five consecutive pulses. Only in the fifth pulse the level of current for PA = 50% remained the same compared to the previous pulse (i.e. fourth pulse) as shown in [180]. The PAs were firstly calculated for first then for last nodes for 100 fibers. A fibre was considered activated when activation potentials were observed in both.

The PAs was measured with different periods for a nerve fibre (e.g.; 1 μs, 10 μs, 25 μs, 40 μs and 50 μs) in NEURON software using Backward Euler integration

Table 3.5: Electrical features of the nerve fibre model.

Features	**Value**
Nodal capacitance (c_n)	2 $\mu F/cm^2$
Internodal capacitance (c_i)	2 $\mu F/cm^2$
Myelin capacitance (c_m)	0.1 $\mu F/cm^2$
Axoplasmic resistivity (ρ_α)	70 Ωm
Periaxonal resistivity (ρ_p)	70 Ωm
Myelin conductance (g_m)	0.001 S/cm^2
MYSA conductance (g_a)	0.001 S/cm^2
FLUT conductance (g_m)	0.001 S/cm^2
STIN conductance (g_m)	0.001 S/cm^2
Maximum fast Na conductance (g_{Naf})	3 S/cm^2
Maximum persistent Na conductance (g_{Nap})	0.1 S/cm^2
Maximum slow K conductance (g_K)	0.08 S/cm^2
Nodal leakage conductance (g_L)	0.007 S/cm^2
Na Nernst potential (E_{Na})	50 mV
K Nernst potential (E_K)	–90 mV
Leakage reversal potential (E_L)	–90 mV

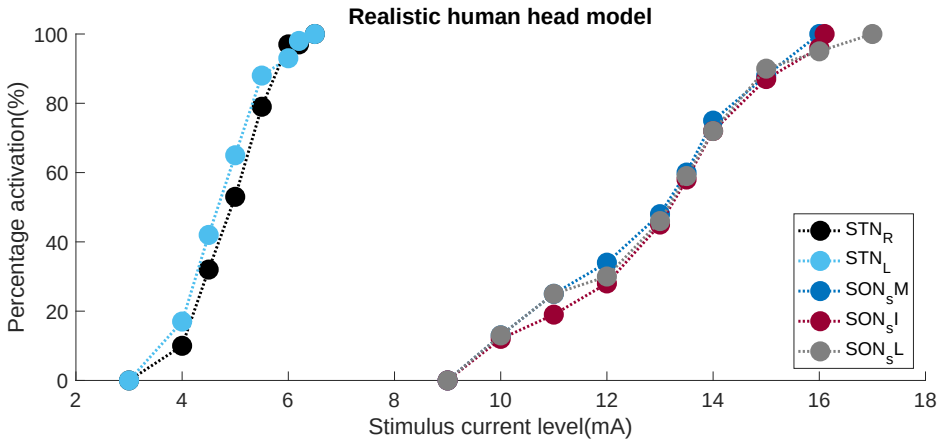

Figure 3.13: The PAs of nerve fibers for realistic human head model. The PAs versus stimulus current levels are shown for realistic head model. The SON branches are superficial medial (SONs-M), intermediate (SONs-I) and lateral (SONs-L). The STN has right(R) and left(L) branches.

method. This method requires solution of a set of nonlinear simultaneous equations at each step. To reduce the extra work, the step size needs to be as large as possible while preserving good quantitative accuracy.

It was observed that there was no vital difference (max. 2%) until 25 μs but there was substantial difference for periods over 25 μs. Thus, the underlying differential equations and the Backward Euler integration method [181] with 25 μs step was used in NEURON to obtain accurate results. To highlight, the same methods of the hybrid modelling (coupling FEM and nerve fibre cable model) is applied throughout the rest of the study.

3.5 Results

3.5.1 Neural excitation and computation cost of realistic and simplified models

The PAs of different nerve branches for different stimulus currents for realistic and simplified models are shown in Figure 3.13 and 3.14, respectively. The stimulus current thresholds at the PAs=50% for the branches of the associated nerves are

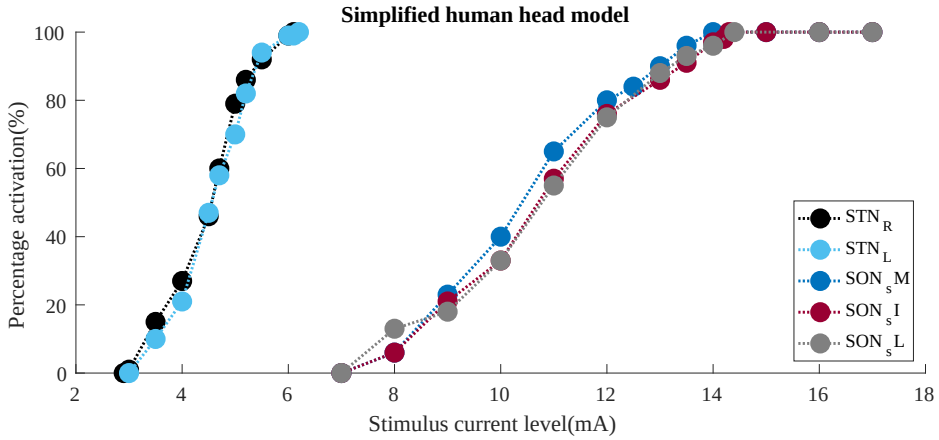

Figure 3.14: The PAs of nerve fibers for simplified human head model. The PAs versus stimulus current levels are shown for simplified head model. The SON branches are superficial medial (SONs-M), intermediate (SONs-I) and lateral (SONs-L). The STN has right(R) and left(L) branches.

compared in Figure 3.15. These results justify the required current range for both nerves in both models are in agreement with the existing device current range. The stimulus current thresholds of the STN is discussed in this paragraph for both realistic and simplified head models. The required current level variations for the branches of the STN nearly follow the same trend in the simplified model. Also, these current variations are approximately the same for the nerve branches in the realistic model. The nerves in the simplified model yield relatively smaller current levels compared to the ones in the realistic human head model. For instance, the current levels of 6.35 mA and 6.25 mA are required to activate all fibres in the right branches of STN (STN_R) for realistic and simplified, respectively. This range is 6.4 mA – 6.3 mA for the left branches of the STN (STN_L). The observation with respect to Figure 3.15 is interesting; the stimulus current thresholds at the PAs=50% for the STN_R between two models is about 2%. This difference for the STN_L is about 2.1%.

In this paragraph, the stimulus current thresholds of the SON is discussed for both realistic and simplified head models. All the SON branches are activated with relatively with high stimulus current levels in the realistic model compared

to the simplified one. Apart from a few cases, when the nerve shifted away from the polarity of the electrode, the required current is increased. Generally, the lateral branch of the SON (SONs-L) is required more current levels compared to medial (SONs-M), intermediate (SONs-I) branches. To stimulate all nerve fibres in all nerve branches of the SON, the required current levels are nearly identical for SONs-M, SONs-I branches in simplified head models. Although these nerve branches are activated with relatively high stimulus current levels in the realistic model, the current thresholds are nearly identical for the SONs-M, SONs-I branches in the realistic head model when considering 100% activation. This similarity is not valid for the SON-L branches. The same variations are valid for these nerve branches. However, the onset activation levels of these nerve fibers are quite different from each other for both models. For the 50% activation, the nerve branches in the simplified model require less stimulus current levels as displayed with bars in Figure 3.15. All fibres of SON-L are activated with 16.5 mA for the realistic and 15 mA for the simplified head models. To activate around 50% of the fibres in the realistic and simplified models, stimulation current level should be at least 4.7 mA for all branches of the STN. On the other hand, to activate 50% of the fibers in the SON, at least 12 mA is needed for simplified and 13.1 mA is required for realistic models.

Overall, diffrence in the stimulus current thresholds vary between about 3– 2% for the STN nerve and approximately 6–4% for the SON while comparing simplified and realistic human head model results.

The computation features for realistic and simplified models are compared in Figure 3.16. The segmentation and discretisation time was approximately 8 days and 26 hours, respectively, for the realistic head model. The number of tetrahedral finite elements (first order) was about 22 million and the simulation time was 19 minutes for this model. On the other hand, the required time for discretisation time was 3 minutes for the simplified head model. The number of obtained tetrahedral elements was about 2.3 million and the simulation time was 2 minutes.

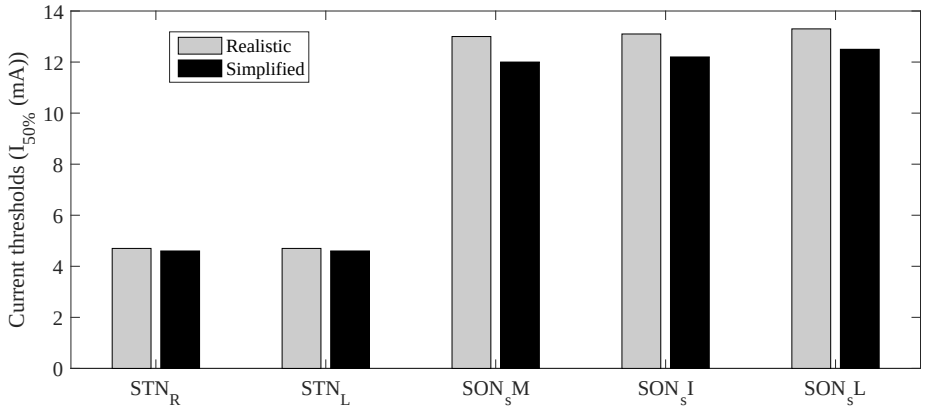

Figure 3.15: The stimulus current thresholds (PAs=50%) for nerve branches. The gray and black bars represents the stimulus current thresholds of the nerve branches in the realistic and simplified human head models, respectively.

3.5.2 Charge density

The charge per phase and charge density are important factors in determining electrode and neural tissue as discussed in safety procedures. It should be noted that current density is independent of stimulation duration and total charge whereas charge per phase and charge density refer to one pulse of stimulation. It is important to take into account that the safety limits are decided based on the charge per phase and charge density (apart from the continuous stimulation (e.g., tDCS safety limit derived based on current density)). To prevent the electrode corrosion, the safe limit for the charge– balanced stimulation is about $0.4\mu C.mm^{-2}$. The safe limit to prevent any tissue damage is about $2\mu C.mm^{-2}$ [182]. As the electrode configuration in this study is bipolar electrode configuration based on the symmetrical current waveform with $250\mu s$ stimulation phase, the charge density per area per phase on the electrode and along the trajectories of the nerves were calculated based on this electrode features as detailed in the results section. Since the same electrodes are used for all models, calculating the charge density on the one electrode should be enough to define

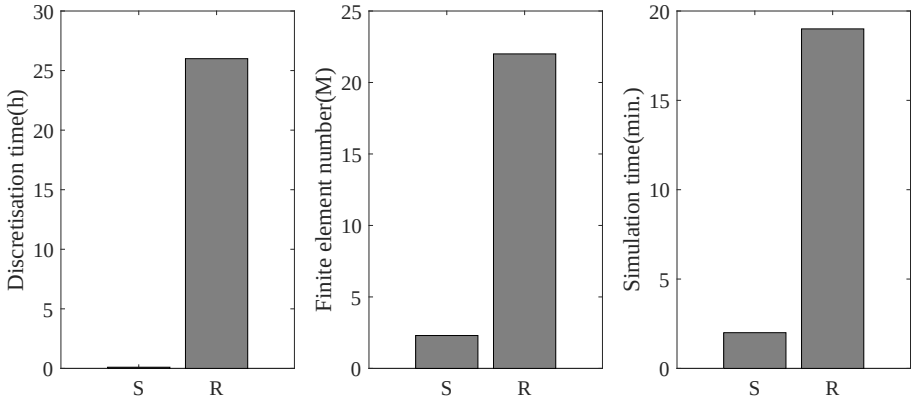

Figure 3.16: The computation features for both realistic and simplified models, R is represents realistic model ans S is used for simplified model. h: hours, M: millions, min: minutes

the limits of the safe charge injection.

The charge per area per phase on the electrode in our study was $7.6\times e^{-4}\mu Ccm^{-2}$ which is far away from the charge safe limit for the electrode. The charge per area per phase density distribution for the associated nerve branches is shown in Figure 3.17. It is clear to observe that the charge per area per phase density is relatively quite small compared to the safe limit for the tissue damage. For all the branches of the nerves, the charge per area per phase density is relatively large in the simplified model compared to the realistic human head model.

3.5.3 Neural excitation and computation cost of simplified and cellular models

The extracellular electrical potential variations across nerve trajectory and the PAs versus the required stimulus current levels for different electrode sizes are shown in Figure 3.18 and 3.19, respectively.

In Figure 3.18, the extracellular potential variations follow the same pattern for both models while the potential variations only introduce a shift along the nerve trajectory. As the electrode size is increased, this difference gets smaller and the electrical potential variation for the largest electrode size (E1) is the same

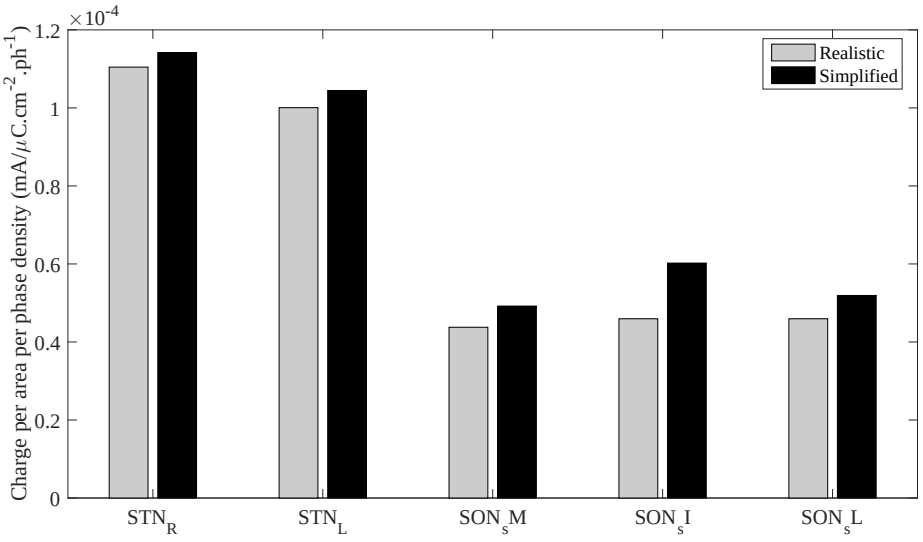

Figure 3.17: Charge per area per phase along for associated nerves. The average charge per area per phase on the trajectory of the nerves are illustrated for both realistic and simplified head models.

for both models. The trends of PAs versus current levels are similar for largest electrodes for both models. Therefore, E1 has the appropriate size for comparing the two models.

The simplified model requires just slightly higher current levels to excite the same number of fibers compared with the cellular model for all electrode sizes, as shown in Figure 3.19. The errors between current thresholds for both models are inversely proportional to the electrode size. The error is lower for larger electrodes. For instance, to activate 50% of the nerve fibers, the required stimulus current errors between the two models are 1.6% for the largest electrode and 6.8% for the smallest electrode size.

The current density variations along nerve fibre trajectory for different electrode sizes is shown in Figure 3.20. Generally, the current density variations along the nerve for the two models are nearly identical. It is higher in the vicinity of the electrode. Meaning that when the nerve away from the polarity of the electrode, the current density is decreased. The current density comparison between the simplified and cellular modes are evaluated based on based on the E1 electrode.

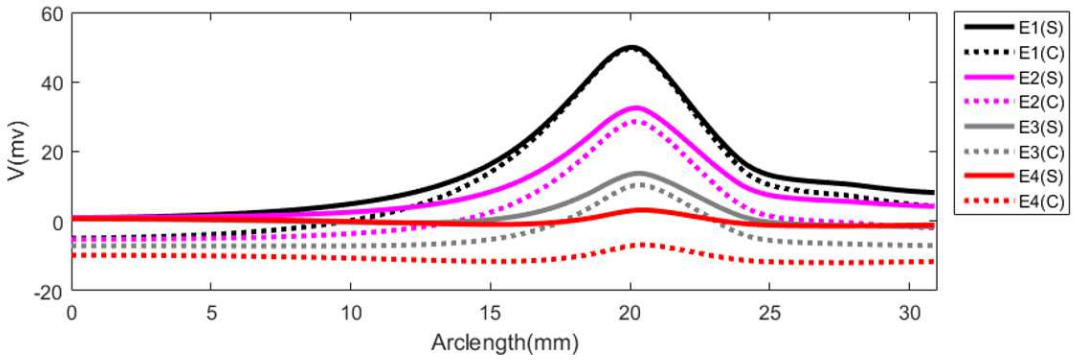

Figure 3.18: The extracellular electrical potential variations versus nerve trajectory (arc-length). The extracellular potential (V) variations across the electrode are displayed with dotted lines for the simplified model and continuous line for cellular model; E1(S): Electrode 1 for S model and E1(C): Electrode 1 for C model. E1 is designed as the largest and E4 is designed as the smallest electrodes in the models [1].

Apart from the value at the peak, the current densities follow nearly the same trend for both models. The average current densities on the nerve trajectory for two models are, in turn, 0.48 and 0.475 A/m^2 which results in $\approx 1\%$ error.

The computation features of the simplified and cellular models are compared in Figure 3.21. The required time for discretization and simulation are 0.4 hours and 0.5 minutes for simplified while these are 21 hours and 35 minutes for the cellular model. The number of elements for the cellular model is nearly 13 times that of the simplified model (1.47 M and 18.2 M, respectively).

3.6 Discussion

It has been shown that the human head can be modeled from geometric shapes (e.g., sphere) to sufficiently accurately model the current flow and electric field in the brain from surface electrodes based on computational models. Also, the effect of the microscopic structures of the skin was assessed using computational models. However, no study has compared the highly detailed, simplified and cellular human head models based on neural excitation for transcutaneous stimulation of the frontal nerve as presented here. It was discussed that bio–modelling is

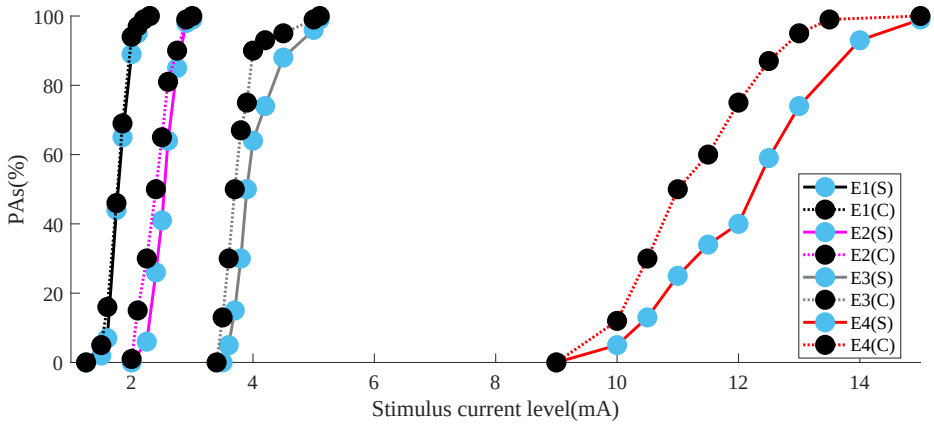

Figure 3.19: The PAs versus required stimulus current levels for four different electrode sizes. The PAs versus required stimulus current across the electrode are displayed with dotted lines for the simplified model and continuous line for cellular model; E1(S): Electrode 1 for S model and E1(C): Electrode 1 for C model. E1 is designed as the largest and E4 is designed as the smallest electrodes in the models. The current density for associated nerves. The variations of the PAs versus excitation current thresholds for simplified and cellular models are represented with circles [1].

increasingly becoming an essential step in the design and optimization of neuroprostheses. The hybrid models are the ones in which the electrical potential field is simulated in a volume conductor and is then exported into a cable model as the extracellular potential to predict the response of the nerve.

A realistic model and a simplified multi–layer volume conductor model were developed to compare the peripheral nerve excitation, charge density and computation size for both models. Also, the influence of the cellular structures on the fibre activation thresholds and computation cost was investigated using hybrid models and the results were then compared with the simplified model to reach an optimal model. To validate generated models, the boundary conditions and discretisation level was meticulously verified to ensure the model is a valid representation of the target structure. The MRG mammalian nerve fibre cable model (based on mammalian fibre data) was used which has been verified to yield reliable results by various contributions in the literature. In particular, the validity of the model for the TENS has been confirmed by Kuhn et al. [132]. It has been shown that

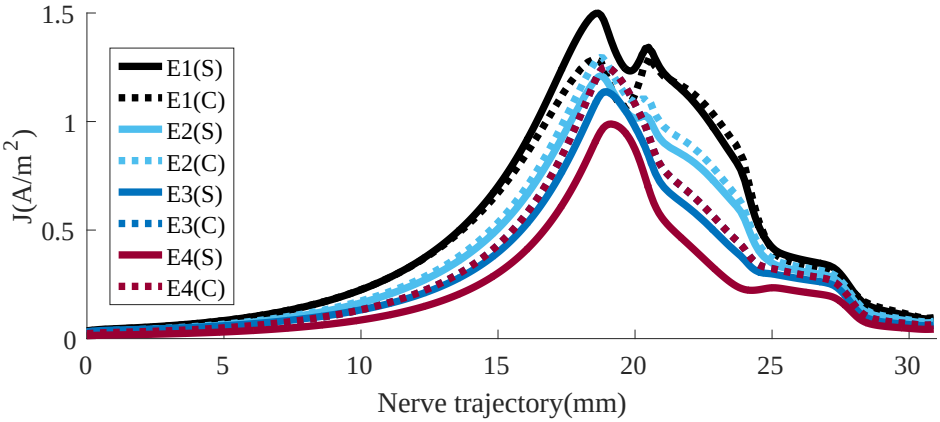

Figure 3.20: The current density for associated nerves. The current density along the trajectory of the nerves are illustrated for both realistic and simplified head models.

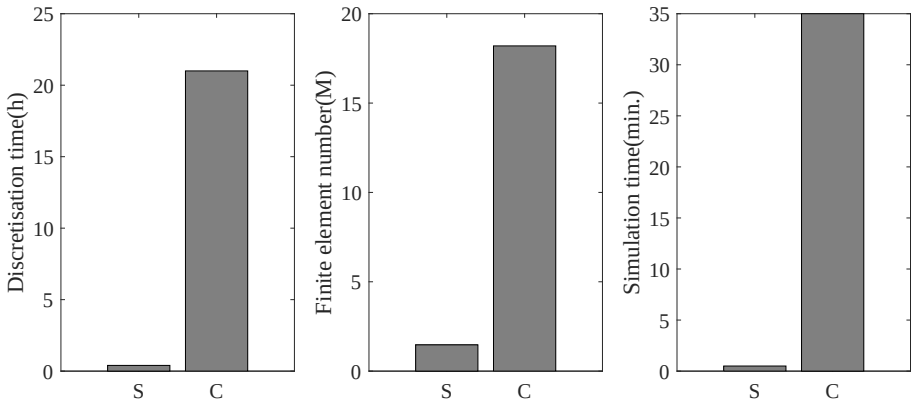

Figure 3.21: The computation features for both simplified and cellular models, S is represents simplified model ans C is used for cellular model [1].

spatial distribution of the fibres in the nerve and different fascicles on the nerve fibre current threshold can be ignored [151].

It is expected that when the nerve is shifted away from the polarity of the electrode, the requires current level is expected to be relatively high. However, this is not valid in all cases. The geometrical distribution of the nerve is vital which decide the variations of the electrical potential. As the activation of the neural tissue can be associated with the variations of the electrical variations, thus electrical potential variations are crucial in the neural excitation. Since charge per

phase determines the total volume within which neurons are excited, it can be deduced that relatively high charge per phase may activate more neural fibers. This value was relatively large in the simplified model compared to the realistic one for all the branches of the nerves as discussed in Result section. Thus, the relatively higher PAs of the nerve fibers in the simplified model was observed under the same stimulus current levels. It was shown that the nerve branches have an impact on the stimulus current level. As the SON has three branches, the current levels difference between the branches are relatively larger than the STN. One of the main reasons for the high current thresholds for the SON may be associated with the distance from of the electrodes which results in low current density. Another reason may be the variation of the trajectory of the nerve when it travels from the skull through the subcutaneous plane. Since the highly realistic human head model is complex compared to the simplified one, the electrical field variations may not be distributed evenly. Thus, all the nerve branches are activated with relatively higher stimulus current levels in the realistic model compared to the simplified one due to the quality of the mesh in the realistic human head model. Also, the results showed that there is a small difference in the charge per area per phase between two models. This can be associated to the finer details and less smooth boundaries which affect the quality of the mesh in the realistic human head model.

Although the detailed head model was constructed by explicitly defining more tissue layers compared with the simplified head model, the simulation results show that there is not a large difference between stimulus current threshold estimates ($\approx 2\%$ for STN and $\approx 3\%$ for SON at PAs=50%). However, there is a substantial difference between their computation cost. The realistic one relatively requires more computation time to solve its volume conductor.

Since the cellular structure of the skin cannot be evaluated in whole simplified and realistic human head models due to the wide spatial difference. The region of the interest was constructed for both the simplified and microscopic structures

of the skin. Both models are discussed based on the region of the interest as presented here. The highly conductive microscopic layer of the cellular model was constructed based on uniform random function in Matlab and other microscopic layers were designed accordingly. Both models were validated with respect to their boundary conditions and discretisation to ensure the model is a valid representation of the target structure.

The extracellular variations and PAs versus current thresholds of nerve fibers were used to quantify the difference between simplified and cellular models as well as electrode sizes. The results show that when the electrode size increased, the potential difference and stimulus current thresholds diffrence between two models are decreased. However, our results show that both the electrical potential field and current thresholds have marginal error in the simplified model compared with the cellular model for electrodes larger than a certain size. The trend in Figure 3.18 indicates that although the electrical potential along the nerve follows nearly the same trend for both models, the values for cellular models are negative at both ends of the nerve. This may be because of the mesh quality of the cellular model. The edge effect for current density happens in highly conductive surfaces like metals. In this study, however, for this transcutaneous setting there exists a metallic contact that is in contact with a layer of a finite but not infinite conductance (part of the electrode) which is in immediate contact with the surface of the skin on its other side. Thus, the edge effect only happens in the metallic surface but not in the electrodes surface in contact with the skin.

Although the error between the simplified and cellular models are increased when using the smaller electrode, it was observed that the slope of the PAs versus current was nearly the same for both models. The results showed that the required current levels are increased for both models when using smaller electrode sizes. This is because the smaller electrodes do not produce a field wide enough to cover the length of the nerve; thus, only the outskirts of the field will reach the nerve in that case which leads to higher required injected current to activate the nerve.

The reason for the large error between the two models may be associated with localisation of the current in the cellular structure. These microscopic structures may be more sensitive to localised changes in the path of current. This may lead to a relatively lower stimulus current being required for the cellular model.

It is noted that the cell structure just below the electrode was only considered in this study due to the high computation cost involved. However, considering a larger cellular area beneath the electrodes may have an impact on the results. This should be investigated in future studies using a workstation with higher computational capabilities.

The discretisation time, simulation time and the number of elements for the cellular model was considerably larger than that of the simplified model, indicating a vast difference in their respective computation cost.

It is very important to note that the safety limit of charge injection for the electrode and tissue should be taken into account during the designing process. The Faradic processes can be seen in the most of the neural stimulation conditions. Thus, it is important to ensure that the stimulation is not beyond the safe charge injection limits for given material and tissue. The stimulus current and current density for all models for different electrodes are within safe limits in this study [182]

Reducing the complexity of models may increase simulation efficiency by reducing simulation and discretization times. Considering the stimulus current thresholds error and computation cost between the realistic, simplified and cellular human head models, this study indicates that the realistic and microscopic features have little effect on the PAs of fibers while impose a larger computation cost. On the other hand, the simplified model is computationally more efficient and has a sufficient level of accuracy at this stage of the design. Thus, it can be used to assess the effect of the neuroanatomical variations across different individuals and electrode settings with different arrangements in future investigations.

3.7 Summary

After summarising the importance of the computational neuromodulation in the design and development of the neurostimulation therapy system, the theory behind of the nerve and volume conductor modelling was detailed. Starting from the fundamental of the HH type cable models, the general principles of the cable theory were elaborated. The fundamentals of the volume conductor models including associate equations, their approximations, the choice of the boundary conditions and the way they are solved numerically were discussed. Then, the chronological and conceptional development of the human head model based on different numerical solutions were tabulated and their key points were discussed. Focus on the main topic of this chapter, the objective of this chapter was reminded the reader as developing a computationally efficient model TES human head

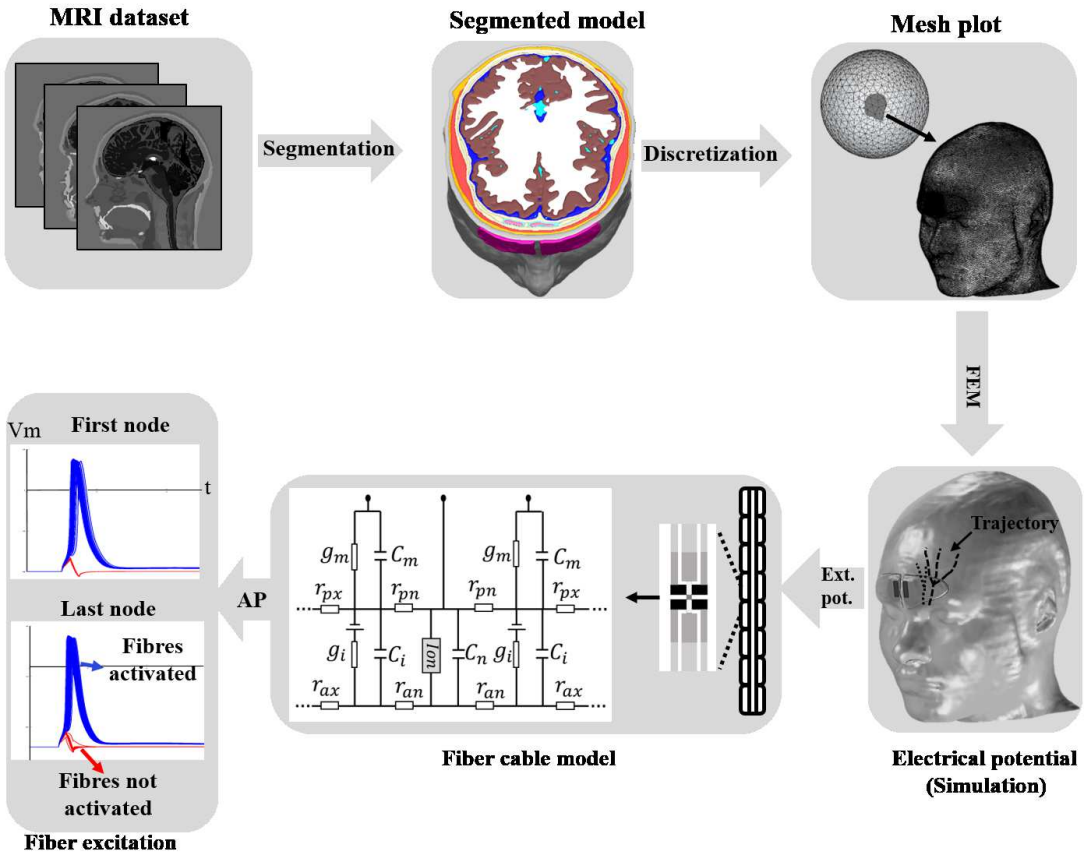

Figure 3.22: Summary of hybrid modelling.

model. Thus, to reduce the complexity and save computation time, the human head model may be built from simplified geometries with marginal error when compared to the highly detailed models. Therefore, the realistic human head was developed from an MRI data set by applying both automatic and manual segmentation processes. The 3D models of the associated nerves were manually constructed in ScanIP based on their anatomical data. Also the volume conductor of the electrodes were generated as CAD in ScanIP and merged with the head model. After generating 3D volume conductor of the human head, a sphere was surrounded the head model to obtain proper electrical potential variations on the neural tissue. Following this, the completed model was discretised with optimal meshing size and exported to the appropriate version of the COMSOL to do the simulation. The associated conductivity of each tissue layer was obtained to solve underlying equations. The electrical potential along the nerve was solved in COMSOL, interpolated in Matlab, and imported as extracellular potentials in NEURON using MRG nerve fibre model to quantify neural excitation as shown in the flow chart in Figure 3.22.

The simplified human head was constructed by mimicking the realistic human head model and the same electrode size and the same trajectories of the associated nerve in the realistic human head were used. The simplified model was constructed in COMSOL using smooth geometric shapes (apart from the trajectory of the nerve). The conductivity of the tissue and electrical simulation settings was identical with the realistic human head model. The same boundary conditions were used however, different discretisation setting was applied to obtain results in a reasonable time. The process in NEURON to measure the stimulus current thresholds of the associated nerve fibers was same for all models.

In addition to this, the skin was divided into the microscopic structures to asses the effect of the cellular structures on the stimulus current levels and electrode size. In this case, the simplified and cellular models were developed based on the

region of the interest to decrease computation cost. All layers in the simplified models were generated by following the same approach as mentioned in the previous paragraph. In the cellular model, only the skin layer was allocated into the microscopic structure and the effect of the lipid lamellae, keratinocytes and uniform random variations of the sweat ducts on the estimated current thresholds and the current density of the nerve fibers were studied using hybrid computational modelling.

This study indicates that a simplified model can be used in future work when assessing the effect of anatomical variations and electrode orientation on the efficacy of the target solution.

Chapter 4

Effect of Neuroanatomical Variations on Stimulus Current Levels

4.1 Introduction

The chapter 3 addresses the hybrid methods and human head simplification processes based on excitation of the neural tissue. Whereas, the aim of this chapter is to demonstrate the effect of the neuroanatomical statistical variations on the stimulus current levels using these hybrid methods and simplified human head models. Thus, the statistical variations of the human head size, anatomical layers (including skin, subcutaneous tissue and muscle) and the nerves and their branches are comprehensively reviewed. After discussing and tabulating the statistical variations of these layers in order, the objective of this chapter is reminded to the reader.

To obtain a comprehensive statistical distribution of human head size and subsequent layers, the variations of these layers, based on the large sample, are elaborated. Then, the variations are converted to the Normal density function in Matlab to obtain single value for both mean and standard deviation. After

designing anatomical layers based on their statistical variations, the designing of the associated of the nerves are detailed. The rest of the chapter presents the modelling of the different human head models using comprehensive automated variable generator script is implemented in Matlab and the effect of neuroanatomical variations in these models on the stimulus current levels are detailed and discussed in the following sections.

4.2 Neuroanatomical variations review

Generally, modelling and simulation are developed to observe the behaviours of real systems (and hence verifying the correctness of abstract models). The simulation results are validated by experimental results, which are considered as an empirical proof of the model's correctness. Thus, it is vital to develop a random function which covers all available significant data in the literature to obtain more accurate results. Therefore, the most accurate and common type of the statistical distribution should be used to consider all neuroanatomical variations in literature to design a random matrix variation of these layers.

The anatomy of the human head with subsequent tissue layers was detailed in Chapter 2. The statistical variations of the human head circumference and other anatomical tissue layers are elaborated in the following subsections. The available statistical distributions of these layers for different individuals were investigated in the literature. To asses the effect of these layers on the stimulus current levels, Normal statistical distributions are applied to generate the statistical relevant group of variations.

4.2.1 Human head size variation

The measurement variations of the adult head circumference are relevant for clinical and research purposes. Although the growth rate of the human head size decreases after birth as shown in Figure 4.1, it usually ends at around 21 years of age. The human head size is traditionally measured based on the occipitofrontal

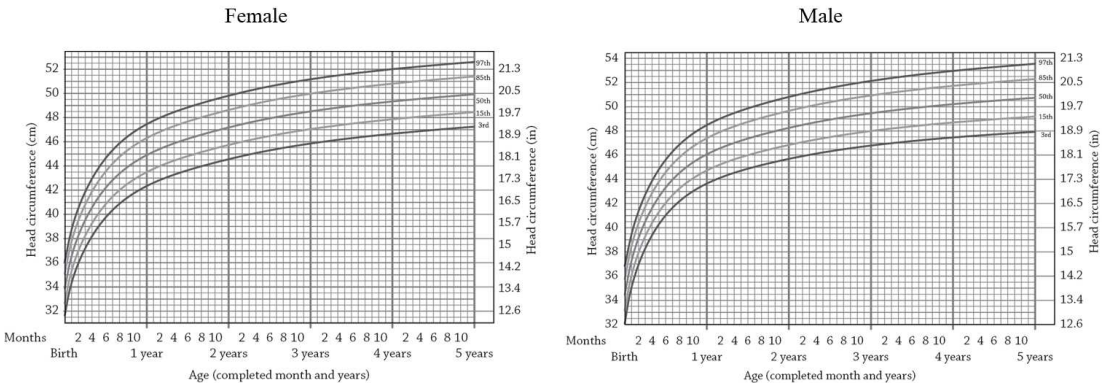

Figure 4.1: Head circumference variation based on different age group for female and male, data obtained from [183].

circumference as it embodies the landmarks of the largest circumference. Meaning that the occipitofrontal circumference has become synonymous with head circumference. Thus, the maximum head size is measured from just above the eyebrows to the area near the top of the occipital bone [183]. Human head size is calculated based on the (human head) circumference which is discussed in more detail in the following sections. During head circumference measurements, all the measurements are generally repeated and the mean is taken for further analysis by the same person. Furthermore, results are expressed as a mean and standard deviation. The variations of the human head circumference is well documented based on different ethnics, ages and genders in literature and associated mean, standard deviations and other features are recorded for each subject as detailed in Table 4.1 [184], [185], [186], [187], [188].

4.2.2 Tissue layers thickness variations

The thickness of the soft tissue layers (e.g., skin, subcutaneous tissue and muscle) varies for different sites, and in the literature, most researchers have tested the thickness of these tissues at several different sites. It is important to have accurate measurements of the variations of these layer thickness for clinical and scientific fields. The statistical variations of these tissues can be measured *in vivo* from living people and *in vitro* from cadavers. Although there is no significant

Table 4.1: Human head circumference statistical variations based on different population and gender.

	Female	**Male**	**Samples size**
Source	$\mu \pm \sigma$**(mm)**	$\mu \pm \sigma$ **(mm)**	
[184]	549.84±20.48	574.54±16.22	376
[185]	542±22	550±27	354
[186]	550±16.6	580±15.2	150
[187]	–	566.9±15.36	280
[188]	534±8	569±27	15

difference between the two studies, most researchers have preferred in the vivo method due to having lower cost and higher efficiency compared to the *in vitro* method. Generally, the thickness of this tissue layer is measured by means of the pulsed ultrasound because of it is easy to use and low risks [189].

To generate effective simulations, it is important to have an appropriate human head model which include accurate segments and their statistical variations. The thickness of the skin layer varies depending on many factors including varies considerably between different races and age–groups, between men and women, and between different regions of the body surface. The statistical variations of the skin at this site is well documented based on aforementioned features in literature [190], [191]. As the forehead site is the region of interest of this study, the variations of the forehead, epidermal and dermal are used to obtain average skin thickness. Tekama *et al.* [192] have calculated the thickness of the human facial skin for a large sample.

The layer below the skin is subcutaneous tissue layer in the forehead site. Although subcutaneous tissue thickness at other sites of the human body has been studied, the data about the thickness of this layer on the healthy human forehead is not available in the literature. The depth of frontalis muscle can vary considerably (2–7 mm) from an individual to another and on average is around 1 mm greater in men than in women [24]. A study based on human cadavers

Table 4.2: The statistical variation of the skin.

Source	Skin thickness($\mu \pm \sigma$(mm))	Sample size
[192]	1.62±0.2	170
[193]	1±0.14	14
[194]	1.9 ± 0.4	44
[191]	2±0.3	10

showed that the thicknesses of the frontal bone varies between 4.6 mm to 9.61 mm [195]. Another study showed that the statistical distribution of the human skull is 5.2±0.8 mm [196] which the variation of the thickness is covered by the previous study.

4.2.3 Statistical variation of nerve trajectory

The supratrochlear nerve (STN) and supraorbital nerve (SON) are the terminal branches of the frontal nerve, which is a major branch of the ophthalmic nerve as discussed in Chapter 2. In this section, the statistical variations of the branches of these nerves and their branches at the various layers are discussed.

The SON exits superior orbital rim and travels beneath the CSM, eventually emerging into the plane beneath the frontalis by piercing through the CSM directly or travelling beneath the CSM and emerging from the superior border of the muscle. It is generally terminated by three superficial branches as it travels in the frontalis muscle. These are classified as superficial medial (SONs–M), intermediate (SONs–I) and lateral (SONs–L). The tiny and thread–like finer nerve strands are not considered for simplification. These three branches pierce the frontalis muscle at various points and trajectories follow different variations in the subcutaneous planes as shown in Figure 4.2. The statistical variation of the branches of SON and STN in the different tissue layers and their exit points from the supraorbital rim as well as their branching points are well documented in literature [197], [160], [198], [199], [200], [201].

The statistical distribution of the SON origin is detailed in [160]. The main tra-

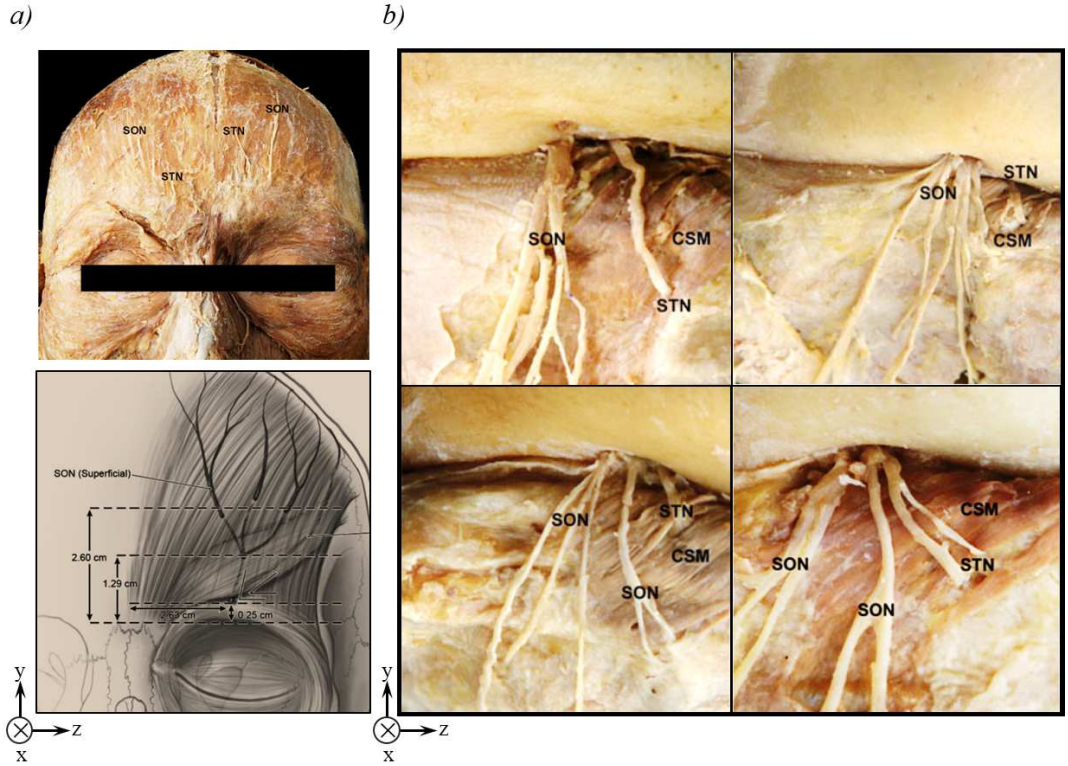

Figure 4.2: Trajectories of STN and SON nerves distribution patterns in the forehead area. The variations of the nerve trajectories over the muscle are shown in (a). The different variations of the nerve trajectories under the muscle and their exit variations are shown in (b). The data obtained from different sources [197], [160] and modified as a figure.

jectory of SON is coursed nearly perpendicular to the superior orbital rim. The average distance from the midline is 26.3±2.7 mm and the range is 21 mm–35 mm. The statistical distributions of the exit points of the SON originate from the skull is 2.5±1.6 mm (range, 0–5mm) with respect to above superior orbital rim. These statistical distributions are supported by other studies with very small error [198], [199], [199], [200]. The average depth of this nerve in the CSM is 7.5±1.6 mm. After having a short trunk in CSM, the nerve divides into multiple branches based on average mean distance (12.9±2 mm) from above superior orbital rim. The depth variation in the frontalis plane is about 4.5±1.3 mm. The SONs branches then transition to the subcutaneous plane by piercing through the frontalis muscle. This occurs at a mean distance of 26±3.2 (range, 19-32)

mm above the superior orbital rim with having 3±1 average depth variation. The horizontal distance distributions between the SON branches at the different tissue layers plane are discussed in [198].

Although there are different distributions of the trajectory of the STN, it generally passes through the CSM either as a single nerve branch or as two branches when it exits from the orbital rim. Then, it pierces through the frontalis muscle to reach the subcutaneous plane as shown in Figure 4.2.

The average distance (horizontal) of the exit point of the STN is 17.67±3.67 mm far from the midline of the forehead and the vertical distance far by 7.37±0.76 mm with respect to supraorbital rim [199], [197]. These statistical distributions are supported by another study with a marginal difference [201]. The transition point of the STN in the CSM has 16.4±4 mm midline distance and 2.3±3.9 mm above supraorbital margin [201]. The variation of the STN in the frontalis and subcutaneous planes are not available in the literature.

4.3 Objectives

As discussed in Chapter 2, the inefficacy of the frontal nerve stimulation may be associated with the neuroanatomical variations in patients where excessively high current levels may be required for some patients. Since this solution is patient-operated, the relatively high levels required are not applied. As high stimulus current levels may lead to the co-excitation of the pain fibres resulting in painful sensation. Despite all these caveats, there has been no robust investigation identifying the underlying causes of inefficacy for some patients. This is partly due to the physical limitations of studying the neuroanatomy of each subject. In computational models, neuroanatomical features can be readily changed using their statistical distributions in anatomical data, creating a powerful tool for assessing how these variations lead to different neural responses for a given electrode setting. Thus, developing realistic human head models by varying neuroanatomical

features including human head size thicknesses of the tissue layers and variations in the courses of the nerve by considering their respective statistical distributions as reported in the literature, the effect of neuroanatomical variations on the stimulus current levels can be readily investigated.

4.4 Materials and methods

4.4.1 Human head size variation design

The variations of human head size were generated based on Table 4.1. These variations are generated based on the adult age range. Thus, most of these studies were based on people 17 to 97 years old. It is important to derive a statistical variation that covers all variations in Table 4.1 to obtain more accurate results. Therefore, the most accurate and common type of the statistical distribution should be used to consider all neuroanatomical variations in literature to design a random matrix variation of these layers. The Normal distribution (also called Gaussian distribution) is the most important and occupies a central position in statistic for independent, randomly generated variables and most of the statistical theories were developed using this method. It is one of the few density functions that can be used for a large number of variables and linear combination these variables lead to new Gaussian variables.

Thus, the available data were converted to Normal density distributions in Matlab based on the given average and standard deviations of the head circumference of these subjects. Then, single mean and standard deviation were calculated based on these density functions which cover all available variation of human head circumference as displayed in Figure 4.3. To have more statistically distributed results, the difference between the circumference of any of the head models was enforced to be at least 10 mm during model designing using the automated variable generator script implemented in Matlab (it was detailed in the flow chart in Figure 4.7). The diameter of each head model was generated based on head

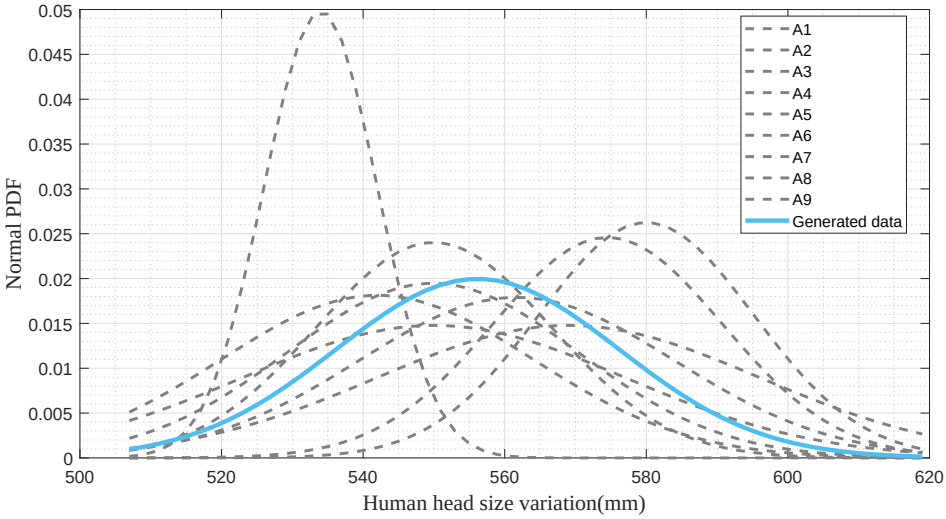

Figure 4.3: Human head circumference variation based on different studies. An average human head circumference and its standard deviation were generated based on given statistical distributions using Normal density function. A1: Available data 1.

circumference for each model to obtain variations of subsequent anatomical layers in the further steps.

4.4.2 Anatomical tissue layers variation design

The skin is an important layer for the electrical stimulation due to having an interface with the stimulation electrode, as detailed in Chapter 3. Thus, the statistical distribution of this layer should be obtained for the region of the interest. Since the electrodes have an interface with the skin at the forehead area, the statistical variation of this region should be taken into account during designing. The variations of the thickness of this layer in the forehead area are shown in Table 4.2. The study which is based on a large samples has been calculated the statistical distributions for female [192]. Since the average scalp thickness difference between male and female is about 1 mm [24], thus, the statistical variation of this layer for the general population was calculated based on this assumption. The statistical variation of the thickness of each of the tissue layer was calculated from its available mean (μ) and standard deviation (σ), as detailed in Table

Table 4.3: Anatomical layers statistical distributions.

Source	**Features**	μ**(mm)**	$\pm\sigma$**(mm)**
Table 4.1	H_c	562	22.8
Table 4.2	δ_s	1.65	0.32
–	δ_f	2.13	0.5
[202]	δ_m	1.62	0.4
[195]	δ_b	6.35	1.12
[160]	Δ_{SONs}	26.3	2.7
[197]	Δ_{STN}	17.67	3.67
[160]	d_b	12.9	2

4.3. However, there is no direct data about the subcutaneous layer thickness (δf) on the healthy human face in the literature [197] as the subcutaneous tissue is anatomically placed between the skin and muscle layers. Thus, the average thickness of the associated tissue was calculated from the difference between the average thickness of the skin (δs) and the average depth of the frontalis muscle. It was assumed that the statistical variations of the frontalis muscle (δm) are similar to the statistical variations of the corrugator supercilii muscle (CSM). Since the outermost layer of the simplified human head was modelled as skin, the radius of this layer was calculated from the normal random distribution of the head circumference (Hc) for each model in Matlab. Then, the remaining neuroanatomical layers were constructed by following the same distributions method to complete the whole head volume conductor. The statistical distributions of these anatomical layers are shown in Figure 4.4. Ten different human head models were generated based on thirteen neuroanatomical variations (eight anatomical layers distributions in Table 4.3, four different nerve variations as presented in **matrix A** and the variation of the diameter of $A\beta$ fibre in myelinated nerve fibre model section). The completed head models were named as Model1 to Model10.

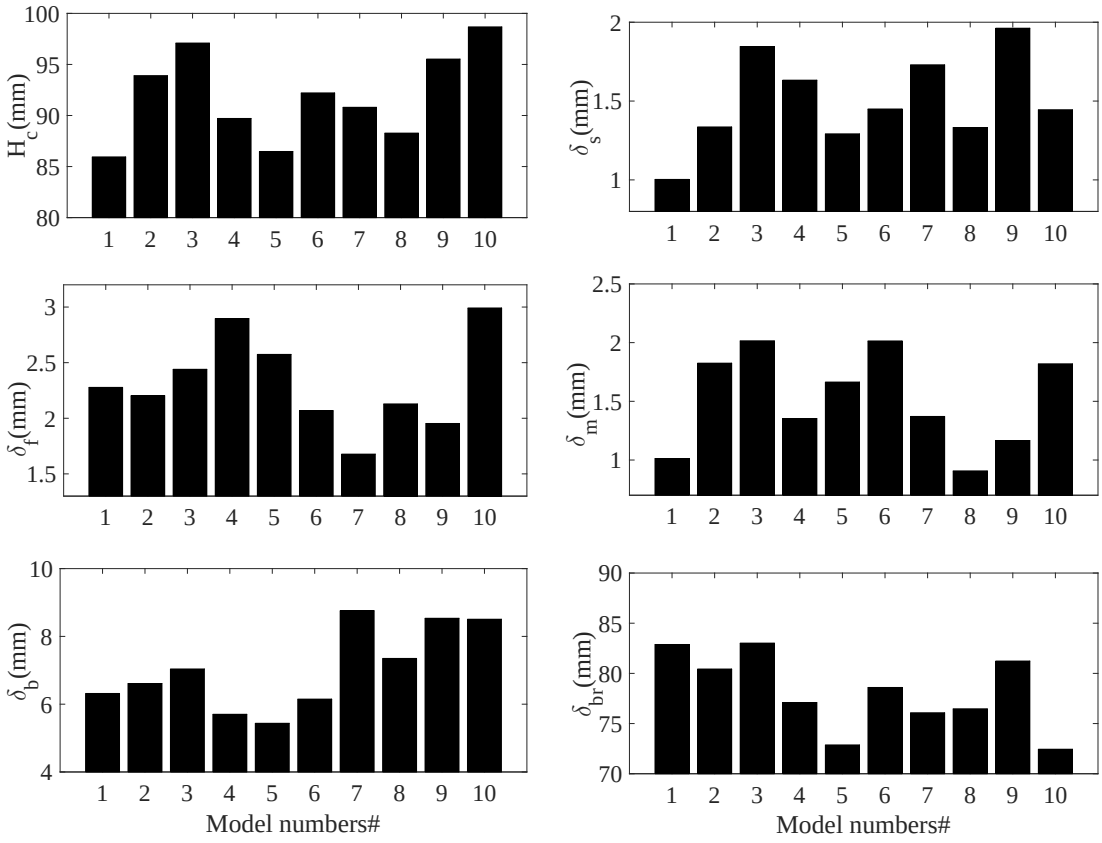

Figure 4.4: The statistical distribution of the anatomical layer of the human head. Hc stands for head circumference variations,δ_s is the variation of the skin thickness, δ_f is used for the subcutaneous tissue thickness variation, δ_m shows the muscle thickness variation and the thickness variations of the skull(bone) and brain are represented by δ_b and δ_{br}, respectively.

4.4.3 Nerve variations design

It has been shown that the variations of the exit points, the course and the branching of the STN and SON in different planes, vary for different individuals. Thus, to explore the impact of the variations on the percentage activations (PAs) of nerve fibres for a given stimulus current, these variations should be considered. The statistical variations of the course of the associated nerve branches and their exit points from the skull have been well documented in the anatomical studies as mentioned in the review section. The SONs–I was considered as a central branch. Since the SON has five transition points from the skull through the subcutaneous plane, five points (from i_1 to i_5, illustrated in Figure 4.5a) were selected along the

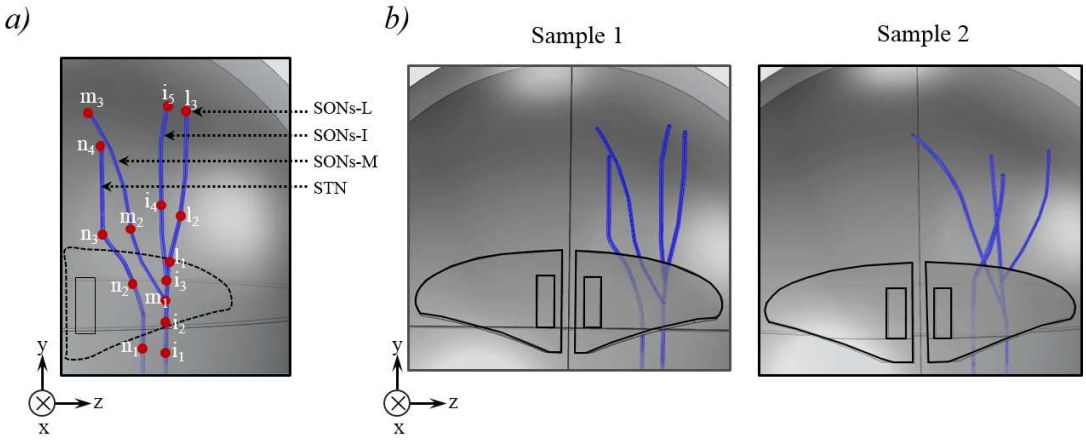

Figure 4.5: Sample variations of the branches of the nerve in the human head model, all branches are displayed in blue and the transition points of the nerves' branches are shown red dots and labelled in white; the dashed line shows the position of electrode in (a). The continuous black line rectangle represents the metal contact. (b) Neuroanatomical variations and same electrode patches. Two different variations of the nerve distribution (blue) in the human head model are illustrated; the borders of the electrode patches delineated by black curved lines.

trajectory of the SONs–I. Although the position of the branching (d_b) along the centre branch is varied, however, it generally occurs in the frontal muscle plane. Thus, to identify the variations of the SONs–M and SONs–L, the SONs–I was chosen as the reference point. The coordinates of the branching points (m_1, m_2, m_3 for SONs–M and l_1, l_2, l_3 for SONs–L, depicted in Figure 4.5a) were calculated based on anatomical studies in the literature [199], [197]. The trajectory of the SON in the skin and subcutaneous tissue layers was assumed 15 mm. Since the anatomical variations of the two branches of the STN were similar, we observed the stimulus current level is identical for these branches based on the PAs [180]. Thus, STN was considered as a single branch in this study. The trajectory and the transition points (n_1 to $n4$) of the nerve are shown in Figure 4.5a.

To generate different anatomically realistic patterns of nerve variations, the **matrix A** was implemented similar to [29] which was proposed for a different application. The variation of the x points are calculated from neuroanatomical

variations as shown in the first column of the **A**.

$$A = \begin{bmatrix} i_1^x = rb - 0.5 & i_1^y \pm 0.5 & i_1^z \pm 2.7 \\ i_2^x = rf + \alpha * \delta m - 0.5 & i_2^y + 2 & i_2^z + 2.7 \\ i_3^x = rm + 0.5 & i_3^y + 3.2 & i_3^z + 3 \\ i_4^x = rf & i_4^y + 3.2 & i_4^z + 3.5 \\ i_5^x = rf + \alpha * \delta s - 0.5 & i_5^y + 3 & i_5^z + 4.5 \end{bmatrix}$$

Here r represents the radius of the associated anatomical layer (e.g., rm: radius of muscle), α stands for uniform random variation.

Since the human head generated from the sphere, the radius (r, which represents x variation in Cartesian coordinate) of the different patterns of the nerve trajectory were calculated based on the first column of **A**. Then, the other spherical coordinates (φ,θ) were generated based on random distribution of each points of y and z in **A**. To obtain Cartesian coordinates *(x, y, z)* of each point of nerve trajectory, equation was applied as shown in Figure 4.7. To generate anatomically more realistic smooth nerve models and prevent any zigzags in the trajectory, the criteria (4.1) and (4.2) were applied for first two points of the nerves for all models. If the difference between these points is negative, the rest of the points must have met the criterion in (4.1). However, if the difference was positive, the rest of the nerve points must have met the criterion (4.2). To assure the trajectory of the nerve was derived from the orbital rim and travel through the upper area section of the forehead, the criterion (4.3) was implemented.

$$\forall(i_{k+1}^z - i_k^z) < 0 \tag{4.1}$$

$$\forall(i_{k+1}^z - i_k^z) > 0 \tag{4.2}$$

$$i_1^y < i_2^y < i_3^y < i_4^y < i_5^y \tag{4.3}$$

Where i represents the point belonging to a nerve and k indicates the transition point number. The criteria in (4.1) implied that the nerve trajectory starts from the orbital rim and travels through the midline of the forehead in z direction. On the other hand, the condition in (4.2) was applied to ensure the nerve travelled away from the midline of the forehead in z direction. The incremental trajectory of the nerve in y direction provided by the criteria given in (4.3). Since the nerve trajectory expected to have a bend in all variations, the identical consecutive points ($i^z_{k+1} - i^z_k = 0$) was not considered. Here these criteria were studied for SONs–I nerve points. The same criteria and conditions were implemented for all nerves' branches in this study.

Note that the head size and anatomical layers were generated based on the statistical distributions then the transition points of each nerve were randomly generated using an automated variable generator script in Matlab. This process was repeated for all models in sequence. Once a nerve trajectory was generated, a difference of at least 1.25 mm between x points, 1.5 mm between z points and 10 mm between y points was imposed in each case. 10 variations of each of SONs branches and STN were generated, leading a total of 40 statistical relevant group of trajectories as shown in Figure 4.6. The transition points of each nerve trajectory interpolated in Matlab then these variations were exported to COMSOL to generate 3D nerve models. Samples are shown in Figure 4.5b.

4.4.4 Electrode modelling

The 3D model of electrode patch was constructed using smooth geometric shapes and applying some available functions in COMSOL. It is important to have the same size of the electrode for all possible head models due to having a serious impact on electric field distribution (the effect of electrode size and their geometric surface are detailed in Chapter 5). Thus, the surface of each electrode was measured for each model to use a constant electrode size. The realistic human head

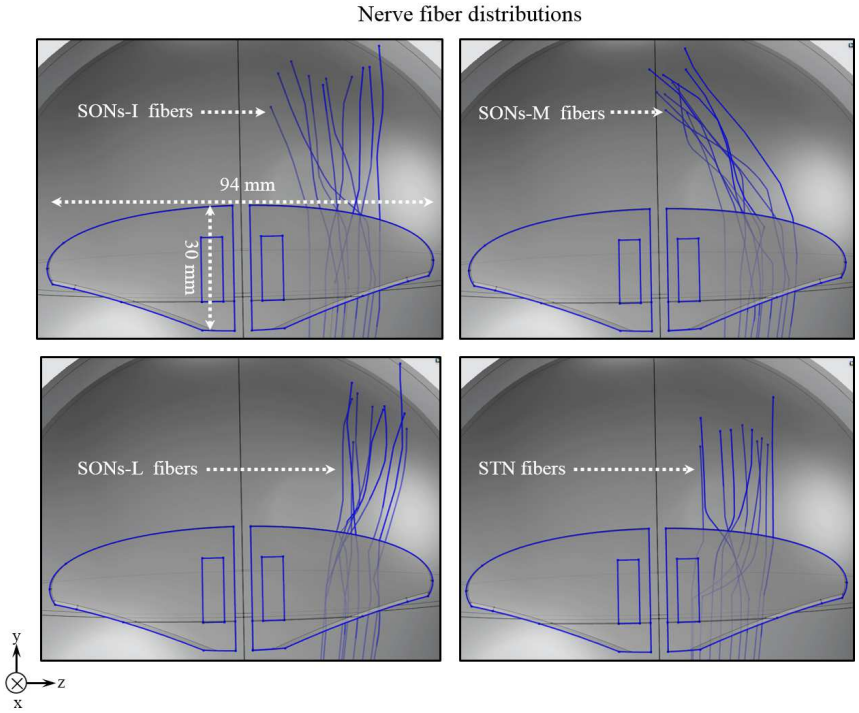

Figure 4.6: Probable and possible variations of the nerve fibre course. Ten variations of the STN and each branches of the SONs and electrode patches are shown in dark blue. Maximum human head size is used to observe all nerve fibre variations on a model.

can be generated from smooth geometric shapes, such as a sphere, as discussed in Chapter 3. To ensure the electrode patch has appropriate contact with the skin layer: an ellipsoid geometric shape (a–axis:94 mm, b–axis:80 mm, c–axis:30 mm) used to generate electrode patch using Boolean operation. After positioned this layer on the forehead area, the difference between ellipsoid shapes and skin layer was obtained. To make sure the electrode patch has full contact with the skin layer, the thickness of the electrode patch was added to the skin layer and the new skin layer was generated. Following this, the intersection of the new skin layer and difference between ellipsoid shapes and skin layer was obtained as an electrode patch. To generate metal contacts as a surface boundary, the metal contacts were unified with the electrode patches then intersection function was applied with keeping interior boundaries. Finally, some modification functions were applied to generate an electrode patch that is identical with the Cefaly electrode. The size of the constructed electrode patch for the different human head

model is depicted in Figure 4.5.

4.4.5 Completion of human head modelling

The generation of human head size, anatomical layers and trajectory of the nerves are summarised in Figure 4.7.

All 3D models were constructed in COMSOL in this section. After designing ten different human head sizes, subsequent anatomical layers and nerve trajectories in Matlab. Since the outermost layer of the human head is skin, the radius of the skin was calculated based on the circumference of the human head for each model. Then, other anatomical layers were modelled based on their statistical thickness variations whose generated in Matlab. Each nerve fibre points were interpolated with higher numbers to obtain a smooth but realistic nerve trajectory before generating the 3D model of nerve model. The trajectories of the nerves were generated using either sweep or Loft tools. Sample nerves are shown in Figure 4.5b. The results show that the branches of the STN nerve have a similar variation of the stimulus current thresholds [180]. Thus, a single branch of the STN was considered during the designing of the nerve variations. After the human head, the electrode patch was merged with the skin which was detailed in the previous section. To have a unique and accurate solution, a large sphere (r=50 cm) was defined around the model. Then, the model was unified and features of each tissue were attained to obtain a solution for this model as detailed in the following sections. This process was repeated for modelling of ten different head models.

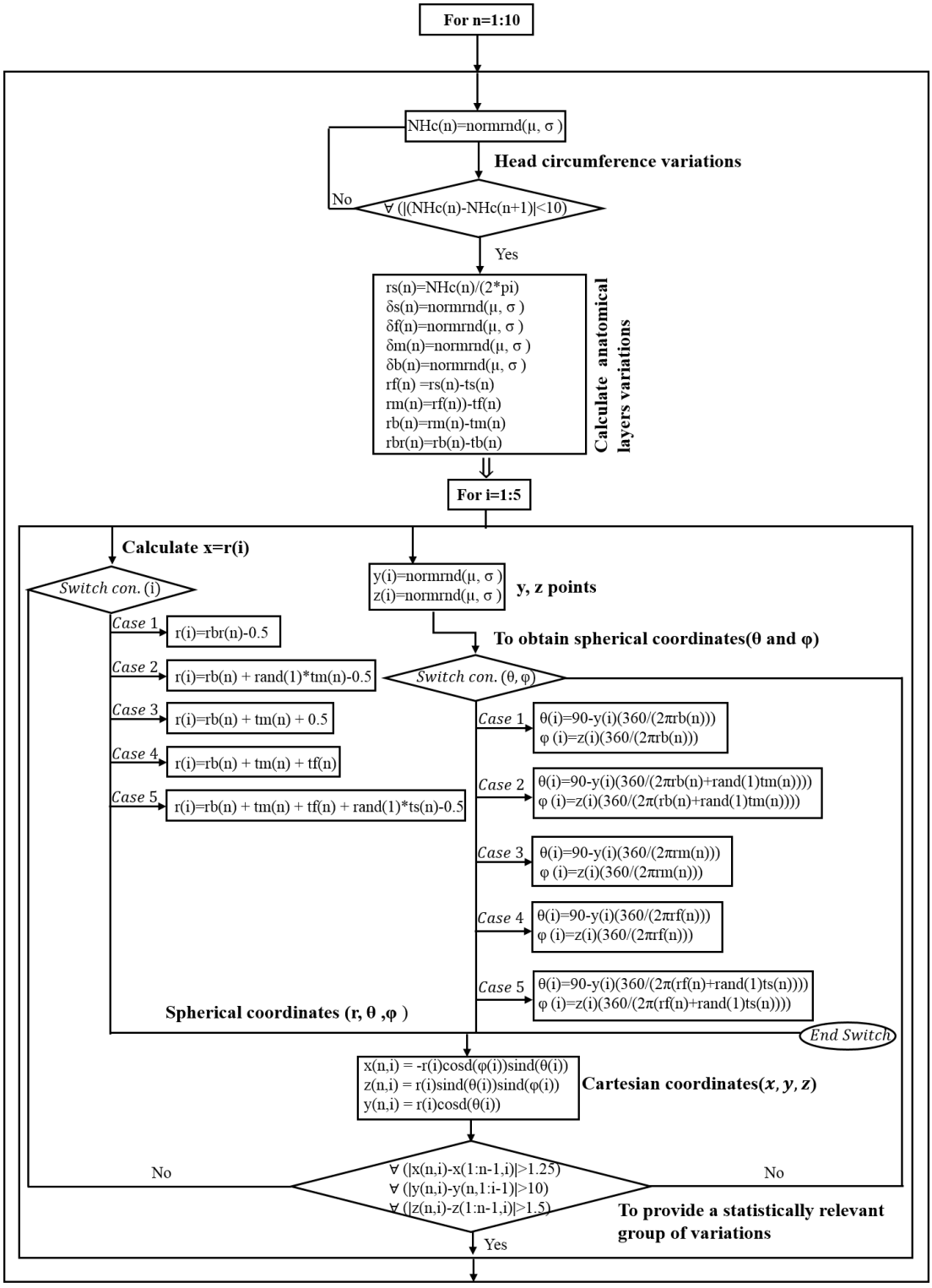

Figure 4.7: The flow chart of the completion human head modelling.

4.4.6 Finite element method discretisation and simulation

The model domains were discretized using tetrahedral finite elements (first order) to solve the numerical solution of partial differential equations in COMSOL. Since the model was composed of geometric shapes, the domains can be meshed with finer discretization settings to obtain optimum meshing quality (without increasing computation cost). Thus, electrode, skin, subcutaneous tissue and muscle were meshed using a minimum element size of 1 μm and the remaining tissue layers had maximum mesh element size of 0.1 mm. Meshing for the nerve model is challenging as the nerve passes through multiple layers. Thus, the mesh settings for the nerves were adjusted to different sizes for different models. Since the outermost layer (sphere) was far from the region of interest, the maximum element size was selected to be larger than the other layers. The number of finite elements varied between approximately between 7–10 million during the discretization process. It is important to note that the discetisation and simulation time was recorded in minutes and seconds levels, respectively.

As the frequency of the applied pulses is relatively low, the simulation results can be obtained by means of a quasi-static approximation of Maxwell's Equations in COMSOL that can be expressed by Laplace equation. In this approximation, the tissues are considered purely resistive with no capacitive and inductive effects.

As it was discussed in Chapter 3, since zero electrical potential is defined at infinity in physics, a sphere with large (50 cm) diameter was determined around the volume conductor model to imitate the appropriate boundary. Thus, the Dirichlet boundary condition was applied to the external boundaries of the sphere. This approximates ground at infinity boundary condition. The current level was set to positive 1 mA for the anode and the same value with opposite polarity for the cathode.

4.4.7 Myelinated nerve fibre modelling

The associated of nerve fibers (frontal nerve) were modelled based on the myelinated $A\beta$ nerve fibre model as introduced in Chapter 3 that are summarised here. The nerve fibre excitation was quantified via TES using the McIntyre-Richardson-Grill (MRG) cable model of a myelinated mammalian axon [24]. Fibre distributions and the number of compartments and their geometric positions along the nerve length were designed based on the previous study [180]. The obtained extracellular electrical potential was then exported into NEURON v7.4 [118] to form voltage pulses and apply them to a population of the double layer cable model of mammalian fibres to simulate responses of fibres' [180]. This process was repeated for all nerve fibres of the STN and SON.

4.4.8 Hybrid modelling

The percentage activation (PA) of fibres was measured based on the fifth current pulse with the Cefaly stimulator parameters (biphasic, symmetric current pulses with a duration of $250\mu s$ and a repetition frequency of 60 Hz were applied) [180]. The nerve cable models were imported in NEURON to solve the underlying differential equations using the (Backward Euler) integration method with 25 s steps. The PAs were (firstly) calculated for the first node for 100 fibres and then for the last node. A fibre was considered activated when activation potentials were observed in both. The PAs versus required stimulus current levels for STN and SON branches(SONs–I, SONs–L and SONs–M) nerve were recorded for each model to compare in the further steps. This process was repeated for ten different head models.

It was observed that the PAs are very sensitive to the stimulus current levels until PAs=50%. Then, relatively high current levels are required to increase the nerve fibres' PAs for all models. Therefore, PAs=50% was chosen to compare nerve models for all generated human head models.

4.5 Results

4.5.1 Nerve variation on stimulus current

The PAs of the fibres with respect to the required stimulus current levels for different nerve branches based on ten different models are shown in Figure 4.8. The variations of the PAs versus stimulus current levels are shown in different colours and modelled as M1 through M10. M1 shows the lowest current levels variations for all SONs–I, SONs–L and STN nerve variations. However, M8 has the lowest pattern of PAs versus stimulus current level for SONs–M. Conversely, the highest requires current range variation is in M6 for STN while, this highest range variation is in M10 for the branches of the SON. It can be derived from Figure 4.8 that the required current levels for STN are relatively smaller than the branches of the SON when comparing each specific model. From the SON nerve branches, generally, the highest current levels are required for the SONs–L nerve branches for all nerve variations.

4.5.2 Neuroanatomical variations on stimulus current

The effects of the neuroanatomical variations on stimulus current levels based on PAs of different nerve branches are shown in Figure 4.9. The nerve fibre current thresholds variations in STN, SONs–M, SONs–I and SONs–L are represented by the first, second, third and fourth bars, respectively, for each model in all subplots figures (except the last subplot figure). The required current levels at the 50% activation of fibres are identified with changes in the jet–scale of the bar for all neuroanatomical variations. The effect of the statistical variation of the skull was not studied as the nerves' emerging points travel from the skull through other planes. The statistical variation of the skull was employed to provide different emerging points based on anatomically realistic nerve variations.

In general, there is no obvious relationship between the current threshold levels

and changes in the thickness of the skin. The only significant changes in the stimulus current thresholds and the thickness of the skin can be seen in M8 for SONs–M nerve fibres where the current threshold and the thickness of the skin show their minimum values. There is a direct relationship between the thickness of the subcutaneous tissue and required current thresholds in M10 (the biggest head size) for all nerve branches. Otherwise, there is no such correlation between remaining models and nerve branches. When the thickness of the muscle varies, the threshold of the STN varies in the same manner (apart from M4). Apart from a few models, the variation in the thickness of the muscle and PAs of the nerve fibres follow the same trend for all SONs branches. The relationship between Hc and $I_{50\%}$ is that the relatively small head size is stimulated with lowest current level while the largest head size is activated with the highest current levels for all neuroanatomical variations. The nerve exit points from the orbital rim with respect to the midline of the head (Δ) are the same for SONs branches, while the STN has different exit point variations. Although a lower current level is needed to activate the nerve fibres for smaller variations of Δ, the results showed that this is not valid for all nerve variations. The results indicate that the variations of the nerve branching point (db) has an impact on the activation of nerve fibres of the SONs–M and SONs–L. In general, the required stimulus current levels are lower for SONs–M branch compared with those of the SONs-L branch for all nerve variation models. Such variations are not observed for the centre branch of the SON for all models.

Overall, it is observed that the minimum required current level is 6.2 mA to stimulate STN fibres and the maximum current level is 33 mA to activate SONs-L fibres. This latter level may be beyond the range of currents which can be safely applied in this application.

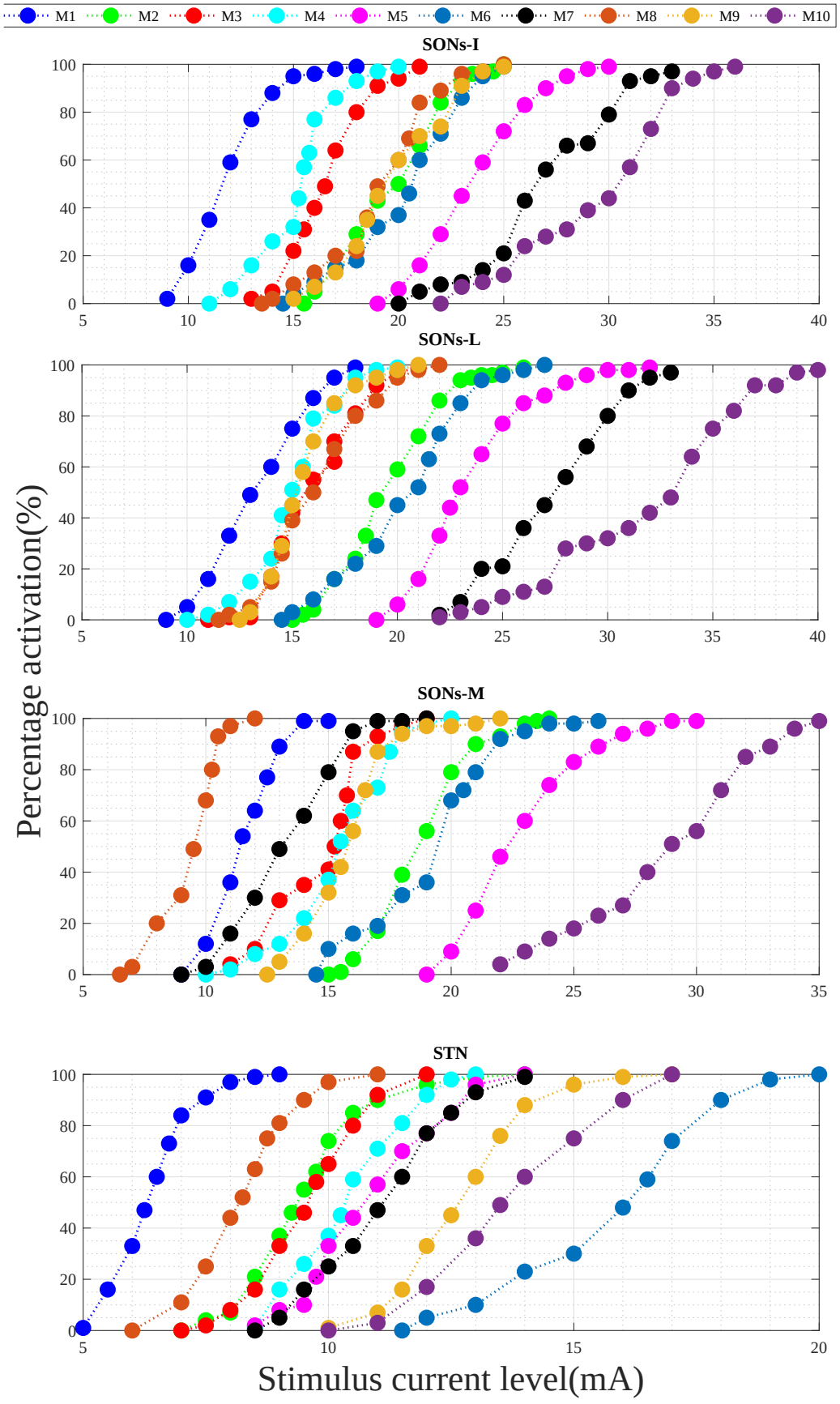

Figure 4.8: The percentage activation versus the required current amplitude for different nerve trajectory using ten different human head model.

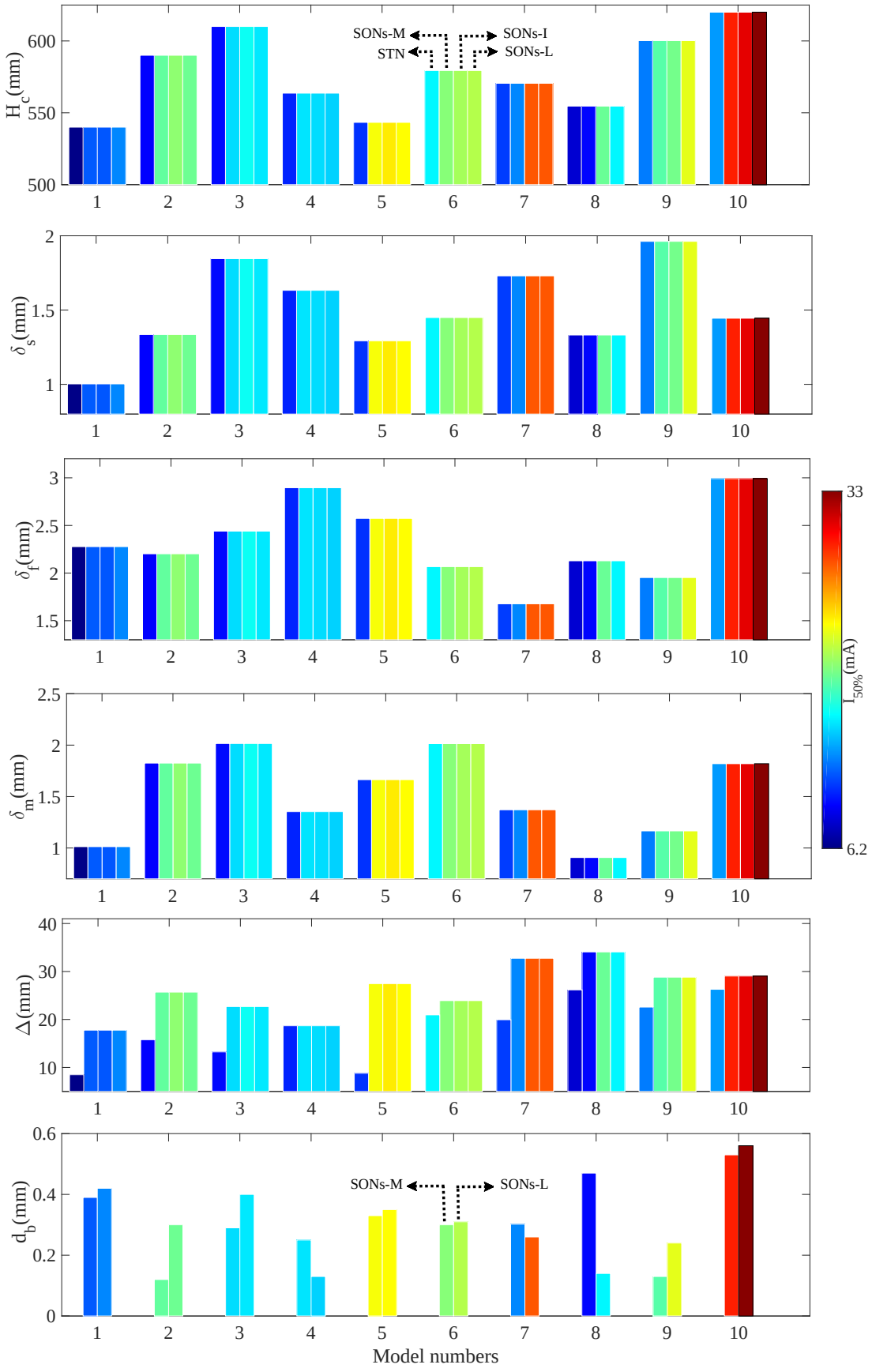

Figure 4.9: The effect of neuroanatomical variations in the human head on the stimulus current levels based on 50% of fibres activation for ten different head models.

4.6 Discussion

Bio–modelling is growingly becoming an essential step in the design and optimization of neuroprostheses [151], [203], [204], [205]. In such models, the electrical potential field is simulated in a VC and is then exported into a cable model as the extracellular potential to predict the response of the nerve.

In Chapter 3 the simplified model is discussed and found to be more computationally efficient and will take considerably less time to obtain extracellular electrical field on the trajectory of the neural tissue. Also, it has a sufficient level of accuracy when comparing the realistic and cellular human head models. Therefore, a more elaborate matrix of variations of neuroanatomical structures and the neuromodulator may be readily developed to produce a statistically relevant model of the patient group using the simplified human head model.

In this chapter, the effect of neuroanatomical variations on nerve fibre activation thresholds was investigated using such models. To provide a statistically relevant group of variations, incorporating the possible variations of the nerve trajectories and other anatomical structures, samples of the entire statistical distribution of each variable was included for each case. This ensured that the variables are sufficiently separated in their respective distributions. The process of generating the entire ensemble (including the Cartesian coordinates of the trajectory of the nerves, the thicknesses of each layer and head sizes) took in excess of a day using the automated variable generator script implemented in Matlab.

The PAs of each of the nerves were assessed and the activation current levels were recorded for each nerve model accordingly, based on Cefaly stimulator parameters (biphasic charge–balanced rectangular 250 μs pulses at 60 Hz) [7]. The variations of the PAs (from 0% to 100%) versus the required stimulus current levels for all nerves and their subsequent branches were recorded and crucial points were analysed. Then, the effect of neuroanatomical variations on the stimulus current levels was investigated based on PAs=50% for all nerves and their

branches. This process was repeated for all generated statistical relevant group of variations. The results suggest that anatomical variations have a substantial influence on stimulus current levels with no feature being dominant, suggesting that it is a combination of variations which contribute to these effects. Additionally, since the trajectories of the nerves emerge from the skull and travel through the subcutaneous plane, the anatomic landmarks of the nerves in these tissue layers vary for each subject [160], [189]. Thus, the activation of nerve fibres may depend on anatomical and electrical features of these elements. Another factor that might affect the outcomes of this study could be the position of the nerve trajectory with respect to the simulation electrodes. Due to some variations of SONs-L being further away from two electrode orientations, this nerve branch generally requires high levels of stimulus current when compared to other nerve branches. The nerve fibres of the STN are generally activated with the lower current thresholds compared to SONs. This may be due to the variations of the exit points of the STN from the orbital rim, which is mostly closer to the centre of the electrode. Also, its trajectory generally travels under the electrode. The importance of variations of the position of the nerve was shown in the previous work [180].

The results based on neuroanatomical variations suggest that the required current levels to activate the target nerve (both STN and SONs branches) in all variations (ranging from 6.2 mA to 33 mA) were beyond the current delivery capabilities of Cefaly device (1 mA to 16 mA) in 50% of variations. This may imply that in 50% of cases the required level of current to stimulate the nerve cannot be delivered, leading to device inefficacy. It was shown in this thesis that in all cases STN is stimulated at relatively low current levels compared to the branches of the SONs. Referring back to existing clinical study, 50% response rate has been observed using Cefaly electrode setting. It may be inferred that the inability of the device to stimulate SONs at relatively low threshold may be cause of the ensuing reported inefficacies. It is noted that the device is patient operated

and referred pain may be induced at considerably at lower current levels below the maximum current capabilities of the device. This can further limit patient compliances and subsequently the efficacious of the solution.

It was assumed that the statistical variations of the human head circumference and thickness of the skin were generated based on normal distributions. Another limitation of the study is to the variations of the human head and the thickness of the skin were calculated based on the mean of mean and mean of the standard deviation. However, the new mean and standard deviation of multiple studies can be generated based on Forest plot using meta–analysis to obtain more accurate variations, as detailed in [206].

4.7 Summary

The statistical distribution of the of the human head size, subsequent soft anatomical layers and trajectories of the nerve and their branches were reviewed. Due to the importance of the human head size, skin layer and nerve trajectories, the statistical distribution of these layers were critically investigated. After reminding the objective of the chapter to the reader, the process of the designing of the neuroanatomical layers were introduced. Starting from the human head size, the design of the anatomical layers and nerve variations were detailed. After discussing the importance of using the same size of the electrode for all models, the process of the generating the statistical relevant group of variations and their modelling (complete human head modelling) were elaborated and summarised with flow chart. Then, the finite element discretisation and simulation processes for generated models were discussed. The importance of the different disctretisation settings for the generated nerve models were detailed with their maximum and minimum element sizes. Then, the methods of obtaining electrical potential distributions in the domains were briefly mentioned. The myelinated nerve fibre and hybrid modelling were summarised then the results and disscussion sections

derived. The required current levels versus stimuls current for all generated statistical nerve distributions and their branches were displayed and detailed. Also, the effect of neuroanatomical variations on the stimulus current levels were displayed (as PAs versus current) and compared in Result sections.Based on available data, the critical points of the effect of neuranatomical statistical variations on the stimulus current levels were analysed.

The findings, in this study, indicate that neuroanatomical variations have a significant impact on the stimulus current thresholds but it is not possible to conclude if these thresholds solely depend on a specific neuroanatomical variation. The relatively high required levels of the stimulus currents are beyond the current capabilities of existing device and possible pain thresholds. Furthermore, considering the previous study, it may be inferred that the stimulation of SONs has a significant role in target solution when compared to the stimulation of STN.Thus, new electrode arrangements was aimed to design as a further study to optimise the required current thresholds levels and reduce the patient discomfort.

Chapter 5

Optimal Electrode Design

5.1 Introduction

In this chapter, the fundamentals of the electrode design are detailed. The effect of electrode orientation (with respect to nerve trajectory), location and the dimensional features (e.g., size) of the electrode on the electrical field shapes and neural activation are discussed. After giving a brief explanation about the electrode edge effects and electrode materials, the electrode–tissue modelling and safety consideration for electrical stimulation are further detailed to take into account for modelling and designing (future work) an optimal electrode configuration setting in subsequent works. After the importance of the electrode array configuration is emphasised, then, the main goal of this chapter is re–called to the reader. Once the modelling procedure of the construction of the electrode orientation and electrode array configurations are explained, the process of obtaining an optimal electrode by applying to generated human head models is explored. Additionally, the effect of electrode orientation and electrode array configurations on the electrical field shapes is compared to assess the impact of this variation on the neural activation in the further section. In the result section, the effect of the electrode orientation (with respect to nerve trajectory) and electrode array on the nerve fibres stimulus current thresholds, for generated human head mod-

els, are compared. Then, the underlying points of the results are detailed in the discussion section. Finally, the feasible future work of this study is highlighted.

5.2 Fundamentals of electrode design

Neural activity is an electrical phenomenon as discussed in Chapter 2. Therefore, establishing a connection between neural tissue and electronics is considerably more complex than simply connecting a wire. Electrodes are electrical conductors made of a metal or polymer which have emerged as a promising technology for generating prosthetic devices that treat neurological disorders and restore the function of the nervous system. Because of the critical role that electrodes play in a bio-instrumentation system, understanding their properties is a prerequisite for system design.

One of the main differences between biology and engineered systems is charge carriers. Bio–electrical currents are ionic which consist of chemical species moving in solution (as it was detailed in Chapter 3, the activation of the neural tissue depend on the variations of these ionic systems). Electrodes provide the necessary transduction of ionic currents into electrical currents, connecting bio–electrical activity and electronic systems to each other.

These neuromodulation systems can be designed either for stimulation and blocking (the information from the engineering system can be readily transferred to the neural system) or for recording (information from the neural system transferred to an engineered system). The principle of the stimulation electrodes: The charge is injected into the neural tissue, the induced current in the tissue generates a distribution of electrical potentials, and the extracellular potentials are generated as a response of the neural tissue by polarising the membrane of electrically excitable cells residing in the tissue according to the cable equations and Hodgkin–Huxley dynamics of the membrane channels. The effect of magnitude of the electrical field on the nerve fibres is determined by the second spatial

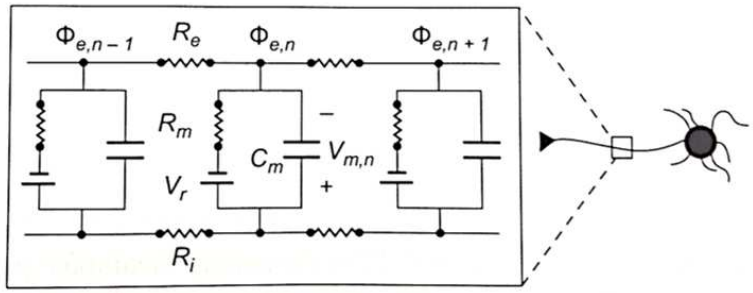

Figure 5.1: Electrical circuit representation of the neuron membrane [210].

derivative of the electrical field along the length of nerve fibre. The temporal characteristics of the field influence the channel, and hence, neural behavior as detailed in Chapter 3. However, the spatial characteristics of the field are significantly affected by the electrode design. Thus, the ability of the electrode to manipulate the field shape depend on the contact shape, placement of the contacts, and insulation. Furthermore, electrodes are able to activate the neural tissue depending on their size, orientation, space and type which are detailed in the following subsections [207], [208].

Additionally, It has been discussed that the electrical potentials along the nerve trajectory may excite or block ongoing neuronal firing depending on the magnitude, distribution, and polarity of the potentials [209].

5.2.1 Electrode orientation and location

In Chapter 3, it was discussed that the stimulation source is proportional to the second centred spatial difference of the extracellular potentials as shown in Equation 5.1 which is derived from circuit in Figure 5.1.

$$C_m \frac{dV_m}{dt} + \frac{V_m - V_r}{R_m} - \frac{\delta^2 V_m}{R_i} = \frac{\delta^2 \Phi_e}{R_i} \tag{5.1}$$

where R_m and C_m are the membrane resistance and membrane capacitance, respectively. R_i is the intracellular/extracellular axoplasmic resistance, V_m, V_r are the membrane and resting membrane potentials while Φ_e is is the extracellular potential along the neural tissue. δ is the centred difference operator.

Thus, stimulation efficiency can be increased or decreased by changing the spatial difference of the extracellular potentials which is called field shaping. It has been shown that the field shaping can be achieved by steering current between two or more electrodes in a multipolar configuration as shown in Figure 5.2 [210]. The neural tissue activation can be changed based on electrode orientation by shaping potential distributions. Meaning that the spatial difference of the extracellular potentials in one direction is relatively larger than other directions. Also this is the case when the monopolar electrode was aligned with the axis of the nerve trajectory, then $\boldsymbol{J}$ in the direction becomes more uniform, $\boldsymbol{\nabla \cdot J}$ approaches zero (under the assumption of the quasi–static approximation). Thus, the spatial difference of the extracellular potentials is reduced along the axis of the align electrode which results in lowering the source driving polarisation of parallel elements, therefore, perpendicular nerve axons are activated first as shown in Figure 5.2.

It has been indicated that orientation–dependent neural activation can be achieved using multipolar electrode configuration. The bipolar electrode is the most basic multipolar electrode configuration which consists of a source (anode) and sink (cathode). It has been demonstrated that when the electrode configuration is aligned parallel with the axis of the of the nerve trajectory, the neural tissue was activated with lower stimulus current levels, compared to the perpendicular aligned version. Although using tripolar configuration which elongated with the axis of the nerve showed the parallel trajectory was stimulated first due to increasing spatial difference of the extracellular potentials based on modelling studies, its performance has not been tested clinically [210].

Furthermore, it is well known that when the distance is increased, the potentials generated by the electrode is decreased. Generally, the spatial difference of the extracellular potentials declines as the magnitude of the potentials declines. Thus, the possibility of the activation of the neural tissue by the electrode depends on how rapidly the extracellular potentials decay. During stimulation of

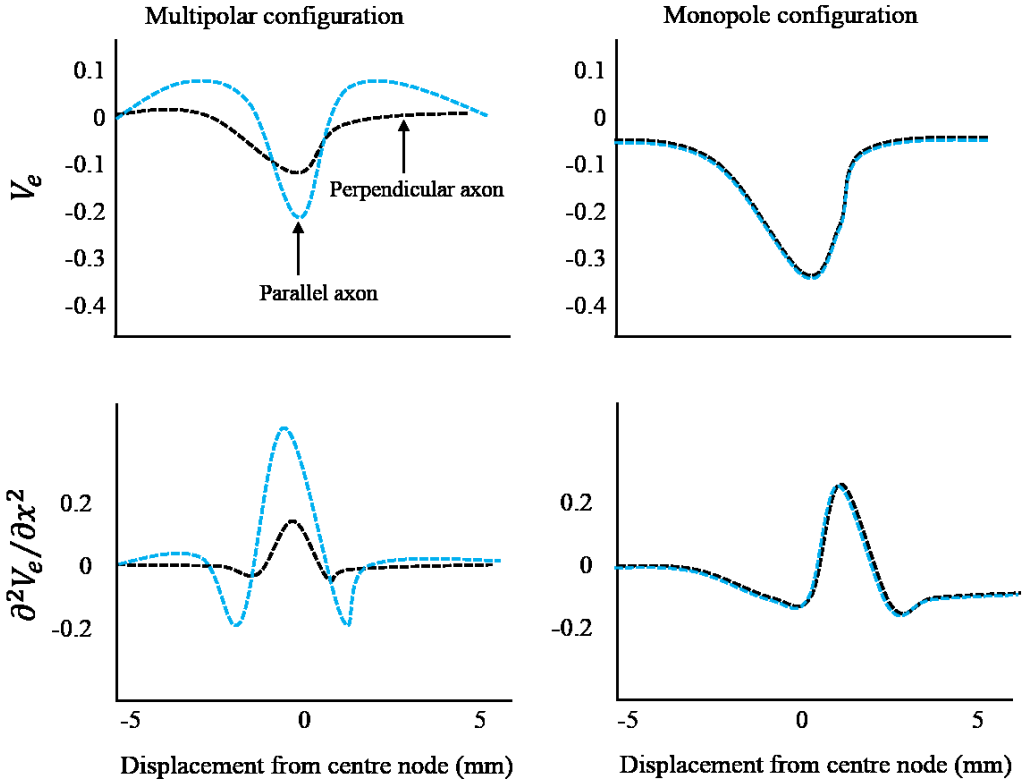

Figure 5.2: The effect of electrode orientation on the nerve activation. The figure was redrawn from with changes [210]. All voltage variations along the axon which parallel aligned with axis of the electrode axon are shown in cyan for both multipolar and monopolar electrode configuration. The perpendicular aligned ones are shown in black. The activation of the nerve can be significantly affected by both electrode orientation with respect to nerve trajectory and electrode configuration type.

peripheral nerves, it is clear that the axons in the vicinity of the electrodes that are activated [211], [212]. Using a multipolar electrode configuration (e.g., bipolar) with interelectrode spacing can be used to increase the spatial selectivity of an electrode. For instance, when the distance the source and sink is smaller than a distance to a bipole, the potentials decay proportional $\approx 1/r^2$. The potentials of the point source decline proportional to $\approx 1/r$. Thus, bipolar electrode configuration has better spatial selectivity than a single electrode [208], [211], [210]. To conclude, to stimulate the nerve fibres with lower current thresholds and with better selectivity, an electrode array (will be detailed in the subsequent sections) which aligned with the trajectory of the nerve and composed of multiple sinks

and sources is assumed to be a better solution. in this way, the polarity of the electrical potentials along the nerve trajectory is changed depending on the sinks and source elements on the electrode array configuration. This may result in lower stimulus current levels to activate the neural tissue.

5.2.2 Electrode size, shape and spacing

The electrodes used in electrical stimulation have different sizes and areas. The real surface and geometric surface area (GSA) are considered for electrodes. The GSA is the traditional idea of surface area (L×W for a rectangular electrode). In practice, if the surface of the electrode is rough or porous, the area of having an interface with electrolyte is much larger than the geometric surface area. This interface area is called real surface area which varies depending on the roughness of the electrode. The chemical reaction can occur more on a rough electrode than a smooth one with the same GSA in the case of Faradic current flow (which will be detailed in the following subsections). It should be noted that a higher real surface increase the double layer capacitance of the electrode [213], [155].
It is clear that the distributions of the extracellular potentials are dependent on the GSA. The charge and current densities are defined by this surface. Since electrochemical surface areas (ESAs) can vary greatly depending on the method and conditions used in its measurement, it is generally not useful to define the electrode features. Thus, using a large electrode size may cause discomfort, insufficient selectivity, and fast fatigue. The discomfort comes from the activation of the pain receptors as well as the activation of the motor nerve fibres [214].

5.2.3 Electrode edge effects

Electrode edge effects have an important role in the electrode design for electrical stimulation. It has been shown that the electric field and thus current density are both sharply enhanced at the periphery of the electrode. It has been observed that the primary current density exhibits a singularity at the very edge, whereas

being only half the average value at the center of the electrode [215]. As it is discussed in the subsequent sections, charge–balanced biphasic stimulation is not enough to prevent locally enhanced current density which may drive electrochemical reactions at the electrode edge and thus may lead to corrode the periphery of the electrode. Tissue damage due to localized stimulation is of concern in biomedical applications [216]. There are several different methods to reduce the edge effects, mainly manipulating the geometric design [217], applying a highly resistive layer over the electrode has shown a more uniform current density distribution in certain applications or increasing the conductivity of the gel layer may result in uniform current density distribution [217], [218].

Although the electrode edge effects are less for TES applications, it should be studied intensively to prevent any damage for both electrode and tissue. Since each electrode has gel layer after metalic contacts, which maintain an electrical interface between neuromodulator, in the target solution. Therefore, the edge effect only happens in the metallic surface but not in the electrodes surface in contact with the skin as detailed in Chapter 3.

5.2.4 Electrode material

There are mainly four different electrode types, composed of different materials. These are metal plate electrodes covered by fabric tissue, carbon electrodes, self adhesive hydrogel electrodes and textile electrodes. The metal plate in the metal plate electrodes often is made from bio–compatible materials such as stainless steel or silver/silver chloride. The fabric tissue can be cotton but is often a polymer textile material that has a certain degree of elasticity. To prevent skin burns, the fabric is made conductive with water or electrode gel to equally distribute the current over the skin.

Carbon electrodes replace fabric covered metal plate electrodes in many TES applications. Since carbon has a higher resistance than metal, the high current concentration in small areas is prevented using the carbon electrodes. Also, hy-

drogel electrodes are not stable at temperatures over 40 degrees and over long time periods, thus, carbon electrodes can be used instead.

Self–adhesive electrodes are generally used for TES application and they consist of a gel to contact with the skin layer. The electrode consists of multiple layers including substrate, hydrogel layers. The conductive gel is made from co–polymer. The skin interface layer includes the conductive gel with relatively low peel strength to easily remove from the subjects skin. The carbon film or other conductive materials are used for the substrate conductive fabric. To make interface between the stimulator and electrode, a metal contact or a wiring cable is used.

The textile electrodes are mainly used for recording and monitoring of the bio–signals. They are composed of multiple fabric layers. These electrodes do not need to use gel to establish connection to the skin, the conductive yarn can be used to build a connection to the skin. Due to the fact that the textile electrodes do not irritate the skin, they can be used for a long term measurement. In addition, they are lightweight, ductile and washable. The limitation of these electrodes is a high impedance in the electrode–skin interconnection which may lead to inaccurate measurement [155], [219], [220].

5.2.5 Surface electrodes

Surface electrodes applied to the skin are widely used in many neuromodulation application due to their simplicity and negligible risk. They vary from transcutaneous electrical nerve stimulation (TENS) for pain management and physical therapy to ECG(electrocardiogram) and EEG (electroencephalogram) measurement. Two basic types of surface electrodes are patch and minimally invasive electrodes. Patch electrodes relatively have large surface area electrodes that adhere to the skin. They can be designed with or without conductive gels. Using conductive gel helps to minimize the electrical impedance of the skin, produce uniform current distribution to prevent electrical burns that could result from

improper stimulation. It should be noted that when the currents pass through the skin, sensory nerves are also activated and this can cause painful sensation. Minimally invasive electrodes are composed of a small percutaneous needle or corkscrew that penetrates the skin. These types of the electrodes are generally used for diagnostic purpose as chronic usage in a therapeutic application would be undesirable.

The limitation of the surface electrodes may include poor selectivity, especially of small or deep neural tissue, inconsistent muscle or nerve activation due to variations in electrode placement and impractical donning time [208], [221], [222].

5.2.6 Safety consideration

The activation of the excitable tissue is achieved by the flow of ionic current between two or more electrodes. Generally, electrical stimulation is applied as a series of biphasic current pulses in neural applications. There are several variations on biphasic current waveforms that have been described in the literature. Also, a number of variations on charge imbalance have been proposed as a way of compensating for irreversibility in charge–injection processes. It is noteworthy to that Faradaic reactions are divided into reversible and irreversible reactions. In the reversible reactions, no effective storage of the charge is generated near the electrode surface. However, irreversible reactions lead to generate chemical species that are damaging to tissue or the electrode. Thus, a general principle of the electrical stimulation design is to avoid an irreversible Faradic reaction. Therefore, the charge–balanced biphasic waveform is widely used to avoid damage to electrodes and surrounding tissue. The fundamental objective of the charge–balance is to keep the potential of the electrode within a range that does not induce irreversible reduction and oxidation reactions which may degrade the electrode, damage tissue, or otherwise limit the charge that can be delivered in a stimulation pulse. However, even when the former criteria are applied, irreversibility may occur during delivery of the pulse due to polarisation of the

electrode. Thus, in addition to charge balance, the current and charge densities of the stimulation waveforms must be limited that allow charge injection by reversible processes. The most common irreversible processes during stimulation are electrolysis of water results in pH changes and gas formation, electrode dissolution due to the oxidative formation of soluble metal complexes and other common damages [155], [182].

5.2.7 Electrode array

Transcutaneous electrical nerve stimulation (TENS) via surface electrodes is being used for various applications (e.g., pain reduction) to restore the function of the neural disorders or to support tasks of daily living using so–called neuroprostheses. Although a single electrode was used in the past for such neuroprosthesis, electrodes array were proposed to improve the efficacy of TENS system in order to observe the spatiotemporal dynamics of the electrical activity. These arrangements consist of multiple elements which can be individually activated to form a virtual electrode of arbitrary size and location. The position and size of the activated region can be dynamically changed. The optimal electrode size and position helps to simplify the use of electrical stimulation systems and to increase their clinical efficacy. However, it is difficult to predict precisely the optimal size and location of the electrodes for neural stimulation although the size and position of the array elements were chosen intuitively in the past. Meaning that the optimal parameters of the stimulation electrodes were built by trial and error and it was unclear how, for example, the gaps between the array elements or the resistivity of the electrode-skin interface material influence the current distribution. It is difficult to test many electrode sizes experimentally which may cause to induce serious effects on patients and also this process is obviously time–consuming [223], [224], [132].

It is noted that the distribution of the extracellular potentials is dependent on the electrode geometry, the electrical properties of the extracellular tissue, and the

stimulation amplitude. The effect of the potentials on neurons is dependent on the nerve cell type, its size and geometry, as well as the temporal characteristics of the stimulus [132], [207], [208]. The diversity of neuronal elements and complexity of the volume conductor make understanding the effects of stimulation more challenging for neural excitation to design optimal stimulation parameters (e.g., design optimal electrode size and space) using experimental methods. Modelling provides a highly flexible environment and has been used since the 1980s to study the effects of extracellular stimulation on neural activity of particular electrode configurations to overcome experimental limitations [121], [138].

5.3 Objectives

The findings of Chapter 4 show that the associated neuroanatomical variations led to excessively high stimulus current levels being required using the electrode setting of the target neuromodulator. As the device is patient–operated, these high levels of the current are not applied. However, such high stimulus current levels may cause patient discomfort by excitation of the pain fibres in the vicinity. Furthermore, since the electrodes are placed near pain –sensitive structures (such as eyes, frontal sinuses, veins and nerves), the pain may be induced even at the low levels of the current which may further limit the efficacy of the neuromodulator. Therefore, a new electrode configuration may be needed to reduce the limitation of the target solution. A potential improvement is to align the axis of electrodes with the target nerve, so that the electrical potential along the trajectory of the nerve changes polarity [210]. This may lead to lower required stimulus current levels. Also in this way, the more superficial distal section of the nerve may be exposed to the stimulus current and the current spread is shifted away from sensitive structures. Furthermore, the required current levels and patients discomfort can be reduced using an electrodes array based on the same concept as detailed in this Chapter.

For all the subsequent simulations and operations, a computer with an Intel Core i7-6700 CPU @ 3.4 GHz with 64 GB RAM was used.

5.4 Methods

5.4.1 Effect of electrode orientation on nerve activation

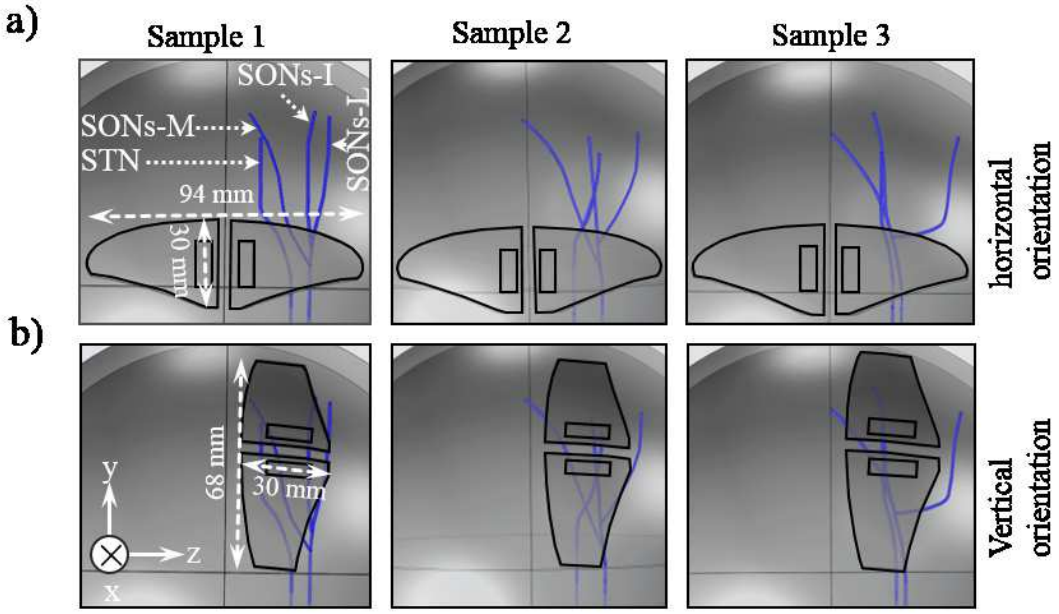

Figure 5.3: The sample of the neuroanatomical variations and different electrode orientation. Three different variations of the nerve distribution in the human head model are illustrated for both horizontal and vertical electrode orientation; the borders of the electrode patches delineated by black curved lines. Sample variations of the branches of the nerve in the human head model, all branches are displayed in blue. The dimensions and nerve name shown in white.

The electrodes are modeled based on the Cefaly design. The samples are shown in Figure 5.3. They consist of a conductive gel, which defines the shape of the skin in contact with the electrode. The metal blades on the surface of the electrodes maintain an electrical interface between neuromodulator and electrodes. The self-adhesive electrode is affixed to the centre of the forehead ad to bilaterally stimulate the branches of the frontal nerve as shown Figure 5.3b [7]. To assess the effect of electrode orientation on the activation current thresholds of nerve

fibres, the variations of each of the nerves and other tissue layers were kept constant as the electrode orientation was rotated by 90 decrees for each model as shown in Figure 5.3b. To conform to the head dimensions the width of a pair of electrodes when used in a vertical orientation was reduced compared with the standard Cefaly electrodes (L×W = 94 mm × 30 mm). Thus, the width of the vertical pair of electrodes (L×W = 30 mm × 68 mm) was designed based on the average human forehead size (from eyebrows to hairline) by cutting the edge of both sides of the standard electrode as shown in Figure 5.3b. Note that the same thickness (1.5 mm) was used for both electrodes arrangements.

5.4.2 Effect of electrode rotation: Preliminary test

The main objective of this test is to causess the device on two subjects to investigate the effect of electrode arrangements on stimulus current levels, pain and paranesthesia sensation levels and record any adverse events during of after test. The study procedure is well detailed in Appendix C and will summarize here. As this study is a straightforward low–risk test, the training and test sessions was applied on the same day. After assuring the device is fully charged and having enough disposable electrodes for each of the session, the training sessions were started to examine the effect of the horizontal electrode orientation and then vertical orientation by placing the electrode on the forehead of each subject as depicted in Figure 5.4. To increase the quality of contact between the skin and electrode patch, the subjects' forehead was wiped. It was reassured the neurostimulator has connection with the metallic area on the electrode patch. Then, the session was started by pressing the button on the stimulator and the levels of the stimulus current was designed based time (1minutes $\approx$ 1 mA is increased) [7]. Each subject was rested for 10 minutes after each sessions to minimise any possible side–affects. Then, the human head schematic was provided during the each session, as shown in Figure 5.5 (without numbers) to record sensation occurrence and its severity on a point scale for both paraesthesia and pain (0: no sensation;

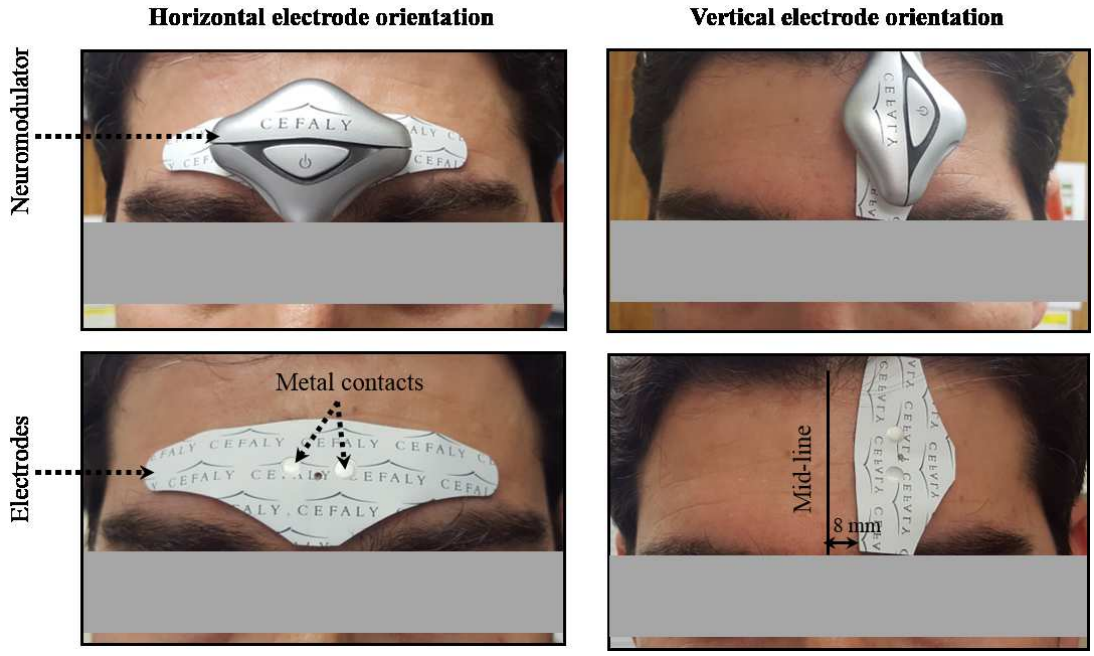

Figure 5.4: Preliminary test on volunteer.

1-6: paraesthesia, 6-10: pain, see Appendix C). Also, another document was provided to record any adverse effect during and just after each session to minimize them in future studies. It should be noted that two measurements were obtained from both horizontal and vertical electrode orientation for each subject and the results were derived from their average variation.

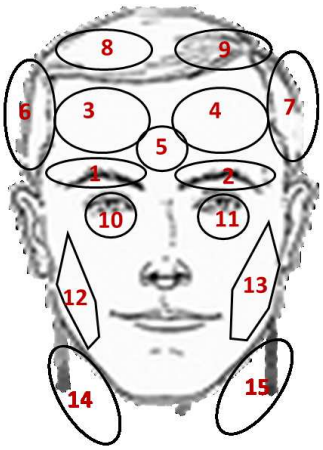

Figure 5.5: Human head schematic.

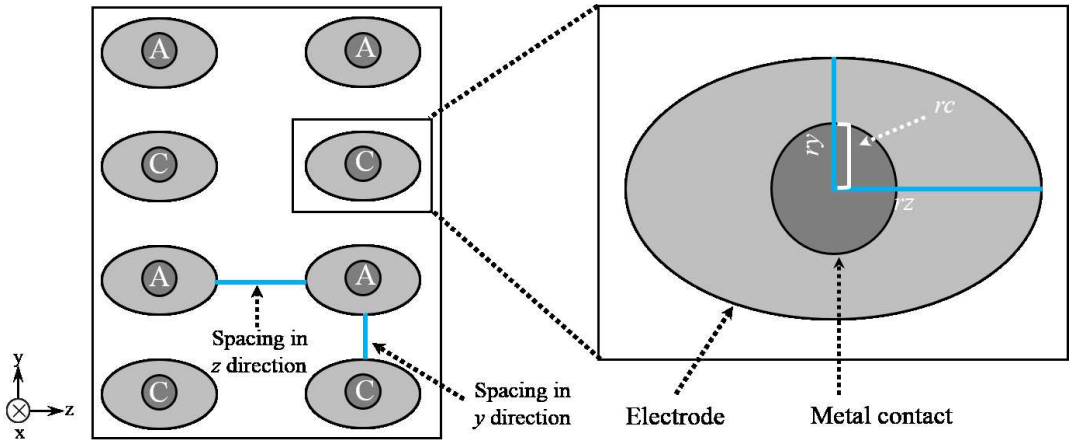

Figure 5.6: The block diagram of the proposed electrode arrangement. 'A' represents source and 'C' is used for sink in electrode diagram; *ry*, *rz* represent the radii of the elliptical shape electrode components in y and z directions, respectively while *rc* shows the radius of the metal contact on the electrode patch.

5.4.3 Design an optimal electrode array

The aim, in this subsection, is to use the TES models of the human head, subsequent layers and neural tissue to obtain optimal electrode configuration based nerve fibres stimulus current thresholds.

As detailed in the earlier sections of this chapter, the activation of the nerve is proportional with the variations of the electrical potentials along the nerve trajectory using multi–polar electrode configuration. This was validated by the electrode orientation. Thus, the electrodes array which composed of multiple sources and sinks may result in more potential distributions that may lead to lower stimulus current being required.

As electrodes form the interface between hardware and living tissue, they must be designed with consideration of the geometry and nature of the target locations. Disk (elliptical) shapes elecrtodes are commonly used in biomedical applications [216]. Thus, the electrode and metal contact was decided to model from the smooth circle shape to prevent possible electrode edge effects. The block diagram of the proposed electrode is shown in Figure 5.6. The procedures of the generations of the electrode in different sizes and spacing are discussed here. The

proposed electrode arrangements (sizes and spacing) were designed based on the average human forehead size (from eyebrows to hairline, 68 mm) in the y– direction and the minimum and the maximum distance (8 mm – 35 mm) of the frontal nerve variation from the midline of the human forehead. The average thickness of the electrode was designed based on the thickness of the Cefaly electrode. Since there are no guidelines on defining the size of components of the electrodes array, the size and space of the components are generally based on the arbitrary selection. However, too small arrangements may not be effective on persons with thick fat layers which prevent the current spread through inner layers (e.g., nerve fibres). Also, it should be noted that small electrodes may cause to induce current densities that may lead to discomfort this limiting the effectiveness of TES. The electrode should be designed from a certain size to be effective. Taking into account these design principles, the thickness of components of the electrodes array were kept constant whereas, the size and spacing of the electrode were increased until the defined border of average human forehead size and the variations of the nerve trajectory range. These results in eight different configurations under mentioned considerations as samples are shown in Figure 5.7. The radius and space of these possible electrode configurations are shown in Table 5.1. Each row of the Table 5.1 represents one electrode and shows the features of the associated electrode. It should be noted that the 3D finite element model was developed based on the average thickness of the human head size and the average thickness of the subsequent layers (this statistical distribution of each layer was discussed in Chapter 4). Also, the average statistical distributions of the STN and SONs were used to obtain the optimal electrodes array arrangements. The same approaches in the previous chapters were used to generate the human head, subsequent layers and the 3D models of the nerves. To construct 3D models of the electrodes, the oval shapes were generated from the ellipse shapes to increase to have more space in the y–direction to obtain more electrical potential variations along the associated nerve trajectory. To make sure the electrode has full contact with the skin

Table 5.1: Array design based on average human forehead size and statistical variations of the associated nerve.

Electrode	r_z**(mm)**	r_y**(mm)**	**y (mm)**	**z (mm)**
E1	5	3	4	4
E2	5	3	4	8
E3	5	3	8	4
E4	5	3	8	8
E5	5	3	12	4
E6	5	3	12	8
E7	6	3.6	4	4
E8	6	3.6	8	4

layer, firstly, the intersection between electrode array component and skin layer was obtained then, metal contact was extruded, finally, the difference was taken based on the thickness of the electrode. This was repeated for each component of the electrode array (sources and sinks).

5.4.4 Optimal array design

The eight different electrodes array were designed, simulated and the required stimulus current levels were recorded for each electrode model to identify the optimal electrode configuration. It was observed that the optimal electrode configuration was 'E6' based on stimulus current threshold of the STN and SONs nerve fibres.

It is necessary to validate this electrode configuration by applying to a large population. Since ten human head models were developed, considering statistical variations of thirteen neuroanatomical features to mimic a large population, the efficacy of this electrode configuration can be confirmed using these models. Thus, the optimal array was generated for all human head models which are previously generated and saved in COMSOL, samples shown in Figure 5.8. Since complete human head models were designed previously, only electrode array was generated for each model as detailed in the previous subsection and briefly mentioned here.

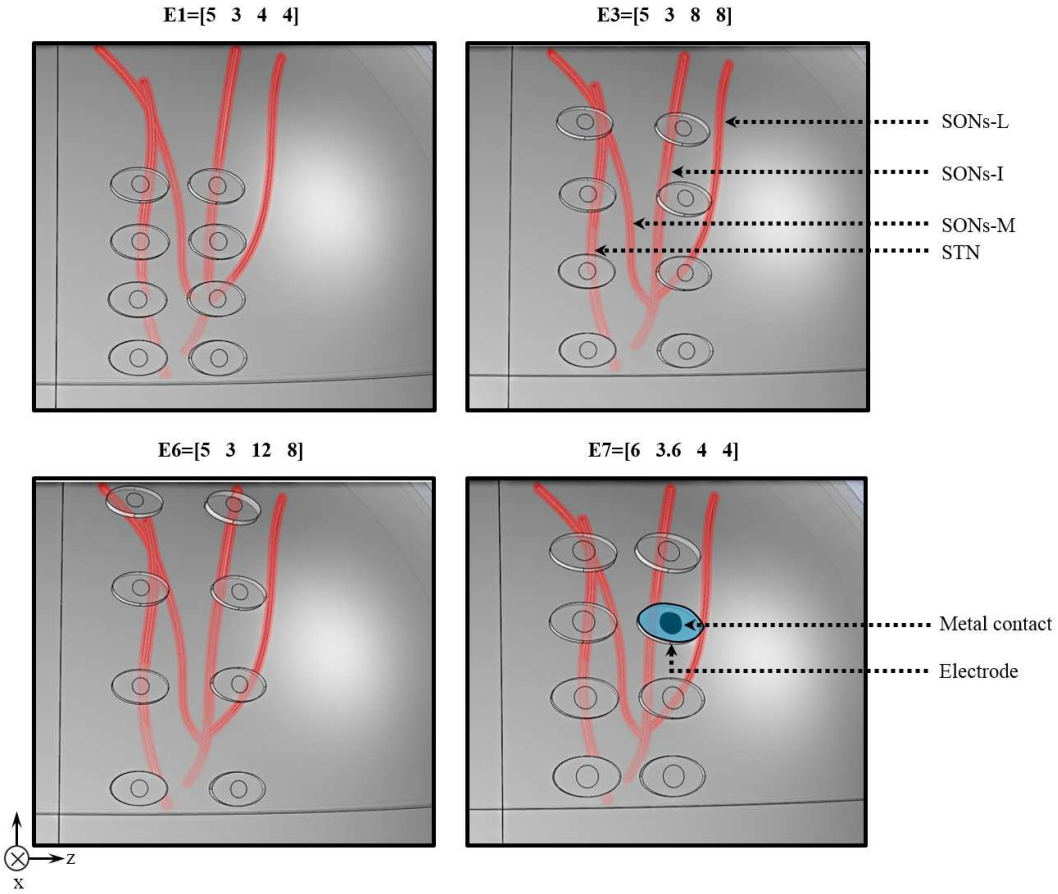

Figure 5.7: Samples of different electrode array on the average human head model. The saturation and transparency of the figure is increased to provide more visibility of the elements on the figure. The nerve branches are shown in red color. An electrode element in the array is displayed with light blue and metal contact is represented in black color.

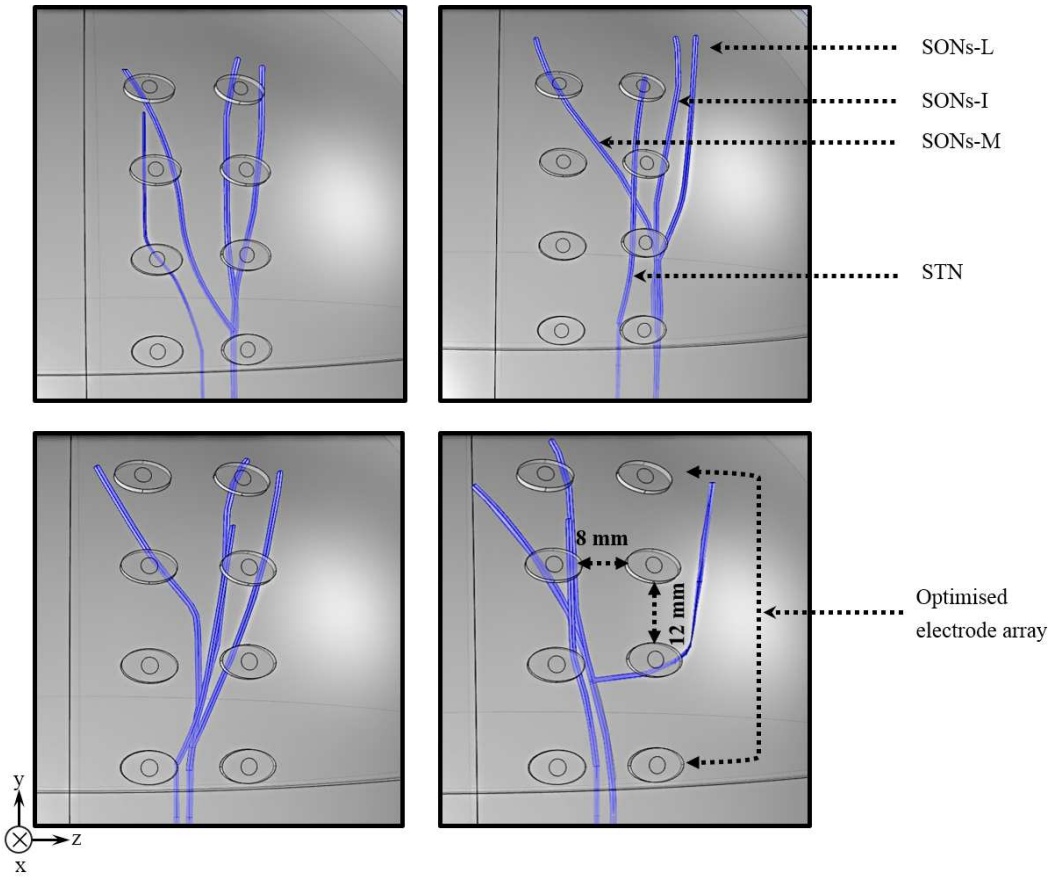

Figure 5.8: Optimal electrodes array on sample variations of the branches of the nerve in the human head model, all branches are displayed in blue. The nerve are labeled with dotted arrow and electrode gaps for different direction are highlighted.

The radius(ry=5mm, rz=3mm) of the elliptical geometric shapes were selected based the optimal electrode settings. After adjusting the electrode thickness, the metal contact (rc=1.5mm) was centred in the electrode with appropriate coordinate settings. The required intersection and difference settings were applied to be able to select the electrode and metal contact as a different material. This process was applied for the rest of the array element. As only 'E6' was the target electrode array, the same procedures were repeated for ten generated human head models.

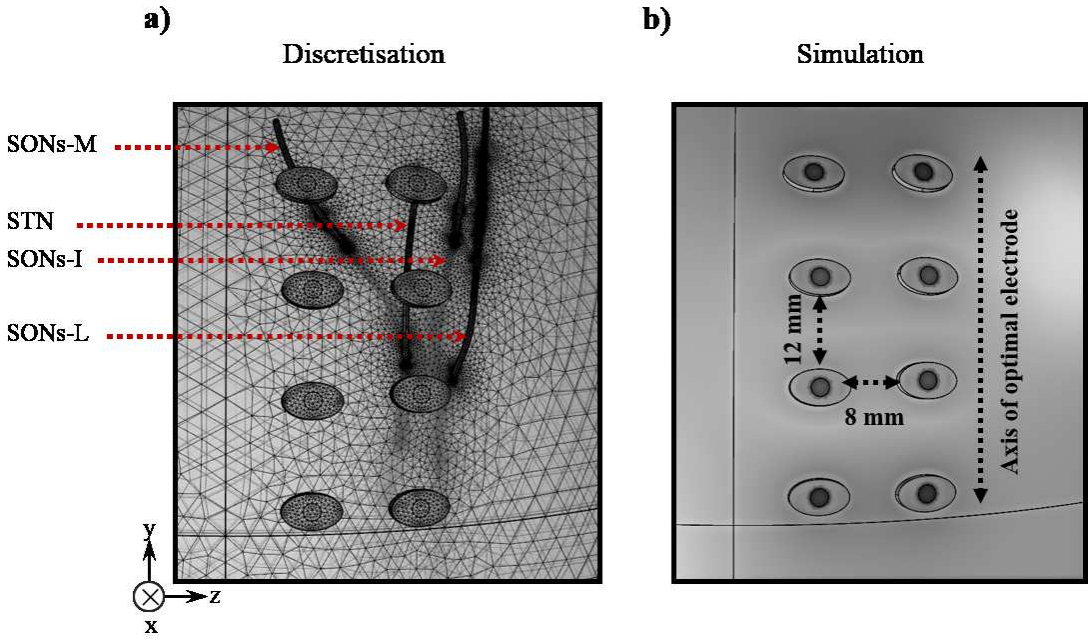

Figure 5.9: Discretisation and simulation of a model using optimal electrode array. (a) The discretisation of a model is shown, some layers are removed to observe the trajectory of the nerve, the nerve branches are labeled with red dot arrow. (b) This electrical potential distribution on the model is shown, the gaps between electrode elements are highlighted with dot arrow and the axis of the electrodes array is shown with dot arrow.

5.4.5 Finite element discretisation and simulation

The same approximation methods and the same boundary conditions were used to obtain electrical potential distributions in the volume conductor as detailed in Chapter 3. The 3D volume conductor of each model was meshed using free tetrahedral discretisation method. Figure 5.9 shows the mesh and simulation plots of the optimal electrode array in COMSOL. Since the simplified human head model was used to obtain the optimal electrode configuration, the domains in the model can be meshed with finer mesh settings without increasing computation cost. The average number of degrees of freedom was between 1 M to 3 M for all models. The average mesh quality was about 0.96 for triangular while this was around 0.7 for tetrahedral. The calculation of the extracellular along the nerve trajectory was varied for all model and this range was between approximately 0.5

minutes to 2 minutes for all models. Since the layers in this model are the same as the model in Chapter 3, the conductivity of each tissue was attained from this table. It is noted that given current levels (±1 mA) was divided by the number of sources or sinks for each model. Meaning that ±1 mA is obtained from the stimulator and induced as ±0.25 mA for each sink or source.

5.4.6 Hybrid modelling

Myelinated afferent fibres in the frontal nerve were modelled as double layer cable models with explicit representation of the node of Ranvier with associated compartments. The response of the nerve fibres to generated electrical potentials was calculated by coupling the FEM results with the NEURON model. For each nerve fibre and each electrode simulation configuration, the extracellular potential was computed in the finite element model in COMSOL then was interpolated on the compartments of nerve fibre and assigned with the extracellular mechanism. Bipolar symmetrical biphasic stimulations (phase duration: 250 μs) were used. The amplitude of stimulus current was increased until generating an action potential (detected at the first node and last node of nerve fibre). A 25 ms time step was used, allowing a reduced error on the activation threshold estimation.

5.5 Results

5.5.1 Effect of electrode configuration on electric field profiles

As it was highlighted in the background of this chapter that multipolar electrode configuration can affect the activation of the neural tissue by varying the polarity of the extracellular potentials along the nerve trajectory. Thus, using electrodes array which composed of multiple sinks and sources may lead to lower stimulus current level being required. Thus, extracellular potentials along the ten different SONS–I nerve branch were compared in Figure 5.10 to validate the

relationship between neural activation and extracellular potentials variations for different electrode arrangements. The simulation result for vertical electrode orientation shown that when the electrode aligns parallel with the nerve trajectory, the polarity of the induced potential along the nerve trajectory varies more due to participating both electrodes in the simulation. Furthermore, using multiple electrode arrays even furthermore change the polarity of electrical potential variations due to participating multiple sources and sinks in the simulation of the neural tissue. Therefore, it is expected that the horizontal orientation is required highest and array configuration is required the lowest stimulus current levels. The neural activation versus required current levels for these electrodes design are elaborated in subsections. It should be noted that the effect of electrode orientation is firstly compared and then this is compared with optimal electrodes array.

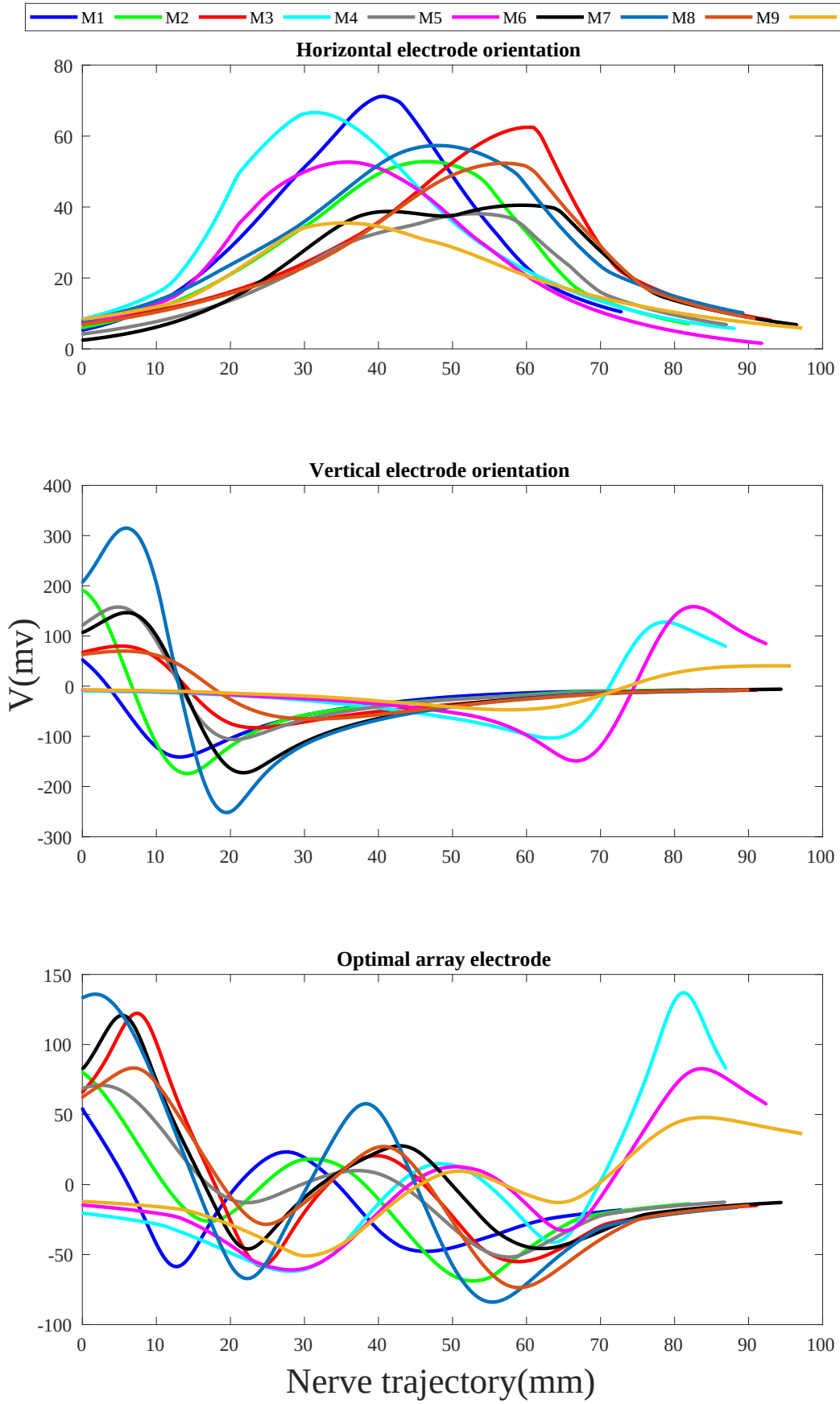

Figure 5.10: Extracellular potentials variation along the nerve trajectory for different electrode arrangements. M1: Head model 1.

5.5.2 Effect of electrode rotation

The influence of the electrode orientation on the PAs of the different nerve fibres versus stimulus current level for various models is shown in Figure 5.15. The order of the nerves is the same for all electrode configurations as identified in the first subplot.

The current density range (not shown here) at the eyebrow level from the skin to the back of the human head for horizontally orientated electrodes is 140 - 20 mA/cm2. However, this range is substantially lower (0.3 – 0.05 mA/cm^2) when using vertically orientated electrodes.

The results show that the vertical electrode orientation requires considerably lower current levels compared to a horizontal orientation for all nerve variations. The required current range to stimulate 50% of the fibres decreased from 6.2 mA – 16 mA to 0.3 mA – 2.7 mA for STN. The current ranges for SONs–M are 9.5 mA – 29 mA for horizontal orientation, which decreased to 1.05 mA – 4.75 mA for vertical electrode orientation. There is also a substantial variation in current ranges for SONs–I that reduced from 11.7 mA – 30.5 mA to 0.68 mA – 14 mA. The required current levels for SONs–L are higher for nearly all models than the other nerve branches in both electrode orientations. However, there is still a substantial reduction in current levels for this nerve branch variation as well. The lower and upper thresholds for horizontal electrodes orientation are 6.2 mA and 33 mA compared with are 0.3 mA and 21 mA for vertical electrodes.

The only similarity between the two arrangements is that the STN requires the lowest and SONs-L requires the highest current levels when the models are compared in order.

5.5.3 Effect of electrode rotation: Preliminary test

The variations scale of both paraesthesia and pain versus stimulus current levels for both horizontal and vertical electrode orientation for each subject is shown in

Figure 5.11.

The sensation of paraesthesia is occurred with relatively lower stimulus current levels and the level of the sensation does not change after a certain current level for subjects when the vertical electrode orientation is used. Using horizontal electrode orientation, the paraesthesia sensation is observed relatively higher stimulus current levels and the painful sensation is occurred at relatively lower current levels (e.g., 5 mA) for subjects. Furthermore, it was claimed that the sensation is so localised and any adverse event is not experienced when the vertical orientation is used. Using horizontal electrode orientation, the sensation zones are varied and both subjects are complaint about painful sensation in the forehead area and eyes as well as one subject is complaint about feeling of fatigue inability of keeping eyes during sessions after a certain time.

The sensation at facial area using horizontal and vertical electrode orientation is illustrated in Figure 5.12. The sensation does not exceed paraesthesia limit and it is localised when the vertical electrode orientation is used.

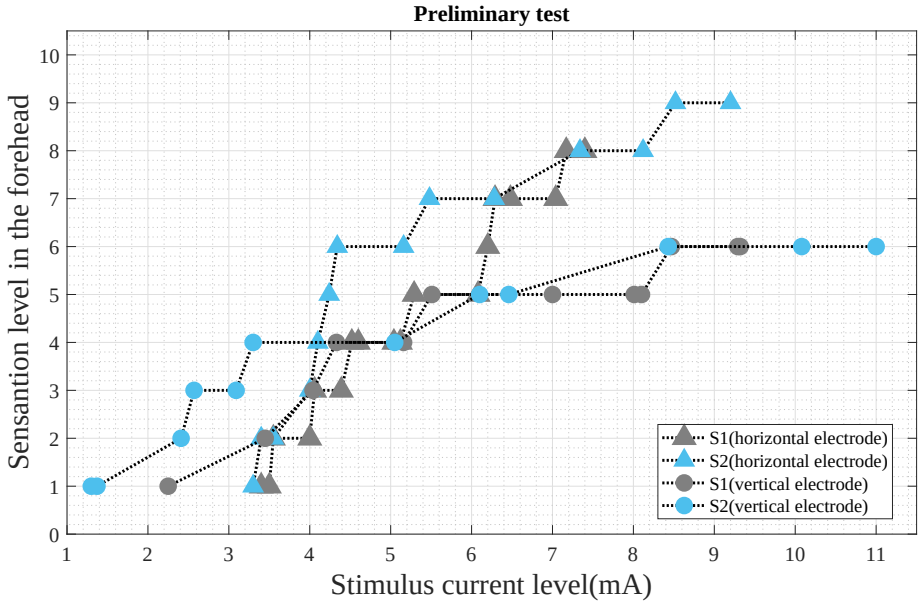

Figure 5.11: Preliminary test. The variations are shown in triangular and circle for horizontal and vertical electrode orientation, respectively. The results are represented in gray for subject 1 and in cyan for subject 2.

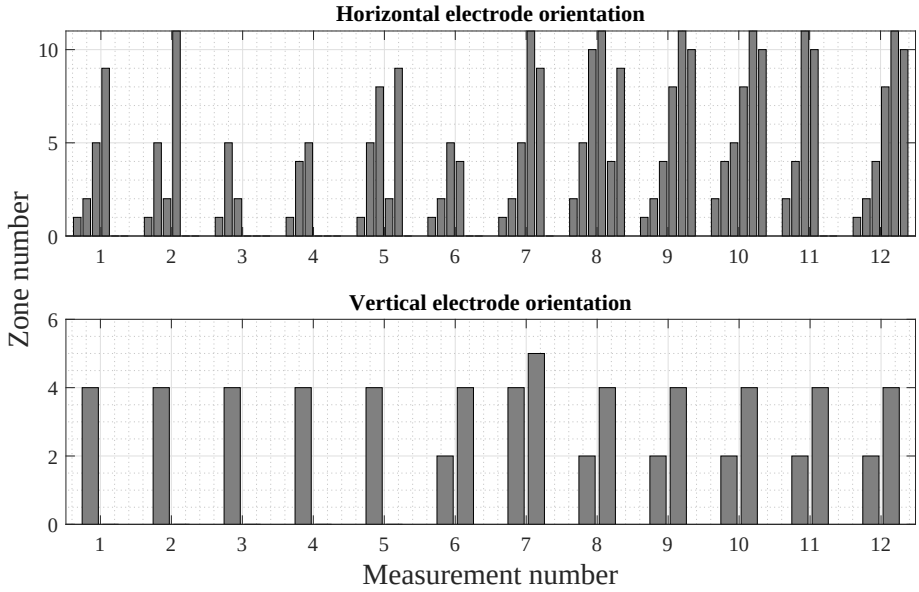

Figure 5.12: Sensation at facial area using horizontal and vertical electrode orientation.

5.5.4 Effect of electrodes array

Figure 5.13 shows the PAs versus the amplitudes of a 250 μs stimulus pulses for the trajectories of the STN and SONs using different electrodes array arrangements. The subplots in Figure 5.13, in turn, show the variations of PAs versus required stimulus current levels for SONs–I, SONs–L, SONs–M and STN. These different electrodes array arrangements were applied on the average human head model and the required current levels for the associated nerves were recorded to identify the optimal electrodes array arrangements.

There are various features of this plot which should be considered. Firstly, the current levels involved should be noted. The required current range level (1 mA–8 mA), to activate all nerve fibres in all nerve, is significantly lower than the current range of the existing transcutaneous frontal nerve stimulator (1 mA–16 mA). The range of the required current changes across different electrode arrangements. To activate the nerve fibres of the SONs–L, relatively more current levels are required in most of the electrode arrangements. Interestingly, using 'E2' arrangement lead to the use of more current for all nerve fibres activations apart

from the fibres in the SONs–L. The figure shows that using 'E1' is not an optimal electrode configuration due to the need for relatively more current levels for all nerve models. For instance, to activate 50% nerve fibres, the required stimulus current levels vary between 1.8 mA to 6.5 mA. For all nerve variations 'E1' and 'E2' are generally require more current levels. However, the variations in Figure 5.13 clearly show that 'E6' is an optimal electrode configuration for all nerve models, it requires relatively less stimulus current levels when compared to other arrangements.

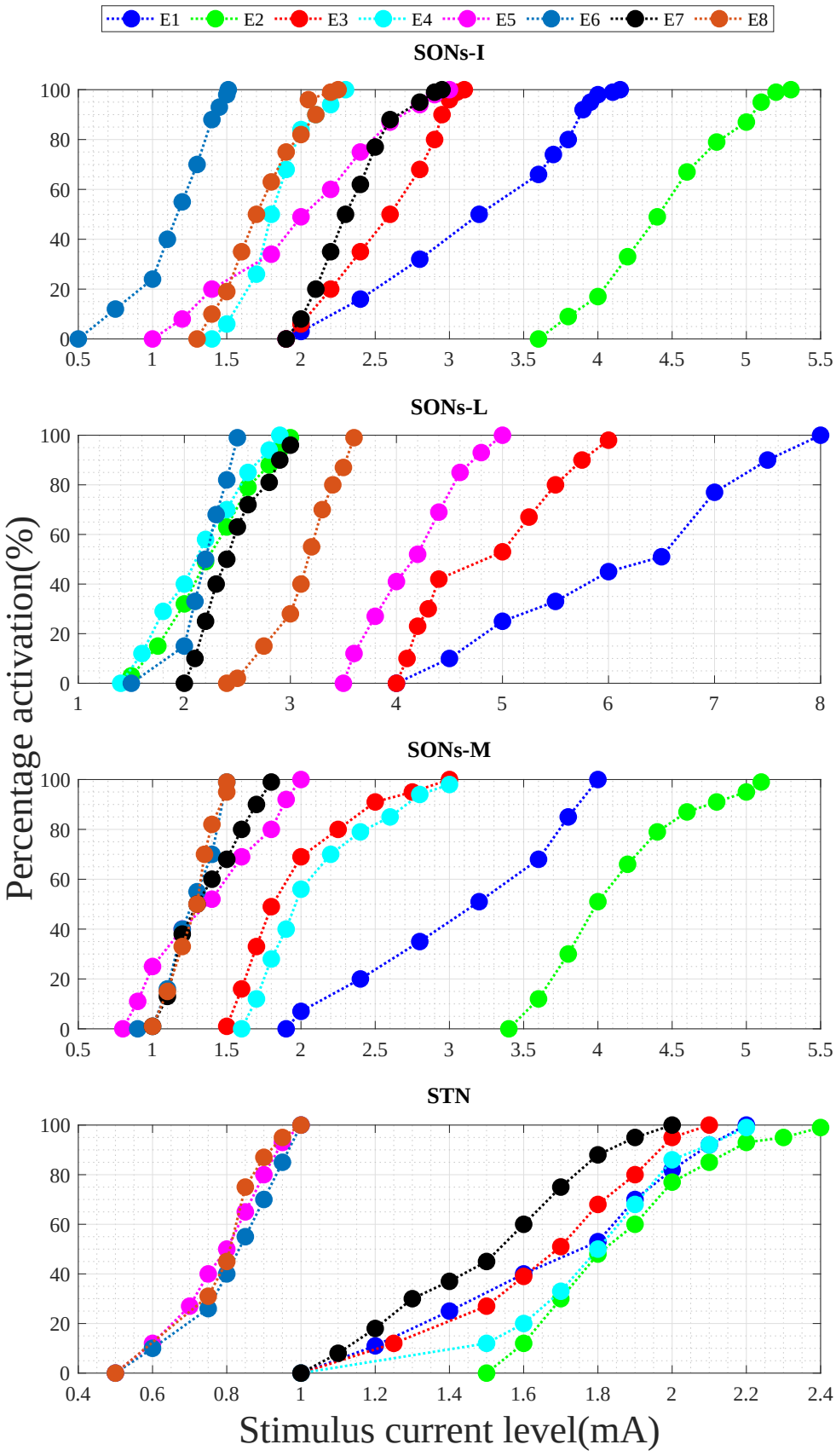

Figure 5.13: PA versus the amplitude of a 250 μs pulse for all of the electrode array configurations in the trajectories of the SONs–I, SONs–L, SONs–M and STN. E1: Electrode configuration 1.

5.5.5 Effect of an optimal electrodes array

The optimal electrode was merged with the ten human head models which were generated based on neuroanatomical statistical distributions. The electrical potential was simulated in the FEM model, interpolated in Matlab and imported to NEURON tool to calculate the response of each nerve fibres. Figure 5.14 shows the PAs versus the amplitudes of a 250 μs stimulus pulses for ten generated nerve models in the human head using an optimal electrodes array.

The figure clearly shows that most of the nerve models can be activated with a lower current range between 1 mA to 3 mA. To activate 50% of nerve all ten models, the required current range is between 0.25 mA and 7.8 mA which is significantly lower than the range of the existing device. Apart from nerve fibres of SONs–L in M5, M5 nerve fibres in other nerves require more stimulus current levels to reach 100% neural activation. It is noted that the required current levels for the branches of the SONs are close to each other and higher than the current levels to activate the STN.

The Figure 5.15 compares the horizontal (standard electrode) electrode, vertical electrode and optimal electrodes array configurations based on the amplitudes of a 250 μs stimulus pulses versus ten head models (40 nerve models). The nerve fibre current thresholds variations in STN, SONs–M, SONs–I and SONs–L are represented by the first, second, third and fourth bars, respectively, for each model in all subplots figures. There is a significant reduction in required stimulus current levels for all nerve branches in all head models while using vertical electrode orientation. Also, using the optimal electrode, these current levels are further minimised. It is very important to note that the required current levels are relatively less fluctuated for all individuals when the optimal electrodes array is used. It is noted that the current density, as shown in Figure 5.16, is within the safe limit [225].

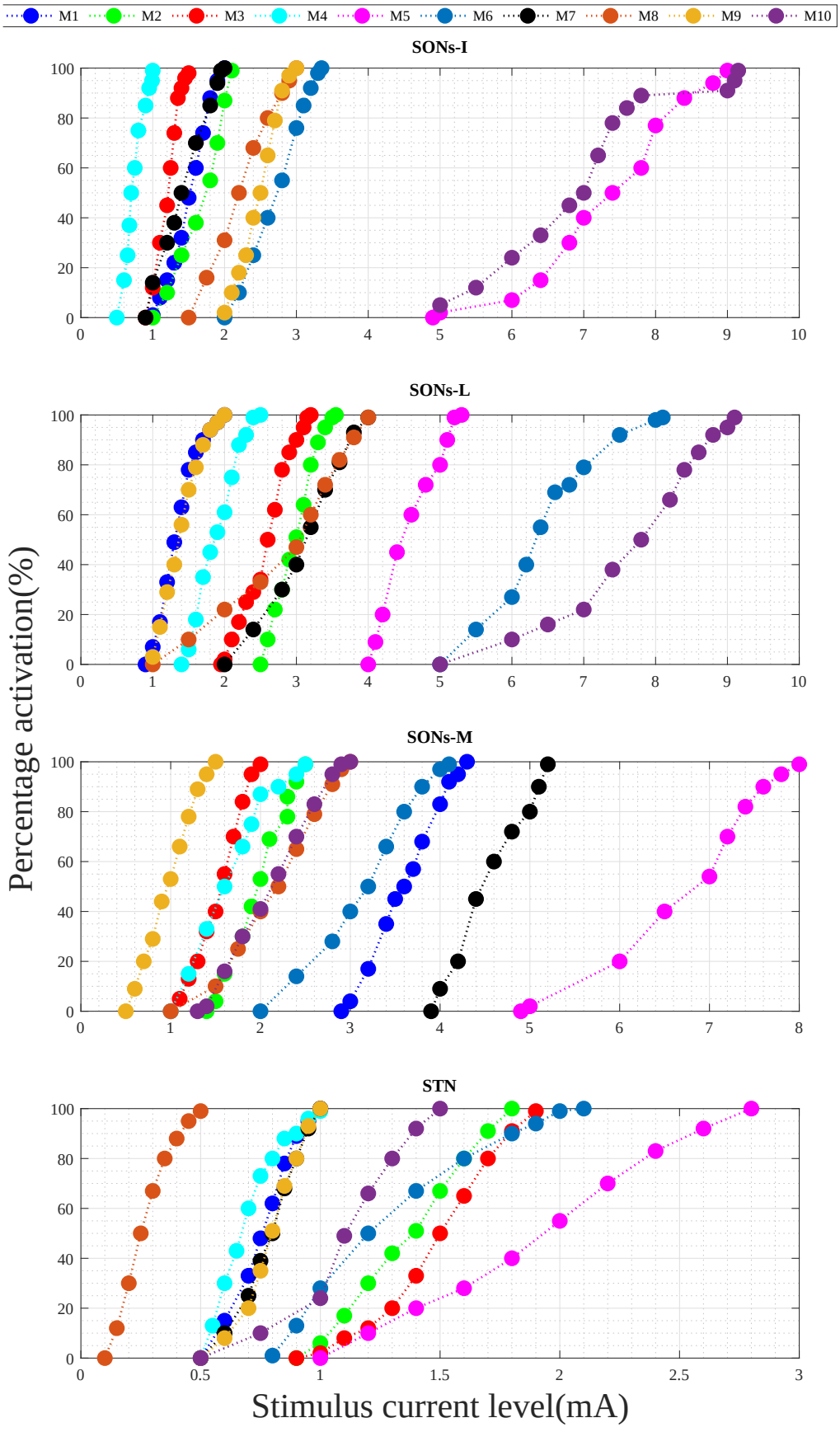

Figure 5.14: Applying optimal electrode array on generated ten human head models. M1: Head model 1.

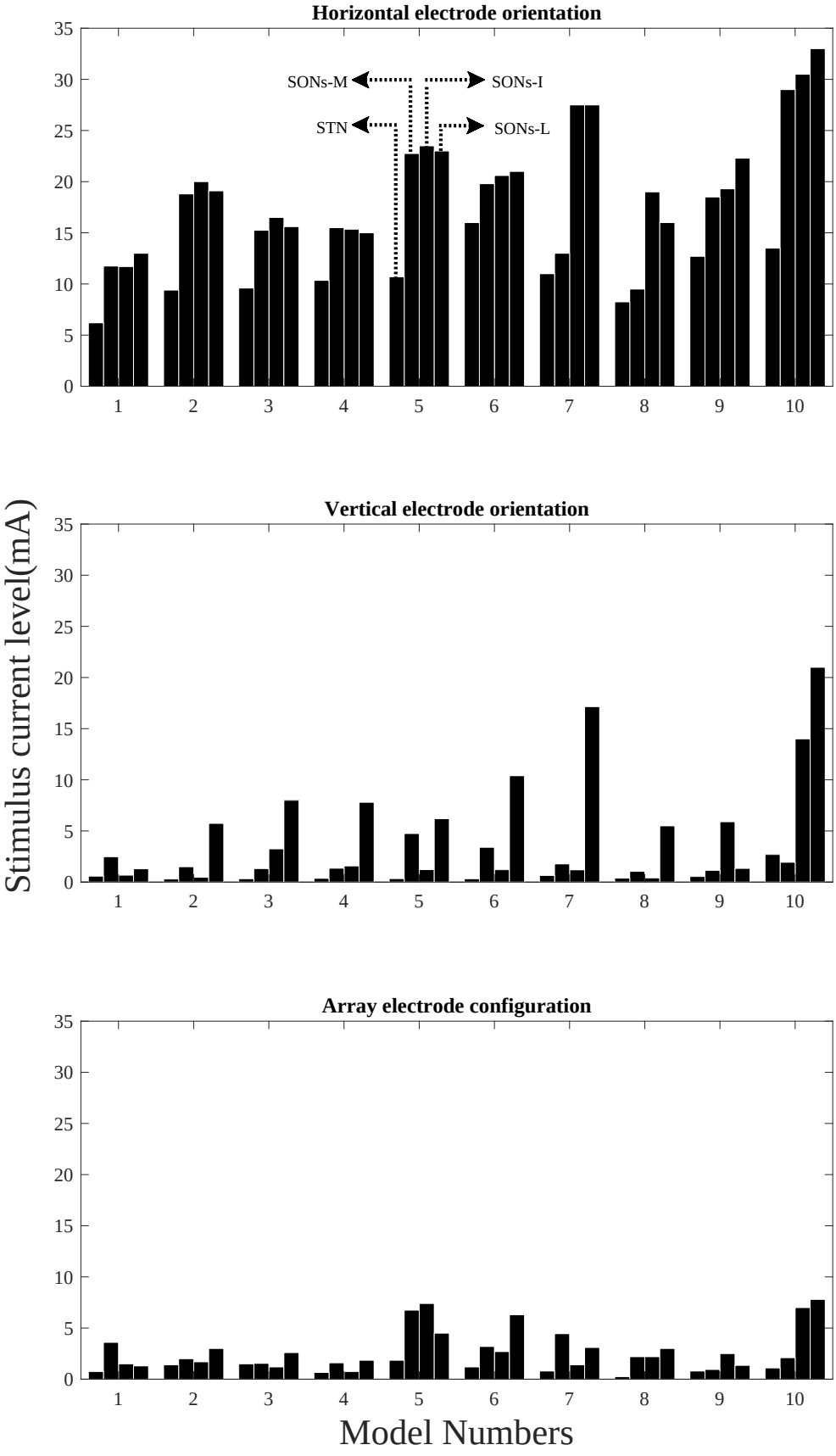

Figure 5.15: The comparison of electrode configurations based on nerve fibres stimulus current levels.

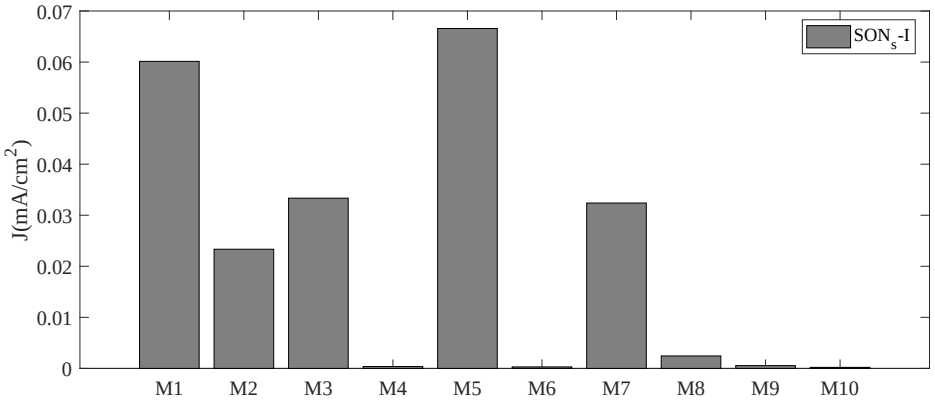

Figure 5.16: Average current density for ten models of the SONs–I nerve branch using optimal electrodes array configuration. J represents current density along the nerve trajectory for ten models.

5.6 Discussion

In chapter 4, it was shown that the neuroanatomical variations have a substantial impact on the required stimulus current levels and these levels were beyond the current delivery capabilities of the Cefaly device. Since the device was patient–operated, the high current levels cannot be applied. Also, the electrode is placed near pain–sensitive structure in the existing device which applied lower current levels may lead to patient discomfort. Thus, there is a need to optimise the existing electrode settings to minimise inefficiency of the solution. In this chapter, the effect of electrode orientation and electrodes array configurations on nerve fibre activation thresholds were investigated. The array technology is a versatile method that can dynamically change the size and position of the stimulation electrode to obtain the optimal design based on the neural activation. It is obviously time–consuming and limited to find the optimal electrode configuration by experiments approach. Alternatively, combined FE models of the human head, tissue layers and nerve model can be used to predict the optimal electrode size and gaps between the array elements.

It has been shown that aligning the axis of the electrodes with the nerve trajectory may reduce the required stimulus current levels. In this way, the polarity of

the electrical potential along the nerve trajectory varies depending on the number of sources and sinks in the electrode configuration [210]. Further, it has been claimed that it is desirable to have a non–uniform electrical distribution to activate the nerve fibres with lower stimulus current levels [209]. Since one electrode participates in the stimulation in the target solution. The first step was to identify if electrode orientation, aligning with the axis of the nerve trajectory, had any effect on the required stimulus current levels by participating two electrodes in the stimulation. Therefore, the electrode orientation was changed to evaluate the effect of non–uniform extracellular potentials along the nerve trajectory on the nerve fibres stimulus current thresholds. To participate both electrodes in simulation in the target solution, the electrode was rotated 90 degrees. The finds for electrode orientations shows relatively lower current levels are required to activate all nerve variations. Thus, it was deduced that the polarity of the simulated electrical potential along the nerve trajectory can be further changed depending on the number of elements (source and sinks) in the electrodes array. Therefore, electrodes array configuration, which composed of multiple sources and sinks, were designed to obtain the optimal configuration based nerve fibre stimulus current thresholds.

One of key improvement of this chapter is the suggestion of using an electrode setting which is aligned with the target nerve based on the theories described in the previous sections. With this new electrode orientation improvement, only in two cases (20%) and only for SONs–L the stimulus current level is above the current capability of the existing device. However, nerve fibres in the STN and the branches of the SONs are activated when the optimal electrodes array configuration is used. It is noted that stimulating other branches may be sufficient to reach the desired outcome. Furthermore, all the results based on 50% activation of the nerve fibres in the nerve branches. This may be slightly pessimistic as even lower activation levels may be sufficient to reach the desired outcome but for designing an optimized electrode setting this can ensure that enough margin

of error is taken into consideration.

It was developed and simulated this optimized arrangement and obtained better results for all variations than the standard arrangement. Using this both new electrode orientation and optimal electrodes array configuration, the STN branch and at least one branch of SONs are stimulated at the current level below 3 mA. This level may be sufficiently low to ensure the desired outcome is achieved in all cases before inducing pain when also considering the current spread of the new design is diverted away from the pain–sensitive structures.

It is noted that reducing the stimulus current level may substantially improve the solution in terms of the safety of delivering the stimulus current, possible side effects and patient compliance. However, the proposed alignment would require using two separate stimulation channels that are appropriately synchronized. While this is not a substantial hardware change but still it adds to the complexity of the system.

Furthermore, the proposed new electrode arrangements have multiple benefits including the reduction of the stimulus current levels and diversion of current spread from possible pain sensitive structures. This improvement can potentially improve the clinical outcome substantially if confirmed in the subsequent clinical studies.

5.7 Summary

In this study, the multilayer FE models of the human head, TENS and cable models of myelinated mammalian nerve fibres with MRG membrane dynamics were used to assess the influence of electrode orientations and electrodes array configurations on the stimulus current thresholds in a device for migraine.

The fundamentals of the electrode design were detailed in the earlier section of the chapter. The importance of the aligning the electrode with the axis of the nerve trajectory was emphasised. Firstly, the effect of participating of two elec-

trodes in the stimulation was investigated using vertical electrode orientation. Based on the findings of this orientation, different size of the electrodes array configuration was designed to identify the optimal electrode configuration based on nerve fibre stimulus current thresholds using the average human head model. Once the optimal electrode configuration was obtained, it was applied to all statistically generated human head models to assess the effect of this configuration for a large population. The stimulus current and PAs were recorded for each model to compare the horizontal (standard) electrode and vertical electrode and electrodes array configurations.

Our findings indicate electrode orientation and electrodes array configurations have a significant impact on the stimulus current thresholds. The nerve fibre stimulus current levels can be considerably decreased using vertical electrode orientation. Furthermore, these current levels are further decreased using optimal electrodes array configuration for all generated nerve models.

It can be deduced that changes in the polarity of the electrical potentials along the nerve trajectory are proportional with the nerve fibres activation.

The proposed new electrode arrangement has multiple benefits including the reduction of the stimulus current levels and diversion of current spread from possible pain sensitive structures. This improvement can potentially improve the clinical outcome substantially if confirmed in the subsequent clinical studies.

Chapter 6

Conclusions and Future Directions

6.1 Introduction

The subsequent sections of this chapter conclude and summarise the narrative of the thesis while the possibilities for improvement and future directions are discussed.

6.2 An optimised design

The target solution, transcutaneous frontal nerve stimulation using Cefaly device, as presented in this thesis can be significantly optimised with respect to stimulation current levels as well as patient discomfort by aligning the electrode with the trajectory of the nerve if proven clinically that it is safe, reliable and efficacious for migraine patients.

The inefficiency of the target solution can be associated with the neuroanatomical variations across different individuals and electrode arrangement that is placed in the vicinity of the pain–sensitive structures which may induce patient discomfort. The computational modelling study presented in this thesis aimed to address these inefficiency limitations. The finding of the hybrid–modelling studies sug-

gest that neuroanatomical variations have a significant impact on the required stimulus current threshold. Additionally, the electrode patch is shifted away in the vicinity of the pain– sensitive structures by aligning the electrode with the axis of the nerve trajectory. In this way, the nerve stimulus current levels are reduced considerably. This may enhance the safety of the neuromodulator while making it more efficacious. Furthermore, the electrode array results show that the required stimulus current thresholds can be further reduced by changing the polarity of electrical potential variations on the nerve. trajectory.

In Chapter 1, the main focus of the thesis outlined and the main novelties and contributions were introduced to the reader. In Chapter 2, the fundamental of the migraine management was detailed. The human head anatomy was reviewed. The key anatomical layers and the human nervous system with underlying neural structures were detailed to provide more information for subsequent works. Furthermore, the generation and propagation of the action potential phenomena, the effect of ion changes on this phenomena with underlying equations were addressed. The pain mechanism and available neural circuitry theories for migraine were discussed. The relationship between the sensory pain mechanism and the neural circuitry of the migraine was compared to have better understanding of migraine pain pathway to provide safe and efficient solution. The existing solutions for a migraine based on pharmaceutical, surgical and neurostimulation techniques and their possible adverse events were addressed to the reader. Since pharmaceutical, surgical and invasive neurostimulation techniques lead to side–effects. Alternatively, non–invasive neuromodulation solutions were introduced and among them, the transcutaneous frontal nerve neuromodulation technique was explored as a possible solution. The possible reasons which are limiting the target solutions efficacy were discussed to put the presented work in this thesis into perspective.

In Chapter 3, the general concept of the hybrid modelling (volume conductor and neural tissue modelling) was introduced. The underlying principles of the neural

tissue excitability based on the existing models are detailed to design the associated nerve models based on the most realistic model. Starting with HH type nerve models, the fundamentals of the cable model and the underlying equations were elaborated to observe the relationship between the cable model and the electrical potential of membrane. The main principles of the volume conductor with underlying equations were discussed to simulate the electrical potentials in the medium. The existing human head modelling studies were tabulated to show the most common numerical approximation in the field of computational modelling. To assess the effect of the simulated extracellular electrical potential variations on the neural tissue, the available mammalian nerve models and their associated channel mechanisms were introduced. It was discussed that highly computational complexity may limit the investigation (e.g., effect of the neuroanatomical variations or different sizes and spacing of electrode arrangements on the stimulus current thresholds). Therefore, to reduce the complexity and save computation time, the simplified human head was extracted by imitating the highly realistic human head model. The MRI based realistic human head model can be simplified with sacrificing a level of error (e.g.,2%). Furthermore, the skin layer was divide into microscopic structures to investigate the effect of the highly conductive and layers on the stimulus current thresholds and their effect on the computation cost. It was shown that the microscopic structures does not a serious impact on the stimulus current thresholds. However, the existence of these layers in the computational model leaded a substantial computational limitation for further work. To conclude, it was shown, in Chapter 3, that the simplified human head model can be used to investigate the effect of neuroanatomical structures and electrode arrangements on the efficacy of the target solution and possible ensuing optimizations.

The work in Chapter 4 provided the effect of neuroanatomical variations on the efficacy of the target solution using state of the art computational bio-models. Different human mead models were developed by varying thirteen key neuroanatom-

ical features including human head size thicknesses of the tissue layers and variations in the courses of the nerve by considering their respective statistical distributions as reported in the literature. After elaborating the anatomical and statistical variations of the associate nerve and their branches, a novel algorithm was developed to account for the variations of the nerve in different individuals and mimic statistically relevant large population. The development of the each human head models, their electrical field simulation process and the neural excitation based on the percentage activation versus current thresholds were introduced the reader. The results suggested that the combined neuroanatomical variations have a significant effect on the neural response for the electrode setting used in Cefaly device, however, it was solely depend on one specific neuroanatomical feature.

In Chapter 5, the fundamentals principles of the electrode design were introduced to the reader. The effect of electrode orientation, location and sizes and shapes on the neural excitation and safety criterion for both electrode design and tissue were detailed to consider these variation parameters while designing the optimal electrode arrangement. The effect of electrical field shaping on the neural tissue excitation was emphasised and it has been shown that the stimulus current thresholds can be reduced by changing the polarity of the electrode using multipolar electrode configuration. This lead to the design of an electrode configuration that induced more variation (changing the polarity) of the electrical field along the nerve trajectory. Thus, the existing device was rotated by 90 decrees to align the axis with nerve trajectory. It was shown that the stimulus current levels are reduced considerably and also the electrode arrangement was shifted away in the vicinity of the pain–sensitive structures. These findings encourage us to design an optimal electrode array configuration. In this way, the polarity of the electrical potentials along the nerve trajectory are changed more compared to standard (horizontal) and vertical electrodes. This results in lower stimulus current levels being required.

6.3 Future work

This section discusses a number of strategies that can be adopted to further develop and improve the work presented in this thesis.

6.3.1 Experiential study: Effect of electrode orientation

Developing computational models of the human head and electrical field and using Hodgkin Huxley type models, we have shown the potential of improving an existing device by changing the way stimulus current is delivered which may result in lower stimulus current being required. Thus, using this new electrode orientation, it may be possible to minimise the existing device complications. This may in turn help in improving the efficacy of the solution. The computational modelling and experimental studies show that using a new electrode orientation, that shifted away from sensitive anatomical layers, result in stimulating all nerve fibre of frontal nerve at a reduced threshold. Also, the experimental study indicates that the painful sensation considerably lower when using the proposed electrode orientation. Although the experimental study of the effect electrode orientation on the stimulus current thresholds and patient discomfort yielded promising results, both standard and the proposed electrode configurations should be applied on a large group of population to have more reliable results.

6.3.2 Protocol and validation procedure

Before validating the computational model results with experimental study in a clinical studying, there is a need to provide a protocol of the study to ensure that there is both a clear idea of how to undertake the experiment and all the materials that are needed. The comprehensive protocol and validation procedures of this study is detailed in Appendix C.

6.3.3 Development of a hardware for novel electrode configuration

The first step was to identify the idea of electrical field shaping using vertical electrode orientation by participating both electrode polarity in stimulation in one phase. The computational study and the experimental tests indicated that the efficacy of the neurostimulator can be improved using vertical electrode orientation. However, the results show that the stimulus current thresholds are still higher for some nerve variations. Thus, the idea of the electrical field shaping encourages the design of an electrode configuration which lead to more variations of the electrical field in one phase. The electrical potential along the nerve fibre can be varied more using an electrode array configuration that is composed of multiple elements. The modelling results indicate that the stimulus current threshold can be further reduced compared to both electrode orientation. Also, the current levels are not fluctuated for different individuals. Thus a novel neuromodulator can be designed if the computational modelling results are proven clinically in terms of the safety and efficacy based on a large sample.

6.3.4 Experiential study: Effect of electrode array configuration

After developing the hardware design for the novel electrode configuration, the experimental study will be applied following the safety criteria. The modelling results may be validated in a small clinical study at first for a short time. Then, if the results are promising, the neuromodulator should be applied in a large sample and a long term based clinical study to assess the efficacy and limitation of the device.

Bibliography

[1] E. Salkim, A. Shiraz, and A. Demosthenous, "Influence of cellular structures of skin on fiber activation thresholds and computation cost," *Biomedical Physics & Engineering Express*, vol. 5, no. 1, p. 015015, 2018.

[2] H. C. C. of the International Headache Society (IHS), "The international classification of headache disorders, (beta version)," *Cephalalgia*, vol. 33, no. 9, pp. 629–808, 2013.

[3] H.-C. Diener, A. Charles, P. J. Goadsby, and D. Holle, "New therapeutic approaches for the prevention and treatment of migraine," *The Lancet Neurology*, vol. 14, no. 10, pp. 1010–1022, 2015.

[4] W. Z. Yeh, L. Blizzard, and B. V. Taylor, "What is the actual prevalence of migraine?" *Brain and behavior*, vol. 8, no. 6, p. e00950, 2018.

[5] X. H. Hu, L. E. Markson, R. B. Lipton, W. F. Stewart, and M. L. Berger, "Burden of migraine in the united states: disability and economic costs," *Archives of internal medicine*, vol. 159, no. 8, pp. 813–818, 1999.

[6] R. B. Lipton, D. C. Buse, D. Serrano, S. Holland, and M. L. Reed, "Examination of unmet treatment needs among persons with episodic migraine: results of the american migraine prevalence and prevention (ampp) study," *Headache: The Journal of Head and Face Pain*, vol. 53, no. 8, pp. 1300–1311, 2013.

[7] F. Riederer, S. Penning, and J. Schoenen, "Transcutaneous supraorbital nerve stimulation (t-sns) with the cefaly® device for migraine prevention: a review of the available data," *Pain and therapy*, vol. 4, no. 2, pp. 135–147, 2015.

[8] R. Melzack, P. D. Wall *et al.*, "Pain mechanisms: a new theory," *Science*, vol. 150, no. 3699, pp. 971–979, 1965.

[9] S. Miller, A. J. Sinclair, B. Davies, and M. Matharu, "Neurostimulation in the treatment of primary headaches," *Practical neurology*, pp. practneurol–2015, 2016.

[10] M. C. Ridding and J. C. Rothwell, "Is there a future for therapeutic use of transcranial magnetic stimulation?" *Nature Reviews Neuroscience*, vol. 8, no. 7, p. 559, 2007.

[11] A. Ambrosini, C. DAlessio, D. Magis, and J. Schoenen, "Targeting pericranial nerve branches to treat migraine: Current approaches and perspectives," *Cephalalgia*, vol. 35, no. 14, pp. 1308–1322, 2015.

[12] J. E. Janis, D. A. Hatef, R. Hagan, T. Schaub, J. H. Liu, H. Thakar, K. M. Bolden, J. B. Heller, and T. J. Kurkjian, "Anatomy of the supratrochlear nerve: implications for the surgical treatment of migraine headaches," *Plastic and reconstructive surgery*, vol. 131, no. 4, pp. 743–750, 2013.

[13] J. Olesen, R. Burstein, M. Ashina, and P. Tfelt-Hansen, "Origin of pain in migraine: evidence for peripheral sensitisation," *The Lancet Neurology*, vol. 8, no. 7, pp. 679–690, 2009.

[14] J. Schoenen, B. Vandersmissen, S. Jeangette, L. Herroelen, M. Vandenheede, P. Gérard, and D. Magis, "Migraine prevention with a supraorbital transcutaneous stimulator a randomized controlled trial," *Neurology*, vol. 80, no. 8, pp. 697–704, 2013.

[15] D. Magis, S. Sava, T. S. dElia, R. Baschi, and J. Schoenen, "Safety and patients satisfaction of transcutaneous supraorbital neurostimulation (tsns) with the cefaly® device in headache treatment: a survey of 2,313 headache sufferers in the general population," *The journal of headache and pain*, vol. 14, no. 1, p. 95, 2013.

[16] S. L. Sava, V. de Pasqua, D. Magis, and J. Schoenen, "Effects of visual cortex activation on the nociceptive blink reflex in healthy subjects," p. e100198, 2014.

[17] P. Hasgall, E. Neufeld, M. Gosselin, A. Klingenböck, and N. Kuster, "Itis database for thermal and electromagnetic parameters of biological tissues," *Version 2.6*, 2015.

[18] C. Gabriel, A. Peyman, and E. Grant, "Electrical conductivity of tissue at frequencies below 1 mhz," *Physics in medicine & biology*, vol. 54, no. 16, p. 4863, 2009.

[19] R. Y. Ha, K. Nojima, W. P. Adams Jr, and S. A. Brown, "Analysis of facial skin thickness: defining the relative thickness index," *Plastic and reconstructive surgery*, vol. 115, no. 6, pp. 1769–1773, 2005.

[20] P. Bertemes Filho, "Tissue characterisation using an impedance spectrosopy probe," Ph.D. dissertation, University of Sheffield, 2002.

[21] U. Birgersson, *Electrical impedance of human skin and tissue alterations: Mathematical modeling and measurements*. Inst för klinisk vetenskap, intervention och teknik/Dept of Clinical Science, Intervention and Technology, 2012.

[22] D. N. Shier, J. Butler, and R. Lewis, *Hole's essentials of human anatomy & physiology*. McGraw-Hill Education, 2017.

[23] J. L. Hiatt and L. P. Gartner, *Textbook of head and neck anatomy*. LWW, 2009.

[24] M. R. Macdonald, J. H. Spiegel, R. B. Raven, S. S. Kabaker, and C. S. Maas, "An anatomical approach to glabellar rhytids," *Archives of Otolaryngology–Head & Neck Surgery*, vol. 124, no. 12, pp. 1315–1320, 1998.

[25] E. Marieb, *Essentials of Human Anatomy and Physiology (10th)*. San Francisco, CA: Benjamin Cummings/Pearson Education, 2011, vol. 10.

[26] M. Z. Siemionow, *The know-how of face transplantation*. Springer, 2011.

[27] E. R. Kandel, J. H. Schwartz, T. M. Jessell, S. A. Siegelbaum, A. J. Hudspeth *et al.*, *Principles of neural science*. McGraw-hill New York, 2000, vol. 4.

[28] D. Purves, G. J. Augustine, D. Fitzpatrick, W. C. Hall, A.-S. LaMantia, J. O. McNamara, and L. E. White, "Neuroscience. 4th," *Sunderland, Mass.: Sinauer Associates*, 2012.

[29] H. Lodish, A. Berk, S. L. Zipursky, P. Matsudaira, D. Baltimore, and J. Darnell, "Molecular cell biology 4th edition," *National Center for Biotechnology Information, Bookshelf*, 2000.

[30] R. Plonsey and R. C. Barr, *Bioelectricity: a quantitative approach*. Springer Science & Business Media, 2007.

[31] S. Monkhouse, *Cranial nerves: functional anatomy*. Cambridge University Press, 2005.

[32] P. J. Goadsby, "Recent advances in understanding migraine mechanisms, molecules and therapeutics," *Trends in molecular medicine*, vol. 13, no. 1, pp. 39–44, 2007.

[33] P. Malmivuo, J. Malmivuo, and R. Plonsey, *Bioelectromagnetism: principles and applications of bioelectric and biomagnetic fields*. Oxford University Press, USA, 1995.

[34] M. N. Levy, B. M. Koeppen, and B. A. Stanton, *Berne & Levy Principles of Physiology*. Elsevier Health Sciences, 2005.

[35] J. Whitwam, "Classification of peripheral nerve fibres," *Anaesthesia*, vol. 31, no. 4, pp. 494–503, 1976.

[36] G. M. Manzano, L. M. Giuliano, and J. A. Nóbrega, "A brief historical note on the classification of nerve fibers," *Arquivos de neuro-psiquiatria*, vol. 66, no. 1, pp. 117–119, 2008.

[37] J. D. Loeser, "Relieving pain in america," 2012.

[38] D. M. Murphy and P. M. O'byrne, "Recent advances in the pathophysiology of asthma," *Chest*, vol. 137, no. 6, pp. 1417–1426, 2010.

[39] E. R. Perl, "Ideas about pain, a historical view," *Nature Reviews Neuroscience*, vol. 8, no. 1, p. 71, 2007.

[40] P. J. Goadsby, "Pathophysiology of migraine," *Neurologic clinics*, vol. 27, no. 2, pp. 335–360, 2009.

[41] M. H. Cameron, *Physical agents in rehabilitation: from research to practice*. Elsevier Health Sciences, 2012.

[42] M. Fischera, M. Marziniak, I. Gralow, and S. Evers, "The incidence and prevalence of cluster headache: a meta-analysis of population-based studies," *Cephalalgia*, vol. 28, no. 6, pp. 614–618, 2008.

[43] T. Wolter and H. Kaube, "Neurostimulation for chronic cluster headache," *Therapeutic advances in neurological disorders*, vol. 5, no. 3, pp. 175–180, 2012.

[44] J. L. Pedersen, M. Barloese, and R. H. Jensen, "Neurostimulation in cluster headache: a review of current progress," *Cephalalgia*, vol. 33, no. 14, pp. 1179–1193, 2013.

[45] T. Vos, R. M. Barber, B. Bell, A. Bertozzi-Villa, S. Biryukov, I. Bolliger, F. Charlson, A. Davis, L. Degenhardt, D. Dicker *et al.*, "Global, regional, and national incidence, prevalence, and years lived with disability for 301 acute and chronic diseases and injuries in 188 countries, 1990–2013: a systematic analysis for the global burden of disease study 2013," *The Lancet*, vol. 386, no. 9995, pp. 743–800, 2015.

[46] R. Burch, P. Rizzoli, and E. Loder, "The prevalence and impact of migraine and severe headache in the united states: figures and trends from government health studies," *Headache: The Journal of Head and Face Pain*, vol. 58, no. 4, pp. 496–505, 2018.

[47] F. Puledda and K. Shields, "Non-pharmacological approaches for migraine," *Neurotherapeutics*, pp. 1–10, 2018.

[48] R. B. Lipton and M. E. Bigal, "The epidemiology of migraine," *The American Journal of Medicine Supplements*, vol. 118, pp. 3–10, 2005.

[49] D. Pietrobon and M. A. Moskowitz, "Pathophysiology of migraine," *Annual review of physiology*, vol. 75, pp. 365–391, 2013.

[50] F. Puledda, R. Messina, and P. J. Goadsby, "An update on migraine: current understanding and future directions," *Journal of neurology*, vol. 264, no. 9, pp. 2031–2039, 2017.

[51] C. F. Marfurt, "The central projections of trigeminal primary afferent neurons in the cat as determined by the tranganglionic transport of horseradish peroxidase," *Journal of Comparative Neurology*, vol. 203, no. 4, pp. 785–798, 1981.

[52] J. P. Okeson, *Bell's orofacial pains: the clinical management of orofacial pain*. Quintessence Publishing Company Chicago, Ill, USA, 2005.

[53] N. M. Schuster and A. M. Rapoport, "New strategies for the treatment and prevention of primary headache disorders," *Nature Reviews Neurology*, vol. 12, no. 11, p. 635, 2016.

[54] J. Olesen, M. Bousser, H. Diener, D. Dodick, M. First, P. Goadsby, H. Göbel, M. Lainez, J. Lance, R. Lipton *et al.*, "New appendix criteria open for a broader concept of chronic migraine," *Cephalalgia*, vol. 26, no. 6, pp. 742–746, 2006.

[55] R. B. Lipton and S. D. Silberstein, "Episodic and chronic migraine headache: breaking down barriers to optimal treatment and prevention," *Headache: The Journal of Head and Face Pain*, vol. 55, pp. 103–122, 2015.

[56] L. Gfrerer and B. Guyuron, "Surgical treatment of migraine headaches," *Acta Neurologica Belgica*, vol. 117, no. 1, pp. 27–32, 2017.

[57] B. Guyuron, J. S. Kriegler, J. Davis, and S. B. Amini, "Comprehensive surgical treatment of migraine headaches," *Plastic and reconstructive surgery*, vol. 115, no. 1, pp. 1–9, 2005.

[58] B. Guyuron, A. Varghai, B. J. Michelow, T. Thomas, and J. Davis, "Corrugator supercilii muscle resection and migraine headaches," *Plastic and reconstructive surgery*, vol. 106, no. 2, pp. 429–434, 2000.

[59] A. Matarasso, "Surgical treatment of migraine headaches," *Archives of facial plastic surgery*, vol. 4, no. 4, pp. 274–275, 2002.

[60] F. Dirnberger and K. Becker, "Surgical treatment of migraine headaches by corrugator muscle resection," *Plastic and reconstructive surgery*, vol. 114, no. 3, pp. 652–657, 2004.

[61] J. T. Poggi, B. E. Grizzell, and S. D. Helmer, "Confirmation of surgical decompression to relieve migraine headaches," *Plastic and reconstructive surgery*, vol. 122, no. 1, pp. 115–122, 2008.

[62] B. Guyuron, D. Reed, J. S. Kriegler, J. Davis, N. Pashmini, and S. Amini, "A placebo-controlled surgical trial of the treatment of migraine headaches," *Plastic and reconstructive surgery*, vol. 124, no. 2, pp. 461–468, 2009.

[63] B. Guyuron, J. S. Kriegler, J. Davis, and S. B. Amini, "Five-year outcome of surgical treatment of migraine headaches," *Plastic and reconstructive surgery*, vol. 127, no. 2, pp. 603–608, 2011.

[64] J. E. Janis, A. Dhanik, and J. H. Howard, "Validation of the peripheral trigger point theory of migraine headaches: single-surgeon experience using botulinum toxin and surgical decompression," *Plastic and reconstructive surgery*, vol. 128, no. 1, pp. 123–131, 2011.

[65] K. Larson, M. Lee, J. Davis, and B. Guyuron, "Factors contributing to migraine headache surgery failure and success," *Plastic and reconstructive surgery*, vol. 128, no. 5, pp. 1069–1075, 2011.

[66] I. Ducic, J. M. Felder III, and J. E. Janis, "Occipital artery vasculitis not identified as a mechanism of occipital neuralgia–related chronic migraine headaches," *Plastic and reconstructive surgery*, vol. 128, no. 4, pp. 908–912, 2011.

[67] K. J. Chepla, E. Oh, and B. Guyuron, "Clinical outcomes following supraorbital foraminotomy for treatment of frontal migraine headache," *Plastic and reconstructive surgery*, vol. 129, no. 4, p. 656e, 2012.

[68] M. T. Liu, B. S. Armijo, and B. Guyuron, "A comparison of outcome of surgical treatment of migraine headaches using a constellation of symptoms versus botulinum toxin type a to identify the trigger sites," *Plastic and reconstructive surgery*, vol. 129, no. 2, pp. 413–419, 2012.

[69] M. T. Liu, H. Chim, and B. Guyuron, "Outcome comparison of endoscopic and transpalpebral decompression for treatment of frontal migraine headaches," *Plastic and reconstructive surgery*, vol. 129, no. 5, pp. 1113–1119, 2012.

[70] L. Chmielewski, M. T. Liu, and B. Guyuron, "The role of occipital artery resection in the surgical treatment of occipital migraine headaches," *Plastic and reconstructive surgery*, vol. 131, no. 3, pp. 351e–356e, 2013.

[71] M. Lee, M. A. Monson, M. T. Liu, D. Reed, and B. Guyuron, "Positive botulinum toxin type a response is a prognosticator for migraine surgery success," *Plastic and reconstructive surgery*, vol. 131, no. 4, pp. 751–757, 2013.

[72] M. Lee, K. Lineberry, D. Reed, and B. Guyuron, "The role of the third occipital nerve in surgical treatment of occipital migraine headaches," *Journal of Plastic, Reconstructive & Aesthetic Surgery*, vol. 66, no. 10, pp. 1335–1339, 2013.

[73] I. Ducic, J. M. Felder III, N. Khan, and S. Youn, "Greater occipital nerve excision for occipital neuralgia refractory to nerve decompression," *Annals of plastic surgery*, vol. 72, no. 2, pp. 184–187, 2014.

[74] S. Polotto, F. Simonacci, E. Grignaffini, M. P. Grieco, and E. Raposio, "Surgical treatment of frontal and occipital migraines: A comparison of results." *Plastic and reconstructive surgery. Global open*, vol. 4, no. 3, pp. e653–e653, 2016.

[75] J. R. Gatherwright, Y. Wu-Fienberg, and B. Guyuron, "The importance of surgical maneuvers during treatment of frontal migraines (site i): A prospective, randomized cohort study evaluating foraminotomy/fasciotomy, myectomy, and arterectomy," *Journal of Plastic, Reconstructive & Aesthetic Surgery*, 2017.

[76] A. Jose, S. A. Nagori, and A. Roychoudhury, "Surgical management of migraine headache," *Journal of Craniofacial Surgery*, vol. 29, no. 2, pp. e106–e108, 2018.

[77] E. S. Krames, P. H. Peckham, A. Rezai, and F. Aboelsaad, "What is neuromodulation?" in *Neuromodulation*. Elsevier, 2009, pp. 3–8.

[78] K. DOstilio and D. Magis, "Invasive and non-invasive electrical pericranial nerve stimulation for the treatment of chronic primary headaches," *Current pain and headache reports*, vol. 20, no. 11, p. 61, 2016.

[79] T. L. Trentman and R. S. Zimmerman, "Occipital nerve stimulation: technical and surgical aspects of implantation," *Headache: The Journal of Head and Face Pain*, vol. 48, no. 2, pp. 319–327, 2008.

[80] R. L. Weiner and K. M. Alo, "Occipital neurostimulation for treatment of intractable headache syndromes," in *Neuromodulation*. Elsevier, 2009, pp. 409–416.

[81] R. L. Verrier, B. D. Nearing, B. Olin, P. Boon, and S. C. Schachter, "Baseline elevation and reduction in cardiac electrical instability assessed by quantitative t-wave alternans in patients with drug-resistant epilepsy treated with vagus nerve stimulation in the aspiresr e-36 trial," *Epilepsy & Behavior*, vol. 62, pp. 85–89, 2016.

[82] P. Martelletti, R. H. Jensen, A. Antal, R. Arcioni, F. Brighina, M. de Tommaso, A. Franzini, D. Fontaine, M. Heiland, T. P. Jürgens *et al.*, "Neuromodulation of chronic headaches: position statement from the european headache federation," *The journal of headache and pain*, vol. 14, no. 1, p. 86, 2013.

[83] S. J. Tepper and A. Caparso, "Sphenopalatine ganglion (spg): stimulation mechanism, safety, and efficacy," *Headache: The Journal of Head and Face Pain*, vol. 57, no. S1, pp. 14–28, 2017.

[84] D. Fontaine, S. Santucci, and M. Lanteri-Minet, "Managing cluster headache with sphenopalatine ganglion stimulation: a review," *Journal of Pain Research*, vol. 11, p. 375, 2018.

[85] D. Rodrigo, P. Acín, and P. Bermejo, "Occipital nerve stimulation for refractory chronic migraine: Results of a long-term prospective study," *Pain physician*, vol. 20, no. 1, pp. 151–159, 2017.

[86] N. A. Mekhail, E. Estemalik, G. Azer, K. Davis, and S. J. Tepper, "Safety and efficacy of occipital nerves stimulation for the treatment of chronic migraines: Randomized, double-blind, controlled single-center experience," *Pain Practice*, vol. 17, no. 5, pp. 669–677, 2017.

[87] S. D. Silberstein, D. W. Dodick, J. Saper, B. Huh, K. V. Slavin, A. Sharan, K. Reed, S. Narouze, A. Mogilner, J. Goldstein *et al.*, "Safety and efficacy of peripheral nerve stimulation of the occipital nerves for the management of chronic migraine: results from a randomized, multicenter, double-blinded, controlled study," *Cephalalgia*, vol. 32, no. 16, pp. 1165–1179, 2012.

[88] S. J. Tepper, A. Rezai, S. Narouze, C. Steiner, P. Mohajer, and M. Ansarinia, "Acute treatment of intractable migraine with sphenopalatine ganglion electrical stimulation," *Headache: The Journal of Head and Face Pain*, vol. 49, no. 7, pp. 983–989, 2009.

[89] M. Lenaerts, K. Oommen, J. Couch, and V. Skaggs, "Can vagus nerve stimulation help migraine?" *Cephalalgia*, vol. 28, no. 4, pp. 392–395, 2008.

[90] A. Mauskop, "Vagus nerve stimulation relieves chronic refractory migraine and cluster headaches," *Cephalalgia*, vol. 25, no. 2, pp. 82–86, 2005.

[91] D. Magis, "Neuromodulation in migraine: State of the art and perspectives," *Expert review of medical devices*, vol. 12, no. 3, pp. 329–339, 2015.

[92] S. Bauer, H. Baier, C. Baumgartner, K. Bohlmann, S. Fauser, W. Graf, B. Hillenbrand, M. Hirsch, C. Last, H. Lerche *et al.*, "Transcutaneous vagus nerve stimulation (tvns) for treatment of drug-resistant epilepsy: a randomized, double-blind clinical trial (cmpse02)," *Brain stimulation*, vol. 9, no. 3, pp. 356–363, 2016.

[93] R. Bhola, E. Kinsella, N. Giffin, S. Lipscombe, F. Ahmed, M. Weatherall, and P. J. Goadsby, "Single-pulse transcranial magnetic stimulation (stms) for the acute treatment of migraine: evaluation of outcome data for the uk post market pilot program," *The journal of headache and pain*, vol. 16, no. 1, p. 51, 2015.

[94] A. Datta, V. Bansal, J. Diaz, J. Patel, D. Reato, and M. Bikson, "Gyri-precise head model of transcranial dc stimulation: Improved spatial focality using a ring electrode versus conventional rectangular pad. brain stimulation. 2009; 2 (4): 201–207," 2010.

[95] S. Miller and M. Matharu, "Non-invasive neuromodulation in primary headaches," *Current pain and headache reports*, vol. 21, no. 3, p. 14, 2017.

[96] T. Usichenko, H. Hacker, and M. Lotze, "Transcutaneous auricular vagal nerve stimulation (tavns) might be a mechanism behind the analgesic effects of auricular acupuncture," *Brain Stimulation: Basic, Translational, and Clinical Research in Neuromodulation*, vol. 10, no. 6, pp. 1042–1044, 2017.

[97] A. Przeklasa-Muszyska, M. Kocotpska, J. Dobrogowski, M. Wiatr, and J. Mika, "Transcranial direct current stimulation (tdcs) and its influence on analgesics effectiveness in patients suffering from migraine headache," *Pharmacological Reports*, vol. 69, no. 4, pp. 714–721, 2017.

[98] H. Matsumoto and Y. Ugawa, "Adverse events of tdcs and tacs: a review," *Clinical Neurophysiology Practice*, vol. 2, pp. 19–25, 2017.

[99] A. J. Starling, S. J. Tepper, M. J. Marmura, E. A. Shamim, M. S. Robbins, N. Hindiyeh, A. C. Charles, P. J. Goadsby, R. B. Lipton, S. D. Silberstein *et al.*, "A multicenter, prospective, single arm, open label, observational study of stms for migraine prevention (espouse study)," *Cephalalgia*, p. 0333102418762525, 2018.

[100] A. Przeklasa-Muszyska, K. Skrzypiec, M. Kocotpska, J. Dobrogowski, M. Wiatr, and J. Mika, "Non-invasive transcutaneous supraorbital neurostimulation (tsns) using cefaly® device in prevention of primary headaches," *Neurologia i neurochirurgia polska*, vol. 51, no. 2, pp. 127–134, 2017.

[101] M. Vikelis, E. V. Dermitzakis, K. C. Spingos, G. G. Vasiliadis, G. S. Vlachos, and E. Kararizou, "Clinical experience with transcutaneous supraorbital nerve stimulation in patients with refractory migraine or with migraine and intolerance to topiramate: a prospective exploratory clinical study," *BMC neurology*, vol. 17, no. 1, p. 97, 2017.

[102] P. Di Fiore, G. Bussone, A. Galli, H. Didier, C. Peccarisi, D. DAmico, and F. Frediani, "Transcutaneous supraorbital neurostimulation for the prevention of chronic migraine: a prospective, open-label preliminary trial," *Neurological Sciences*, vol. 38, no. 1, pp. 201–206, 2017.

[103] D. E. Chou, G. J. Gross, C. H. Casadei, and M. S. Yugrakh, "External trigeminal nerve stimulation for the acute treatment of migraine: Open-label trial on safety and efficacy," *Neuromodulation: Technology at the Neural Interface*, vol. 20, no. 7, pp. 678–683, 2017.

[104] L. Grazzi, G. Egeo, E. Liebler, A. M. Padovan, and P. Barbanti, "Non-invasive vagus nerve stimulation (nvns) as symptomatic treatment of migraine in young patients: a preliminary safety study," *Neurological Sciences*, vol. 38, no. 1, pp. 197–199, 2017.

[105] L. Grazzi, G. Egeo, A. H. Calhoun, C. K. McClure, E. Liebler, and P. Barbanti, "Non-invasive vagus nerve stimulation (nvns) as mini-prophylaxis for menstrual/menstrually related migraine: an open-label study," *The journal of headache and pain*, vol. 17, no. 1, p. 91, 2016.

[106] S. D. Silberstein, A. H. Calhoun, R. B. Lipton, B. M. Grosberg, R. K. Cady, S. Dorlas, K. A. Simmons, C. Mullin, E. J. Liebler, P. J. Goadsby *et al.*, "Chronic migraine headache prevention with noninvasive vagus nerve stimulation the event study," *Neurology*, vol. 87, no. 5, pp. 529–538, 2016.

[107] A. Russo, A. Tessitore, F. Conte, L. Marcuccio, A. Giordano, and G. Tedeschi, "Transcutaneous supraorbital neurostimulation in de novo patients with migraine without aura: the first italian experience," *The journal of headache and pain*, vol. 16, no. 1, p. 69, 2015.

[108] P. Goadsby, B. Grosberg, A. Mauskop, R. Cady, and K. Simmons, "Effect of noninvasive vagus nerve stimulation on acute migraine: an open-label pilot study," *Cephalalgia*, vol. 34, no. 12, pp. 986–993, 2014.

[109] A. Straube, J. Ellrich, O. Eren, B. Blum, and R. Ruscheweyh, "Treatment of chronic migraine with transcutaneous stimulation of the auricular branch of the vagal nerve (auricular t-vns): a randomized, monocentric clinical trial," *The journal of headache and pain*, vol. 16, no. 1, p. 63, 2015.

[110] A. Viganò, T. S. DElia, S. L. Sava, M. Auvé, V. De Pasqua, A. Colosimo, V. Di Piero, J. Schoenen, and D. Magis, "Transcranial direct current stimulation (tdcs) of the visual cortex: a proof-of-concept study based on interictal electrophysiological abnormalities in migraine," *The journal of headache and pain*, vol. 14, no. 1, p. 23, 2013.

[111] B. M. Clarke, A. R. Upton, M. V. Kamath, T. Al-Harbi, and C. M. Castellanos, "Transcranial magnetic stimulation for migraine: clinical effects," *The journal of headache and pain*, vol. 7, no. 5, pp. 341–346, 2006.

[112] C. J. Wright, S. R. Haqshenas, J. Rothwell, and N. Saffari, "Unmyelinated peripheral nerves can be stimulated in vitro using pulsed ultrasound," *Ultrasound in medicine & biology*, vol. 43, no. 10, pp. 2269–2283, 2017.

[113] C. R. Butson, "Computational models of neuromodulation," in *International review of neurobiology*. Elsevier, 2012, vol. 107, pp. 5–22.

[114] R. Christopher, "Computational methods and software for bioelectric field problems."

[115] J. J. Pods, "Electrodiffusion models of axon and extracellular space using the poisson-nernst-planck equations," Ph.D. dissertation, 2014.

[116] A. L. Hodgkin and A. F. Huxley, "A quantitative description of membrane current and its application to conduction and excitation in nerve," *The Journal of physiology*, vol. 117, no. 4, pp. 500–544, 1952.

[117] C. Koch, "Cable theory in neurons with active, linearized membranes," *Biological cybernetics*, vol. 50, no. 1, pp. 15–33, 1984.

[118] M. L. Hines and N. T. Carnevale, "The neuron simulation environment," *Neural computation*, vol. 9, no. 6, pp. 1179–1209, 1997.

[119] L. Goldman and J. S. Albus, "Computation of impulse conduction in myelinated fibers; theoretical basis of the velocity-diameter relation," *Biophysical journal*, vol. 8, no. 5, pp. 596–607, 1968.

[120] R. Fitzhugh, "Computation of impulse initiation and saltatory conduction in a myelinated nerve fiber," *Biophysical journal*, vol. 2, no. 1, pp. 11–21, 1962.

[121] D. R. McNeal, "Analysis of a model for excitation of myelinated nerve," *IEEE Transactions on Biomedical Engineering*, no. 4, pp. 329–337, 1976.

[122] J. Sweeney, J. Mortimer, and D. Durand, "Modeling of mammalian myelinated nerve for functional neuromuscular stimulation." in *IEEE/Engineering in Medicine and Biology Society Annual Conference*. IEEE, 1987.

[123] I. Tasaki, "New measurements of the capacity and the resistance of the myelin sheath and the nodal membrane of the isolated frog nerve fiber," *American Journal of Physiology-Legacy Content*, vol. 181, no. 3, pp. 639–650, 1955.

[124] A. Huxley and R. Stämpeli, "Evidence for saltatory conduction in peripheral myelinated nerve fibres," *The Journal of physiology*, vol. 108, no. 3, pp. 315–339, 1949.

[125] J. W. Moore, R. W. Joyner, M. H. Brill, S. D. Waxman, and M. Najar-Joa, "Simulations of conduction in uniform myelinated fibers. relative sensitivity to changes in nodal and internodal parameters," *Biophysical journal*, vol. 21, no. 2, pp. 147–160, 1978.

[126] J. T. Rubinstein, "Analytical theory for extracellular electrical stimulation of nerve with focal electrodes. ii. passive myelinated axon," *Biophysical journal*, vol. 60, no. 3, pp. 538–555, 1991.

[127] M. Capogrosso, N. Wenger, S. Raspopovic, P. Musienko, J. Beauparlant, L. B. Luciani, G. Courtine, and S. Micera, "A computational model for epidural electrical stimulation of spinal sensorimotor circuits," *Journal of Neuroscience*, vol. 33, no. 49, pp. 19 326–19 340, 2013.

[128] A. Richardson, C. McIntyre, and W. Grill, "Modelling the effects of electric fields on nerve fibres: influence of the myelin sheath," *Medical and Biological Engineering and Computing*, vol. 38, no. 4, pp. 438–446, 2000.

[129] A. Blight and S. Someya, "Depolarizing afterpotentials in myelinated axons of mammalian spinal cord," *Neuroscience*, vol. 15, no. 1, pp. 1–12, 1985.

[130] E. F. Barrett and J. N. Barrett, "Intracellular recording from vertebrate myelinated axons: mechanism of the depolarizing afterpotential," *The Journal of physiology*, vol. 323, no. 1, pp. 117–144, 1982.

[131] C. C. McIntyre, A. G. Richardson, and W. M. Grill, "Modeling the excitability of mammalian nerve fibers: influence of afterpotentials on the recovery cycle," *Journal of neurophysiology*, vol. 87, no. 2, pp. 995–1006, 2002.

[132] A. Kuhn, "Modeling transcutaneous electrical stimulation," Ph.D. dissertation, ETH Zurich, 2008.

[133] P. K. Stys and S. G. Waxman, "Activity-dependent modulation of excitability: implications for axonal physiology and pathophysiology," *Muscle & Nerve: Official Journal of the American Association of Electrodiagnostic Medicine*, vol. 17, no. 9, pp. 969–974, 1994.

[134] G. David, B. Modney, K. A. Scappaticci, J. N. Barrett, and E. F. Barrett, "Electrical and morphological factors influencing the depolarizing after-potential in rat and lizard myelinated axons." *The Journal of Physiology*, vol. 489, no. 1, pp. 141–157, 1995.

[135] D. Bourbeau, J. Hokanson, J. Rubin, and D. Weber, "A computational model for estimating recruitment of primary afferent fibers by intraneural stimulation in the dorsal root ganglia," *Journal of neural engineering*, vol. 8, no. 5, p. 056009, 2011.

[136] K. Lindsay, J. Rosenberg, and G. Tucker, "From maxwell's equations to the cable equation and beyond," *Progress in biophysics and molecular biology*, vol. 85, no. 1, pp. 71–116, 2004.

[137] A. Agudelo-Toro, "Numerical simulations on the biophysical foundations of the neuronal extracellular space," 2012.

[138] S. Joucla and B. Yvert, "Modeling extracellular electrical neural stimulation: from basic understanding to mea-based applications," *Journal of Physiology-Paris*, vol. 106, no. 3-4, pp. 146–158, 2012.

[139] S. Joucla, A. Glière, and B. Yvert, "Current approaches to model extracellular electrical neural microstimulation," *Frontiers in computational neuroscience*, vol. 8, p. 13, 2014.

[140] A. Tizzard, L. Horesh, R. J. Yerworth, D. S. Holder, and R. Bayford, "Generating accurate finite element meshes for the forward model of the human head in eit," *Physiological measurement*, vol. 26, no. 2, p. S251, 2005.

[141] multiphysics CYCLOPEDIAL. (2017) Detailed explanation of the finite element method (fem). [Online]. Available: https://www.comsol.com/multiphysics/finite-element-method

[142] S. Mahdavi, F. Towhidkhah, A. D. N. Initiative *et al.*, "Computational human head models of tdcs: Influence of brain atrophy on current density distribution," *Brain stimulation*, vol. 11, no. 1, pp. 104–107, 2018.

[143] P. Dixit and G. Liu, "A review on recent development of finite element models for head injury simulations," *Archives of Computational Methods in Engineering*, vol. 24, no. 4, pp. 979–1031, 2017.

[144] A. Indahlastari, M. Chauhan, B. Schwartz, and R. J. Sadleir, "Changing head model extent affects finite element predictions of transcranial direct current stimulation distributions," *Journal of neural engineering*, vol. 13, no. 6, p. 066006, 2016.

[145] R. Cotton, C. W. Pearce, P. G. Young, N. Kota, A. Leung, A. Bagchi, and S. Qidwai, "Development of a geometrically accurate and adaptable finite element head model for impact simulation: the naval research laboratory–simpleware head model," *Computer methods in biomechanics and biomedical engineering*, vol. 19, no. 1, pp. 101–113, 2016.

[146] J. Gomez-Tames, Y. Sugiyama, I. Laakso, S. Tanaka, S. Koyama, N. Sadato, and A. Hirata, "Effect of microscopic modeling of skin in electrical and thermal analysis of transcranial direct current stimulation," *Physics in Medicine & Biology*, vol. 61, no. 24, p. 8825, 2016.

[147] A. Indahlastari and R. J. Sadleir, "A comparison between block and smooth modeling in finite element simulations of tdcs," in *Conference proceedings:... Annual International Conference of the IEEE Engineering in Medicine and Biology Society. IEEE Engineering in Medicine and Biology Society. Annual Conference*, vol. 2015. NIH Public Access, 2015, p. 3403.

[148] C. Schmidt, S. Wagner, M. Burger, U. van Rienen, and C. H. Wolters, "Impact of uncertain head tissue conductivity in the optimization of transcranial direct current stimulation for an auditory target," *Journal of neural engineering*, vol. 12, no. 4, p. 046028, 2015.

[149] S. M. Rampersad, A. M. Janssen, F. Lucka, Ü. Aydin, B. Lanfer, S. Lew, C. H. Wolters, D. F. Stegeman, and T. F. Oostendorp, "Simulating transcranial direct current stimulation with a detailed anisotropic human head model," *IEEE Transactions on Neural Systems and Rehabilitation Engineering*, vol. 22, no. 3, pp. 441–452, 2014.

[150] D. Kim, H. Seo, H.-I. Kim, and S. C. Jun, "Computational study on subdural cortical stimulation-the influence of the head geometry, anisotropic conductivity, and electrode configuration," *PLoS One*, vol. 9, no. 9, p. e108028, 2014.

[151] A. N. Shiraz, M. Craggs, B. Leaker, and A. Demosthenous, "Minimizing stimulus current in a wearable pudendal nerve stimulator using computational models," *IEEE Transactions on Neural Systems and Rehabilitation Engineering*, vol. 24, no. 4, pp. 506–515, 2016.

[152] J. R. Macdonald and E. Barsoukov, "Impedance spectroscopy: theory, experiment, and applications," *History*, vol. 1, no. 8, pp. 1–13, 2005.

[153] E. McAdams, A. Lackermeier, J. McLaughlin, D. Macken, and J. Jossinet, "The linear and non-linear electrical properties of the electrode-electrolyte interface," *Biosensors and Bioelectronics*, vol. 10, no. 1-2, pp. 67–74, 1995.

[154] W. Franks, I. Schenker, P. Schmutz, and A. Hierlemann, "Impedance characterization and modeling of electrodes for biomedical applications," *IEEE Transactions on Biomedical Engineering*, vol. 52, no. 7, pp. 1295–1302, 2005.

[155] S. F. Cogan, "Neural stimulation and recording electrodes," *Annu. Rev. Biomed. Eng.*, vol. 10, pp. 275–309, 2008.

[156] P. Shah and Y. Luximon, "Three-dimensional human head modelling: a systematic review," *Theoretical Issues in Ergonomics Science*, pp. 1–15, 2018.

[157] M. I. Iacono, E. Neufeld, E. Akinnagbe, K. Bower, J. Wolf, I. V. Oikonomidis, D. Sharma, B. Lloyd, B. J. Wilm, M. Wyss *et al.*, "Mida: a multimodal imaging-based detailed anatomical model of the human head and neck," *PloS one*, vol. 10, no. 4, p. e0124126, 2015.

[158] Y. Huang, J. P. Dmochowski, Y. Su, A. Datta, C. Rorden, and L. C. Parra, "Automated mri segmentation for individualized modeling of current flow in the human head," *Journal of neural engineering*, vol. 10, no. 6, p. 066004, 2013.

[159] J. E. Janis, D. A. Hatef, R. Hagan, T. Schaub, J. H. Liu, H. Thakar, K. M. Bolden, J. B. Heller, and T. J. Kurkjian, "Anatomy of the supratrochlear nerve: implications for the surgical treatment of migraine headaches," *Plastic and reconstructive surgery*, vol. 131, no. 4, pp. 743–750, 2013.

[160] K. N. Christensen, N. Lachman, W. Pawlina, and C. L. Baum, "Cutaneous depth of the supraorbital nerve: a cadaveric anatomic study with clinical applications to dermatology," *Dermatologic Surgery*, vol. 40, no. 12, pp. 1342–1348, 2014.

[161] Y.-C. Gil, K.-J. Shin, S.-H. Lee, W.-C. Song, K.-S. Koh, and H. J. Shin, "Topography of the supraorbital nerve with reference to the lacrimal caruncle: danger zone for direct browplasty," *British Journal of Ophthalmology*, vol. 101, no. 7, pp. 940–945, 2017.

[162] A. Datta, M. Elwassif, F. Battaglia, and M. Bikson, "Transcranial current stimulation focality using disc and ring electrode configurations: Fem analysis," *Journal of neural engineering*, vol. 5, no. 2, p. 163, 2008.

[163] Y. A. Chizmadzhev, A. V. Indenbom, P. I. Kuzmin, S. V. Galichenko, J. C. Weaver, and R. O. Potts, "Electrical properties of skin at moderate voltages: contribution of appendageal macropores," *Biophysical Journal*, vol. 74, no. 2, pp. 843–856, 1998.

[164] C. K. Ho, "Probabilistic modeling of percutaneous absorption for risk-based exposure assessments and transdermal drug delivery," *Statistical Methodology*, vol. 1, no. 1-2, pp. 47–69, 2004.

[165] Y. A. Chizmadzhev, V. G. Zarnitsin, J. C. Weaver, and R. O. Potts, "Mechanism of electroinduced ionic species transport through a multilamellar lipid system." *Biophysical journal*, vol. 68, no. 3, p. 749, 1995.

[166] G. Szabo, "The regional anatomy of the human integument with special reference to the distribution of hair follicles, sweat glands and melanocytes," *Phil. Trans. R. Soc. Lond. B*, vol. 252, no. 779, pp. 447–485, 1967.

[167] S. R. Tripathi, E. Miyata, P. B. Ishai, and K. Kawase, "Morphology of human sweat ducts observed by optical coherence tomography and their frequency of resonance in the terahertz frequency region," *Scientific reports*, vol. 5, p. 9071, 2015.

[168] F. Rattay, "Analysis of models for external stimulation of axons," *IEEE transactions on biomedical engineering*, no. 10, pp. 974–977, 1986.

[169] A. Kuhn, T. Keller, M. Lawrence, and M. Morari, "A model for transcutaneous current stimulation: simulations and experiments," *Medical & biological engineering & computing*, vol. 47, no. 3, p. 279, 2009.

[170] T. Yamamoto and Y. Yamamoto, "Electrical properties of the epidermal stratum corneum," *Medical and biological engineering*, vol. 14, no. 2, pp. 151–158, 1976.

[171] P. Dimbylow, "Development of the female voxel phantom, naomi, and its application to calculations of induced current densities and electric fields from applied low frequency magnetic and electric fields," *Physics in Medicine & Biology*, vol. 50, no. 6, p. 1047, 2005.

[172] G. Schmid, S. Cecil, and R. Überbacher, "The role of skin conductivity in a low frequency exposure assessment for peripheral nerve tissue according to the icnirp 2010 guidelines," *Physics in Medicine & Biology*, vol. 58, no. 13, p. 4703, 2013.

[173] V. De Santis, X. L. Chen, I. Laakso, and A. Hirata, "An equivalent skin conductivity model for low-frequency magnetic field dosimetry," *Biomedical Physics & Engineering Express*, vol. 1, no. 1, p. 015201, 2015.

[174] C. Gabriel, S. Gabriel, and y. E. Corthout, "The dielectric properties of biological tissues: I. literature survey," *Physics in Medicine & Biology*, vol. 41, no. 11, p. 2231, 1996.

[175] A. Kuhn, T. Keller, S. Micera, and M. Morari, "Array electrode design for transcutaneous electrical stimulation: a simulation study," *Medical engineering & physics*, vol. 31, no. 8, pp. 945–951, 2009.

[176] M. A. Schiefer, R. J. Triolo, and D. J. Tyler, "A model of selective activation of the femoral nerve with a flat interface nerve electrode for a lower extremity neuroprosthesis," *IEEE transactions on neural systems and rehabilitation engineering*, vol. 16, no. 2, pp. 195–204, 2008.

[177] S. B. Baumann, D. R. Wozny, S. K. Kelly, and F. M. Meno, "The electrical conductivity of human cerebrospinal fluid at body temperature," *IEEE transactions on biomedical engineering*, vol. 44, no. 3, pp. 220–223, 1997.

[178] T. F. Oostendorp, J. Delbeke, and D. F. Stegeman, "The conductivity of the human skull: results of in vivo and in vitro measurements," *IEEE transactions on biomedical engineering*, vol. 47, no. 11, pp. 1487–1492, 2000.

[179] M. L. Hines, T. Morse, M. Migliore, N. T. Carnevale, and G. M. Shepherd, "Modeldb: a database to support computational neuroscience," *Journal of computational neuroscience*, vol. 17, no. 1, pp. 7–11, 2004.

[180] E. Salkim, A. Nasrollahy Shiraz, and A. Demosthenous, "Effect of nerve variations on the stimulus current level in a wearable neuromodulator for migraine: A modeling study." IEEE, 2017.

[181] N. T. Carnevale and M. L. Hines, *The NEURON book*. Cambridge University Press, 2006.

[182] D. R. Merrill, M. Bikson, and J. G. Jefferys, "Electrical stimulation of excitable tissue: design of efficacious and safe protocols," *Journal of neuroscience methods*, vol. 141, no. 2, pp. 171–198, 2005.

[183] K. W. Gripp, A. M. Slavotinek, and J. E. Allanson, *Handbook of physical measurements*. Oxford University Press, 2013.

[184] J. W. Young, "Head and face anthropometry of adult us civilians," FEDERAL AVIATION ADMINISTRATION WASHINGTON DC OFFICE OF AVIATION MEDICINE, Tech. Rep., 1993.

[185] K. Bushby, T. Cole, J. Matthews, and J. Goodship, "Centiles for adult head circumference." *Archives of disease in childhood*, vol. 67, no. 10, pp. 1286–1287, 1992.

[186] S. J. Bale, C. I. Amos, D. M. Parry, and A. E. Bale, "Relationship between head circumference and height in normal adults and in the nevoid basal cell carcinoma syndrome and neurofibromatosis type i," *American journal of medical genetics*, vol. 40, no. 2, pp. 206–210, 1991.

[187] A. Nguyen, A. Simard-Meilleur, C. Berthiaume, R. Godbout, and L. Mottron, "Head circumference in canadian male adults: development of a normalized chart," *Int. j. morphol*, vol. 30, no. 4, pp. 1474–1480, 2012.

[188] R.Ching, "Relationship between head mass and circumference in human adults," Tech. Rep.

[189] M. Xu and J. Yang, "Human facial soft tissue thickness and mechanical properties: A literature review," in *ASME 2015 International Design Engineering Technical Conferences and Computers and Information in Engineering Conference*. American Society of Mechanical Engineers, 2015, pp. V01AT02A045–V01AT02A045.

[190] D. E. Barker, "Skin thickness in the human," *Plastic and Reconstructive Surgery*, vol. 7, no. 2, pp. 115–116, 1951.

[191] K. Chopra, D. Calva, M. Sosin, K. K. Tadisina, A. Banda, C. De La Cruz, M. R. Chaudhry, T. Legesse, C. B. Drachenberg, P. N. Manson *et al.*, "A comprehensive examination of topographic thickness of skin in the human face," *Aesthetic surgery journal*, vol. 35, no. 8, pp. 1007–1013, 2015.

[192] Y. Takema, Y. Yorimoto, M. Kawai, and G. Imokawa, "Age-related changes in the elastic properties and thickness of human facial skin," *British Journal of Dermatology*, vol. 131, no. 5, pp. 641–648, 1994.

[193] Y. Lee and K. Hwang, "Skin thickness of korean adults," *Surgical and radiologic anatomy*, vol. 24, no. 3-4, pp. 183–189, 2002.

[194] H. Hori, G. Moretti, A. Rebora, and F. Crovato, "The thickness of human scalp: normal and bald," *Journal of Investigative Dermatology*, vol. 58, no. 6, pp. 396–399, 1972.

[195] J. Ruan and P. Prasad, "The effects of skull thickness variations on human head dynamic impact responses," *Stapp Car Crash J*, vol. 45, no. 11, pp. 395–414, 2001.

[196] S. K. Law, "Thickness and resistivity variations over the upper surface of the human skull," *Brain topography*, vol. 6, no. 2, pp. 99–109, 1993.

[197] H.-J. Lee, K.-S. Choi, S.-Y. Won, P. Apinuntrum, K.-S. Hu, S.-T. Kim, T. Tansatit, and H.-J. Kim, "Topographic relationship between the supratrochlear nerve and corrugator supercilii musclecan this anatomical knowledge improve the response to botulinum toxin injections in chronic migraine?" *Toxins*, vol. 7, no. 7, pp. 2629–2638, 2015.

[198] Y.-C. Gil, K.-J. Shin, S.-H. Lee, W.-C. Song, K.-S. Koh, and H. J. Shin, "Topography of the supraorbital nerve with reference to the lacrimal caruncle: danger zone for direct browplasty," *British Journal of Ophthalmology*, pp. bjophthalmol–2016, 2016.

[199] K.-J. Shin, H. J. Shin, S.-H. Lee, W.-C. Song, K.-S. Koh, and Y.-C. Gil, "Emerging points of the supraorbital and supratrochlear nerves in the supraorbital margin with reference to the lacrimal caruncle: implications for regional nerve block in upper eyelid and dermatologic surgery," *Dermatologic Surgery*, vol. 42, no. 8, pp. 992–998, 2016.

[200] P. Konofaos, M. A. Soto-Miranda, J. Ver Halen, and J. C. Fleming, "Supratrochlear and supraorbital nerves: an anatomical study and applications in the head and neck area," *Ophthalmic Plastic & Reconstructive Surgery*, vol. 29, no. 5, pp. 403–408, 2013.

[201] S. M. Jeong, K. J. Park, S. H. Kang, H. W. Shin, H. Kim, H. K. Lee, and Y. G. Chung, "Anatomical consideration of the anterior and lateral cutaneous nerves in the scalp," *Journal of Korean medical science*, vol. 25, no. 4, pp. 517–522, 2010.

[202] Y. Pinar, F. Govsa, M. A. Ozer, and I. Ertam, "Anatomocosmetic implication rules of the corrugator supercilii muscle for youthful eye appearance," *Surgical and Radiologic Anatomy*, vol. 38, no. 9, pp. 1045–1051, 2016.

[203] S. Raspopovic, M. Capogrosso, and S. Micera, "A computational model for the stimulation of rat sciatic nerve using a transverse intrafascicular multichannel electrode," *Ieee Transactions On Neural Systems And Rehabilitation Engineering*, vol. 19, no. 4, pp. 333–344, 2011.

[204] S. Raspopovic, F. M. Petrini, M. Zelechowski, and G. Valle, "Framework for the development of neuroprostheses: from basic understanding by sciatic and median nerves models to bionic legs and hands," *Proceedings of the IEEE*, vol. 105, no. 1, pp. 34–49, 2017.

[205] P. Marianelli, M. Capogrosso, L. B. Luciani, A. Panarese, and S. Micera, "A computational framework for electrical stimulation of vestibular nerve," *IEEE Transactions on Neural Systems and Rehabilitation Engineering*, vol. 23, no. 5, pp. 897–909, 2015.

[206] M. Borenstein, L. V. Hedges, J. P. Higgins, and H. R. Rothstein, *Introduction to meta-analysis*. John Wiley & Sons, 2011.

[207] R. A. Blum, "An electronic system for extracellular neural stimulation and recording," Ph.D. dissertation, Georgia Institute of Technology, 2007.

[208] D. J. Tyler and K. H. Polasek, "Electrodes for the neural interface," in *Neuromodulation*. Elsevier, 2009, pp. 181–213.

[209] W. M. Grill, "Principles of electric field generation for stimulation of the central nervous system," in *Neuromodulation*. Elsevier, 2009, pp. 145–155.

[210] K. Kilgore, *Implantable Neuroprostheses for Restoring Function*. Elsevier, 2015.

[211] A. R. Kent and W. M. Grill, "Model-based analysis and design of nerve cuff electrodes for restoring bladder function by selective stimulation of the pudendal nerve," *Journal of neural engineering*, vol. 10, no. 3, p. 036010, 2013.

[212] J. D. Sweeney, D. A. Ksienski, and J. T. Mortimer, "A nerve cuff technique for selective excitation of peripheral nerve trunk regions," *IEEE Transactions on Biomedical Engineering*, vol. 37, no. 7, pp. 706–715, 1990.

[213] N. P. Aryan, H. Kaim, and A. Rothermel, *Stimulation and recording electrodes for neural prostheses*. Springer, 2015, vol. 1.

[214] N. M. Malešević, L. Z. P. Maneski, V. Ilić, N. Jorgovanović, G. Bijelić, T. Keller, and D. B. Popović, "A multi-pad electrode based functional electrical stimulation system for restoration of grasp," *Journal of neuroengineering and rehabilitation*, vol. 9, no. 1, p. 66, 2012.

[215] J. Newman, "Resistance for flow of current to a disk," 1965.

[216] B. Wang, A. Petrossians, and J. D. Weiland, "Reduction of edge effect on disk electrodes by optimized current waveform," *IEEE Transactions on Biomedical Engineering*, vol. 61, no. 8, pp. 2254–2263, 2014.

[217] S. Papazov, Z. Kostov, and I. Daskalov, "Electrical current distribution under transthoracic defibrillation and pacing electrodes," *Journal of medical engineering & technology*, vol. 26, no. 1, pp. 22–27, 2002.

[218] C. C. McIntyre and W. M. Grill, "Finite element analysis of the current-density and electric field generated by metal microelectrodes," *Annals of biomedical engineering*, vol. 29, no. 3, pp. 227–235, 2001.

[219] S. Day, "Important factors in surface emg measurement," *Bortec Biomedical Ltd publishers*, pp. 1–17, 2002.

[220] T. Keller and A. Kuhn, "Electrodes for transcutaneous (surface) electrical stimulation," *Journal of Automatic Control*, vol. 18, no. 2, pp. 35–45, 2008.

[221] R. Waters, D. McNeal, W. Faloon, and B. Clifford, "Functional electrical stimulation of the peroneal nerve for hemiplegia. long-term clinical follow-up." *JBJS*, vol. 67, no. 5, pp. 792–793, 1985.

[222] E. Marsolais and R. Kobetic, "Functional walking in paralyzed patients by means of electrical stimulation." *Clinical Orthopaedics and Related Research*, no. 175, pp. 30–36, 1983.

[223] M. E. Spira and A. Hai, "Multi-electrode array technologies for neuroscience and cardiology," *Nature nanotechnology*, vol. 8, no. 2, p. 83, 2013.

[224] A. Popović-Bijelić, G. Bijelić, N. Jorgovanović, D. Bojanić, M. B. Popović, and D. B. Popović, "Multi-field surface electrode for selective electrical stimulation," *Artificial organs*, vol. 29, no. 6, pp. 448–452, 2005.

[225] R. V. Shannon, "A model of safe levels for electrical stimulation," *IEEE Transactions on Biomedical Engineering*, vol. 39, no. 4, pp. 424–426, 1992.

[226] R. M. Gallagher and R. Kunkel, "Migraine medication attributes important for patient compliance: concerns about side effects may delay treatment," *Headache: The Journal of Head and Face Pain*, vol. 43, no. 1, pp. 36–43, 2003.

[227] S. Hann and A. Sharan, "Dual occipital and supraorbital nerve stimulation for chronic migraine: a single-center experience, review of literature, and surgical considerations," *Neurosurgical focus*, vol. 35, no. 3, p. E9, 2013.

[228] J. R. Saper, D. W. Dodick, S. D. Silberstein, S. McCarville, M. Sun, and P. J. Goadsby, "Occipital nerve stimulation for the treatment of intractable chronic migraine headache: Onstim feasibility study," *Cephalalgia*, vol. 31, no. 3, pp. 271–285, 2011.

[229] D. Magis and J. Schoenen, "Advances and challenges in neurostimulation for headaches," *The Lancet Neurology*, vol. 11, no. 8, pp. 708–719, 2012.

[230] J. E. Janis, J. C. Barker, C. Javadi, I. Ducic, R. Hagan, and B. Guyuron, "A review of current evidence in the surgical treatment of migraine headaches," *Plastic and reconstructive surgery*, vol. 134, no. 4S-2, pp. 131S–141S, 2014.

[231] P. Gérardy, D. Fabry, A. Fumal, and J. Schoenen, "A pilot study on supra-orbital surface electrotherapy in migraine: Pd. 22," *Cephalalgia*, vol. 29, no. 1, p. 134, 2009.

[232] G. Bussone, H.-C. Diener, J. Pfeil, and S. Schwalen, "Topiramate 100 mg/day in migraine prevention: a pooled analysis of double-blind randomised controlled trials," *International journal of clinical practice*, vol. 59, no. 8, pp. 961–968, 2005.

[233] G. Landmann, L. Stockinger, C. Lustenberger, M. Schmelz, and R. Rukwied, "Effects of current density on nociceptor activation upon electrical stimulation in humans," *Pain Practice*, vol. 16, no. 3, pp. 273–281, 2016.

[234] Food, D. Administration *et al.*, "De novo classification request for cefaly device. 2012."

Appendix A

HH-type channel parameters

A.1 HH-type channel parameters

Table A.1: HH-type channel parameters [131].

Current	Equation
Fast Na^+	$I_{Naf} = g_{Naf} m^3 h (V_m - V_{Na})$
	$\alpha_m = \frac{6.57(V_m+20.4)}{1-e^{\frac{-V_m-20.4}{10.3}}}$
	$\alpha_h = \frac{0.34(-V_m-114)}{1-e^{\frac{V_m+114}{11}}}$
	$\beta_m = \frac{0.304(-V_m-25.7)}{1-e^{\frac{V_m+25.7}{9.16}}}$
	$\beta_h = \frac{12.6}{1+e^{\frac{V_m-31.8}{13.4}}}$
Persistent Na^+	$I_{Nap} = g_{Nap} p^3 (V_m - V_{Na})$
	$\alpha_p = \frac{0.0353(V_m+27)}{1-e^{\frac{-V_m-27}{10.2}}}$
	$\beta_p = \frac{0.000883(-V_m-34)}{1-e^{\frac{V_m+34}{10}}}$
Slow K^+	$I_{Ks} = g_{Ks} s (V_m - V_K)$
	$\alpha_s = \frac{0.3}{1+e^{\frac{V_m+53}{-5}}}$
	$\beta_s = \frac{0.03}{1+e^{\frac{V_m+90}{-1}}}$

Appendix B

Electrode-tissue interface

The R_{ct} can be expressed by Butler–Volter formulation in Equation (B.1) [152], [153], [154].

$$R_{ct} = \frac{RT}{nFJ_0} \tag{B.1}$$

where R is the universal gas constant, T is the temperature(K), F is the Faraday constant, n is the number of electrons involved the reaction and J_0 is the current density at which the rate of oxidation and reductions are equilibrium. The R_{ct} is is highly dependent upon the current density at ETI, the frequency of the applied signal as well as the electrode surface area. At the high frequency, it has a high value; it has inverse proportional variations with J_0. The R_t in Figure B.1 represents tissue resistance which the electrode is attached. Electrodes are typically applied onto the surface of the skin in TES applications.

Since faradic currents are dependent on the existence of the ions at the surface and the diffusion of these ions requires time (especially at low frequency), an extra element which referred to as the Warburg element should be placed with R_{ct} in the equivalent circuit representing the interface as shown in Figure B.1b. The Warburg impedance can be expressed by Equation (B.2) [153], [154].

$$Z_W = \frac{(1-j)D}{\sqrt{w}} \tag{B.2}$$

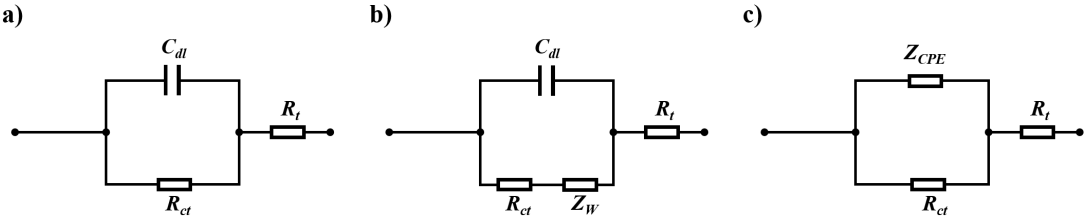

Figure B.1: Electrical circuit model of ETI impedance. a) Simple ETI circuit model. b) Warburg element is connected with simple ET circuit to represent the ion diffusion dependent Faradaic current. c) Frequency-dependence of ETI is represented using CPE instead of basic capacitor.

where D is the ions diffusion coefficient and w is the angular frequency.

According to experimental results, interfacial double layer does not behave as a pure capacitor but instead reveals frequency–dependent behaviour. This is maybe because of the physiochemical effects at the interface and the surface roughness and can be modeled by replacing C_{dl} with a constant phase element (CPE). There are different representation of the impedance of the CPE in the literature but one representation was shown in Figure B.1c. The effect of CPE is formulated by Equation (B.3) [154].

$$Z_{CPE} = \frac{1}{Q(jw)^{\alpha}} \tag{B.3}$$

where Q is a coefficient capacitance and α is an is a measure of the deviation from pure capacitive behaviour and it is an exponent between zero and one. Electrodes with higher surface area has lower Z_{CPE} [153], [154]. In addition, the impedance of the ETI also heavily depends on the electrode geometry. The large electrodes have low impedance due to having a large effective area. Therefore, big electrodes need a higher current than small ones to generate the same voltage and thus electric field strength. As relatively bigger electrodes induce a much larger electric field result in affecting a large population of neurons. Depending on the application, the size of the electrode can vary.

Appendix C

Protocol for clinical study

Project ID: 13151/001

C.1 Transcutaneous electrical frontal nerve stimulation

C.1.1 Introduction

Migraine is a highly disabling disorder of the brain which may affect patients both socially and economically. The pharmacotherapeutic, injectable and invasive neurostimulation treatments used to treat migraine may have undesirable side effects and associated risks. It has recently been shown that non-invasive transcutaneous supraorbital neuromodulation is effective at preventing episodic migraine attacks. However, the results indicated that it has modest efficacy. Neuroanatomical variations in the branches of the frontal nerves often require relatively high currents during stimulation, which then may result in pain sensation due to activation of the both Aδ and C fibers. Furthermore, as the electrode patch is close to the sensitive anatomical structures (e.g. eyes and sinuses) in the existing device, this may cause discomfort.

Using a new electrode orientation that shifted away from these sensitive anatom-

ical layers, it may be possible to stimulate all nerve fibre of frontal nerve at a reduced threshold with a lower risk of inducing pain. The computational model results indicated that the electrode orientation has an important influence on the stimulus current levels for nerve fibres. It was shown that the required currents to stimulate all nerve fibres could be minimised considerably using vertical electrode orientation (vertically aligned) rather than using horizontal orientation (horizontally aligned). Thus, using this new electrode orientation, it may be possible to minimise the existing device complications. This may in turn help in improving the efficacy of non-invasive transcutaneous frontal nerve stimulation. The aim of the proposed study is to validate the computational model results by assessing the effect of electrode orientations on the current levels required and threshold for pain and paraesthesia.

C.1.2 Background

Migraine is a common neurological disorder characterized by episodes of unilateral or bilateral headache lasting for hours to days, which may be accompanied by photophobia, phonophobia, nausea and vomiting. The available pharmaceutical treatments are limited due to their modest efficacy and often troublesome side-effects [7]. Available pharmaceutical treatments of migraine have contraindications and are associated with moderate to severe side effects such as the overuse of some drugs may lead to medication overuse headache [6]. These side effects lead to insufficient efficacy, dissatisfaction and/or discontinuation of medication. It was demonstrated that 80% of patients would be willing to use an alternative treatment method to pharmaceutical solution, if provided with similar or better efficacy, and most importantly fewer side effects [226]. Thus, there is a need for alternative, more efficient and tolerable therapies.

Neuromodulation method may represent such an alternative. This technique has been considered as an option to manage migraine which aims to manipulate peripheral or central pain pathways using electrical stimulation of peripheral nerve

branches. This stimulation is achievable either invasively via implantable devices or non-invasively delivered transcutaneously via surface electrodes connected to an external stimulator [7], [9], [227]. According to Melzack and Walls gate control theory [8] it is believed that the peripheral nerve stimulation (PNS) works through activation of large Aβ afferent nerve fibers and inhibition of small Aδ and C pain fibers . Additionally, the neural plasticity is defined as the ability of the central nervous system (CNS) adapt to modifications. The therapeutic plasticity can be achieved over a period of time, often weeks to months [7].

Although invasive electrical nerve stimulation (IENS) methods, such as occipital nerve stimulation, have shown encouraging results to prevent migraine, this method is only used in the most medically intractable patients due to the inevitable exposure of the patients to the associated risks [87], [228], [229]. Transcutaneous electrical nerve stimulation (TENS) has fewer complications compared with the IENS. Although transcutaneous vagus nerve and transcranial magnetic stimulation provide a degree of positive results, most of this techniques are based on small numbers of participants and lack long term data about their tolerability, convenience, effectiveness and side effects in the treatment of migraine [15], [78]. In addition, as the vagus nerve contains sensory and motor nerve fibers, stimulation of this nerve caused neck muscle contractions in some patients [11].

Clinical studies show that migraine sufferers commonly report that the pain centered in the frontal region of the head [12], [230], in the territories of the supraorbital (SON) and supratrochlear (STN) nerves. These sensory peripheral nerves are branches of the frontal nerve, which derives from the ophthalmic division of the trigeminal nerve. These nerves are responsible for receiving most of the frontal pain sensation and transmit to the brain through the trigeminal nucleus caudalis [13], [230].

Transcutaneous frontal nerve stimulation (t–FNS) with Cefaly (Cefaly, CEFALY Technology, Liege, Belgium) stimulator has been developed to prevent episodic migraine by stimulating the frontal nerve [7]. There is no well-controlled evidence

for the use of the Cefaly device in the acute treatment of episodic migraine. A single pilot study of 10 patients using the Cefaly device for acute treatment of migraine showed that the device had no effect on 57% of treated attacks and was associated with pain freedom in only 13% of attacks [231]. Evidence for the use of the Cefaly device in the prevention of episodic migraine comes from one small, manufacturer sponsored sham-controlled trial, the PREvention of MIgraine using the STS Cefaly (the PREMICE study) and company post–marketing survey data. The sham-controlled study involved only 67 subjects with episodic migraine, who after a one month run-in period of normal treatment used the Cefaly or sham device for 3 months reported a significant reduction in migraine days by 29.7% from 6.94 to 4.88 (p=0.023) in the active group compared to a non-significant change of 4.9% from 6.54 to 6.22 (p=0.608) in the sham group [14]. For comparison, topiramate at a dose of 100mg daily decreases migraine days by 44% in a pooled analysis of controlled studies [229]. The therapeutic gain for the 50% responder rate of supraorbital nerve stimulation was 26.1% compared to 23.5% for topiramate but the therapeutic gain in migraine day reduction is much higher in pooled studies of topiramate at 24.5% compared to the PREMICE trial at 12% [232]. The post-marketing survey of 2313 subjects using the device as a preventative treatment of episodic migraine reported 53% of users were 'satisfied' with the treatment as determined by the number continuing treatment after a 40 day trial period. 46.6% of the patients were not satisfied with the Cefaly device(among them 40% of patients using the device at least 20 days) [15]. It is assumed the principal reasons for interruption of the stimulation are sensation of the paranesthesia and pain with high current stimulation [16].

Neuroanatomical variations result in the use of relatively high currents based on our computational modelling study which then may result in painful sensations due to activation of both Aδ and C fibers [233]. Furthermore, as electrode patch is close to sensitive anatomical structures (e.g., eyes and sinuses) in the existing device, this may cause patient discomfort. The device efficacy can be improved

with optimize those complications.

Using a new electrode orientation that shifted away from these sensitive anatomical layers, it may be possible to stimulate all nerve fibre of frontal nerve at a reduced threshold with a lower risk of inducing pain. The electrical potential variations is greater using vertically aligned electrode orientation than horizontally aligned one. Thus it may be possible to activate the nerve fibers with the lower threshold using vertically aligned electrode orientation rather than horizontal aligned orientation.

It was shown that the required currents to stimulate all nerve fibres could be minimised considerably using vertical electrode orientation (vertically aligned) rather than using horizontal orientation (horizontally aligned). Thus, using this new electrode orientation, it may be possible to minimise the existing device complications. This may in turn help in improving the efficacy of non-invasive transcutaneous frontal nerve stimulation. To assess the effect of electrode orientations on the pain and current levels, we would like to validate our computational results in a clinical study.

C.1.3 Aim of study

Using computational models of the human head and electrical field, we have shown the potential of improving an existing device by shifting the electrode orientation from the sensitive anatomical structures as well as alignment of the electrode (Manuscript in preparation). Using vertically aligned electrodes, we may reduce the adverse effects of the existing device. To assess current threshold and stimulus sensations, we need to compare both orientations on healthy subjects. Thus, we would like to validate our computational results in a small clinical study.

C.2 Objective

The objectives of this study are to investigate

- The effect of electrode arrangements on stimulus current levels.
- The effect of electrode arrangements on the pain and paranesthesia sensation levels.
- The effect of human head size on the current threhold levels

C.3 Hypothesis

It was shown that there is no well-controlled evidence for the use of the Cefaly device in the acute treatment of episodic migraine. The clinical control studies were shown that the efficacy of the device is low. Based on post market study, 46.6% of the patients were not satisfied with the Cefaly device (among them 40% of patients using the device at least 20 days). This may be because of high current levels which cause to sensation of the paranesthesia and pain.

Our computational modelling results showed that neuroanatomical variations resulting in high currents and it is known that the high current may cause to activate both Aδ and C fibers which result in painful sensations [233]. Furthermore, the transcutaneous electrical stimulation electrode patch is close to the sensitive anatomical structures (e.g.; eyes and sinuses) in the existing device and this may cause patient discomfort. Thus, using new electrode arrangements, which may be shifted away from these sensitive anatomical layers, it may be possible to stimulate all nerve fiber of frontal nerve at a reduced threshold with a lower risk of inducing pain. It was shown that the required currents to stimulate all nerve fibers could be minimized considerably using vertical electrode orientation rather than using horizontal orientation. Thus, we hypothesize that using this new electrode orientation will reduce the complications of the existing device. This may in turn help in improving the efficacy of the solution. To assess the effect of electrode orientations on the pain and current levels, we would like to validate our computational results in a clinical study.

C.3.1 Study design

Randomised control study is proposed to obtain more accurate and objective results in this study.

C.3.2 Study setting/ location

The study will be a single centre study and will be conducted at UCL Institute of Neurology.

C.3.3 Study population

The population the subjects will be drawn from UCL and UCLH staff and students. We will perform this controlled study on healthy subjects. The age range will be from 18 to 65 years.

C.3.4 Eligibility criteria

Inclusion criteria

The participant will be volunteers from UCL and UCLH staffs and students (they should be at least 18 years old). They will be asked to sign the consent form. The medical history will be asked to reassure they do not have any exclusion criteria.

Exclusion criteria

- The device cannot be used by an individual who has an implanted metallic or electronic device in their head.

- The device should not be used by an individual with chronic migraine, refractory migraine, medication overuse headache, or chronic tension-type headaches. The safety and effectiveness of the device have not been demonstrated for individuals with these conditions.

- The device should not be applied on the neck or chest, and it should not be used in the presence of electronic monitoring equipment (e.g., cardiac

monitors), in the bath or shower, while sleeping, while driving, or while operating machinery [234].

- The participants who have any physiological and psychological medical disorders will be excluded.

C.4 Study outcomes

- Comparison of amplitude of pain threshold with horizontal versus vertical alignment
- Comparison of paranesthesia threshold with horizontal versus vertical alignment
- Comparison of paranesthesia and pain threshold for usage of one vertical electrode versus two vertical electrodes alignment
- Record any adverse effect to minimize for future study.

C.4.1 Study procedures

Recruitment of participants

The potential participants of this study will be from UCL and UCLH staffs and students. We will make an advertisement to invite participants to be a volunteer for our study and we will pay 20 pounds as cash for each volunteer. We will inform each participant that they do not feel coerced into taking part, that they are able to decline participation if they wish to and if they do agree to take part that they can withdraw at any time without having to give a reason.

Randomisation

We will assess the effect of four different electrode arrangements on pain and paresthesia thresholds. Thus, we will number these arrangements then we will generate a computer code to randomize the selection of these arrangements.

Study procedure

After participant signed the consent form, we will divide four group (as shown in Table D.1) and train each participant before the session. As this study is a straightforward low-risk test, we will do training and test sessions on the same day. Then, we will provide document which shows the sensation occurrence and its severity on a point scale for both paraesthesia and pain (0: no sensation; 1–6: paraesthesia, 6–10: pain, see Table D.3) to fill in during the session. Also, it worthy to provide a document (see Table D.4) to record any adverse effect during the study to minimize them in future studies.

We will make sure the device fully charged and use disposable electrodes for each volunteer. The maximum time is 20 minutes for each session. The device will be off automatically after 20 minutes. We will test the effect of four different electrode arrangements on each subject. These are, in turn, horizontal on the forehead, vertical on the right side of the forehead, vertical on the left side of the forehead, and vertical on the left and right side of the forehead. After training session, the below steps will be followed for each participant.

- We will wipe the volunteers forehead with available wipes to increase the quality of contact between skin and electrode patch.
- We will put Cefaly electrode patch on the forehead.
- We will place the Cefaly stimulator on the electrode patch and make sure magnet connected with the metallic area on electrode patch.
- We will press the button on the stimulator to activate it.
- We will show the human head schematic to the subject asking where he/she feels sensations and we will cross this areas and record time and sensation frequency for each updated sensation.

Table C.1: Schedule of the experiments for each group.

Morning	Afternoon
Group 1	Group3
Group 2	Group 4

- As the intensity of the current is increased step by step automatically, we will ask the participant to update us regarding the place where he/she feels the sensation and we will record the time accordingly.

- We will carry on the session unless the subject wants to withdraw. As volunteers do not have to carry on 20 minutes, we will calculate resting time for next session by 50% of total stimulation time (e.g.; 20 minutes stimulation requires 10 minutes resting).

- We will repeat sections 1 to 8 for each randomized selected electrode arrangement.

Measurement tools used

We will provide the human head schematic (as shown in Figure D.1) and we will mark locations to assess sensation occurrence and its severity on a point scale for both paresthesia and pain (0: no sensation; 1–6: paresthesia, 6–10: pain) to fill in during the session as shown in Figure D.3. Also we will provide a schedule to record any adverse effects as depicted in Table D.4 . We will also provide the timer to calculate total usage of the device by each subject which can be related to current threshold levels.

C.4.2 Safety considerations/patient safety

The Cefaly device bears the CE mark for the medical devices. It is certified to the IS Medical standard, authrised by GMP (Gd Manufacturing Practices) and GCP (Gd Clinical Practice). The company also obtains FDA license. In 2016, the UKs National Institute of Health and Care Excellence (NICE) issued full guidance on

Table C.2: Sample size calculation, $Z_{a/2}$, Z_β are critical values of the standard normal distribution.

P	$Z_{a/2}$	$1-\beta$	Z_β	μ_1	μ_2	SD
0.01	2.576	0.95	1.645	89.4	68	17

the device. That means that NHS experts thoroughly reviewed its clinical data and safety evidence. Since usage of the device is safe and we will follow the eligibility criteria, we do not expect any medical emergencies. Furthermore, Dr. Matharu will be supervise as a neurologist and principal researcher. Moreover, any indications of severe psychological distress during the therapy will be explored and, if necessary, appropriate referrals for concurrent therapy/psychiatric consultation will be made.

Data monitoring

The participants data will be collected and stored in UCL network with a specified password. The data will not share with any third parties.

C.5 Statistical considerations and data analysis

Sample size and statistical power

Anatomical variations are significant for both electrode orientations. To calculate number of the participants, the human head size (average radius) and the forehead distance from the eyebrows to hairline are selected as significant elements for this study. Average human head size (μ_1) and average human forehead distance from the eyebrows to hairline (μ_2) are 89.4 mm and 68 mm, respectively. The pooled standard deviation (SD) is calculated as 17. We assumed the clinical significance (p) is 0.01 and the power ($1-\beta$) is estimated 95% to increase accuracy. The total estimated sample size is quantified from the given information as shown in Table D.2 and in Equation D.1.

$$N = \frac{2(Z_{a/2} + Z_{\beta})^2}{(\mu_1 - \mu_2)} \tag{C.1}$$

As N is the total number of the sample size, we need to be conservative when we calculate N. Thus, the required sample size for this study is 30.

C.5.1 Statistical methods

The statistical analysis will performed in MATLAB software version R2015b (MathWorks, Inc., Natic M, USA). For all analysis, we will use the paired t-test with threshold for statistical significance set as $p<0.01$

C.6 Ethical considerations

This study will be carried out in accordance with the recommendations of the UCL Research Ethics Committee of with written informed consent from all subjects. All subjects will be given written informed consent in accordance with the Declaration of Helsinki after the study procedure had been explained We will inform the participants that they do not feel coerced into taking part, that they are able to decline to participate or if they wish to and if they do agree to take part that they can withdraw at any time without having to give a reason. The data will be saved and stored in UCL network.

C.7 Outcomes and significance

The potential benefits of this study are:

- The patient discomfort and unknown effects may be reduced by minimizing current thresholds using optimise electrode orientation.
- The stimulation may be more comfortable using an arrangement that shifts the electrode orientation away from the sensitive structure.
- Any adverse effects during this study will be recorded to enable us to min-

imise them in any future studies.

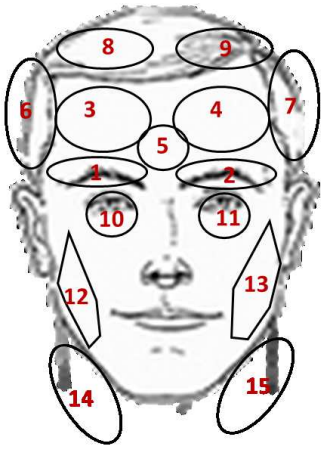

Figure C.1: Human head schematic.

Table C.3: Sensation intensity of paresthesia and pain on human head schematic.

	Paraesthesia						**Pain**			
Sensation intensity	1	2	3	4	5	6	7	8	9	10
Sensation zone										
Stimulus current threshold										

Table C.4: Adverse events during study.

Adverse events		**Time(s)**
Reversible forehead skin irritation		
Feeling of fatigue		
Feeling of stress		
Allergic skin reaction		
Dental pain during the session or at the beginning		
Inability to keep eyes open during sessions		
Do not like the feeling		
Others		